Switches in trypanosome differentiation:

ALBA proteins acting on post-transcriptional mRNA control

Dissertation zur Erlangung des

naturwissenschaftlichen Doktorgrades

der Julius-Maximilians-Universität Würzburg

vorgelegt von

Ines Subota

geboren in Groß-Sankt-Nikolaus

Würzburg, August 2011

Eingereicht am: 22. August 2011

Mitglieder der Promotionskommission:

Vorsitzender: Prof. Dr. Thomas Dandekar

1. Gutachter : Prof. Dr. Markus Engstler

2. Gutachter : Prof. Dr. Thomas Rudel

Tag des Promotionskolloquiums: 12. Oktober 2011

Doktorurkunde ausgehändigt am:

Diese Arbeit wurde betreut von: Dr. Philippe Bastin und Prof. Dr. Markus Engstler

Die experimentellen Arbeiten wurden am
Institut Pasteur (Paris, Frankreich), in der Gruppe
Trypanosome Cell Biology Unit durchgeführt.

Die vorliegende Arbeit wurde gefördert vom
Fonds National de la Recherche, Luxembourg

FÜR MEINE MAMA,

Du hast mich Kraft und Ehrgeiz gelehrt,
dieses Abenteuer zu unternehmen.

CONTENTS

1 ZUSAMMENFASSUNG

SUMMARY

1.1 Zusammenfassung

Trypanosoma brucei ist ein digenetischer, eukaryotischer Parasit, der zwischen Säugetier und Tsetsefliege alterniert, in welchen er unterschiedliche Gewebe besiedelt. Er ist die Ursache für die Schlafkrankheit in Afrika südlich der Sahara. Der Lebenszyklus der Trypanosomen besteht aus mehr als neun Parasitenstadien, die eindeutig anhand ihrer Morphologie, ihres Metabolismus und der Positionierung ihrer DNA Organellen unterschieden werden können. Trypanosomen bleiben ausschließlich extrazellulär und kommen im Laufe ihres Infektionszyklus mit sich verändernden Umwelteinflüssen in Berührung, z. B. Temperaturschwankungen, Variation in vorhandenen Energiequellen, erhöhte Viskosität usw. In Übereinstimmung mit der anerkannten sensorischen Funktion die Cilien in Vielzellern ausüben, wurde für diese Rolle das strukturverwandte Flagellum in Trypanosomen vorgeschlagen. Die Erkennung wechselnder Umweltparameter ist der vermutliche Auslöser für Differenzierungsprozesse, die ein Entwicklungsstadium hervorbringen, welches am besten an die neue Umgebung angepasst ist. Dies wird durch eine Modifizierung der Genexpression erreicht, die in Trypanosomen fast ausschließlich auf posttranskriptioneller Ebene erfolgt.

Diese Arbeit zeigt, dass die RNA bindenden Proteine ALBA3 und ALBA4 an der Differenzierung von Trypanosomen in der Tsetsefliege beteiligt sind. Immunfluoreszenzanalyse und Lebendvideomikroskopie von Zellen, die eine an YFP gekoppelte Variante der Proteine enthalten, haben gezeigt, dass sich ALBA3/4 im Zytosol befinden und dass sie in jedem Parasitenstadium exprimiert sind, mit Ausnahme derer, die im Proventrikel der Tsetsefliege zu finden sind. Das Herunterregulieren der Proteine in vorangehenden Stadien, führt zu markanten Veränderungen, die mit denjenigen, die in Parasiten im Proventrikel zu finden sind, vergleichbar sind: z. B. Verlängerung der Zelle, Zellzyklusarrest und Lokalisierung des Zellkerns in eine posteriore Position. Im Gegenteil dazu findet die Umpositionierung des Zellkerns nicht statt, wenn ALBA3 während der Entwicklung des Parasiten in der Tsetsefliege überexprimiert wird. Ein vergleichbarer Effekt wird mit ALBA4 Überexpression nicht erreicht, welches die Entwicklung nicht negativ zu beeinflussen scheint. Wenn Trypanosomen Hungerstress ausgesetzt sind, reichern sich beide ALBA Proteine zusammen mit DHH1, einem anerkannten RNA bindenden Protein, in zytoplasmatischen Aggregaten an, die nur teilweise mit denjenigen kolokalisieren, die durch polyA$^+$ RNA in diesen Bedingungen verursacht werden. Diese Arbeit zeigt, dass ALBA Proteine eine wichtige Rolle in der Entwicklung von Trypanosomen spielen und legt nahe,

dass sie an der entwicklungsbedingten Kontrolle eines Teils der mRNA Expression beteiligt sind.

Der zweite Teil dieser Arbeit handelt von der Identifizierung neuer flagellarer Proteine, die eine sensorische Funktion haben könnten. Hierfür wurden mehrere Proteinkandidaten aus einer durchgeführten Proteomanalyse intakter Flagellen gewählt. Die vorliegende Arbeit bestätigt die flagellare Lokalisierung der Proteine mit großem Erfolg (85% der untersuchten Proteine) und zeigt, dass sie unterschiedliche Verteilungsmuster vorweisen. Zwei der Proteine werden während der Infektion des Parasiten in der Tsetsefliege untersucht, was aufdeckt, dass eines davon in den Stadien im Proventrikel herunterreguliert ist. Die Funktionsstudie eines neu identifizierten flagellaren Membranproteins weist seine schnelle Dynamik im Flagellum auf, führt jedoch zu keinem sichtbaren Phänotyp in Laborbedingungen. Diese Beobachtung passt zu der Annahme, dass Proteine mit sensorischer Funktion in stabilen Laborverhältnissen nicht essentiell sind aber eine wichtige Rolle während der Entwicklung des Parasiten in natürlichen Bedingungen spielen.

Zusammenfassend fügt diese Arbeit Teile zum Puzzle der Identifizierung molekularer Schalter, die in Trypanosomenstadien in der Tsetsefliege an der mRNA Kontrolle und der Erkennung der Umwelt beteiligt sind.

1.2 Summary

Trypanosoma brucei is a digenetic eukaryotic parasite that develops in different tissues of a mammalian host and a tsetse fly. It is responsible for sleeping sickness in sub-saharan Africa. The parasite cycle involves more than nine developmental stages that can be clearly distinguished by their general morphology, their metabolism and the relative positioning of their DNA-containing organelles. During their development, trypanosomes remain exclusively extracellular and encounter changing environments with different physico-chemical properties (nutritional availability, viscosity, temperature, etc.). It has been proposed that trypanosomes use their flagellum as a sensing organelle, in agreement with the established role of structurally-related cilia in metazoa and ciliates. Recognition of environmental triggers is presumed to be at the initiation of differentiation events, leading to the parasite stage that is the best suited to the new environment. These changes are achieved by the modification of gene expression programmes, mostly underlying post-transcriptional control of mRNA transcripts.

We first demonstrate that the RNA-binding proteins ALBA3/4 are involved in specific differentiation processes during the parasite development in the fly. They are cytosolic and expressed throughout the parasite cycle with the exception of the stages found in the tsetse fly proventriculus, as shown by both immunofluorescence and live cell analysis upon endogenous tagging with YFP. Knock-down of both proteins in the developmental stage preceding these forms leads to striking modifications: cell elongation, cell cycle arrest and relocalization of the nucleus in a posterior position, all typical of processes acting in parasites found in the proventriculus region. When ALBA3 is over-expressed from an exogenous copy during infection, it interferes with the relocalization of the nucleus in proventricular parasites. This is not observed for ALBA4 over-expression that does not visibly impede differentiation. Both ALBA3/4 proteins react to starvation conditions by accumulating in cytoplasmic stress granules together with DHH1, a recognized RNA-binding protein. ALBA3/4 proteins also partially colocalize with granules formed by polyA$^+$ RNA in these conditions. We propose that ALBA are involved in trypanosome differentiation processes where they control a subset of developmentally regulated transcripts. These processes involving ALBA3/4 are likely to result from the specific activation of sensing pathways.

In the second part of the thesis, we identify novel flagellar proteins that could act in sensing mechanisms. Several protein candidates were selected from a proteomic analysis of intact flagella performed in the host laboratory. This work validates their flagellar localization with high success (85% of the proteins examined) and defines multiple different patterns of protein distribution in the flagellum. Two proteins are analyzed during development, one of them showing down-regulation in proventricular stages. The functional analysis of one novel flagellar membrane protein reveals its rapid dynamics within the flagellum but does not yield a visible phenotype in culture. This is coherent with sensory function that might not be needed in stable culture conditions, but could be required in natural conditions during development.

In conclusion, this work adds new pieces to the puzzle of identifying molecular switches involved in developmental mRNA control and environmental sensing in trypanosome stages in the tsetse fly.

2 INTRODUCTION

2.1 The *Trypanosoma brucei* parasite

The "tsetse fly disease" was first described by David Livingstone in 1857 during his exploratory travels in South-eastern Africa (Livingstone, 1857). It was David Bruce who made the link between the tsetse fly and the parasitic agent in the blood of animals (Bruce, 1895) later called *Trypanosoma brucei* (Plimmer and Bradford, 1899). In the beginning of the 20th century, trypanosome parasites were identified in human blood and cerebrospinal fluid of patients suffering from sleeping sickness and the pathogen could be linked to this disease. The cyclical transmission of trypanosomes from fly to mammal and back was described later by Friedrich Kleine (Kleine, 1909).

Today, Human African Trypanosomiasis (HAT) or sleeping sickness is considered as a neglected tropical disease with more than 60 million people at risk in Central and Sub-Saharan Africa. It has re-emerged in the late eighties, but due to stronger control and surveillance efforts, the annual number of newly reported cases fell under 10,000 for the first time in 50 years (WHO, 2010). However, this number is considered to be underestimated (Brun et al., 2009) as infection events occur mostly in remote rural areas that do not benefit from the WHO surveillance and where infection rates can reach up to 14% of the population (Chappuis et al., 2010). If left untreated, the disease is fatal. Five drugs are currently used to treat HAT in various combinations: pentamidine, suramin, melarsoprol, eflornithine and nifurtimox, but all show a certain level of side-effects and toxicity (melarsoprol contains derivatives of arsenic) (Schlitzer, 2009). Although these drugs were developed in the beginning of the last century and although evidence of resistances has accumulated, new drugs are still out of reach (Barrett, 2010).

African trypanosomes are transmitted by the bite of a tsetse fly of both genders that are exclusively blood-feeding. Several trypanosome species and subspecies can cause fatal disease in various animal species, for instance *T. brucei brucei*, *T. congolense* and *T. vivax* that are all able to infect livestock as well as dogs, horses and camels. Therefore, trypanosomes have a severe impact directly on public health by causing disease, but also lead to high socio-economic losses that influence the well-being of the African populations.

When a human gets infected with trypanosomes after the bite of an infected tsetse fly, the parasites develop in the blood, lymph and tissues and provoke non-specific symptoms such as headache, fever, joint pain and weakness. The second phase of the disease is initiated when the parasites cross the blood-brain barrier and develop in the brain and central nervous system. This leads to muscular failure, uncontrolled sleep-wake phases, coma and finally

death. Two trypanosome subspecies can survive in the human blood: *T. brucei rhodesiense* and *T. brucei gambiense*. They cause different forms of infections, the first one leads to an acute disease, lasting from a few weeks to several months, while the second one provokes a chronic disease that can persist several years without major symptoms (Brun et al., 2009). Both subspecies are resistant against the human trypanolytic factor, a combination of apolipoprotein1 and haptoglobin-related protein that is able to destroy all other trypanosome subspecies (Pays et al., 2006; Thomson et al., 2009).

T. brucei is exclusively extracellular and hence has to cope with the immune defence system in the mammalian host. Their survival is ensured by a sophisticated system of antigenic variation (Cross, 1977). The parasite surface is densely covered by a coat made of $5x10^6$ copies of the same variant surface glycoprotein (VSG) that are linked to the cell membrane by a GPI-anchor (Field et al., 2009). At a given time, a population exposes only one type of VSG on the cell surface and proliferates until the host mounts a typical antibody response that clears these parasites. However, a small proportion of cells can switch to a distinct VSG, a phenomenon that occurs with a rate of 10^{-2} to 10^{-3} (Lythgoe et al., 2007). These parasites are not recognized by existing antibodies and proliferate until the host has produced a new response. This vicious circle can continue for a long time, as the parasite genome contains more than 1000 different genes encoding VSG (Berriman et al., 2005). Moreover, these genes are able to recombine between each other to generate an almost unlimited repertoire.

African trypanosomes are members of the kinetoplastid family that is characterized by the presence of concatenated DNA in the single mitochondrion, a structure called the kinetoplast (Fig 2.1). This family also includes other protozoa such as *Trypanosoma cruzi*, the infective agent responsible for American trypanosomiasis or Chagas disease (Rassi et al., 2010), and numerous *Leishmania* species responsible for visceral and cutaneous leishmaniases (Murray et al., 2005).

Trypanosomes are eukaryotic organisms and possess several typical organelles such as a nucleus surrounded by a nuclear membrane, a Golgi apparatus, an endoplasmic reticulum network, an exo- and endocytosis machinery consisting of endosomes and lysosomes, a single mitochondrion and a flagellum (Fig 2.1). They swim with the flagellum leading, defining the narrow anterior and the larger posterior ends (Fig 2.1). The shape of the cell is defined by a cytoskeleton made of a corset of regularly spaced sub-pellicular microtubules with the plus-ends at the posterior pole of the cell. This network is enveloped by the plasma membrane and is only interrupted where the flagellum exits the cell body. There, a specialized part of the plasma membrane defines the flagellar pocket, the only site where endo- and exocytosis can

take place (Field and Carrington, 2009). The kinetoplast is physically linked to the basal body of the flagellum that controls its segregation during the cell cycle (Robinson and Gull, 1991). A kinetoplast that is positioned posterior to the nucleus as in Fig 2.1 defines the cell as trypomastigote, while a kinetoplast in an anterior position is found in epimastigote stages. In both cases, the flagellum is attached to the cell body along its whole length with the exception of its distal tip. This adhesion is ensured by the flagellum attachment zone (FAZ) that follows the flagellum on the cell body side and consists of a filament and a set of four specialized microtubules (Kohl et al., 1999).

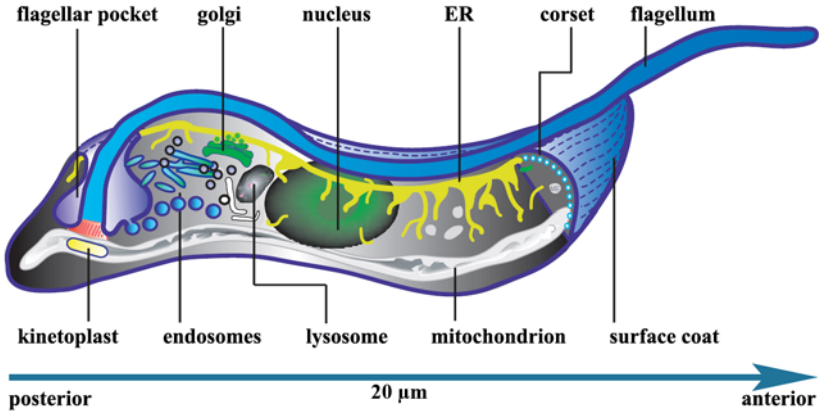

Figure 2.1: The trypanosome cell. Adapted and modified from (Overath and Engstler, 2004). Schematic model with the location of the major organelles and the anterior and posterior pole. The corset of microtubules, the flagellum and the surface coat are also represented. The swimming direction is indicated by an arrow.

Two trypanosome stages can be grown in culture: those originating from the mammalian blood (bloodstream form) and those issued from the midgut of the tsetse fly (procyclic form). They can reach high densities ($5x10^5$-$5x10^7$) and exhibit short doubling times (6 h for bloodstream and 8 h for procyclic forms). These two forms divide by binary fission (movie 1) after duplication of all organelles in a highly defined timeline. The first duplicating organelle is the basal body that leads to the formation of a new flagellum that is found in a more posterior position compared to the old one (Sherwin and Gull, 1989a) (Fig 2.2). Then, kinetoplast DNA replication begins shortly before nuclear S-phase (Woodward and Gull, 1990). It is completed faster and hence, kinetoplast segregation is visible well before nuclear mitosis. This results in a cell with 2 kinetoplasts and one nucleus (2K1N) (Fig 2.2, indicated by G2). Elongation of the microtubule corset takes place at the posterior part of the cell (Sherwin and Gull, 1989b) and leads to an increase in cell volume by more than 20% (Rotureau et al., 2011a). The tip of the new flagellum remains attached to the old one by the flagellar connector (Moreira-Leite et al., 2001). This particular configuration, coupled to the flagellum elongation leads to the re-localization of the new kinetoplast/basal-body complex in an increasingly posterior position as the whole cell elongates (Absalon et al., 2007). This

elongation is accompanied by the formation of a new FAZ that ensures adhesion of the new flagellum (Fig 2.2). Mitosis occurs without breakdown of the nuclear membrane, leading to a cell with two kinetoplasts and two nuclei 2K2N (Fig 2.2). When the new flagellum has reached a certain length, the anterior end of the new FAZ defines the position of the cleavage furrow (Kohl et al., 2003). Cleavage proceeds from the anterior to the posterior, in such a way that each daughter cell inherits one set of every individual organelle. During cytokinesis, the tip of the new flagellum detaches from the old one (Briggs et al., 2004) and two distinct cells become visible, only held together by thin remnants of membrane. Flagellum motility contributes to separation (Branche et al., 2006; Ralston et al., 2006), producing two daughter cells that can re-enter the cell division process.

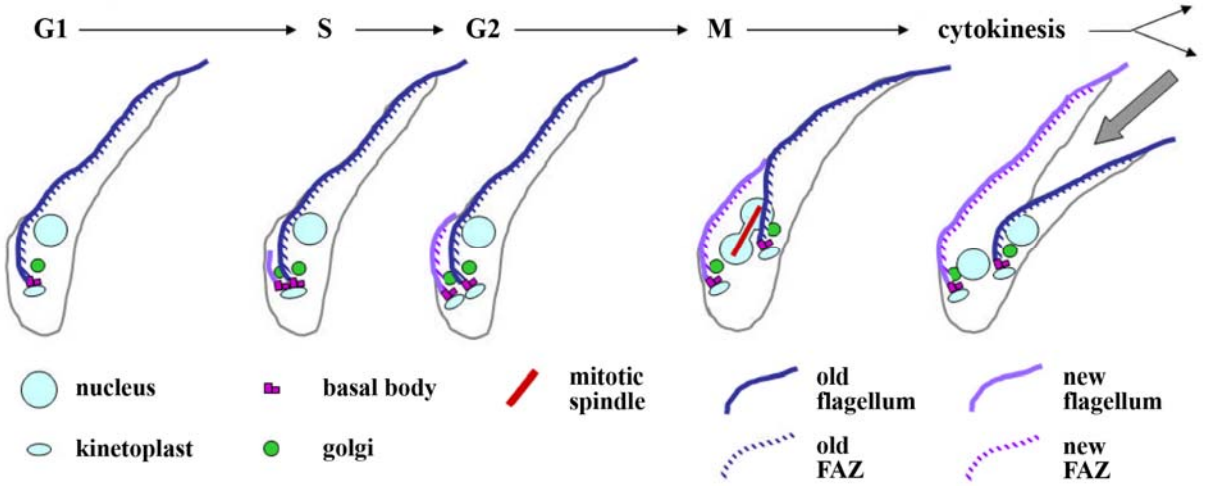

Figure 2.2: The trypanosome cell cycle. Adapted and modified from (Hammarton, 2007). The progression in the cell cycle is shown in phases G1, S, G2, mitosis (M) and cytokinesis. The organelles present in the cell at each phase are indicated: the kinetoplasts and nuclei (light blue), the basal bodies (pink), the Golgi (green), the old flagellum (dark blue) and the new flagellum (violet). The FAZ follow each flagellum on the cell body side (indicated as dashed lines in the same colour as the corresponding flagellum). The mitotic spindle in the dividing nucleus is represented as red line.

This type of cell division actually opens up the possibility to compare "new" and "old" organelles in the same cell, a feature that is highly interesting in fundamental research. Research on trypanosomes revealed important information on these parasites as disease causing agent but they also turned out to be important model organisms. Trypanosomes show several advantages: their genome is sequenced and is almost devoid of introns, a fact that facilitates reverse genetics such as RNAi that is a highly potent tool in these organisms (Balana-Fouce and Reguera, 2007; Berriman et al., 2005). Major discoveries such as the GPI anchor of surface proteins (Ferguson et al., 1985; Ferguson et al., 1988) and RNA editing in the mitochondrial DNA (Benne et al., 1986) were first described in *T. brucei*. Nevertheless,

trypanosomes diverged early in the eukaryotic lineage and developed unique biological features in comparison to other eukaryotes, sometimes being described as “freaky eukaryotes” (Talbert and Henikoff, 2009). The most divergent phenomena are found in transcription and RNA metabolism described in chapter 2.3.

2.2 The *Trypanosoma brucei* parasite cycle and its control mechanisms

Trypanosomes alternate between an insect and a mammalian host to complete their parasite cycle. This is achieved by numerous differentiation steps with drastic changes in cell morphology, metabolism and surface coating. Environmental sensing is likely to trigger these differentiation processes by activating distinct signalling cascades and gene expression programs (Parsons and Ruben, 2000). We are far from having a complete picture of these signals and control mechanisms but the genome sequencing project (Berriman et al., 2005) and new technical advantages such as reverse genetics should accelerate their identification. Knowledge of the differentiation processes of the parasite in the tsetse fly are limited to morphology and to some surface proteins (Sharma et al., 2009). This is mostly due to technical difficulties: culture and differentiation conditions have not been set up for these developmental stages and a limited number of cells that are difficult to obtain from fly infections, often complicated by mixed trypanosome stages and bacteria/fungi populations. So far, the best analyzed parasite stages are those that can be grown in culture, the slender bloodstream form and the proliferative procyclic form. As the transition between one form to the other can be reproduced *in vitro*, it is the best understood differentiation step of the trypanosome parasite cycle.

2.2.1 Differentiation from the bloodstream to the procyclic form

The population of bloodstream parasites is not uniform but consists of long slender forms and parasites with a stumpy shape (Vickerman, 1985) (Fig 2.3). This is observed in parasite strains that are termed “pleomorphic” but can be missing in bloodstream cell strains that have been kept in culture for a long time. These became monomorphic with only slender forms and loose infectivity. Stumpy formation is induced at a high parasite densities in the blood and is comparable to a quorum sensing mechanism involving a parasite derived factor: the stumpy inducing factor (SIF) (Hamm et al., 1990; Lythgoe et al., 2007; Reuner et al., 1997; Robertson, 1912; Vassella et al., 1997). The exact biochemical identification of SIF is still elusive, although several compounds have been proposed (Penketh et al., 1991; Scory et al.,

2007; Vassella et al., 1997). SIF would act as an external trigger that is transformed into an intracellular signalling cascade involving two described kinases: a zinc finger kinase and TbMAPK5, a member of the MAP kinase family (Domenicali Pfister et al., 2006; Vassella et al., 2001). SIF accumulation would lead to a specialized cell division from a proliferative long slender form to produce a stumpy form progeny (Tyler et al., 2001) (Fig 2.3). This differentiation process is characterized by cell cycle arrest in G0/G1, changes in cell shape to a stumpy form and the expansion of the mitochondrial network (Reuner et al., 1997; Vassella et al., 1997). When bloodstream parasites are ingested by the insect host during its bloodmeal, the slender forms die while the stumpy forms are able to differentiate into the procyclic forms (Robertson, 1913). The cell cycle arrest of the stumpy forms is supposed to be important for their synchronous differentiation to the procyclic stage that is characterized by several changes happening in a defined timeline (Fig 2.3). First, the GPI-anchored procyclin proteins start to coat the surface before the complete disappearance of VSG (Overath et al., 1983; Roditi et al., 1989). Second, the kinetoplast repositions from a terminal posterior position into a position midway between the posterior end and the nucleus by elongation of the posterior microtubule corset (Matthews et al., 1995). Third, the metabolism is adapted from a glucose-rich medium in the blood to an environment in which amino acids become the main nutritional source (Overath et al., 1986; Priest and Hajduk, 1994). Finally, the cells exit the cell cycle arrest and switch to a proliferative state (Matthews and Gull, 1994; Pays et al., 1993).

In vitro, the stumpy to procyclic differentiation is triggered by the combination of a drop in temperature from 37° C to 27° C and the addition of citrate and/or cis-aconitate to the medium (Brun and Schonenberger, 1981; Czichos et al., 1986; Engstler and Boshart, 2004) (Fig 2.3). These conditions mimic the parasite transfer from the mammalian to the insect host occurring during a bloodmeal *in vivo*. This transfer to the insect host subjects trypanosomes to a cold-shock that influences the thermo-regulated transporter protein PAD2 (proteins associated with differentiation) (Dean et al., 2009). The temperature-drop leads to higher protein expression and re-localization of PAD2 from the flagellar pocket membrane to the whole cell surface. This allows a higher citrate/cis-aconitate influx (Dean et al., 2009) that is available in µM concentrations in the fly midgut (Hunt et al., 1994). The temperature drop is also responsible for the expression and trafficking of the procyclin protein to the surface of stumpy cells, a phenomenon that did not occur in slender bloodstream forms, possibly explaining the survival of only the stumpy forms in the fly midgut (Engstler and Boshart, 2004). The procyclic surface coat was proposed to have a protective function against the immune attack of the

invertebrate host but this is controversial as trypanosomes deficient in procyclin proteins can, despite lower efficiency, fulfil the parasite cycle in laboratory infection experiments (Vassella et al., 2009).

The downstream effect of the citrate/cis-aconitate influx is the inhibition of the tyrosine phosphatase PTP1 (Szoor et al., 2010) (Fig 2.3). PTP1 normally prevents differentiation of the stumpy parasites in the mammalian bloodstream and specific inhibitors of this enzyme induce prompt differentiation to the procyclic form (Szoor et al., 2006). When PTP1 is active in stumpy parasites, it dephosphorylates its target PIP39 that is another phosphatase. When citrate/cis-aconitate molecules enter the cell in the tsetse host, the PTP1 activity is reduced and PIP39 in its phosphorylated state possibly initiates a signalling cascade that promotes stumpy to procyclic form differentiation (Szoor et al., 2010). In addition to PTP1 and PIP39, kinases might also be involved in these signalling pathways (Ellis et al., 2004; Garcia-Salcedo et al., 2002; Hammarton et al., 2003; Hua and Wang, 1994; Li and Wang, 2006; Muller et al., 2002; Rotureau et al., 2009).

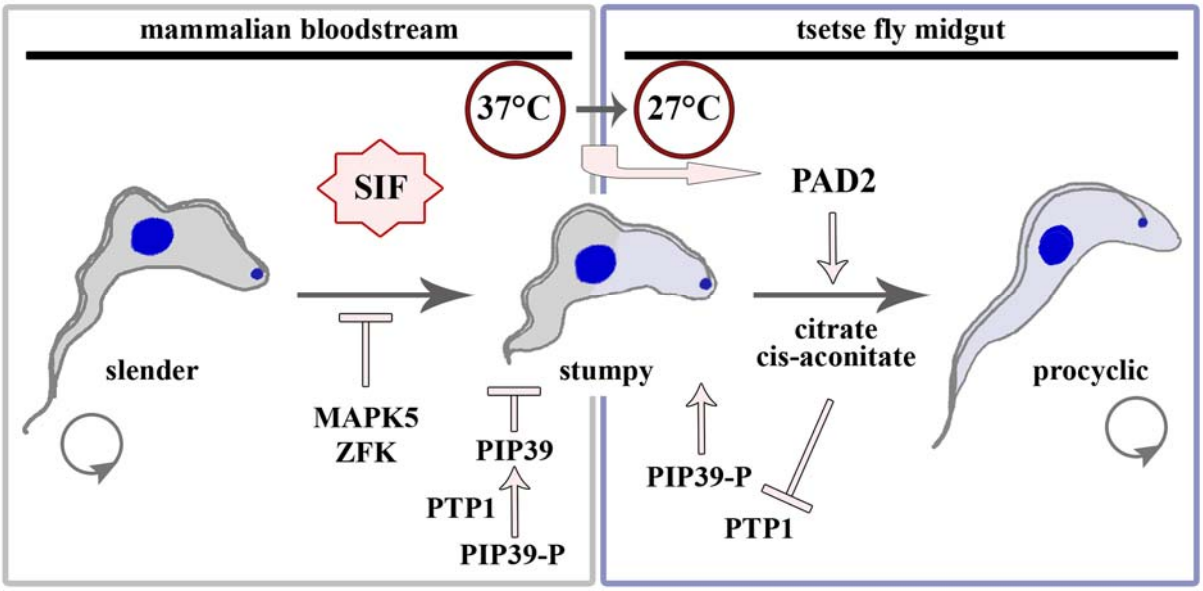

Figure 2.3: Differentiation from bloodstream to procyclic form. Slender bloodstream forms proliferate in the mammalian bloodstream and produce stumpy inducing factor (SIF); leading to stumpy cells that are arrested in G0. This differentiation is controlled by the kinases MAPK5 and ZFK. In the bloodstream, the stumpy to procyclic differentiation is inhibited by the phosphatase PIP39 that gets dephosphorylated by the PTP1 phosphatase. Slender and stumpy forms are coated by VSG (in dark grey). When stumpy parasites are transferred to the tsetse fly they are subjected to a temperature drop provoking the establishment of a procyclin coat (indicated in light blue) and to the re-localization of the carboxylate-transporter PAD2 to the whole surface. This allows the influx of citrate and cis-aconitate that leads to an inhibition of PTP1. PIP39 is thus available in a phosphorylated state and promotes differentiation to the procyclic form. These parasites re-enter the cell cycle and colonize the tsetse midgut. The posterior kinetoplast and the nucleus are shown in blue.

2.2.2 Development of *T. brucei* in the tsetse fly

The bloodstream parasites enter the tsetse fly when the fly takes its bloodmeal on an infected mammal. The meal is shortly stored in the crop before reaching the anterior midgut tract (Fig 2.4). At this step, trypanosome bloodstream trypomastigotes differentiate into the procyclic trypomastigote form. The infected bloodmeal can contain from hundreds to thousands of parasites, a population that is reduced by at least three orders of magnitude in the 3-5 days following ingestion (Oberle et al., 2010; Van Den Abbeele et al., 1999). This reduction in parasite number is not due to failure in trypanosome differentiation from stumpy to procyclic, as laboratory infections directly with procyclic parasites provoke a similar drop (Van Den Abbeele et al., 1999). Infection with trypanosomes stimulates the innate immunity of the tsetse fly and leads to the production of anti-pathogenic compounds in the midgut such as proteases and lectins (Aksoy et al., 2003). In principle, one trypanosome cell is sufficient to lead to fly infection (Maudlin and Welburn, 1989) but in natural conditions, the interplay between trypanosome populations and tsetse species is more complicated. Some tsetse fly species are more susceptible to infection and specific factors such as gender and age also come to play (Aksoy et al., 2003; Roditi and Lehane, 2008; Welburn and Maudlin, 1999). Procyclic parasites proliferate exponentially (shown in movie 1) and move further in the midgut together with the bloodmeal, in order to colonize the posterior midgut (Fig 2.4). This can lead to a parasite load of $5x10^5$ parasites per whole midgut (Van Den Abbeele et al., 1999).

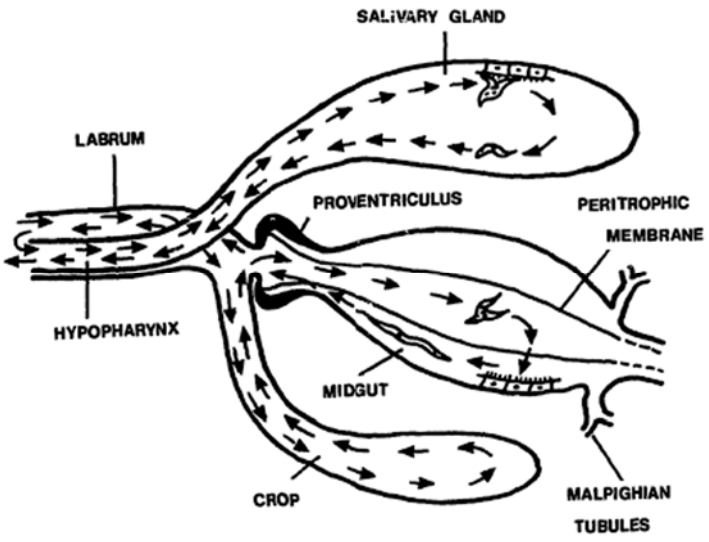

Figure 2.4: The route of trypanosomes in the tsetse fly organs. Adapted from (Vickerman et al., 1988). Trypanosomes enter the fly during its bloodmeal that is stored in the crop before reaching the midgut. There, procyclic trypanosomes proliferate. They can cross the peritrophic membrane and migrate towards the anterior region. The mesocyclic forms invade the proventriculus and differentiate into the epimastigote form. After an asymmetric division, the short epimastigote is supposed to be the precursor of the salivary gland epimastigote. The latter is a proliferative stage that is attached to the epithelium and colonizes the gland. An asymmetric division leads to the metacyclic form that is released in the saliva and gets expelled during the next bloodmeal.

After a successful infection, the procyclic parasites can cross the peritrophic membrane, a semi-permeable chitinous membrane that separates the meal from the midgut epithelium, and proliferate in the ectoperithrophic space, between the midgut epithelium and the peritrophic membrane (Robertson, 1913) (Fig 2.4). This penetration was shown to be direct through the midregion of the anterior midgut (Ellis and Evans, 1977; Evans and Ellis, 1975) and is accompanied by a change in the surface coat of the procyclic trypomastigote cells. Procyclic cells express procyclin surface proteins, glycoproteins that are characterized by internal glu-pro (EP) or gly-pro-glu-glu-thr (GPEET) repeats (Roditi and Clayton, 1999; Roditi et al., 1998). Early procyclics in the midgut predominantly express GPEET, but once found in the peritrophic space they replace GPEET by EP (Acosta-Serrano et al., 2001; Sharma et al., 2008; Vickerman et al., 1988). When the cells are in the peritrophic space, they gain in length and become thinner than in the midgut lumen (Rotureau et al., 2011a; Sharma et al., 2008) giving rise to cells of up to 60 µm length according to the strains (Vickerman, 1985). This developmental stage is named mesocyclic trypomastigote (Fig 2.5) and its long and thin aspect is presumably an adaptation to high cell densities and to facilitate swimming against the liquid flow and the peristaltic movement towards the proventriculus, a muscular part of the digestive tract between the foregut and the midgut. Mesocyclics are characterized by a cell cycle arrest in G2 in which the nucleus has undergone S-phase but has not proceeded to mitosis while the kinetoplast has not divided (Sharma et al., 2008; Van Den Abbeele et al., 1999), in sharp contrast to procyclic or bloodstream form proliferation in which kinetoplast segregation is always concomitant to nuclear S-phase. The mesocyclic form is a transient developmental stage that can re-transform to a proliferating stage when transferred to *in vitro* culture conditions optimal for procyclic cells (Van Den Abbeele et al., 1999). Mesocyclic forms possess an oval nucleus found in the centre of the cell that, once the cell has reached the proventriculus, elongates and relocates in a juxta-lateral position past the kinetoplast towards the posterior end of the cell (Sharma et al., 2008) (Fig 2.5). The resulting developmental stage adopts the epimastigote configuration where the nucleus is found in a more posterior position to the kinetoplast (Fig 2.5). At this stage, the two events of kinetoplast segregation and nuclear mitosis are initiated and lead to a dividing epimastigote form (Sharma et al., 2008; Van Den Abbeele et al., 1999). This division does not occur symmetrically, but leads to the production of a long and a short progeny both in the epimastigote configuration (Fig 2.5 and movie 2). In all these stages, the flagellum length follows the length of the cell body (Rotureau et al., 2011a). Asymmetrically dividing forms have already been reported in the early description of the parasite (Lewis and Langridge, 1947; Robertson, 1913), but the

mechanisms governing this asymmetric division are unknown (Rotureau et al., 2011a; Sharma et al., 2009). We have shown that this cell division is not accompanied by an increase in cell volume but consists in a rearrangement of the existing cytoskeleton corset which is in contrast to other dividing stages (Rotureau et al., 2011a). The long and short epimastigotes are the result of one cell cycle that was initiated from one procyclic trypomastigote, as no proliferating forms have been described in the proventriculus.

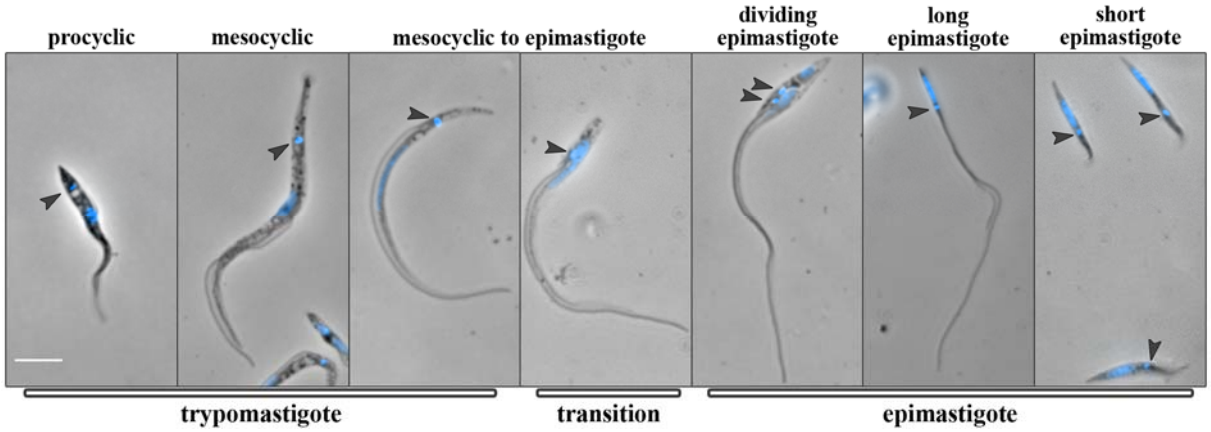

Figure 2.5: Development of trypanosomes in the tsetse fly midgut and proventriculus. The cells are shown in the order of appearance during the infection and adopt different morphotypes as shown by DNA staining with DAPI (in blue superposed on the phase contrast image). From procyclic to mesocyclic, the cells elongate and the kinetoplast is posterior to the nucleus, hence the cells show trypomastigote configuration. In the mesocyclic to epimastigote differentiation, the nucleus elongates and re-localizes past the kinetoplast in a more posterior position giving rise to an epimastigote cell. This will proceed to kinetoplast segregation and mitosis and will divide asymmetrically. The daughter cells are a long and a short epimastigote cell. The position of the kinetoplasts is indicated by arrowheads. The scale bar represents 5 µm.

These cell types are also present in the foregut, suggesting that they migrate towards the salivary glands (Lewis and Langridge, 1947; Sharma et al., 2008) (Fig 2.4). Among all trypanosomes, *T. brucei* is the only species that invades the salivary glands to fulfil its development in the fly. In contrast to dividing and long epimastigotes, the short form parasites are poor swimmers, so they are presumably brought to the salivary glands by their long sibling (movie 2). The long epimastigote is presumably dying (Sharma et al., 2008; Van Den Abbeele et al., 1999), while the short epimastigote is believed to be the progenitor of the epimastigote cell that is found tightly attached to the epithelium of the salivary glands via its flagellar membrane (Tetley and Vickerman, 1985; Vickerman, 1985) (Fig 2.6). This is a proliferative stage and is assumed to colonize the whole gland epithelium. The invasion of the salivary gland appears to be a narrow bottleneck in trypanosome development (Oberle et al., 2010) and a high proportion of flies infected in the midgut do not establish mature infections (Aksoy et al., 2003; Rotureau et al., 2011a; Van Den Abbeele et al., 1999). The production of

meiotic cells and thus sexual exchange, have been observed exclusively at this particular stage (Gibson et al., 2008; Peacock et al., 2011). Four developmental stages of trypanosomes in the salivary gland were initially described by Tetley and Vickerman in 1985: the attached epimastigote, the attached premetacyclic, the nascent metacyclic and the mature metacyclic that is free in the fly saliva (Tetley and Vickerman, 1985) (Fig 2.6).

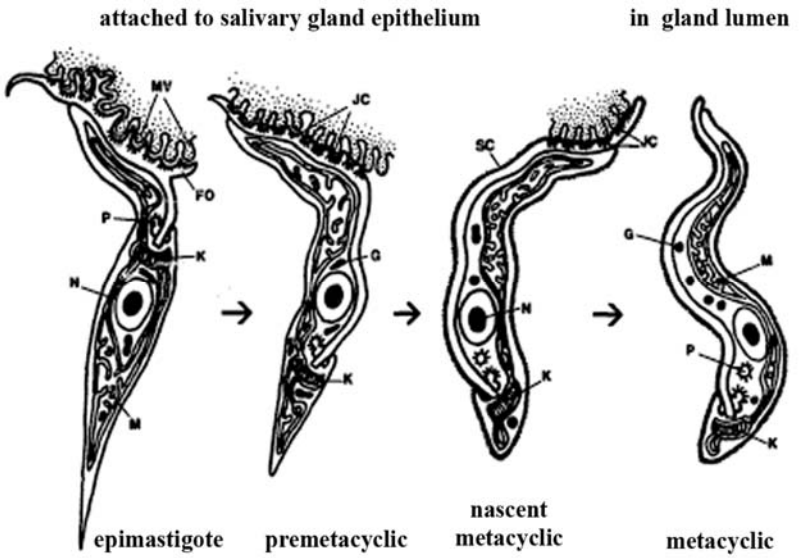

Figure 2.6: Trypanosome stages in the salivary gland of the tsetse fly. Modified from (Vickerman et al., 1988). The epimastigotes proliferate to colonize the salivary gland. In a specialized asymmetric division, they produce pre-metacyclic cells that adopt the trypomatigote configuration. Both are attached to the microvillar salivary gland epithelium (MV) via flagellar membrane outgrowths (FO) forming hemi - desmosome - like junctions (JC). Premetacyclics mature to the mammalian infective metacyclic stage by the acquisition of the VSG surface coat (SC), the rounding-up of the posterior pole and the re-localization of the kinetoplast (K) to the extreme posterior. The intermediary nascent metacyclic is only partially attached to the epithelium and the mature metacyclic is free in the saliva.

In the last decade, the surface proteins of the insect stages were shown to evolve during the parasite development. EP procyclin is present on the surface of dividing and long epimastigotes but is absent from the surface of the short daughter cells and the salivary gland epimastigotes (Sharma et al., 2008). The surface membrane spanning protein PSSA-2 is observed in all developmental forms in the midgut, proventriculus and salivary gland epimastigotes and is required by the parasite to establish efficient infection in the salivary gland (Fragoso et al., 2009). BARP (Brucei alanine rich protein) is a GPI-anchored protein, present on the surface of salivary gland epimastigotes, that will be substituted by the metacyclic VSG in the premetacyclic cell (Hajduk, 1984; Urwyler et al., 2007) (Fig 2.6). Recent data from the host laboratory revealed that attached epimastigotes divide asymmetrically to produce the premature metacyclic trypomastigote cell (Rotureau et al., 2011b) (Fig 2.6). This results in the production of two different daughter cells, one showing the epimastigote morphology like its mother and one adopting the trypomastigote

morphotype. This daughter is presumably the previously reported premetacyclic that develops into the mature metacyclic by progressively rounding-up its posterior pole, repositioning the kinetoplast to the extreme posterior, acquiring the VSG coat and detaching from the gland epithelium (Rotureau et al., 2011b; Tetley and Vickerman, 1985) (Fig 2.6). The full trypanosome development in the tsetse fly is completed in 20 to 30 days according to the strain and laboratory conditions (Aksoy et al., 2003; Sharma et al., 2009). Metacyclic parasites are expelled with the saliva when the fly takes its bloodmeal and their VSG surface coat enables them to survive the first defences of the mammalian host immune system. Inoculated metacyclics are thought to multiply in the skin for a few days and then reach the lymphatic system and the bloodstream of the mammal (Aksoy et al., 2003). They undergo differentiation to the long slender trypomastigote form.

Trypanosome development is likely governed by environmental triggers that are transduced to internal signalling cascades. These play a role in the regulation of gene expression programs to cope with the newly encountered surroundings.

2.3 Regulation of gene expression during trypanosome development

In most eukaryotes, individual gene expression is mainly controlled at the level of transcription initiation and can also be regulated at the level of mRNA elongation. The expression of the mature mRNA is also subjected to post-transcriptional control by different mechanisms.

In trypanosomatids, the "classical" mechanisms of gene expression are divergent and present a number of specific features (Daniels et al., 2010; Fernandez-Moya and Estevez, 2010; Martinez-Calvillo et al., 2010). The *T. brucei* genome has a size of 70 megabases and consists of eleven pairs of large chromosomes (with a size of 1.1 to 5.4 Mb), five intermediate size chromosomes (between 200-900 kb) and around 100 minichromosomes (30 to 150 kb) (Hertz-Fowler et al., 2007). In the large chromosomes, clusters of tens to hundreds protein-coding genes are transcribed by Pol II in a run-through fashion, generating polycistronic pre-mRNA (Johnson et al., 1987; Mottram et al., 1989). These polycistronic gene clusters are either divergent or convergent, and separated by strand switch regions (SSR). As Pol II transcription initiation seems to operate without apparent promoter sequences, it has been proposed that epigenetic signals at the SSR fulfil this function (Siegel et al., 2009; Wright et al., 2010). Histones with different post-translational modifications mark the divergent gene

clusters as sites of transcription initiation while convergent organization is linked to transcription termination. The transcribed pre-mRNA is processed into individual mature mRNAs by two coupled processes: trans-splicing and polyadenylation (Liang et al., 2003). Trans-splicing consists in the addition of a splice leader (SL) RNA, a short sequence of 39 nucleotides, to the 5' end of each mRNA that provides the mRNA cap. This SL is also transcribed by Pol II and contains the only identified Pol II promoter sequence in trypanosomes (Campbell et al., 2003). As the majority of trypanosome coding genes lack introns (Berriman et al., 2005), cis-splicing is not required and thus polyadenylation of the 3' end completes mRNA maturation.

When high amounts of transcripts are needed (for example for tubulin), the genes are found in multiple copies in the genome. An exception to this rule consists in recruiting Pol I for mRNA transcription from specialized Pol I promoter regions (Martinez-Calvillo et al., 2010). The highly abundant surface proteins VSGs and procyclins are translated from such Pol I derived transcripts (Rudenko et al., 1991; Zomerdijk et al., 1991). Pol I also transcribes the mRNAs of metacyclic VSG, which is the only example of monocistronic transcription for protein-coding genes and so far the only example of an exclusive control at the level of transcription initiation (Ginger et al., 2002; Graham et al., 1990; Graham et al., 1999).

As a consequence of polycistronic transcription, all mRNAs of one gene cluster are transcribed at the same rate but these genes do not code for functionally related proteins and are neither arranged according to developmental regulation (Archer et al., 2008; Hendriks and Matthews, 2007). Therefore, to ensure the timely correct expression of proteins during the development of the parasite, the abundance of specific mRNAs needs to be regulated at the post-transcriptional level by mRNA turn-over and translation efficiency. These processes are linked to specific cellular substructures: the processing (P-) bodies and stress granules. They are microscopically visible accumulations of mRNA and RNA-binding proteins (but not membrane-delimited) that are thought to play an important role in post-transcriptional control (Anderson and Kedersha, 2009). P-bodies are the site of mRNA degradation as they contain the decapping enzymes DCP1 and DCP2, the enhancer of decapping RNA-helicase DHH1 and the 5'-3' exoribonuclease XRN1. In trypanosomes, P-bodies are constitutively present in the cytoplasm and contain all major proteins described in other eukaryotic organisms (Cassola et al., 2007; Kramer et al., 2008). However, despite the presence of decapping activity in trypanosomes, the identification of genes encoding DCP homologs remained unsuccessful (Milone et al., 2002). Stress granule formation is induced by various changing environmental conditions, such as heat shock and nutritional starvation (Cassola et al., 2007; Kramer et al.,

2008). They share many proteins with P-bodies such as DHH1 and XRN1, but also contain poly(A) binding proteins, translation-initiation factors, small ribosomal subunits as well as several RNA-binding proteins (Anderson and Kedersha, 2009). Polysomes containing mRNAs that are about to be translated get stalled in stress conditions, dissociate and the mRNAs are relocated to stress granules (Kramer et al., 2008). It has been proposed that this accumulation sequesters the mRNA from translation until growth resumes upon better environmental conditions (Cassola et al., 2007). Since P-bodies and stress granules are exchanging material with each other, the storage and degradation functions could be intertwined (Kedersha et al., 2005; Wilczynska et al., 2005). Their interplay suggests that changing environmental conditions could influence the mRNA translation efficiency, which might be an important feature in the developmental biology of trypanosomes. This could be influenced by the RNA-binding proteins associated to the mRNA. During bloodstream to procyclic differentiation, microarray analysis initially revealed that 2% of the mRNA transcripts show different abundance between bloodstream and procyclic forms (Brems et al., 2005). More recent studies indicate that this was largely underestimated and revealed differential expression for up to 25% of the mRNA when the setting of the threshold was less stringent (Jensen et al., 2009; Kabani et al., 2009; Nilsson et al., 2010; Queiroz et al., 2009; Siegel et al., 2010).

As gene expression in trypanosomes is almost exclusively controlled at the post-transcriptional level, the abundance of mRNAs that are differentially expressed during development should be regulated by *trans*-acting RNA-binding proteins. The decisive regulatory information is often found in the 3'UTR (untranslated region) of the transcript (Clayton and Shapira, 2007; Haile and Papadopoulou, 2007). Prominent examples are the 3' UTRs of procyclins or that of the phosphoglycerate kinase B (PGKB) that contains AU-rich motifs, responsible for destabilization of the transcript in the bloodstream but not in the procyclic form (Furger et al., 1997; Quijada et al., 2002). The 3'UTRs contain structural or sequence elements that are recognized and bound by RNA-binding complexes. Trypanosomes encode a multitude of RNA binding proteins (RBP), many of them are distinct to those encoded in other eukaryotic species suggesting a specialized function (Berriman et al., 2005; De Gaudenzi et al., 2005; Kramer and Carrington, 2010). Binding of these proteins can either have a stabilizing effect on the mRNA target or inversely promote its degradation. Several examples have been shown to stabilize specific subsets of mRNA that are functionally related: *Tb*DRBD3 is found associated with transcripts encoding membrane proteins (Estevez, 2008;

Stern et al., 2009), while *Tb*PUF9 is found with transcripts that are co-regulated in the cell cycle (Archer et al., 2009).

Examples of such RBP have been identified to be important in bloodstream to procyclic differentiation. TbZFP1 (zinc finger protein) is enriched during this differentiation step and is necessary for the repositioning of the kinetoplast from a very posterior position in stumpy parasites to a more anterior position in procyclic parasites, while the related protein TbZFP2 is necessary at the bloodstream stage for efficient differentiation (Hendriks et al., 2001). Proteins with a zinc finger (CCCH motif) have been described to bind to 3' UTRs of transcripts, leading to their destabilization in other eukaryotes. Homologues in *T. cruzi* were shown to be involved in developmental gene expression by binding mRNA at regulatory elements (Paterou et al., 2006).

In a recent study, DHH1 was identified to play a role in regulating mRNA abundance during development (Kramer et al., 2010). The inducible expression of a mutant version of this protein, lacking the ATPase function due to a point mutation, was achieved from an exogenous locus in the procyclic form and the consequences on mRNA levels were analyzed by microarrays (Kramer et al., 2010). Indeed, expression of the DHH1 functional mutant led to the inversion of the abundance of mRNA levels in procyclic cells. A large set of transcripts normally abundant at this parasite stage were down-regulated, while several others only present in bloodstream parasites were up-regulated (Kramer et al., 2010). For example the *ISG75* transcript, encoding a plasma-membrane protein of unknown function, normally more abundant in bloodstream forms, was shown to be stabilized and accumulated during the induction time of the DHH1 mutant in procyclics. No effect was observed for constitutively expressed mRNA showing the selective function of DHH1 on developmentally regulated transcripts. However, while DHH1 revealed to be an important factor in adjusting the mRNA amounts in development, it did not affect all developmentally regulated RNA, suggesting the existence of a different control pathway independent of DHH1 (Kramer et al., 2010). Moreover, the effect of DHH1 could be influenced by the interaction with additional protein factors.

Procyclin expression is highly post-transcriptionally controlled by its 3' UTR. The *GPEET* 3' UTR contains a glycerol responsive element and its expression can also be regulated by the activity of mitochondrial enzymes (Vassella et al., 2000; Vassella et al., 2004). EP procyclins are present in three gene copies (*EP1-3*) that can be distinguished by different sequences in their 3' UTR (Konig et al., 1989). Each contains three regulatory loops: the first one acts as a positive regulator, the second one contains a 26-mer motif that leads to destabilization of the

transcript in bloodstream form parasites, while the 16-mer distal stem loop in the same UTR promotes translation in procyclics (Hehl et al., 1994; Hotz et al., 1997). Interestingly, a third zinc finger protein called TbZFP3 is able to bind to the 3' UTR of *GPEET* and *EP1*, but not *EP2* and *EP3* (Walrad et al., 2009). The interaction with the *EP1* 3' UTR was demonstrated to be mediated by its loops II and III. Ectopic over-expression or down-regulation of ZFP3 did not lead to altered levels of procyclin mRNAs, but strikingly, the investigation of protein amounts revealed an increase in EP1 levels and a decrease of GPEET abundance (Walrad et al., 2009). ZFP3 is constitutively expressed in bloodstream and procyclic forms, but it interacts only in procyclics directly with the translational machinery (Paterou et al., 2006). This interaction could lead to an increased translation of *EP1* mRNA while *GPEET* transcripts are translationally repressed, possibly explaining the molecular switch between GPEET to EP in procyclic parasites. It also indicates how an RNA-binding protein can control the fate of its mRNA target in different parasite developmental stages.
The transcript of *BARP* is also controlled by its 3'UTR (Urwyler et al., 2007). A reporter protein under the control of the *BARP* 3'UTR is exclusively expressed at the salivary gland epimastigote stage, a regulation that could be mediated by RNA-binding proteins. Interestingly, *BARP* mRNA levels also increased in procyclic cells expressing a mutant version of the DHH1 protein (Kramer et al., 2010).

The RNA-controlling proteins recently discovered are likely to be just a small piece in the puzzle of the stage specific regulation of protein expression by multiple RBP of the same transcript or group of transcripts. One can imagine competition events between different RBP complexes for the same RNA, allowing fine tuning of a very complex regulatory system (Fernandez-Moya and Estevez, 2010).

2.4 ALBA as RNA-binding protein candidates in parasite development

In the search for potential trypanosomal RNA-binding proteins, we focussed on the Alba protein family as potential candidates that could contribute to developmental control or switches.
Alba proteins were first identified in a screen for archaeal DNA-binding proteins in the eighties (Lurz et al., 1986). Since then, Alba proteins have been studied in a multitude of Archaeabacteria where they were found in most of the sequenced genomes (Forterre et al., 1999). These proteins were initially named according to the species of origin and to their

molecular mass of 10 kDa: Sso10b from *Sulfolobus solfataricus*, Ssh10b from *Sulfolobus shibatae*, etc. (Forterre et al., 1999). It was in 2002 that the nomenclature was unified defining the Alba proteins, for "acetylation lowers binding affinity" (Bell et al., 2002) (see below). Alba proteins were grouped into one family by Aravind and colleagues, with members that are largely distributed in organisms of the Archaebacteria and Eukaryota superkingdoms (Aravind et al., 2003).

Alba structure and function in Archaea

Alba protein structure was analyzed by crystallography in a variety of archaeal species (Chou et al., 2003; Hada et al., 2008; Wang et al., 2003; Wardleworth et al., 2002; Zhao et al., 2003). They all revealed a high conservation of the Alba domain (Pfam PF01918), a mix of two α-helices and four β-strands showing (β1 α1 β2 α2 β3 β4) topology (Fig 2.7A). This fold is reminiscent of the RNA-binding structure in the C-terminus of the translation initiation factor IF3 and of the N-terminal DNA binding domain of DNase I (Biou et al., 1995; Lahm and Suck, 1991; Wardleworth et al., 2002).

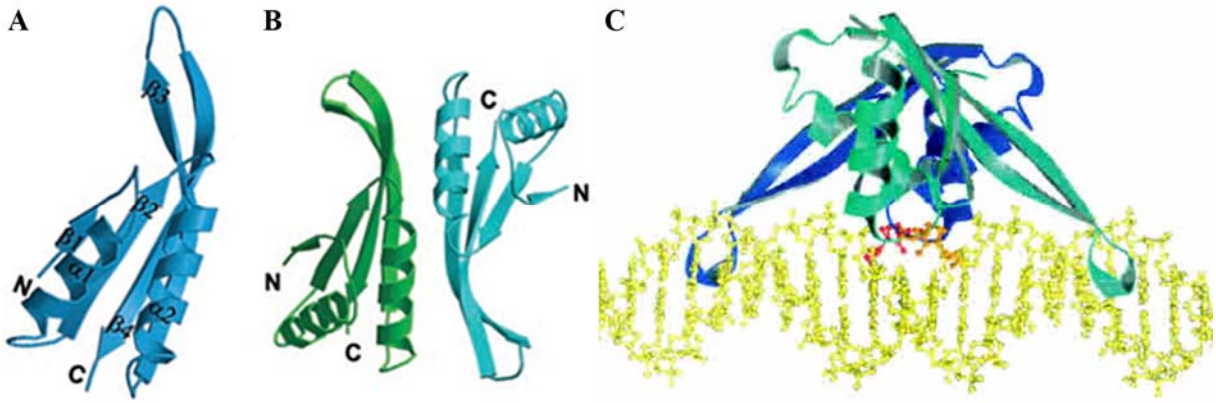

Figure 2.7: Alba structure and DNA-binding model. (A,B) adapted from (Zhao et al., 2003). Crystal structure of (A) an Alba monomer and (B) dimer. The N- and C-terminal ends are indicated as well as the α-helices and β-sheets. (C) adapted from (Wang et al., 2003). Model of the binding of Alba dimers (blue, green) to a DNA-helix (yellow) in a side view.

Alba proteins are present in high quantities in most archaeal cells and were first described as DNA-binding proteins (Lurz et al., 1986). Two Alba monomers of 10 kDa are forming dimers for DNA binding to the DNA helix (Fig 2.7) (Chou et al., 2003; Wardleworth et al., 2002; Xue et al., 2000). The dimerisation occurs via the second α-helix (α2) and the two C-terminal β-strands (β3 and β4) (Chou et al., 2003; Wardleworth et al., 2002). By different techniques, it was possible to show that one Alba dimer spans between 5-10 bp of plasmid DNA (Wardleworth et al., 2002). Crystallography and NMR studies show that Alba proteins adopt a

dimer-dimer stacking to form a linear rod-like structure around the DNA helix (Wang et al., 2003; Wardleworth et al., 2002; Zhao et al., 2003) (Fig 2.7C).

Histone proteins are found in some Archaea species to form nucleosomes, but their abundance may not be sufficient to fulfil a similar role in DNA compaction as in eukaryotes (Sandman and Reeve, 2000). It was suggested that Alba proteins are acting as histones in Archaebacteria as they are binding dsDNA without sequence specificity (Bell et al., 2002; Xue et al., 2000). More recently, Alba proteins were found associated to specific DNA sequence motifs (Liu et al., 2009). In studies using electron microscopy, the analysis of Alba proteins together with DNA made clear that Alba forms DNA-protein complexes in a cooperative manner by enveloping DNA without compacting it or inducing supercoiling (Lurz et al., 1986). However, supercoiling of DNA by Alba was shown to be induced at higher temperatures, corresponding to the natural environment of hyperphilic Archaea (Xue et al., 2000). In Archaea that possess two different Alba proteins, such as *Sulfolobus*, heterodimerisation of Alba1 and Alba2 can result in a highly compacted protein-DNA interaction (Jelinska et al., 2005). Most studies investigating the nucleic acid binding abilities of Alba in Archaea were conducted using recombinant protein together with DNA or RNA and showed similar binding affinity to double-stranded DNA, single-stranded DNA or RNA (Guo et al., 2003). However, in UV cross-linking experiments, performed on crude cell extracts to freeze protein-nucleic acid interaction, Alba proteins revealed to be only bound to RNA, for instance mRNA and rRNA, and thus to ribosomes, suggesting their role in stabilizing RNA in extreme environments (Guo et al., 2003). The fact that DNA is a true *in vivo* binding target of Alba was provided by Marsh and colleagues, who demonstrated that archaeal Alba proteins bind DNA and RNA *in vivo* (Marsh et al., 2005).

Aravind and colleagues suggested that Alba were initially RNA-binding proteins in the common ancestor, before Archaea and eukaryotes separated in the evolution, only being recruited as DNA-binding protein in some Archaeal species (Aravind et al., 2003). They hypothesize that Alba still retained RNA-binding capacities in some archaeal species where they fulfil an additional role to DNA binding. They propose that Alba proteins are derived within the IF3 fold (translation initiation factor) that has RNA binding capacities and is the closest to the CRM domain found in proteins of bacteria (YhbY proteins), archaea and plants that are involved in several processes of RNA metabolism (Fig 2.8A) (Ostheimer et al., 2002).

Acetylation and deacetylation

The name Alba stands for “acetylation lowers binding affinity” and was first proposed by Bell and colleagues (Bell et al., 2002). This name reflects the discovery that Alba proteins have an

important lysine residue (Lys-16 in the *Sulfolobus* Alba protein) that can be acetylated and thereby influence the binding efficiency of Alba to DNA. Native Alba in its acetylated state is not able to prevent transcription in an *in vitro* transcription assay, whereas recombinant protein, that has no posttranslational modifications, shows significant transcriptional repression (Bell et al., 2002). In Archaebacteria, Alba interacts directly with the Sir2 (silent information regulator, sirtuin) protein, leading to the deacetylation of the Alba residues (Bell et al., 2002). This process is dependent on the Sir2 cofactor NAD but independent of DNA (Bell et al., 2002). In contrast, acetylation of lysins is performed by the Pat acetyltransferase that lowers the affinity of Alba to DNA (Marsh et al., 2005). With this acetylation control system, it is possible for Archaebacteria to tune transcription directly through DNA coating by Alba proteins. This situation can be compared with eukaryotic histones that are subjected to multiple posttranscriptional modifications, such as acetylation, methylation, phosporylation and ubiquitination to control gene regulation, DNA replication and repair (Iizuka and Smith, 2003; Strahl and Allis, 2000). Acetylation renders chromatin more accessible for transcription while hypo-acetylated histones efficiently compact DNA leading to transcriptional repression (Wu and Grunstein, 2000).
This acetylation system might also play a role for Alba as RNA binding protein, as acetylated Alba proteins show a 2-fold reduced affinity for RNA (Marsh et al., 2005).

Alba in Eukaryotes

Sequence profile searches, using archaeal Alba proteins as baits, revealed that they share significant homology with some eukaryotic proteins (Aravind et al., 2003). Alba homologs were found in numerous organisms such as kinetoplastids, apicomplexans, plants and animals. The search for homologs detected MDP2 (macronuclear development protein) present in the ciliate *Stylonychia* (Fetzer et al., 2002) and the proteins Pop7/Rpp20 and Rpp25, key subunits of the RNase P/RNase MRP endoribonucleases that are involved in tRNA and rRNA processing respectively (Chamberlain et al., 1998; Guerrier-Takada et al., 2002; Stolc et al., 1998). The construction of a phylogenetic tree with all Alba proteins found in the sequence profile searches, split the superfamily into three groups (Fig 2.8B) (Aravind et al., 2003). One encompassed all archaeal Alba while the two others branched the eukaryotic members into one group with the Pop7/Rpp20 like proteins and the other containing the Rpp25/MDP2 proteins. In the latter, many uncharacterized proteins are found that share C-terminal extensions, downstream of the Alba domain, with a characteristic GYQXP signature and often a stretch of RGG repeats that are frequently associated with RNA binding (Godin and Varani, 2007).

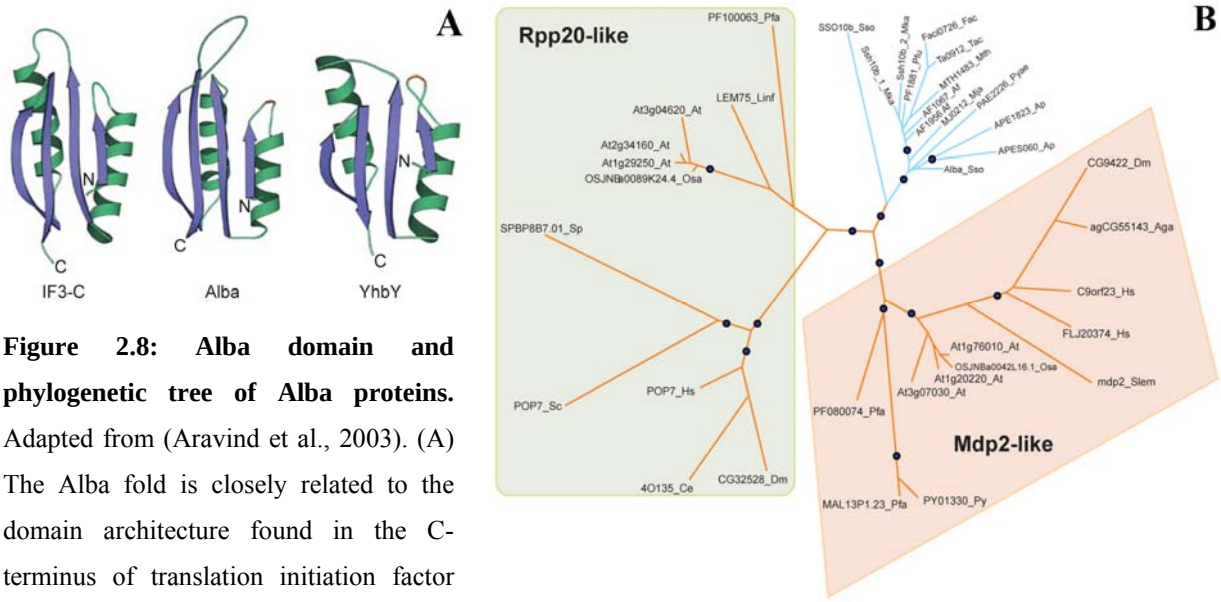

Figure 2.8: Alba domain and phylogenetic tree of Alba proteins. Adapted from (Aravind et al., 2003). (A) The Alba fold is closely related to the domain architecture found in the C-terminus of translation initiation factor IF3 (left) and to the CRM domain (YhbY on the right), both involved in mRNA metabolism. (B) Phylogenetic tree of Alba proteins in Archaea and Eukaryota. Members of the Archaea group together (blue lines) while the eukaryotic Alba proteins (orange lines) separate into two groups: the Rpp20-like (grey shading) and the MDP2-like (pink shading).

MDP2

In ciliates, two distinct nuclei are present: the macronucleus (containing multiple copies of housekeeping genes) ensuring the production of RNA needed for vegetative growth and the micronucleus that is diploid, transcriptionally silent and serves as a germline nucleus (Ammermann et al., 1974). After a meiotic cycle and sexual reproduction involving the exchange of haploid micronuclei, the old macronucleus degenerates. The haploid micronuclei fuse and the newly formed diploid micronucleus undergoes mitosis to produce a micronucleus and a macronucleus. The maturation of the latter is characterized by massive DNA rearrangements: deletion of almost 90% of sequences, amplification, fragmentation, and splicing of DNA sequences such as transposable elements (Prescott, 1994). These processes were shown to be partially RNA-mediated, possibly by using RNA sequences to match on the old nucleus as proofreading system (Jonsson et al., 1999). Some proteins are exclusively expressed at this stage of development (Fetzer et al., 2002). This is the case of a protein termed MDP1 (macronuclear development protein) that contains a Piwi and a PAZ domain (Fetzer et al., 2002; Meyer and Garnier, 2002), typical of Argonaute (AGO) and PIWI proteins. These proteins are binding to small RNA and some have been shown to possess slicer (RNA cleaving) activity. Exclusively during macronuclear development, ciliates express an Alba protein member named MDP2, predicted to localize to the nucleus (Fetzer et al., 2002). MDP2 and MDP1 could coordinate this developmental step of macronucleus

development jointly by their RNA binding properties, but further characterization of ciliate MDP2 is still pending.

Rpp20 and Rpp25

The endoribonuclease RNase P occurs in all three domains of life and contains an RNA molecule in combination with either one (in bacteria) or multiple protein subunits (in Archaea and Eukaryotes). The related RNase MRP (mitochondrial RNA processing) is only found in eukaryotes (Zhu et al., 2006). RNase P and RNase MRP share most of their protein composition, with Rpp20 and Rpp25 Alba proteins as key subunits in both complexes (Walker and Engelke, 2006). In eukaryotes RNase P is localized in the nucleus, where it is involved in the processing of pre-tRNA (Gopalan et al., 2002; Jarrous, 2002). RNase MRP localizes to the nucleus and also to mitochondria and is involved in the processing of ribosomal RNA and mitochondrial replication (Chang and Clayton, 1987; Schmitt and Clayton, 1993). RNase MRP also participates in cell-cycle regulation by controlling the degradation of specific cell-cycle mRNA (Gill et al., 2004). Recent data suggest that this degradation process takes place in a single cytoplasmic focus, presumably a P-body, and leads to a cell-cycle dependent re-localization of the RNase MRP complex from the nucleus to the cytoplasm in early mitosis (Gill et al., 2006).

Both Rpp20 and Rpp25 proteins interact with the RNA moiety in RNase MRP (Pluk et al., 1999; Yuan et al., 1991). This RNA is very important for protein-RNA interaction and accumulation of the complex in the nucleolus (Jacobson et al., 1995). Rpp25 binds not only to the RNA but also to the other protein subunits of the macromolecular complex (Welting et al., 2004). Rpp20 and Rpp25 form highly stable heterodimers and their expression is co-dependent as shown by RNAi studies (Welting et al., 2007). Dimerisation of Rpp20/Rpp25 is mediated by the core Alba domain which is also the only determinant necessary for interaction with the RNA unit of the RNase (Hands-Taylor et al., 2010). However, the Rpp20/Rpp25 heterodimer is not as stably linked to the RNase MRP complex as the other protein subunits and possibly dissociates from the complex before RNA processing (Welting et al., 2007). The exact function of the Rpp20/25 dimer for RNase function remains to be determined. In Archaea, Alba proteins are not a part of the RNase P complex that consists of an RNA molecule and four protein subunits (Ellis et al., 2007).

Alba proteins are RNA-binding proteins in Eukaryotes and are, at least in Ciliates, exclusively expressed in particular developmental stages, suggesting specific functions. As DNA-binding proteins, Alba are able to suppress transcription, so their role as RNA-binding proteins could

be the control of translation. These properties place Alba in a good position to be RNA-binding proteins in trypanosomes where they would act in developmental control of gene expression.

2.5 How to sense the environment: the flagellum hypothesis

Sensing the environment is a key element in the life of all organisms. In trypanosomes changing environments are believed to initiate developmental switches that allow the parasite to survive in different hosts and their tissues.

Sensory function is achieved by variable means according to the cell type. In the recent past, cilia and flagella have emerged as prominent sensory organelles of many eukaryotic organisms (Singla and Reiter, 2006). The terms cilia and flagella are interchangeably used for a defined organelle that is build from a specialized centriole, the basal body. There, tubulin nucleates to form the main structure called the axoneme that is composed of nine doublets of microtubules and can contain an additional central pair. The ciliary compartment is separated from the cell body by transition fibres that restrict transport to and from the cilia (Garcia-Gonzalo et al., 2011). The ciliary structure is assembled at its distal tip and, as protein synthesis does not occur in cilia, all structural components need to be actively transported from the cell body by the intraflagellar transport machinery (IFT) to the site of assembly. IFT consists of kinesin and dynein motors that ensure the anterograde and retrograde transport respectively, together with IFT protein complexes that transport ciliary components to the tip and back to the basal body for recycling or degradation. This IFT movement is likely to be crucial in the transport of signalling molecules (Singla and Reiter, 2006).

In mammals the possibility to see and smell are coupled to sensory cilia: the photoreceptors and the olfactory sensory neuron respectively. These possess specialized cilia that concentrate sensory receptors whose activation triggers the production of second messengers such as cyclic nucleotides (Boekhoff et al., 1990; Elias et al., 2004; Strissel et al., 2005). When IFT is blocked in photoreceptors, the maintenance of the specialized cilium is affected, leading to progressive degeneration, apoptosis and blindness (Marszalek et al., 2000). Sensing the environment via cilia is well understood in two model organisms, *Drosophila* and *Caenorhabditis elegans* (Vincensini et al., 2011). In *Drosophila*, sensory neurons function in its antenna as audition system to react to sound vibrations (Gong et al., 2004). Ciliary sensory neurons in *C. elegans* are located at the nose and allow perception of changes in osmolarity and mechanical nose touch (Tobin et al., 2002). In vertebrates, almost every mammalian cell

possesses an immotile primary cilium. It is assembled at the G0 phase of the cell cycle and is made of nine doublets of microtubules whose length is variable from one cell type to the other. This cilium is able to sense a large variety of extracellular stimuli that are transduced to intracellular signalling pathways important in cell development (Singla and Reiter, 2006). In mammalian cells, defects in IFT components have direct implication on the hedgehog and Wnt signalling pathways whose members are concentrated in the primary cilium (Huangfu et al., 2003). Sensing in mammals was thought to occur in immotile cilia only, a hypothesis recently broken by a study of motile cilia in lung tissues that are able to sense toxic compounds via taste receptors and react by enhanced ciliary beating for mucus evacuation (Shah et al., 2009).

In Protozoa, motile flagella unify the function of propelling the cell in a directional movement and simultaneously sense their environment (Vincensini et al., 2011). In the ciliate *Paramecium*, cilia are able to detect obstacles and modulate the beating pattern to redirect swimming accordingly (Eckert et al., 1972). In the green algae *Chlamydomonas*, the flagellum is not only equipped with proteins involved in photoreception (Huang et al., 2004) but is also critical for gamete fusion and sexual reproduction. Indeed, gametes attach via their flagella and the IFT machinery is necessary for cell signalling processes that initiate cell fusion (Pan and Snell, 2003; Wang et al., 2006).

Several clues indicate that the flagellum could function as a sensory organelle in *T. brucei*. During the whole parasite cycle, the trypanosome swims will the flagellum leading, so that its tip is the first part of the cell to be in contact with a new environment. In addition, trypanosomes attach to the salivary gland epithelium of the fly via their flagellum membrane that grows and acquires some electron-dense structures proposed to mediate adhesion (Tetley and Vickerman, 1985) (Fig 2.6). The axoneme is highly conserved in structure and protein composition, as well as its IFT machinery (Fig 2.9A). But trypanosome flagella possess an additional distinct structure called the paraflagellar rod (PFR) that is physically linked to the flagellum attachment zone (FAZ) by cross-links through the membranes of flagellum and cell body (Fig 2.9A). Flagellum attachment could ensure a rapid interaction with the cell body. Although the flagellar membrane is in continuity with the plasma membrane, it contains a unique composition of proteins. Many proteins predicted to be involved in signalling processes are targeted to, and enriched in the flagellar membrane. Examples are the calcium-binding proteins named calflagins (Godsel and Engman, 1999) and ESAG4, possibly involved in sensing by cAMP regulation (Paindavoine et al., 1992). The membrane of the trypanosome flagellum is enriched in lipid rafts that were proposed to serve as platform for signalling

events (Tyler et al., 2009). Several enzymes (two adenylate kinases and the R-subunit of the polo-like kinase A (PKA)) and a calcium binding protein of the calmodulin family, have been found to localize to the PFR, suggestion that the PFR could act as a structural matrix (Oberholzer et al., 2011; Pullen et al., 2004; Ridgley et al., 2000).

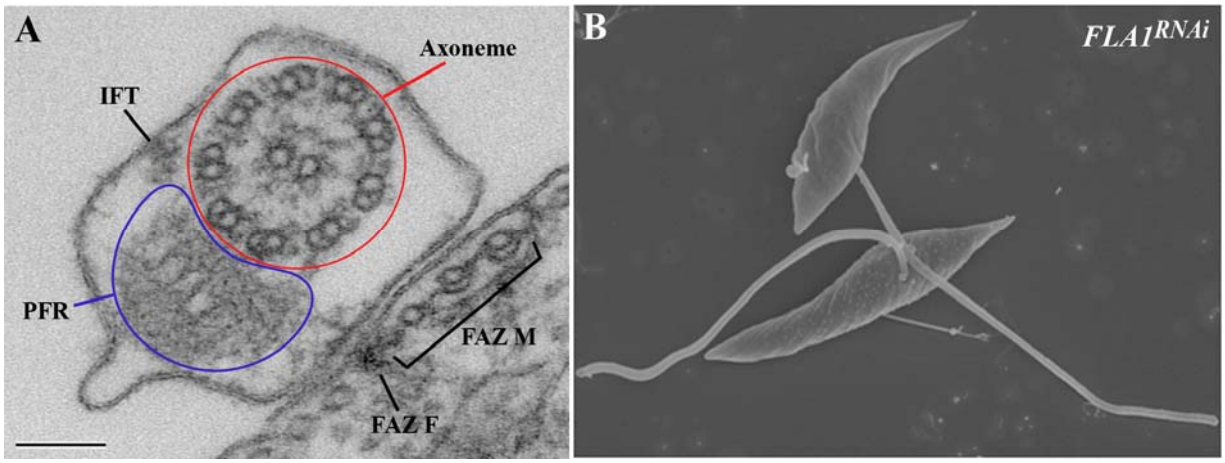

Figure 2.9: The structure of the trypanosome flagellum and the *FLA1*^{RNAi} cell line. (A) Transmission electron microscopy of a cross section through a trypanosome flagellum (kind gift of Johanna Buisson). The flagellum consists in an axoneme with 9 doublets of microtubules and a central pair (in red). The PFR lattice is indicated in blue. The electron dense structure between PFR and axoneme is presumably an IFT particle. The flagellum is attached to the cell body by the FAZ structure composed of four microtubules (FAZ M) and the FAZ filament (FAZ F) that is physically linked to the PFR. Scale bar represents 100 nm. (B) Scanning electron microscopy of *FLA1*^{RNAi} cells that detach flagella when knock-down of the protein FLA1 is induced by RNAi (kind gift of Thierry Blisnick).

However, signalling protein candidates are scarce and the flagellar proteomes were carried out from preparations purified with detergent and high salt treatment, eliminating all the flagellar membrane and matrix components (Broadhead et al., 2006; Portman et al., 2009).

Recently, a protocol was set up in the host laboratory to purify intact flagella from trypanosomes (Julkowska et al., manuscript in preparation). This was achieved from the mutant *FLA1*^{RNAI} cell line that displays detached flagella when the FLA1 protein is down-regulated by inducible RNA interference (LaCount et al., 2002) (Fig 2.9B). FLA1 (flagellum adhesion glycoprotein 1) is anchored to the cell membrane via a C-terminal transmembrane domain interacting with the FAZ filament, while its extracellular N-terminus binds to an unknown partner presumably linked to the PFR to confer flagellum attachment (Rotureau unpublished). Flagella from induced *FLA1*^{RNAI} procyclic cells were separated from the cell body by mechanical forces (vortex) and purified by differential centrifugation in detergent-free buffer (Julkowska et al., manuscript in preparation). The purity of the obtained flagellar fraction was confirmed by scanning and transmission electron microscopy (Fig 2.10). Few

contaminants were detected and 80% of the flagella were intact, displaying a membrane surrounding axoneme and PFR structures. The detachment has been shown to occur at the level of the basal body, excluding the kinetoplast (Fig 2.10C-E).

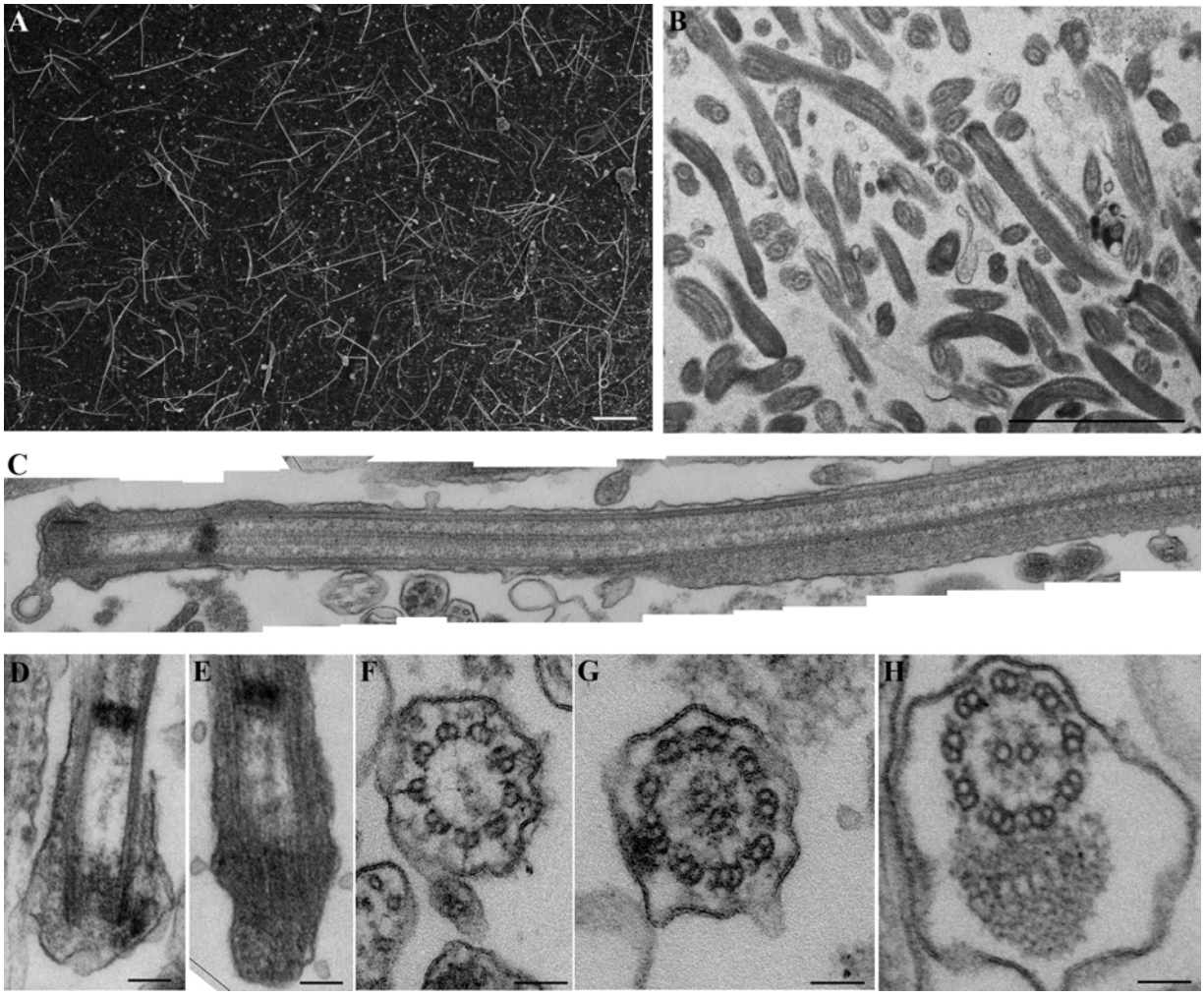

Figure 2.10: Purified flagella are intact and contain all typical structural elements. (A,B) low magnification of flagella preparations analyzed by scanning (A) and transmission (B) electron microscopy. More than 80 % of the flagella still possess their membrane. (C) longitudinal section through the base of a purified flagellum reveals all the typical elements of the organelle (from left to right): the basal body, the transition zone, the axoneme as it would be within the flagellar pocket and the axoneme associated to the PFR. (D-E) sections through the base of the flagellum showing that the organelle is severed from the kinetoplast and that the membrane seals at this area. (F-H) sections through different portions of the purified flagella showing the typical organisation of the transition zone (F), the axoneme (G,H) and the PFR (H). (Julkowska et al., manuscript in preparation)

Immunofluorescence analysis (IFA) confirmed the presence of soluble proteins in the flagellum matrix, such as IFT. Western blot analysis showed the enrichment of flagellar proteins in the flagella versus whole cell protein samples, when comparable protein amounts were loaded (Fig 2.11). The markers for structural proteins of the PFR (PFR2) and the axoneme (mAb25) where enriched as well as membrane and matrix proteins: the calflagins

(three different proteins) as representatives for flagellar membrane proteins, and the IFT proteins IFT172 and Rab-like RABL5 (Adhiambo et al., 2009) for the matrix pool. The ER marker BiP was used to show the level of contamination of the flagellar preparation with cell body proteins (Fig 2.11).

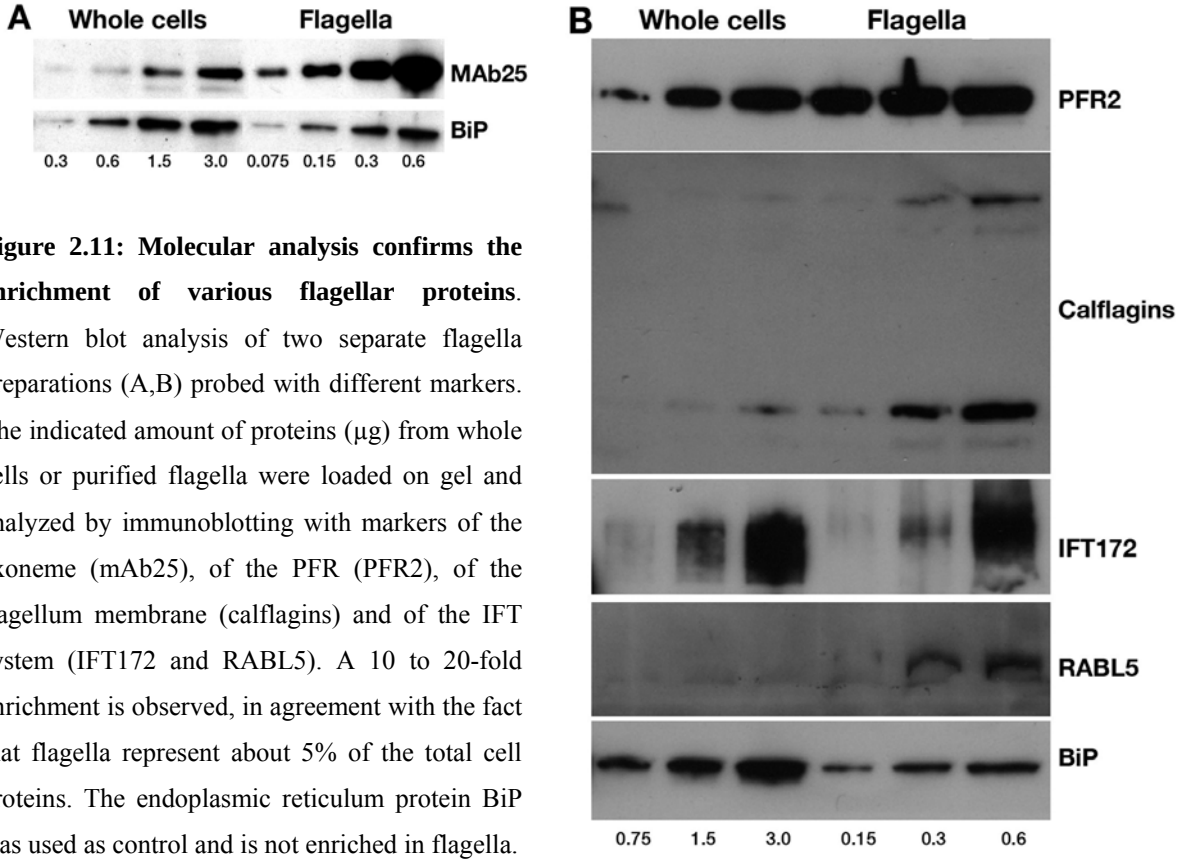

Figure 2.11: Molecular analysis confirms the enrichment of various flagellar proteins. Western blot analysis of two separate flagella preparations (A,B) probed with different markers. The indicated amount of proteins (µg) from whole cells or purified flagella were loaded on gel and analyzed by immunoblotting with markers of the axoneme (mAb25), of the PFR (PFR2), of the flagellum membrane (calflagins) and of the IFT system (IFT172 and RABL5). A 10 to 20-fold enrichment is observed, in agreement with the fact that flagella represent about 5% of the total cell proteins. The endoplasmic reticulum protein BiP was used as control and is not enriched in flagella. (Julkowska et al., manuscript in preparation)

The purified flagella were analyzed by mass spectrometry in five separate experiments (Table 1.1). Only proteins found in at least three data sets were taken into account. A total of 388 identified proteins included most of the flagellum markers, such as axoneme and PFR components but also most of the known membrane (calflagins) and matrix proteins (different IFT). None of the markers for membrane and matrix had been detected in the previous study of flagella skeletons (Broadhead et al., 2006) (Table 1.1). Almost half of the newly identified proteins have not been previously reported to be associated to the flagellum. To increase confidence in the purity of the flagella, two mass-spectrometry experiments were carried out in parallel with the cell body fraction. Comparative analysis revealed proteins that were enriched in flagella versus cell bodies, present in equivalent proportion or depleted. 83 out of the 88 identified known flagellar markers were found to be enriched in flagella, confirming the validity of the approach. Out of the 194 novel proteins, 115 turned out to be enriched.

These were screened more closely using criteria such as the existence of domains known to be enriched in flagella, the conservation of the protein in other species or their restriction to kinetoplastids.

Structure	This study	Broadhead et al., 2006
Dynein arms	19/19	16/19
Central pair	3/4	4/4
Others	14/17	15/17
Total axoneme	*36/40*	*35/40*
Basal body	2/5	2/5
PFR	29/35	22/35
Total flagellar skeleton	*67/80*	*59/80*
IFT	9/26	0/26
Other membrane/matrix	5/7	0/7
Total membrane/matrix	*14/33*	*0/33*
Total flagellum markers	*81/113* (93/113)*	*59/113*
Cytoskeletal-associated**	0/6	5/6

*including proteins found in 1 or 2 experiments (case of 11 IFT proteins)
**proteins associated to the flagellum but not part of it

Table 2.1: Summary of various markers found in proteomes of intact flagella or flagella skeletons. The results of the mass-spectrometry analyses of intact flagella in this study, was compared with the skeletal proteome of Broadhead et al., 2006. The screen includes known proteins of the axoneme, basal body and PFR that are markers for the flagellar skeleton. In the intact flagella several known flagellar membrane and matrix proteins were identified but are absent in the flagellar skeleton study. In total, more recognized flagellar proteins were identified in this study that in the analysis of the flagellar skeleton. (Julkowska et al., manuscript in preparation)

Among the hypothetical proteins identified in the study we selected ten candidates with interesting domains to study their flagellar localization as a prerequisite for sensory function. Those were named by their likely localization as flagellar membrane and matrix proteins (FLAMM). In addition, we got particularly interested in two obvious sensing candidates, the PAD2 protein that has been identified as a citrate transporter triggering differentiation from stumpy to procyclic forms (Dean et al., 2009), and the arginine kinase protein that was already described to play a role in resistance against environmental stresses in the related parasite *T. cruzi* (Miranda et al., 2006; Pereira et al., 2003).

2.6 Aims of the thesis

Post-transcriptional control is the major possibility for trypanosomes to control mRNA transcripts that need to be expressed in certain developmental stages and not in others. Regulatory structures were identified in the 3' UTRs of many transcripts and several RNA-binding proteins have been shown to recognize them and to control their fate. Control could take place at the level of stabilization, degradation or translation efficiency. Some examples of RNA-binding proteins were described to act during differentiation from bloodstream to procyclic form but investigations on such proteins beyond the procyclic stage in the tsetse fly have never been conducted.

We searched to assess the role of the predicted RNA-binding proteins ALBA in trypanosome development. Their involvement in processes that are developmentally controlled raised their status for being good candidates of RNA-binding proteins controlling differentiation processes. Former lab members had generated antibodies against trypanosome ALBA proteins (Ngwabyt, Blisnick) and preliminary RNAi knock-down experiments suggested important roles for the survival of the procyclic form in culture (Durand-Dubief). My aim was to perform a thorough study on the function of ALBA in the developmental stages of the parasite in the tsetse fly. First by analyzing the phenotype in the $ALBA^{RNAi}$ knockdown cell line and then to assess ALBA expression levels in the fly stages by fluorescent tagging experiments.

In the context of trypanosome differentiation, the sensing of environmental cues is indispensable for the parasite to "know" in which host and which organ it is living, to trigger the necessary developmental program. The flagellum has been emphasized as an important sensory organelle (Rotureau et al., 2009). However, molecular actors have not been identified yet. In the host laboratory, intact flagella containing membrane and matrix proteins were purified from procyclic trypanosomes (Julkowska et al., manuscript in preparation). Mass spectrometry analysis revealed some known sensing proteins and identified a multitude of proteins with hypothetical functions. The aim of the last part of my thesis consisted in the validation of the flagellar localization of selected proteins and to proceed, at least for one of them, to their functional analysis to assign their role as possible sensing proteins.

3 RESULTS

3.1 ALBA as candidate proteins to act in developmental control

3.1.1 The ALBA protein family in *Trypanosoma brucei*

The genomes of *T. brucei*, *T. cruzi* and *T. vivax* encode four proteins containing an Alba domain, whereas only two are found in *T. congolense* and in all *Leishmania* species. In *T. brucei*, two *ALBA* genes are found on chromosome four: *ALBA3* (Tb927.4.2040) and *ALBA4* (Tb927.4.2030) and two on chromosome eleven: *ALBA1* (Tb11.02.2040) and *ALBA2* (Tb11.02.2030). Multiple sequence analysis of ALBA proteins found in several kinetoplastids (*T. brucei*, *T. cruzi* and *Leishmania major*) and in some metazoan organisms (human and mouse) revealed two main characteristics (Fig 3.1A). First, the kinetoplastid ALBA proteins split in two groups, one including ALBA1 and ALBA2 and the other one containing ALBA3 and ALBA4. Second, the ALBA1/2 group was more closely related to the metazoan Rpp20 proteins while ALBA3/4 proteins were closer to the Rpp25/Alba-like proteins. This is due to the fact that all Rpp25 and ALBA3/4 proteins contain C-terminal extensions with a characteristic GYQXP signature and often a stretch of RGG repeats (Aravind et al., 2003).

The *T. brucei* ALBA1 and ALBA2 are small proteins of 12 and 14 kDa that contain the Alba domain only (Pfam PF01918) and that show 53% identity at the amino-acid level between each other. ALBA3 and ALBA4 are very divergent from ALBA1 and ALBA2 with whom they share only 16% overall identity. This is restricted to a few residues within the Alba domain (Fig 3.1B). ALBA3 and ALBA4 show high conservation between each other, with 80% identity not considering the C-terminal extension of ALBA4. The encoded proteins have a molecular weight of 21 and 25 kDa respectively.

I will focus my investigation on ALBA3 and ALBA4 as they display, in addition to the predicted RNA-binding Alba domain, a C-terminal stretch of multiple RGG repeats that are thought to be important for RNA-binding (Godin and Varani, 2007). Moreover, they are more closely related to the Rpp25/MDP2 group that contains the MDP2 protein that might be involved in developmental processes in ciliates.

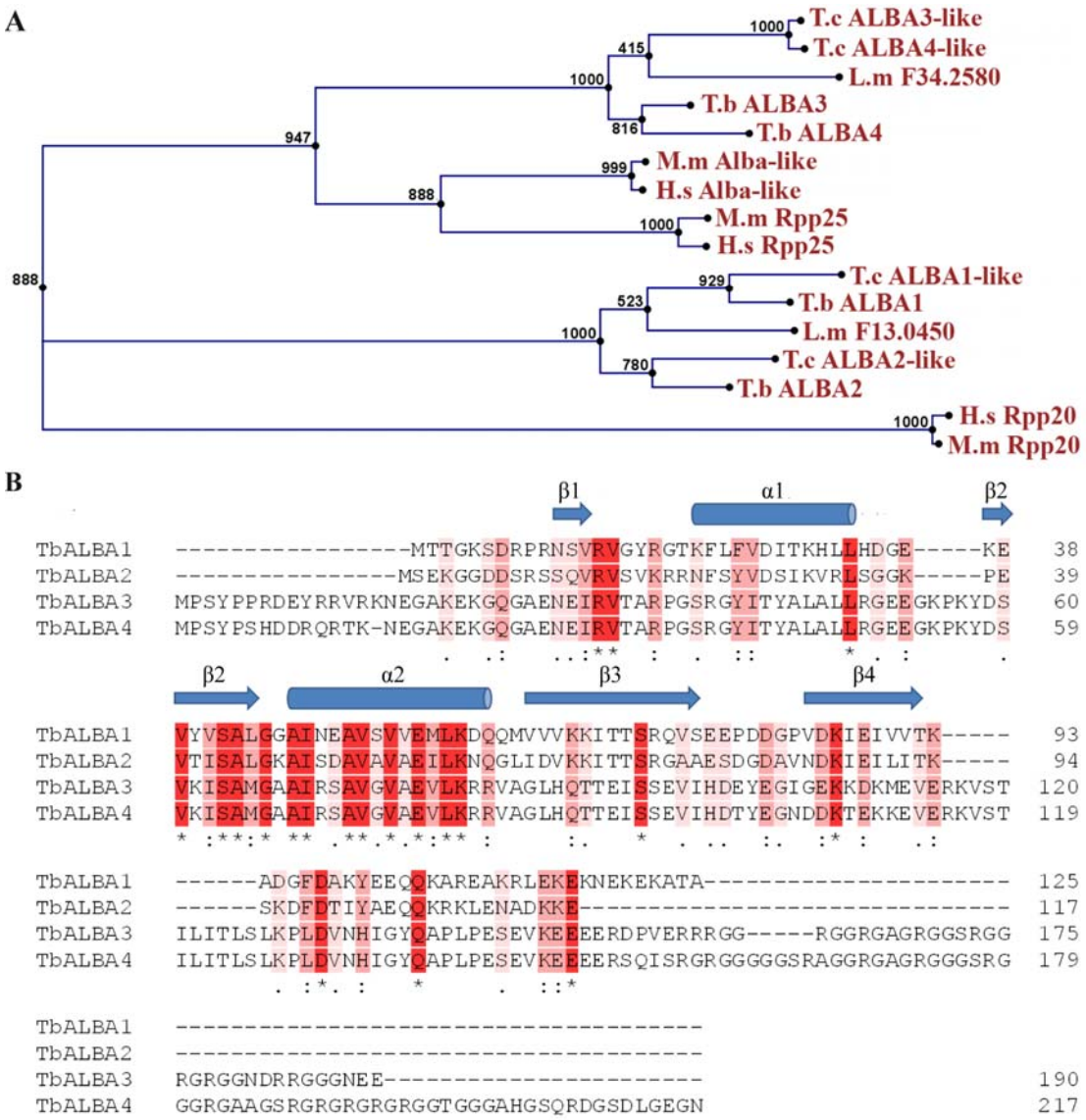

Figure 3.1: Conservation of ALBA proteins. (A) A phylogenetic tree of ALBA and Alba-like proteins was generated from a multiple sequence alignment. Bootstrap values (1000 replicates) for neighbourhood joining are indicated at each node. The following protein sequences were chosen for the alignment: *H. sapiens* Ribonuclease P protein subunit p20 (Rpp20) (Uniprot Reference: O75817), *M. musculus* Rpp20 (Q9DCH2), *H. sapiens* Ribonuclease P protein subunit p25 (Rpp25) (Q9BUL9), *M. musculus* (Rpp25) (Q91WE3), *H. sapiens* Alba-like protein C9orf23 (Q8N5L8), *M. musculus* Alba-like protein C9orf23 (Q99JH1). For comparison, all Alba-domain containing protein sequences of *T. brucei* and the related organisms *T. cruzi* and *L. major* were chosen: *T. brucei* ALBA1 (Tb11.02.2040), ALBA2 (Tb11.02.2030), ALBA3 (Tb927.4.2040), ALBA4 (Tb927.4.2030); *T. cruzi* ALBA1-like (Tc00.1047053504089.60), ALBA2-like (Tc00.1047053504089.70), ALBA3-like (Tc00.1047053510877.40) and ALBA4-like (Tc00.1047053510877.30); *L. major* (L.m F13.0450 and L.m F34.2580) (B) Multiple sequence alignment of *T. brucei* ALBA proteins: TbALBA1, TbALBA2, TbALBA3 and TbALBA4 using ClustalW2 (* identical residue dark red, **:** high conservation red, **.** low conservation pale red). The predicted Alba domain fold is indicated in blue (arrows represent β-sheets and cylinders α-helices). This is an assumption based on the crystal structure of the archaeal Alba1 protein from *S. solfataricus* (Wardleworth et al., 2002) and its alignment with *T. brucei* ALBA1 (Bell et al., 2002).

3.1.2 Tools for the detection of ALBA proteins

To investigate the localization and the function of ALBA3 and ALBA4, both full-length proteins had been expressed as GST fusions and injected in mice to produce antisera (Ngwabyt & Blisnick). I carried out western blot analysis on total protein extracts and confirmed that both proteins were expressed in procyclic (PC) and slender bloodstream form (BS) parasites in culture (Fig 3.2). ALBA proteins migrated at positions corresponding to their predicted size of 21 kDa and 25 kDa for ALBA3 and ALBA4 respectively. Out of the 16 antisera produced, most of them recognised both bands with various efficiencies (example in Fig 3.2A), whereas one antibody turned out to react preferentially with ALBA3 and one with ALBA4 (Fig 3.2B,C).

Next, for the detection of ALBA proteins in living cells, cell lines expressing YFP fusion proteins with either ALBA3 or ALBA4 were generated in procyclic cells of Lister 427. The plasmid p3329 containing a fragment of the C-terminal coding sequence of *ALBA3* or *ALBA4* was linearized in the *ALBA* sequence to target integration in the endogenous locus and achieve the subsequent expression of the fusion construct. Protein expression was first verified by western blot using either the antibody reacting preferentially with ALBA3 or with ALBA4. The YFP tagged versions migrated at positions in agreement with their molecular weights of 46 kDa (ALBA3::YFP) and 50 kDa (ALBA4::YFP) respectively (Fig 3.2B,C). These results also confirmed that these antibodies indeed recognize ALBA3 or ALBA4. Therefore we will refer to the tested antibodies as anti-ALBA3 (preferentially recognizing ALBA3), anti-ALBA4 (preferentially recognizing ALBA4) and anti-ALBA3/4 (recognizing both ALBA3 and ALBA4). Moreover, as expected from the endogenous tagging procedure, the amount of untagged protein seemed reduced for both ALBA3 and ALBA4 (Fig 3.2B,C).

Upon paraformaldehyde (PFA) fixation, all antibodies tested by immunofluorescence analysis (IFA) produced a clear signal in the cytoplasm of cultured procyclic and bloodstream forms. No signal was detected in the nucleus or in the kinetoplast at any step of the cell cycle (Fig 3.2D,E). In contrast, signal was lost upon methanol fixation suggesting that ALBA3/4 are soluble proteins or that the recognized epitopes were denatured. For most IFA studies the anti-ALBA3 was used because it showed the best signal-to-noise ratio. Observation of the ALBA::YFP direct fluorescence in live and fixed cells confirmed the exclusively cytoplasmic localization initially observed by IFA and the absence of visible changes in the staining pattern during the cell cycle (Fig 3.2F).

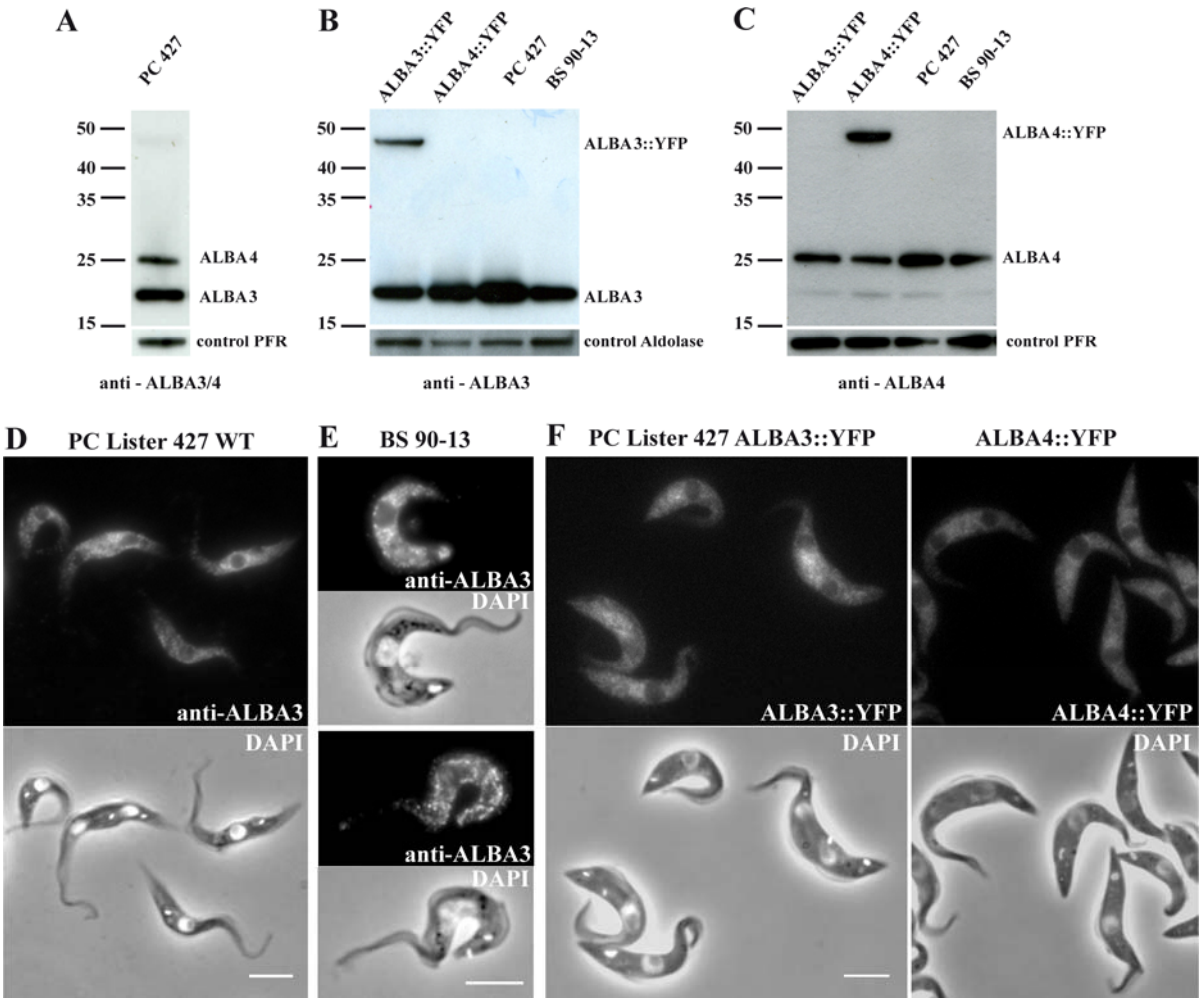

Figure 3.2: Reactivity of ALBA antibodies and ALBA::YFP cell lines. (A-C) ALBA antibodies in western blot on total protein samples from PC 427 WT, 427 expressing either ALBA3::YFP or ALBA4::YFP fusion protein and BS 90-13 (2 µg total protein per lane). Cell lines are indicated on top of the gels and the antibodies at the bottom of each panel. The positions of the bands of the molecular weight marker are shown on the left and the expected positions of various proteins are shown on the right-hand side of each gel. (A) Anti-ALBA3/4 recognizes ALBA3 (21 kDa) and ALBA4 (25 kDa), (B) anti-ALBA3 the endogenous ALBA3 and the ALBA3::YFP fusion (46 kDa) and (C) anti-ALBA4 recognizes ALBA4 and ALBA4::YFP (50 kDa). (D,E) IFA with the anti-ALBA3 on (D) PC 427 WT and (E) BS 90-13 counterstained with DAPI (in white merged with the phase contrast image). (F) Cell lines expressing either ALBA3::YFP (left panel) or ALBA4::YFP (right panel) fusion proteins were fixed in PFA, counterstained with DAPI (in white merged with the phase contrast image) and direct ALBA::YFP fluorescence was observed. Scale bar represents 5 µm.

3.1.3 ALBA localization in environmental stress conditions

ALBA3 and ALBA4 are cytosolic proteins and are therefore unlikely to be involved in DNA binding. Due to the intrinsic ability of the Alba domain and the several RGG repeats they could interact with RNA. In trypanosomes, several RNA-interacting proteins have been

shown to accumulate in cytoplasmic foci that harbour mRNA and are formed in starvation conditions or upon heat shock (Cassola et al., 2007; Kramer et al., 2008).

3.1.3.1 ALBA3/4 aggregate to foci during starvation and co-localize with DHH1

The localization of ALBA3/4 was investigated in procyclic cells upon heat shock and starvation, first by IFA with the anti-ALBA3 and an antibody against the RNA-helicase DHH1, a marker for cytoplasmic foci (Kramer et al., 2008). In contrast to DHH1, the ALBA signal did not reveal small foci in non-stressed conditions (Fig 3.2D) and heat shock did not provoke a concentration of ALBA to granules (Fig 3.3A). However, the ALBA signal was clearly concentrated in foci after starvation stress where it co-localized with DHH1 (Fig 3.3B).

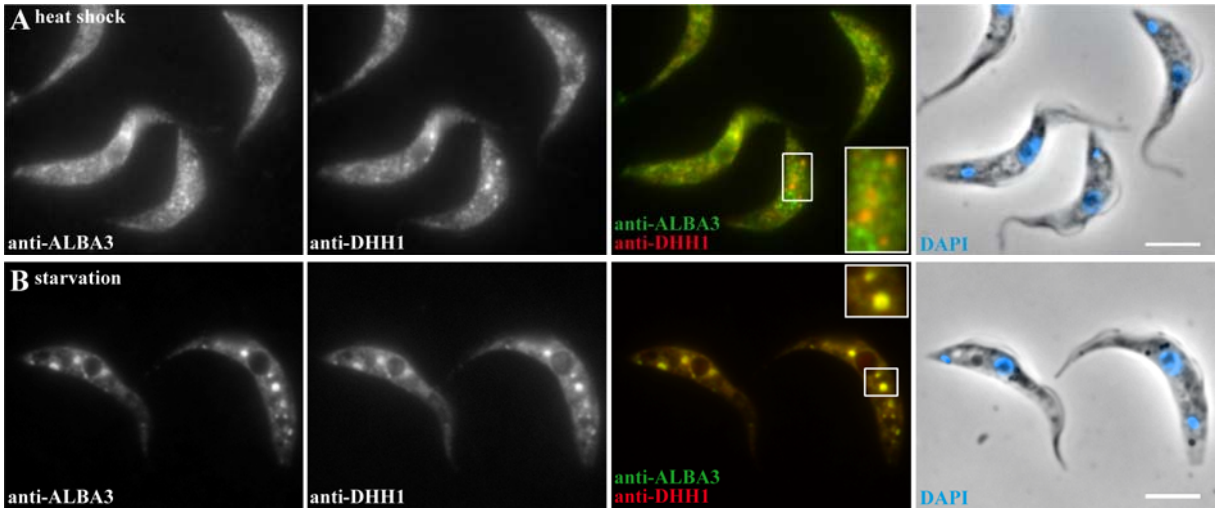

Figure 3.3: Localization of ALBA and DHH1 in stress conditions. (A) heat shock (42 °C for 2 h) or (B) starvation (incubation in PBS for 2 h) followed by IFA with the anti-ALBA3 (green) and the anti-DHH1 (red) antibody. Cells were counterstained with DAPI (in blue merged with the phase contrast, right panel), scale bars represent 5 µm. White boxes indicate areas of magnification.

As the access of the antibody to the antigen in the foci could be limited, these results were confirmed by analysing the cell lines expressing endogenous ALBA3::YFP and ALBA4::YFP fusion proteins. After transfer in PBS, both ALBA::YFP fusion proteins aggregated into cytoplasmic foci confirming the IFA results (Fig 3.4). The kinetics of granule formation was analysed after 30 min, 1 h, 2h and 3 h incubation in PBS, not including the time of washes that was less than 15 min (Fig 3.4). After 30 min of stress, granule formation was observed in more than half of the cells, the number of foci as well as their size varying among different cells. A minority of cells presented a uniform cytoplasmic localization of ALBA as in non-stressed conditions. Starvation for 1 h led to the formation of ALBA granules that seemed in size and number equivalent to those present after 2 h and 3 h. For the following experiments

we decided to perform starvation experiments for 2 h in PBS, as granule formation is surely completed and will not change upon longer incubation times.

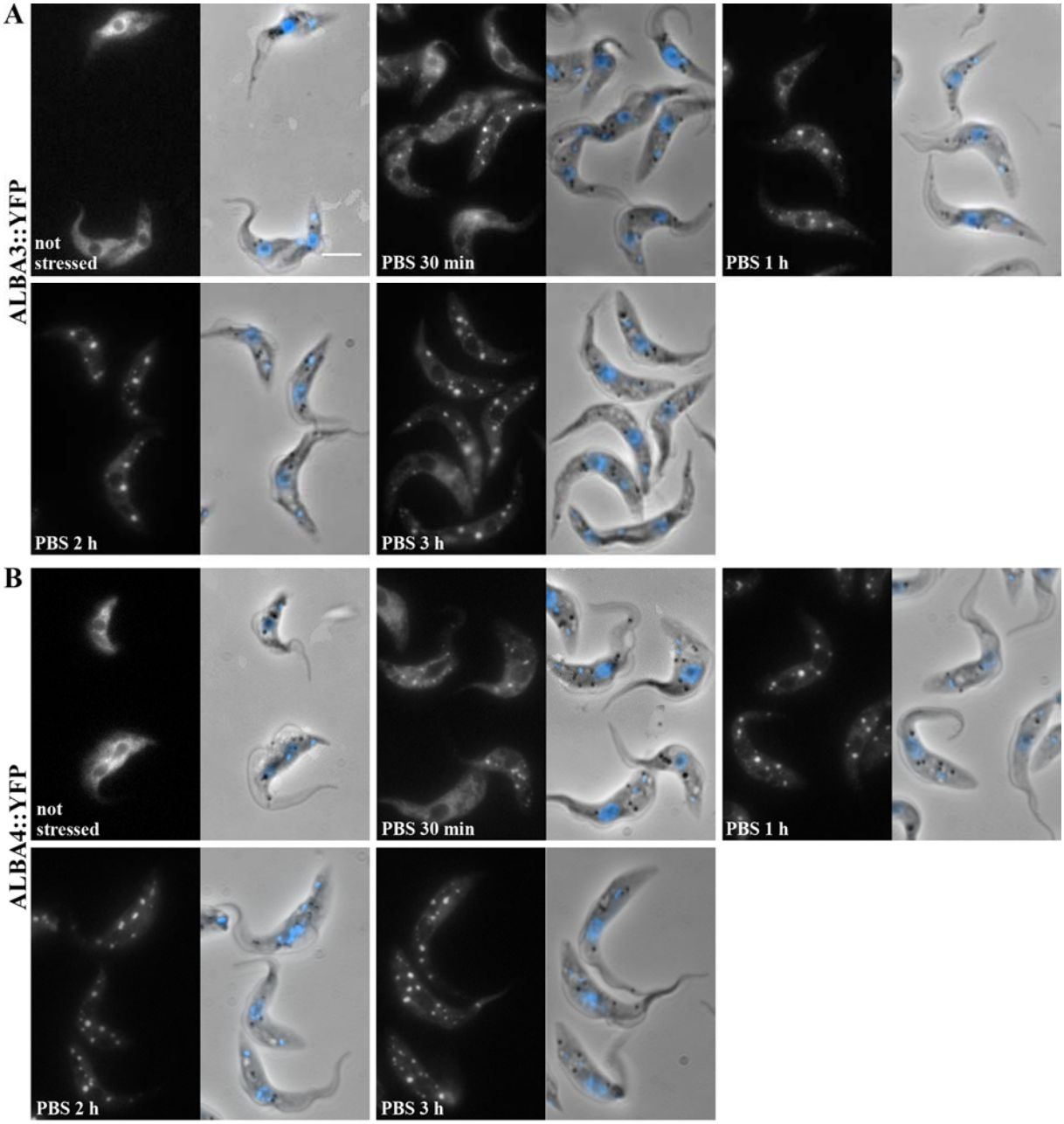

Figure 3.4: Kinetics of ALBA granule formation in starvation conditions. Cells expressing either (A) ALBA3::YFP or (B) ALBA4::YFP were starved in PBS for the indicated time points: 30 min, 1 h, 2 h and 3 h. As control, cells in non-stressed conditions are shown. Cells were counterstained with DAPI, in blue superimposed with the phase contrast image. Scale bar represents 5 µm and is the same for all images.

In order to further define ALBA localization, a mCherry::DHH1 construct (Kelly et al., 2007; Kramer et al., 2008) was added to the ALBA3::YFP or ALBA4::YFP expressing cell lines. The cells were fixed and YFP and mCherry signal analysed before and after starvation stress. Both proteins co-localized in cytoplasmic granules after 2 h of nutritional stress (Fig 3.5).

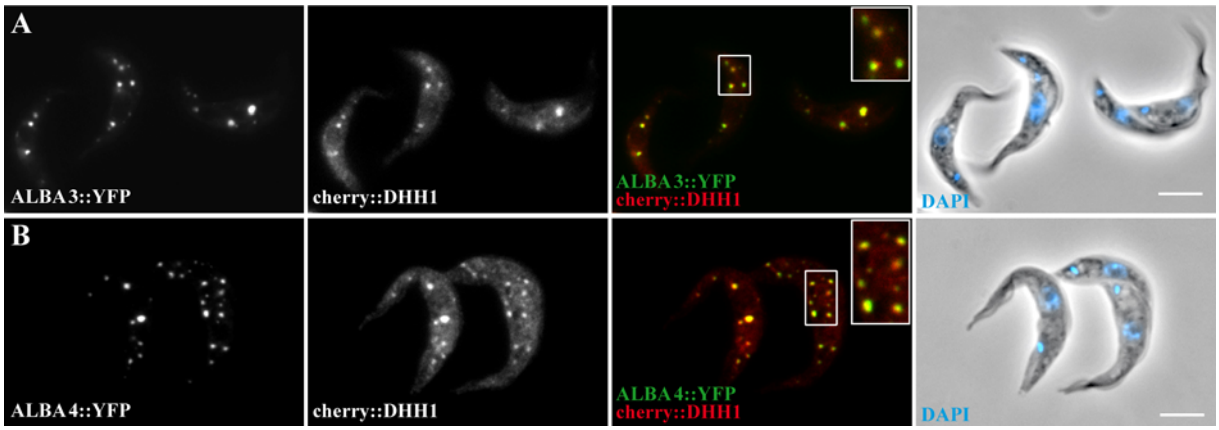

Figure 3.5: Localization of ALBA and DHH1 fluorescent fusion proteins in starvation conditions. PC cells of the strain Lister 427 expressing endogenous (A) ALBA3::YFP or (B) ALBA4::YFP together with mCherry::DHH1 were starved (incubation in PBS for 2 h) and fixed in PFA. Cells were counterstained with DAPI (in blue merged with the phase contrast image, right panel) and direct YFP and mCherry fluorescence observed. Scale bars represent 5 µm. White boxes indicate areas of magnification.

3.1.3.2 ALBA3 and ALBA4 co-localize in starvation granules

Both ALBA::YFP fusion proteins fully co-localize with the DHH1 protein (Fig 4.5). We can therefore hypothesize that ALBA3 and ALBA4 co-localize with each other in the same foci during nutritional stress. To test this, we created a construct allowing expression of ALBA4 coupled to a mCherry fluorescent protein. After its introduction into the cell line already expressing ALBA3::YFP, we were able to visualize the behaviour of both proteins in starvation conditions. Indeed ALBA3 and ALBA4 perfectly co-localize in starvation granules at any step of the cell cycle (Fig 3.6).

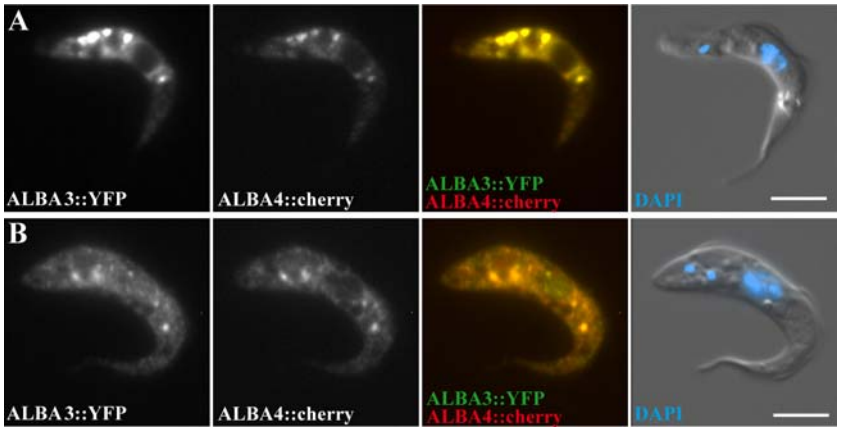

Figure 3.6: ALBA3 and ALBA4 co-localize in starvation stress. Cells expressing ALBA3::YFP (green) and ALBA4::mCherry (red) after 3 h of starvation in PBS. (A) 1K1N cell and (B) 2K1N cell. The step in the cell cycle was determined using DAPI (in blue on the DIC image). Scale bars represent 5 µm.

3.1.3.3 Partial co-localization of ALBA with polyA$^+$ RNA in starvation granules

The co-localization of ALBA with a described RNA-binding protein in cytoplasmic foci prompted the investigation of polyA$^+$ RNA that was shown to co-localize with the DHH1

protein upon starvation stress (Cassola et al., 2007). Therefore, the RNA-FISH method to detect polyA$^+$ RNA was coupled to IFA using the anti-ALBA3 antibody (Fig 3.7). The analysis by confocal microscopy revealed three types of foci in starved parasites (Fig 3.7 magnification in the white box): (1) those containing polyA$^+$ RNA and ALBA protein displaying equal signal intensity, (2) those containing polyA$^+$ RNA but no detectable ALBA protein and (3) those showing a signal for ALBA protein but no detectable polyA$^+$ RNA signal. In conclusion, both ALBA3 and ALBA4 proteins formed foci upon starvation stress conditions that showed partial co-localization with polyA$^+$ RNA (Fig 3.7).

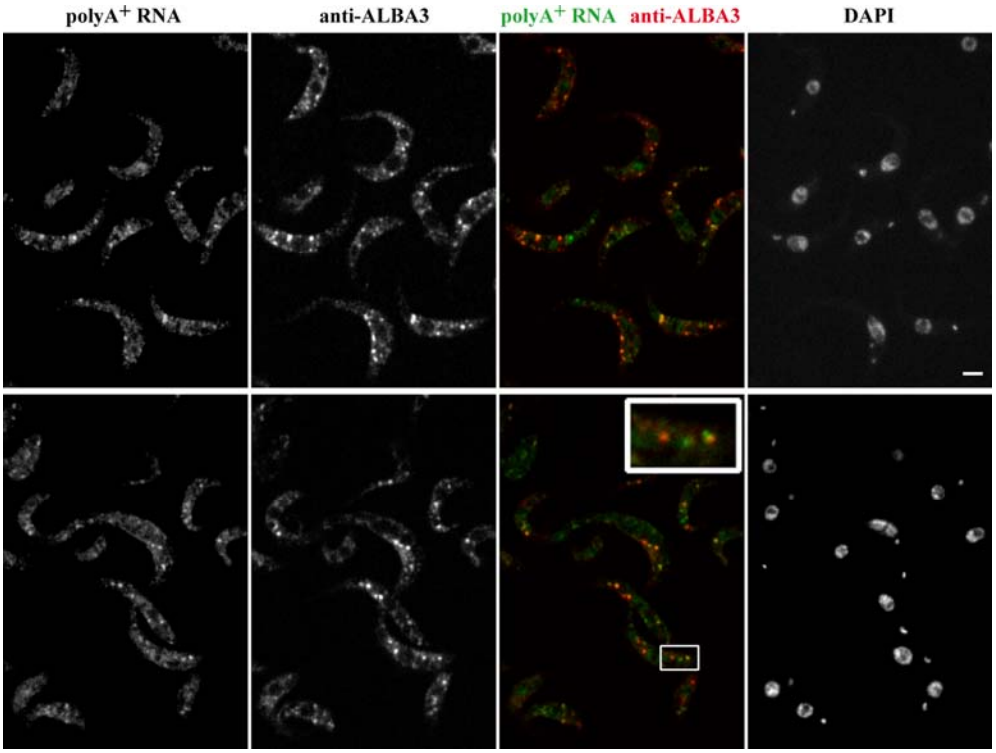

Figure 3.7: Localization studies of ALBA and polyA$^+$ RNA in starvation conditions. PC cells of Lister 427 WT were starved for 2 h and analysed by FISH-RNA to detect polyA$^+$ RNA using a fluorescent polyT probe (green in merged image), coupled to IFA with the anti-ALBA3 antibody (red in merged image). Cells were counterstained with DAPI (right panel). White box shows a magnification with the three types of foci: (right, yellow) ALBA and polyA$^+$ RNA co-localization, (middle, green) polyA$^+$ RNA signal only and (left, red) anti-ALBA3 signal only. Scale bar represents 5 µm.

3.1.3.4 Puromycin and cycloheximide treatment

The concentration of RNA-binding proteins and mRNA into cytoplasmic foci is induced by various stress situations. The drug puromycin has a destabilizing effect on polysomes and enhances the granule formation during the stress response. In contrast, cycloheximide is able to prevent formation of stress granules by blocking translation elongation and thus stabilizing polysomes. Procyclic WT cells were starved for 2 h in PBS without drug treatment or in the

presence of puromycin or cycloheximide. IFA with the anti-ALBA3 antibody revealed that foci were present in cells starved in PBS without and with puromycin treatment (Fig 3.8A,B), while addition of cycloheximide prevented granule formation in starvation conditions (Fig 3.8C). ALBA3 co-localized with DHH1 in these situations and behaved as described for other RNA-binding proteins upon starvation stress and drug treatment (Cassola et al., 2007) (Fig 3.8).

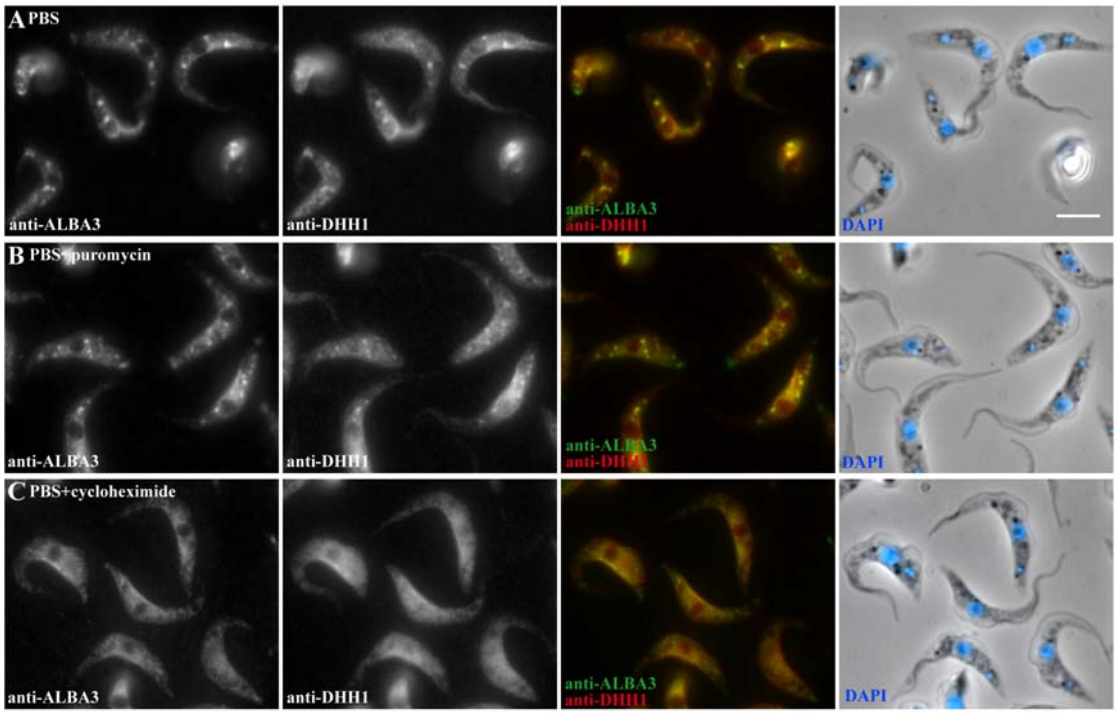

Figure 3.8: Effect of puromycin and cycloheximide on granule formation in starvation conditions. IFA on PC WT parasites starved for 2 h in PBS (A) in the absence of drugs or in the presence of (B) puromycin or (C) cycloheximide, followed by IFA with the anti-ALBA3 (green) and the anti-DHH1 (red) antibody. Cells were counterstained with DAPI (in blue merged with the phase contrast image). Scale bar represents 5 µm.

3.1.4 RNAi against ALBA in procyclic parasites

To investigate the function of ALBA3 and ALBA4 proteins in trypanosomes, their expression was depleted either simultaneously or individually using RNAi in the Lister 427, 29-13 procyclic parasites in culture. The first 400 base pairs of the *ALBA3* and *ALBA4* coding region show 94% identity and were targeted for knocking-down ALBA3 and ALBA4 simultaneously by RNAi (Fig 3.9A). The *ALBA4* sequence (1-400 bp) was cloned in-between two T7 promoters under the control of the Tet-repressor, ensuring tetracycline-inducible production of *ALBA4* dsRNA targeting *ALBA3/4*. An alignment of the *ALBA4* DNA sequence with those of *ALBA1,2* ruled out the possibility of cross-RNAi since the nucleotide identity is too low

(maximum stretch of identity is limited to 8 consecutive nucleotides for *ALBA1* and 5 for *ALBA2*) to generate efficient siRNA against *ALBA1* or *ALBA2* transcripts (Fig 3.9B).

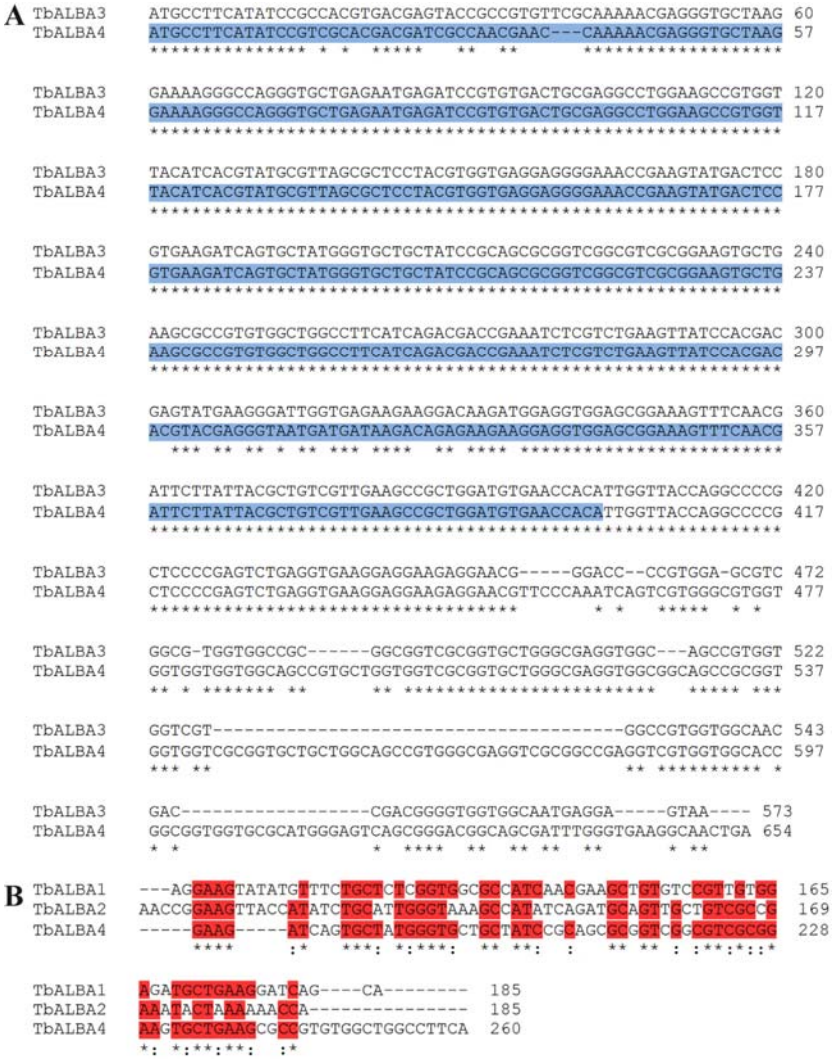

Figure 3.9: Conservation of *ALBA* DNA sequences in *T. brucei*. (A) Sequence alignment of *ALBA3* and *ALBA4* using ClustalW2 (* marks identical bases). The blue shading indicates the fragment cloned into the pZJM plasmid to create the *ALBA3/4*^{RNAi} cell line. (B) Sequence alignment of *ALBA1* and *ALBA2* with *ALBA4* ClustalW2 (* identical base pairs in all sequences, **:** conservation of *ALBA4* with either *ALBA1* or *ALBA2*). This alignment represents only a region of the genes and was chosen because of the high conservation of the encoded residues (see Fig 3.1B). Therefore, it was selected to exclude cross-RNAi against *ALBA1* or *ALBA2* in the *ALBA3/4*^{RNAi} cell line.

3.1.4.1 Kinetics and efficiency of ALBA3/4 silencing

The silencing efficiency of *ALBA3/4* was first assessed by semi-quantitative RT-PCR using *ALBA4* or *ALBA3* specific primers, which confirmed that mRNA levels of both *ALBA3* and *ALBA4* were significantly reduced after 2 days of induction (Fig 3.10A). As control we used primers against *ODA7* that encodes a cytoplasmic protein important for the correct assembly of flagellar skeletal components (Duquesnoy et al., 2009). At the protein level, ALBA3/4 amounts were already reduced in the non-induced *ALBA3/4*^{RNAi} cell line in comparison to Lister 427 WT as shown by western blot using either the antibody recognizing both ALBA3/4 (Fig 3.10B) or an antibody recognizing exclusively ALBA3 (Fig 3.10C). Nevertheless, protein levels of both ALBA significantly dropped further, once tetracycline was added to the medium, until maximal silencing was achieved after 3 to 4 days (Fig 3.10B,C).

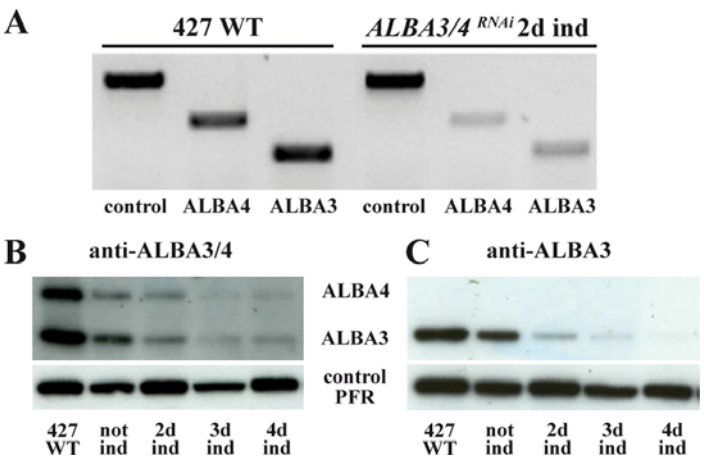

Figure 3.10: Silencing of ALBA3 and ALBA4 upon induction of the *ALBA3/4*^{RNAi} cell line. (A) Semi-quantitative RT-PCR of strains Lister 427 WT versus *ALBA3/4*^{RNAi} induced for 2 days. Primers were specific of either *ALBA4*, *ALBA3* or the control *ODA7*. 50 ng of RNA were used for the assay. (B,C) Western blot to assess protein levels of ALBA in Lister 427 WT as control versus the *ALBA3/4*^{RNAi} cell line not induced or induced for 2, 3 or 4 days with tetracycline using the (B) anti-ALBA3/4 or (C) the anti-ALBA3. The expected position of the proteins is indicated in the middle. 2µg of total protein were loaded per lane.

The anti-ALBA3 antibody was used in IFA to show protein down-regulation at the single cell level. The number of ALBA positive cells dramatically decreased during the first days of RNAi induction. At day 3 almost 100% of the cells were ALBA negative (Fig 3.11).

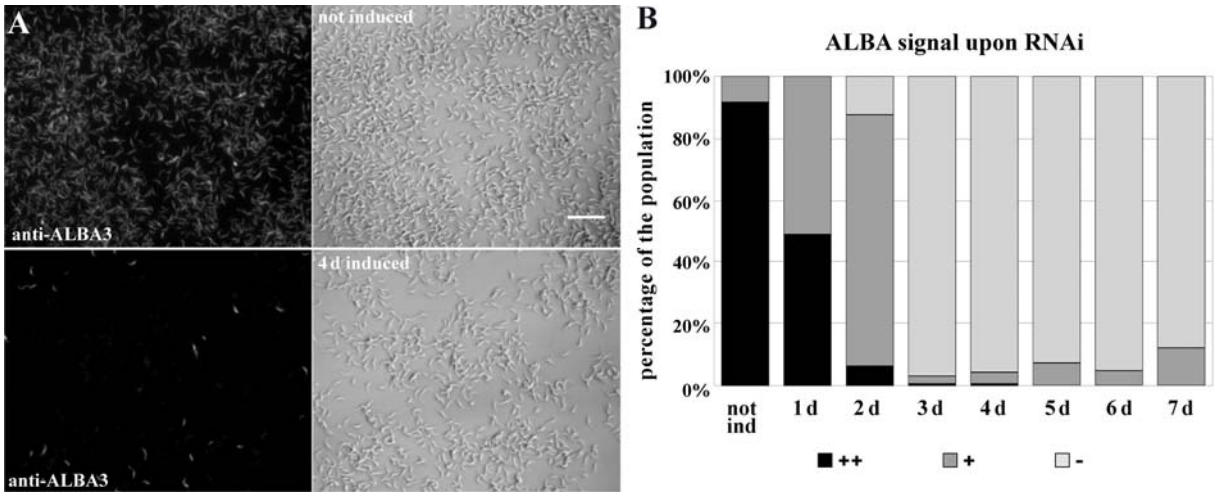

Figure 3.11: Efficiency of ALBA silencing investigated at the cellular level. (A) IFA signal with the anti-ALBA3 antibody in *ALBA3/4*^{RNAi} cells not induced (top panel) and induced for 4 days (bottom panel). Scale bar represents 40 µm. (B) Percentage of ALBA bright positive cells (++ black), weakly positive (+ dark grey) and negative cells (- light grey) during the time course of RNAi induction in a population of cells (n≥200 per time point). Counts were determined by single cell analysis upon IFA with the anti-ALBA3 antibody.

3.1.4.2 Silencing of ALBA3/4 leads to cell cycle arrest

Once proven that the ALBA proteins were efficiently knocked-down in the *ALBA3/4*^{RNAi} cell line, growth in culture was monitored with and without tetracycline (Fig 3.12A). After a comparable proliferation in the first 2 days, the induced cells showed a slightly slowed-down growth after the first dilution step but almost stopped to duplicate after the second dilution step. In contrast, the non-induced control was subsequently diluted every 2 days. To verify if the slow growth phenotype resulted from a specific cell cycle arrest, cells were scored for DNA containing organelles during the induction period to determine G1/S (1K1N), G2/M (2K1N) and the post-mitotic cells (2K2N). Aberrant cell types were also recorded: cells without nucleus called zoids (1K0N) (Robinson et al., 1995), 1K2N and cells with multiple nuclei (>2N). The non-induced state was considered as the control situation in which the population was split in 79% 1K1N, 14% 2K1N, 4% 2K2N cells and a minority of various aberrant cell types (<3%). No major changes in these proportions were observed up to three days of induction, in agreement with the growth curve (Fig 3.12B). However, after the fourth day of RNAi, the proportion of 2K1N cells decreased while the percentage of zoids (1K0N) went up to 10%. After 6 days of RNAi, up to 15% of zoids were present in the population indicating cell cycle defects that could result from a delayed or defective mitosis (Ploubidou et al., 1999). In contrast to many RNAi mutants in *T. brucei*, we did not observe the emergence of multinucleated cells (Fig 3.12B).

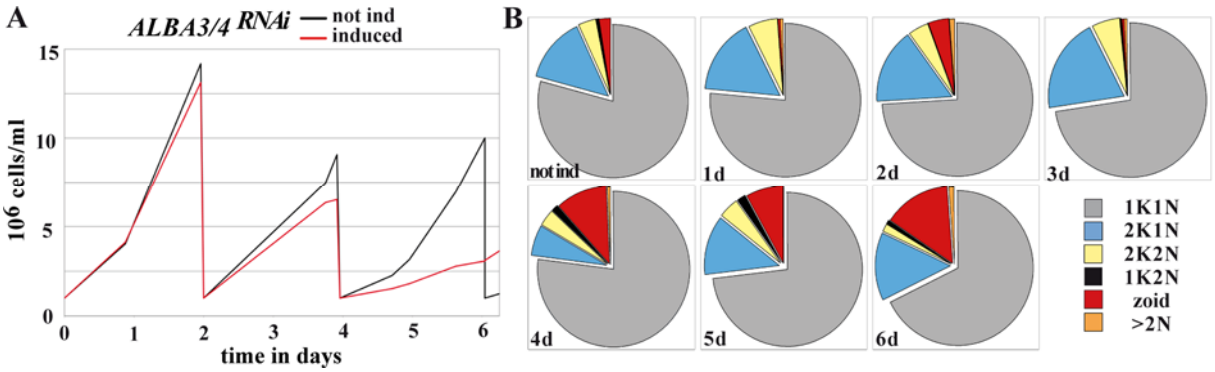

Figure 3.12: Slow growth and cell cycle arrest in the *ALBA3/4*^{RNAi} cell line. (A) Growth curves of the *ALBA3/4*^{RNAi} not induced (black line) and induced with tetracycline (red line). (B) Proportion of individuals in the different cell cycle steps during the time course of induction of RNAi (n=200 cells per time point). 1K1N (grey), 2K1N (blue), 2K2N (yellow), 1K2N (black), zoid 1K0N (red) and multinucleated cells >2N (orange).

The hypothesis of delayed or defective mitosis in ALBA knock-down cells was investigated using the DNA-FISH method. Fluorescent probes were prepared in order to visualize duplication and segregation of minichromosomes and large chromosomes during mitosis (Ersfeld and Gull, 1997). In *ALBA3/4*^{RNAi} non-induced cells minichromosomes localized in

multiple small clusters at the periphery of the nucleus during interphase, as previously described (Fig 3.13A). At mitosis they showed a defined localization, first as one cluster in the centre of the spindle and finally as expected, at the poles of the dividing nucleus until completion of cytokinesis. Large chromosomes were detected as dots duplicating during mitosis that segregated in a quite central position of the spindle (Ersfeld and Gull, 1997). However, in the induced state, several cells showed aberrations in this pattern. Multiple nuclei were enlarged (Fig 3.13B, arrowheads) and showed an accumulation of minichromosomes and dots corresponding to large chromosomes in a loose distribution in the nucleus. These results are consistent with a nucleus that is very likely blocked after completion of one round of S-phase and that does not proceed to segregation of the chromosomes in mitosis. Some cells were clearly undergoing mitosis but with an aberrant distribution of their chromosome content. The minichromosomes were either not concentrated in defined clusters or these clusters were not localized at opposite poles (Fig 3.13B, stars).

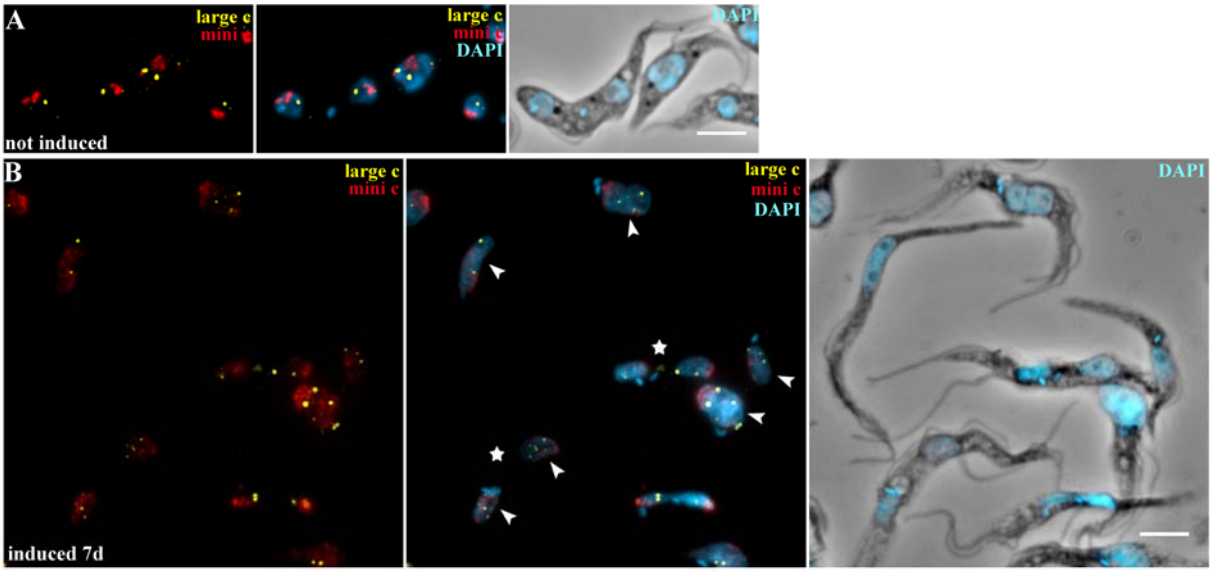

Figure 3.13: Impaired chromosome segregation in the absence of ALBA3/4. *ALBA3/4*^{RNAi} cells (A) not induced or (B) induced for 7 days. Large chromosomes (in yellow) were detected using a probe against the repetitive *r5S* locus and minichromosomes (in red) were visualized using a probe against a 177 bp repetitive motif. Nuclei and kinetoplasts were stained with DAPI (in blue on the phase contrast image). Scale bars represent 5 µm, arrowheads show nuclei that are of unusually large shape and stars indicate aberrant distribution of chromosomes during mitosis.

3.1.4.3 ALBA3/4 silencing leads to morphogenetic defects

To further investigate the consequences of the ALBA3/4 knock-down, cells induced at various time points were fixed and stained by IFA with the anti-ALBA3 antibody. A high

proportion of cells were very elongated, reaching up to 40 µm in length (non-induced cell length in 1K1N state is ~25 µm). As early as 2 days after the induction of protein knock-down, 24% of the cells showed an elongated posterior end, reaching up to 50% after 5 days (Fig 3.14A). This phenotype has previously been reported in some mutants and termed "nozzle" (Hammarton et al., 2004; Hendriks et al., 2001; Li et al., 2003). The question whether the elongation in nozzle cells was due to an active polymerization of microtubules at the posterior pole was then assessed by staining with the YL1/2 antibody that recognizes newly assembled tyrosinated α-tubulin (Kilmartin et al., 1982; Sherwin and Gull, 1989b). The staining was found at the basal bodies and the daughter flagellum as well as at the posterior end in both the control and *ALBA3/4*^{RNAi} induced cells (Fig 3.14B). *ALBA3/4*^{RNAi} cells with an elongated posterior end displayed bright staining indicating active microtubule elongation (Fig 3.14B, stars).

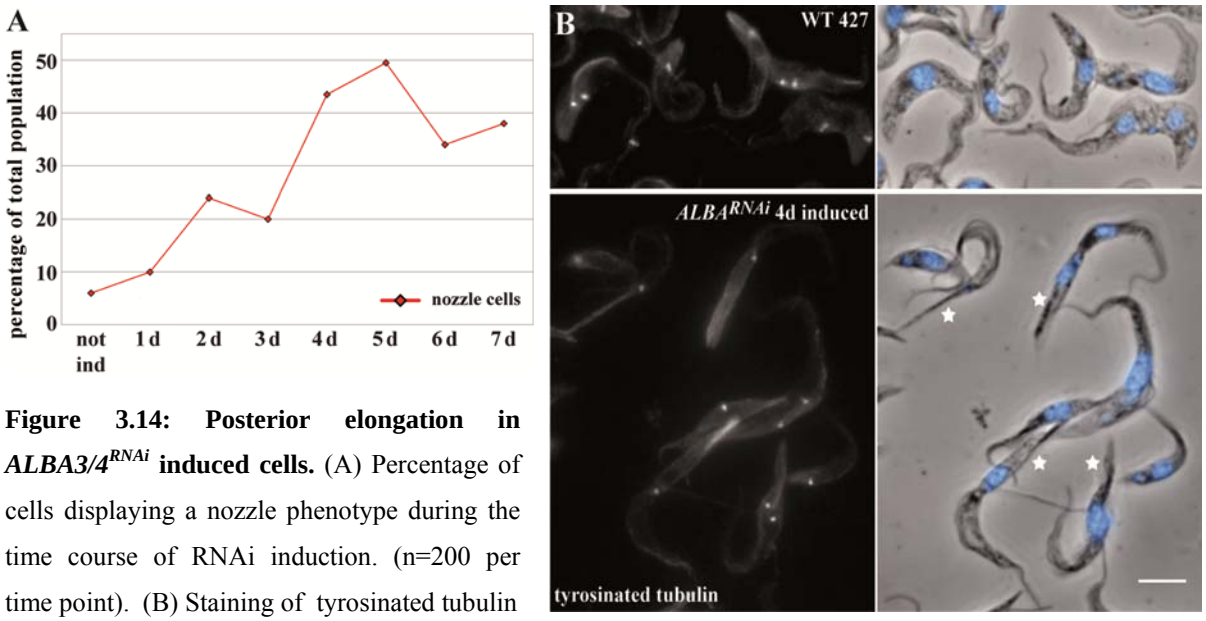

Figure 3.14: Posterior elongation in *ALBA3/4*^{RNAi} induced cells. (A) Percentage of cells displaying a nozzle phenotype during the time course of RNAi induction. (n=200 per time point). (B) Staining of tyrosinated tubulin in WT 427 and *ALBA3/4*^{RNAi} cells induced for 4 days. Stars indicate cells with nozzle phenotype. Scale bar represents 5 µm.

Cell body size has been linked to flagellum length (Kohl et al., 2003), therefore we assessed if this parameter increased concomitantly to cell elongation. A second question was if the elongation of the posterior pole occurred before or after cell division, looking at the future daughter cell that inherits the more posterior flagellum, the posterior half of the duplicated organelles and of the cell body (Ploubidou et al., 1999). To answer these questions, we analysed the zoids and measured their total cell length (from the posterior end to the tip of the flagellum), the distance of the kinetoplast to their posterior pole and their flagellar length on phase contrast images. The values of the distance from the kinetoplast to the posterior end

versus the cell length (Fig 3.15, left panels) showed linear trend lines at each induction time point with R^2 values between 0.59 and 0.73. This indicated the high probability of a linear relationship of the parameters that can be explained by an exhaustive microtubule elongation at the posterior pole. No matter the cell length and the RNAi induction time point (day 4-6), the length of the flagellum remained in the normal range of 15 to 22 µm in the majority of the cells measured (Fig 3.15, right panels). The R^2 values between 0.33 and 0.39 show an absence of linear relationship between flagellum length and cell length.

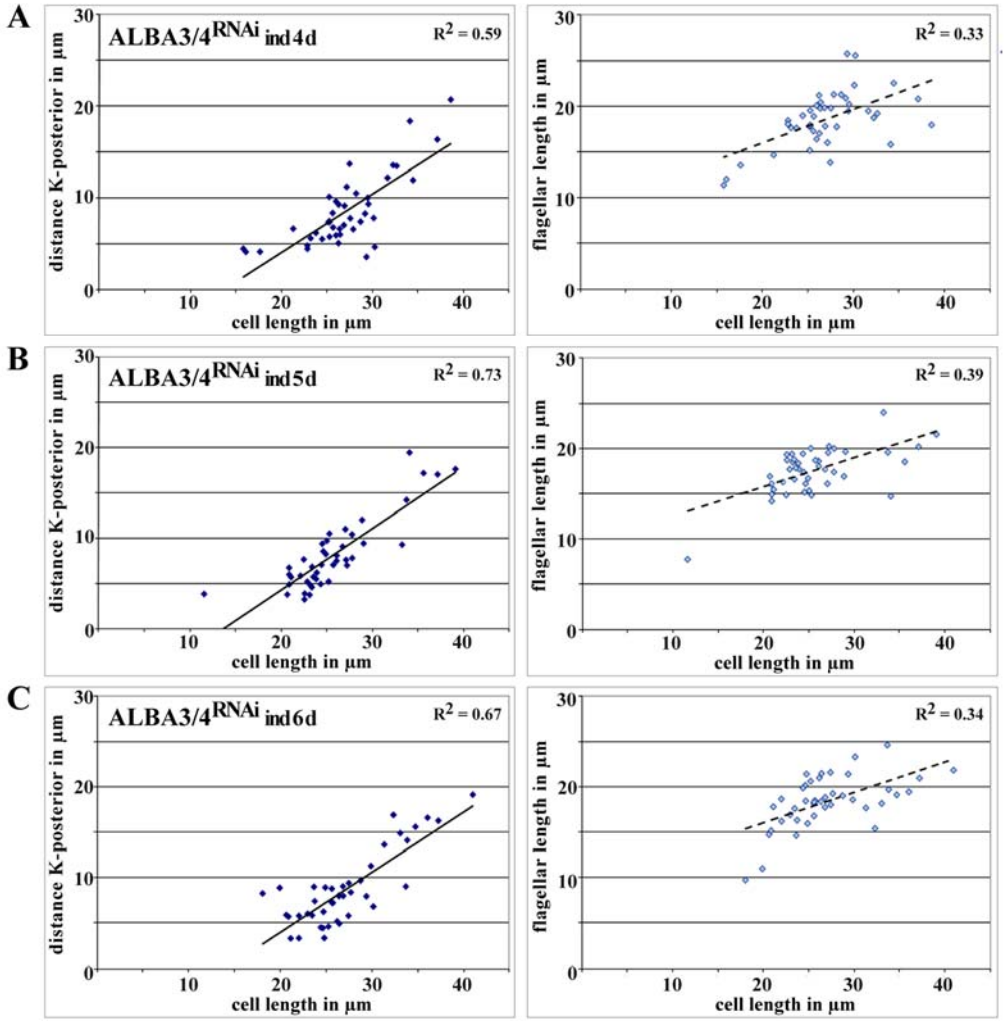

Figure 3.15: Cellular parameters of zoid cells in the *ALBA3/4*^{RNAi} cell line. Cells (A) induced for 4 days, (B) 5 days and (C) 6 days. The plots on the left show the distance of the kinetoplast to the posterior end in relation to the cell length (dark blue squares), the plots on the right show the flagellar length versus the cell length (light blue squares). Linear trend lines were added in black and their corresponding R^2 values are indicated. ($n \geq 40$ cells for each induction time point).

Taken together these data suggest that (1) elongation of the posterior end of the *ALBA3/4*^{RNAi} induced cells already occurred before cell division, as no major difference was observed from

one time point to the other and (2) that this elongation does not depend on flagellar length but occurs at the posterior end.

A second phenotype was observed: the nucleus frequently appeared in a posterior position relative to the kinetoplast (Fig 3.16A). The percentage of such cells increased constantly during the course of RNAi induction. The aberrant nucleus positioning was scored as juxtaposed anterior or posterior of the kinetoplast, or being clearly posterior. In contrast to the non-induced control, after one and two days of induction a small percentage of cells with the three forms of aberrant nucleus positioning were already detected (Fig 3.16B). This went up steadily to reach a maximum at 6 days of induction with 28% of the cell population. Whereas cells with a juxtaposed anterior positioning of the nucleus were detected throughout the induction course, the percentage of cells with a juxtaposed posterior nucleus increased to 16% at day 6. An increase in abundance was also observed for cells showing a posterior nucleus positioning.

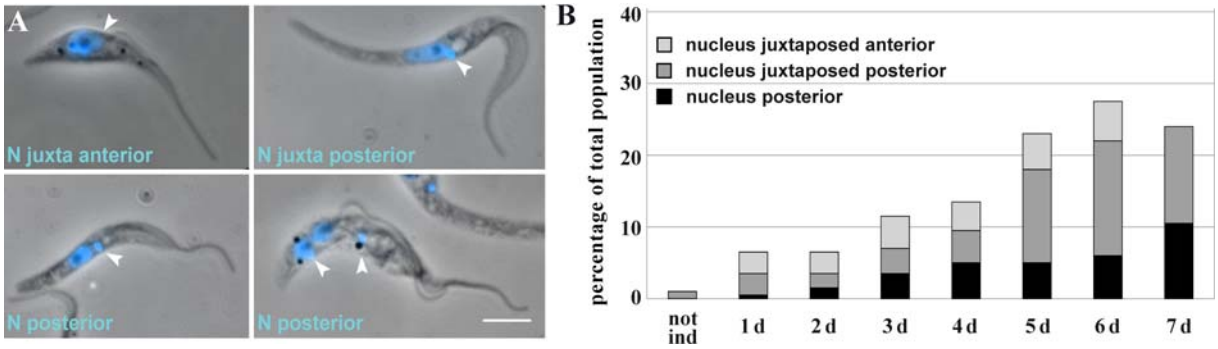

Figure 3.16: Posterior nucleus positioning in the *ALBA3/4*^{RNAi} cell line. (A) Examples of cells scored with DAPI staining (blue): a juxtaposed anterior (upper left), a juxtaposed posterior (upper right) and posterior nuclei (bottom panels). Scale bar represents 5 µm and arrowheads indicate kinetoplasts. (B) Percentage of cells in the population of the *ALBA3/4*^{RNAi} cell line displaying a juxtaposed anterior (light grey), a juxtaposed posterior (grey) and a posterior nucleus (dark grey) during the time course of RNAi induction (n≥200 cells per time point).

The flagellum attachment zone (FAZ) was shown to be essential for the trypanosome cell cycle i.e. correct morphogenesis and cytokinesis (Kohl et al., 2003; Kohl et al., 1999; Robinson et al., 1995). Furthermore, it was speculated that the FAZ controls nuclear positioning (Rotureau et al., 2011a; Vaughan et al., 2008). Thus, we monitored the FAZ in the *ALBA3/4*^{RNAi} cell line by staining the FAZ1 protein with the antibody L3B2 (Kohl et al., 1999) in a double IFA with the mAb25 antibody that stains the flagellar axoneme (Pradel et al., 2006) (Fig 3.17). In all *ALBA3/4*^{RNAi} cells investigated, both the flagellum and the FAZ1 staining exhibited normal aspect and length. This was also the case in cells that show a nucleus positioned posterior to the kinetoplast (Fig 3.17, arrowheads). Nevertheless, we could

not exclude that other FAZ components could be modified in these cells or that nuclear repositioning in the absence of ALBA involved completely different players.

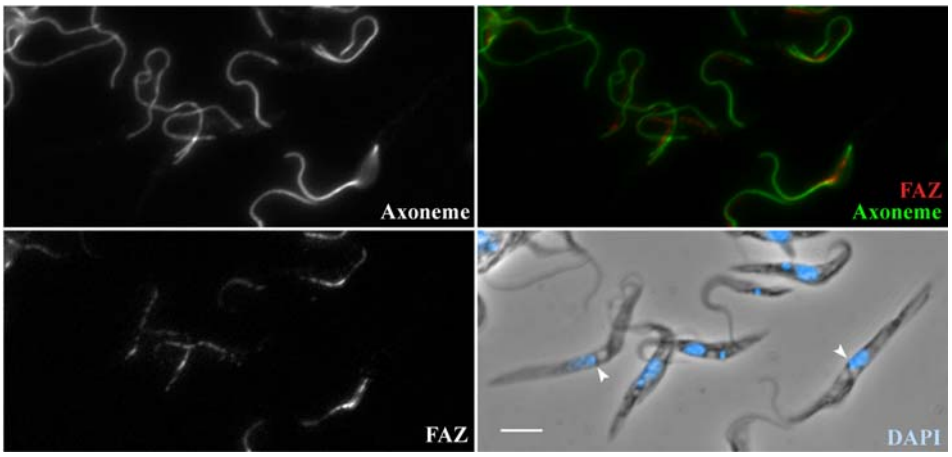

Figure 3.17: FAZ and flagellar analysis in induced cells of the *ALBA3/4*^{RNAi} cell line. Cells induced for 4 days were fixed in methanol and analysed by IFA with the antibodies mAb25, staining the axoneme (in green), L3B2, staining the FAZ (in red) and counterstained with DAPI (in blue merged with the phase contrast). Scale bar represents 5 µm and arrowheads show kinetoplasts that are positioned anterior to the nucleus.

3.1.4.4 Specific silencing of ALBA3 or ALBA4

The silencing of both ALBA3 and ALBA4 led to multiple phenotypes. These were caused either by silencing of only one of the proteins or by simultaneously silencing both proteins. Therefore we created cell lines that allowed knock-down of either ALBA3 or ALBA4 individually. Considering the similarity in the coding sequence of both genes, silencing was achieved by producing strains expressing dsRNA against the 3' coding sequence and 3'UTR of either *ALBA3* or *ALBA4* that were divergent enough to exclude cross-RNAi (Fig 3.18A).

The ALBA silencing was first assessed by semi-quantitative RT-PCR in the cell populations after transfection. For ALBA3, two transfection experiments were needed to obtain two populations that showed silencing. Further sub-cloning of these transfectants failed to recover any living cells. ALBA4 silencing was observed in several populations issued from the first round of transfection and were sub-cloned by limited dilution. We recovered 2 clones showing clear silencing of ALBA4 by RT-PCR analysis. We decided to continue our set of experiments with one cell line for each *ALBA*^{RNAi} that showed the highest silencing efficiency on the mRNA level (Fig 3.18B). Next, the growth rate was recorded for these cell lines in the non-induced and induced state. Over the whole period of induction, the growth of the *ALBA4*^{RNAi} cell line was comparable to the parental cell line even in the induced state (Fig 3.18C). The *ALBA3*^{RNAi} non-induced cell line grew slightly more slowly in comparison to *ALBA4*^{RNAi} and when induced manifested a slow-growth phenotype after 3 days. However, it

recovered after 150 hours to adopt a growth rate comparable to the non-induced culture (Fig 3.18C).

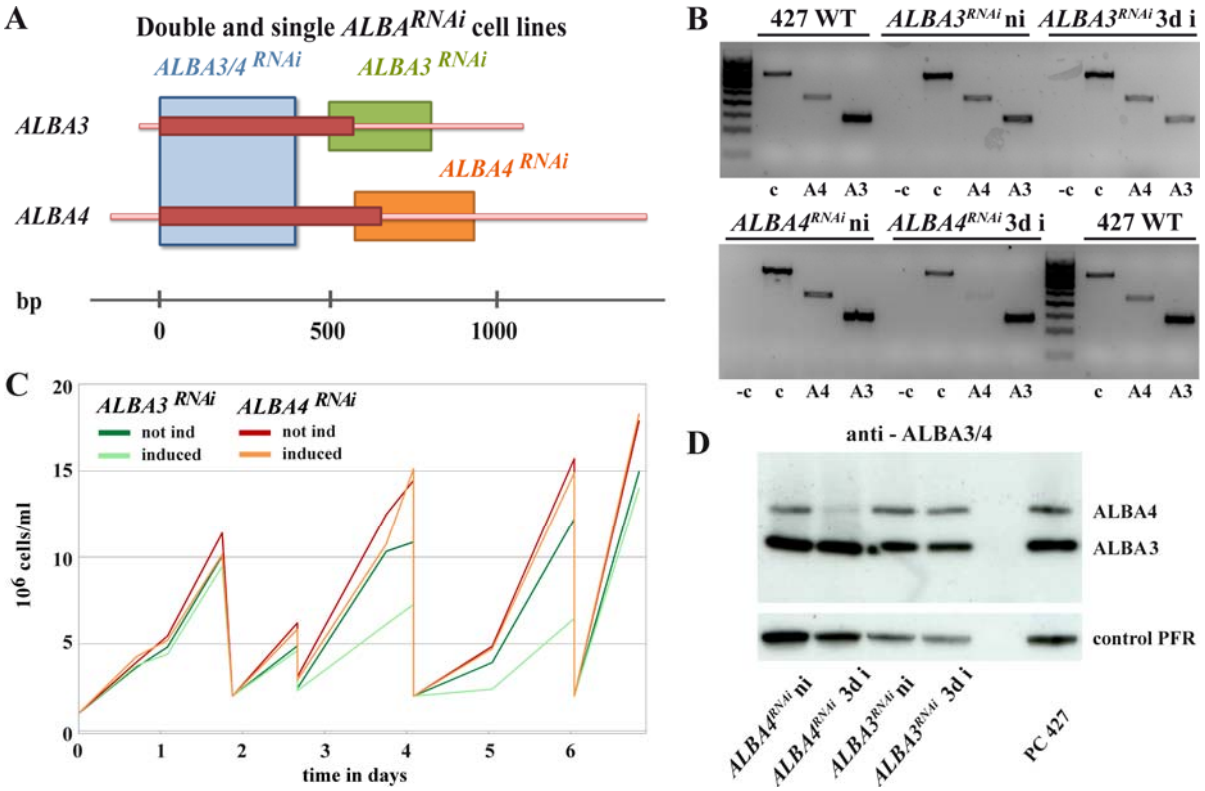

Figure 3.18: Silencing of ALBA proteins in *ALBA3*^{RNAi} or *ALBA4*^{RNAi} cell lines. (A) Schematic representation of the DNA sequences of *ALBA3* and *ALBA4*, coding sequences are shown in dark red and UTRs in pale red. Boxes indicate the region used to generate dsRNA against both *ALBA3/4* (blue box) or single RNAi against either *ALBA3* (green box) or *ALBA4* (orange box). The cartoon was drawn to scale, the number of base pairs is represented as scale. (B) Semi-quantitative RT-PCR of strains Lister 427 WT versus *ALBA3*^{RNAi} and *ALBA4*^{RNAi} non-induced or induced for 3 days. Primers were specific for either *ALBA4* (A4), *ALBA3* (A3) or the control *ODA7* (c). 50 ng of RNA were used for the assay and its DNA-free state verified in a PCR assay without reverse trancriptase (-c). (C) Growth curves of the single RNAi cell lines measured during 7 days. *ALBA3*^{RNAi} curves in green and *ALBA4*^{RNAi} in orange (dark colours correspond to the non-induced state, light colours indicate induced cells). (D) Western blot with the anti-ALBA3/4 antibody to assess ALBA protein levels in the single RNAi cell lines, non-induced and induced with tetracycline for 3 days, versus the WT strain Lister 427. The expected position of the proteins is indicated on the right. 2 µg of total protein were loaded per lane and the loading control is the PFR protein detected with the L13D6 antibody.

We verified the silencing efficiency in western blot using the anti-ALBA3/4 antibody that recognized both proteins (Fig 3.18D). In the *ALBA4*^{RNAi} samples, the amount of protein in the non-induced state was comparable to a wild-type cell line and silencing of ALBA4 was achieved after 3 days of induction without altering the amount of ALBA3. In the *ALBA3*^{RNAi} samples, the levels of the ALBA3 protein were reduced to half the amount in the non-induced

cells and tetracycline induction did not lead to a further knock-down. However, the PFR control for these samples indicated that a lower amount of total protein was loaded. Nevertheless, the amount of ALBA4 in the *ALBA3*^{RNAi} samples is comparable to that of the wild-type (Fig 3.18D).

To verify these results obtained by western blot, we performed IFA with the anti-ALBA antibodies and used the anti-DHH1 staining as internal control (Fig 3.19).

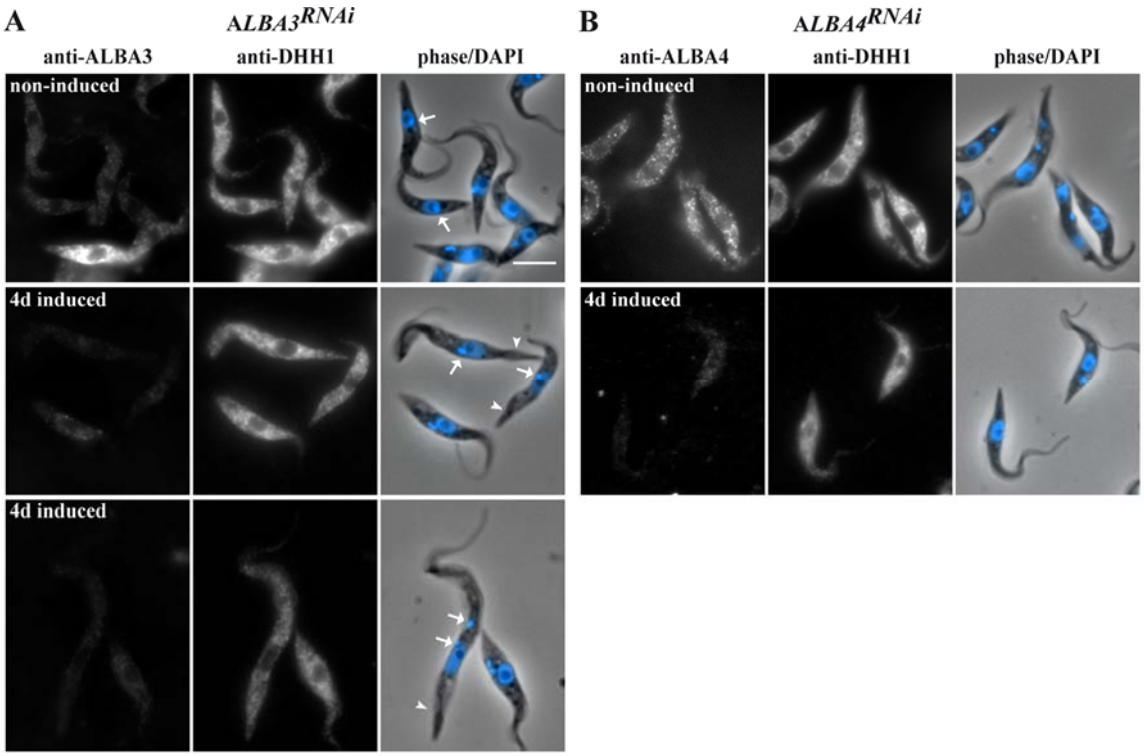

Figure 3.19: Silencing of ALBA led to phenotypes in the *ALBA3*^{RNAi} cell line. (A) *ALBA3*^{RNAi} and (B) *ALBA4*^{RNAi} cells non-induced or induced for 4 days were analysed by IFA with the anti-ALBA3 (for the *ALBA3*^{RNAi}) and the anti-ALBA4 (for the *ALBA4*^{RNAi}). We stained the cells with the anti-DHH1 as control and with DAPI (in blue merged with the phase contrast image). The scale bar represents 5 µm. Morphogenetic phenotypes in the *ALBA3*^{RNAi} cell line are indicated by arrowheads (nozzle, long posterior) and arrows (wrong positioning of the kinetoplast: anterior or juxtaposed anterior).

As seen for the *ALBA3/4*^{RNAi}, DHH1 level remained constant. Experiments with the anti-ALBA3 showed that in the *ALBA3*^{RNAi} non-induced population, the level of ALBA protein was already down-regulated in a high proportion of the cells and that this proportion was not considerably higher in the induced state. This is in agreement with the western blot result. Some of the cells devoid of ALBA3 signal showed the phenotypes already observed after silencing ALBA3/4: posterior elongation and nucleus repositioning (Fig 3.19A). Cells of the *ALBA4*^{RNAi} cell line were stained with the anti-ALBA4 antibody in IFA. The signal generated by this antibody was weak in the non-induced cells and disappeared almost completely in

cells induced for 4 days. Cells devoid of ALBA4 did not show a visible cellular phenotype (Fig 3.19). These results suggest that ALBA3 and not ALBA4 knock-down was responsible for the phenotypes observed in the *ALBA3/4*^{RNAi} cell line, but due to the leakiness of RNAi in the *ALBA3*^{RNAi} cell line and the fast generation of revertant cells (described in (Chen et al., 2003)), its investigation was not further pursued.

3.1.5 ALBA3/4 expression during parasite development in the fly

3.1.5.1 Analysis of ALBA protein levels in *ex vivo* trypanosomes by IFA

The observations made from the *ALBA3/4*^{RNAi} and *ALBA3*^{RNAi} cell line suggest that ALBA knock-down is mimicking some of the typical changes happening in cells that undergo a trypomastigote to epimastigote differentiation during trypanosome development in the anterior midgut of a tsetse fly: elongation by active polymerization of microtubules at the posterior end, relocation of the nucleus to the posterior side of the kinetoplast and cell cycle arrest. However, this differentiation step is not reproducible in the laboratory. In order to assess ALBA protein levels *in vivo* during the parasite cycle, tsetse flies were fed with procyclic parasites of the AnTat1.1 strain. Flies were dissected at various time-points of infection and the obtained parasites were fixed in PFA to perform IFA with the anti-ALBA3 antibody (Fig 3.20). DNA was stained by DAPI allowing assessment of kinetoplast and nucleus position and thus unambiguous determination of the parasite cycle stage (Rotureau et al., 2011a; Sharma et al., 2008).

The procyclic form (PC) obtained from the fly midgut showed a cytoplasmic ALBA staining equivalent to that observed with the cultured form (Fig 3.20A). As the cell elongated to differentiate into the non-proliferative mesocyclic trypomastigote form (MS), no visible changes in ALBA signal intensity or profile were detected (Fig 3.20B). The following stage in the parasite cycle, the mesocyclic to epimastigote form (MS-E) is found mainly in the proventriculus of the fly. These forms do not proliferate and are characterized by an elongated nucleus migrating towards the posterior end of the cell. The MS-E parasites showed highly reduced ALBA level (Fig 3.20C-E,K,M). Cells having adopted the epimastigote configuration duplicate their kinetoplast and proceed to mitosis, leading to the asymmetrically dividing epimastigote form (DE) that also showed low ALBA abundance (Fig 3.20F,K). After an asymmetric division into a long (LE) and a short epimastigote (SE), the short form reacquired ALBA signal whereas the LE remained negative (Fig 3.20G,H,L).

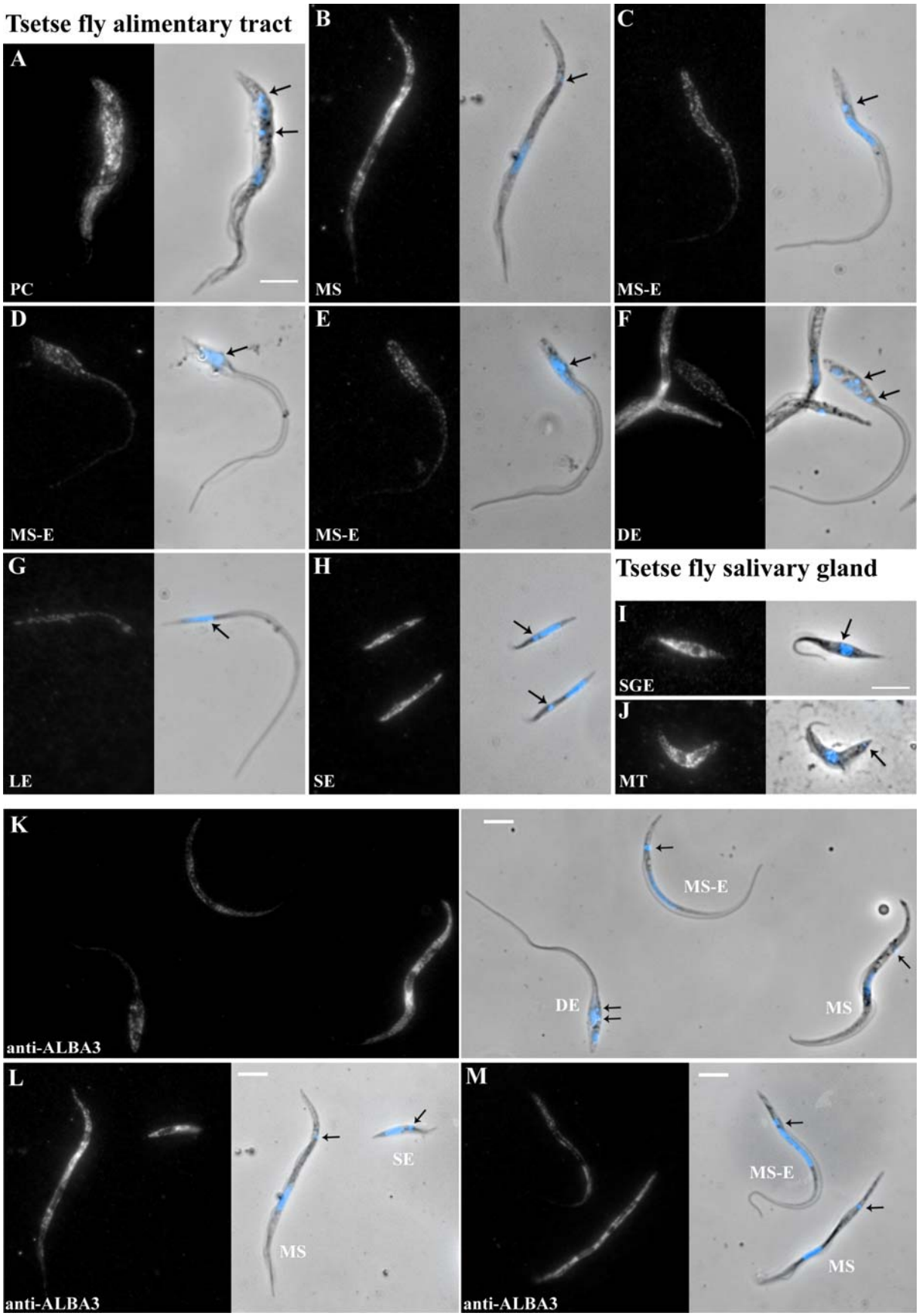

Figure 3.20: ALBA3/4 expression level during parasite development in the tsetse fly. Evolution of ALBA3/4 expression level assessed by IFA with the anti-ALBA3 antibody (left panel) and counterstained with DAPI (in blue on the phase contrast image). (A-H) ALBA signal in AnTat1.1 parasites derived from the digestive tract and

(I-J) salivary glands of the tsetse fly. (K-M) Fields of parasites in different developmental stages in the proventriculus. Fluorescent signal was normalized by setting the PC maximal signal intensity as 100% in all acquired images (in parasites on the same slide). (A-J) Cells are shown in the order of appearance during the infection cycle in the tsetse fly: procyclic (PC), mesocyclic trypomastigote (MS), parasites in transition from mesocyclic trypomastigote to epimastigote (MS-E), asymmetrically dividing epimastigote (DE) into a long (LE) and a short epimastigote (SE), salivary gland epimastigote (SGE) and metacyclic (MT). Scale bars represent 5 µm (scale bar in A is the same in A-H, scale bar in I is the same in J), arrows indicate the localization of kinetoplasts.

All the forms in the salivary glands were positive for ALBA: the salivary gland epimastigotes (SGE) (Fig 3.20I) and the infective metacyclic trypomastigote parasites (MT) (Fig 3.20J). These data indicate a precise control of at least ALBA3 during trypanosome development in the fly.

In order to validate the drop of ALBA we searched for an internal control protein that also shows cytosolic localization and stays stable during differentiation, but in the literature no such proteins have been reported. We decided to use the DHH1 protein as possible candidate for several reasons. First, we showed that DHH1 protein abundance is not influenced by ALBA down-regulation at least in the procyclic form. Second, DHH1 is an RNA-binding protein as we hypothesized for ALBA so it is interesting to investigate its abundance during development in the tsetse fly. After co-staining with the anti-ALBA3 antibody we assessed signal intensities produced by the antibodies in the different trypanosome forms in the fly (Fig 3.21). In the ImageJ software the whole cell (on the phase contrast image) was determined as a region of interest (ROI) and mean signal intensities of ALBA and DHH1 were then calculated by the program within this ROI on the fluorescence images. Although only low numbers of parasites could be analysed, the results confirmed the observed drop of ALBA signal in the MS-E, DE and LE cells and also the re-emergence of ALBA signal in the SE. In contrast, the cells found in the salivary glands showed an ALBA signal comparable to MS-E cells (Fig 3.21 dark grey bars). To visualize the evolution of DHH1 signal versus ALBA signal in the different forms we calculated the ratio of the mean signal intensities (Fig 3.21 light grey bars). It revealed an ALBA/DHH1 ratio of 1.6-1.8 in midgut and proventricular stages, with the exception of SE, where the ratio goes up to 2.4. In all stages found in the salivary glands ALBA signal intensity was comparable to that of DHH1. Thus, we could not use the DHH1 protein as negative control protein in this set of experiments, as its abundance seemed to follow the pattern of ALBA proteins during the trypo- to epimastigote transition.

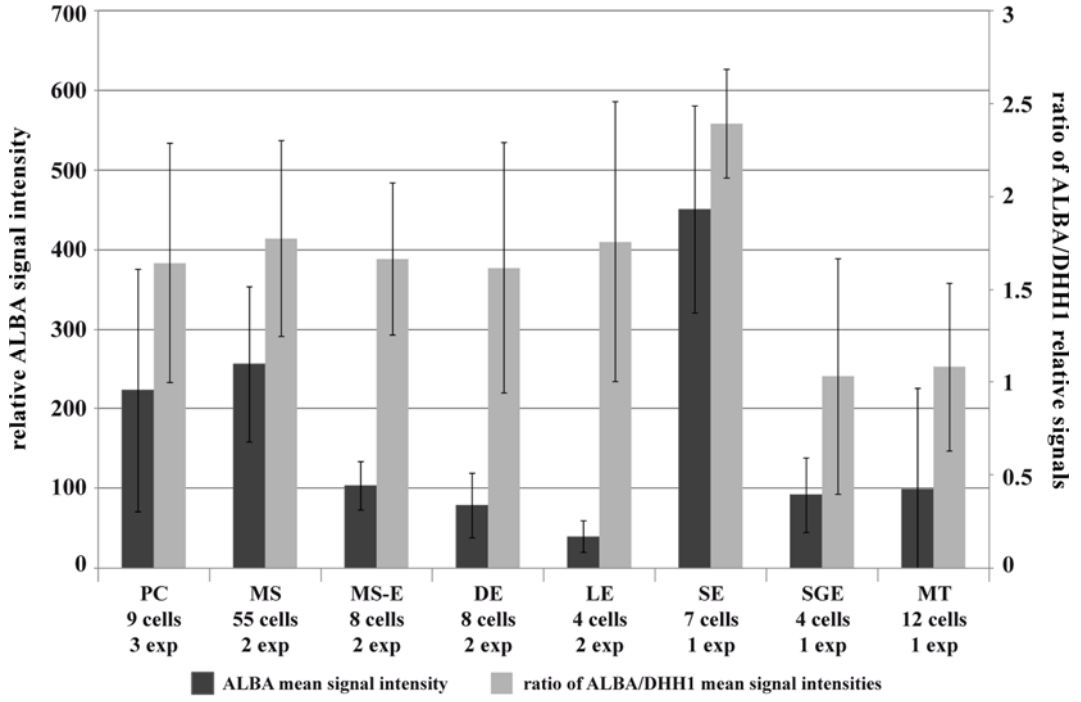

Figure 3.21: Signal intensities of ALBA and DHH1 in parasite stages in the tsetse fly. Data were obtained on measurements on cells by IFA with the anti-ALBA3 and anti-DHH1 antibodies. In dark grey: ALBA mean signal intensities, values on the left y-axis. In light grey: ratio of ALBA/DHH1 mean signal intensities, right y-axis. The parasite stage, the number of cells analysed in the number of different experiments is shown. Parasite stages: procyclic (PC), mesocyclic trypomastigote (MS), parasites in transition from mesocyclic to epimastigote (MS-E), asymmetrically dividing epimastigote (DE) into a long (LE) and a short epimastigote (SE). In the salivary glands: salivary gland epimastigote (SGE) and metacyclic (MT).

Although we obtained useful information by the IFA technique and signal measurements, we realized that higher cell numbers were needed to better quantify ALBA signal intensities. Only low numbers of parasites could be analysed, as ALBA3 and ALBA4 require the use of PFA fixation and cells of some parasite stages fixed in these conditions do not adhere well on microscope slides. In addition, most trypanosome stages found in the tsetse fly are only present in low numbers that makes statistical analysis difficult. Finally, antibody accessibility could be different depending on the properties of particular stages and the degree of elimination of other contaminants (bacteria and tissue) before fixation and IFA. To overcome the technical limitations, we decided to work with live cells expressing ALBA::YFP fusion proteins.

3.1.5.2 Analysis of ALBA::YFP fusion protein levels in *ex vivo* trypanosomes

Tsetse flies were fed with either one of the ALBA::YFP AnTat1.1 cell lines (the comparable Lister427 cell lines are shown in Fig 3.2) and dissected at different time points of infection. For both strains, the rates of infection in the midgut (MG) and salivary glands (SG) were comparable with the parental WT AnTat1.1 strain (control MG 40%, SG 10.7%; ALBA3::YFP MG 54%, SG 10.3%; ALBA4::YFP MG 33%, SG 11%). The expression of the ALBA fusion proteins in trypanosomes *ex vivo* was first verified by observing the direct YFP signal in fixed parasites. Figure 3.22 shows a typical example of ALBA3::YFP cells released from the proventriculus of an infected fly: mesocyclic parasites showed strong ALBA signal, in contrast to the mesocyclic to epimastigote forms. In this experiment, parasites were released from fly tissues into PBS, demonstrating that the formation of cytoplasmic starvation granules also occurs in parasites issued from an infection. We avoided starvation conditions in subsequent analyses of ALBA fluorescent cell lines by releasing parasites directly into culture medium.

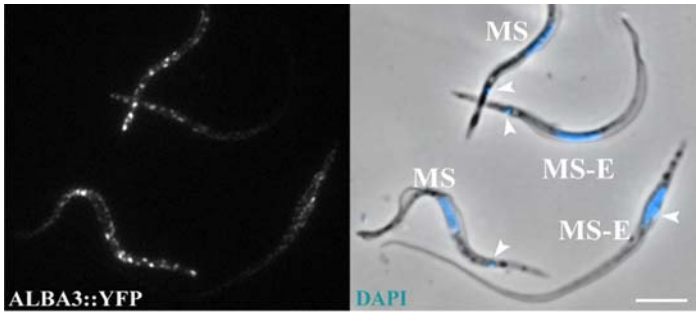

Figure 3.22: Starvation granules in parasites issued from fly infection. Trypanosomes of the strain AnTat1.1 expressing endogenous ALBA3::YFP, derived from the tsetse proventriculus were released in PBS, fixed and stained with DAPI. Scale bar represents 5 µm and arrowheads indicate the localization of the kinetoplast. Parasite stages: mesocyclic trypomastigote (MS), cells in transition from mesocyclic to epimastigote (MS-E).

As endogenous ALBA fusion protein expression reflected the results obtained by IFA, the aim was to monitor the ALBA expression profile by live video microscopy. However, one has to remember that parasites can only be seen upon dissection and that after fly sacrifice trypanosomes only survive for a limited amount of time, restricting the time window for analysis. We selected to acquire images by analogue video recording. This is not a digital system and therefore absolute quantification cannot be performed but three categories of cells can be clearly visually defined: negative (-), positive (+), and bright (++). By this mean, it was possible to analyse a sufficiently large number of cells not reachable otherwise (1216 for ALBA3::YFP and 775 for ALBA4::YFP issued from two and one independent infection experiments respectively). The differentiation stage was determined by imaging the phase

contrast (for morphology) coupled with DNA staining by DAPI, a dye that penetrates easily in live trypanosomes.

Movie 3 shows representative cells for each parasite stage of ALBA3::YFP found in the fly, and movie 4 shows fields of cells of the same strain to illustrate how relative fluorescence intensity was evaluated. Still images of movie 3 were extracted and are shown in Figure 3.23. Fluorescence in ALBA4::YFP parasites was assessed in movie 5 and still images are presented in Figure 3.24.

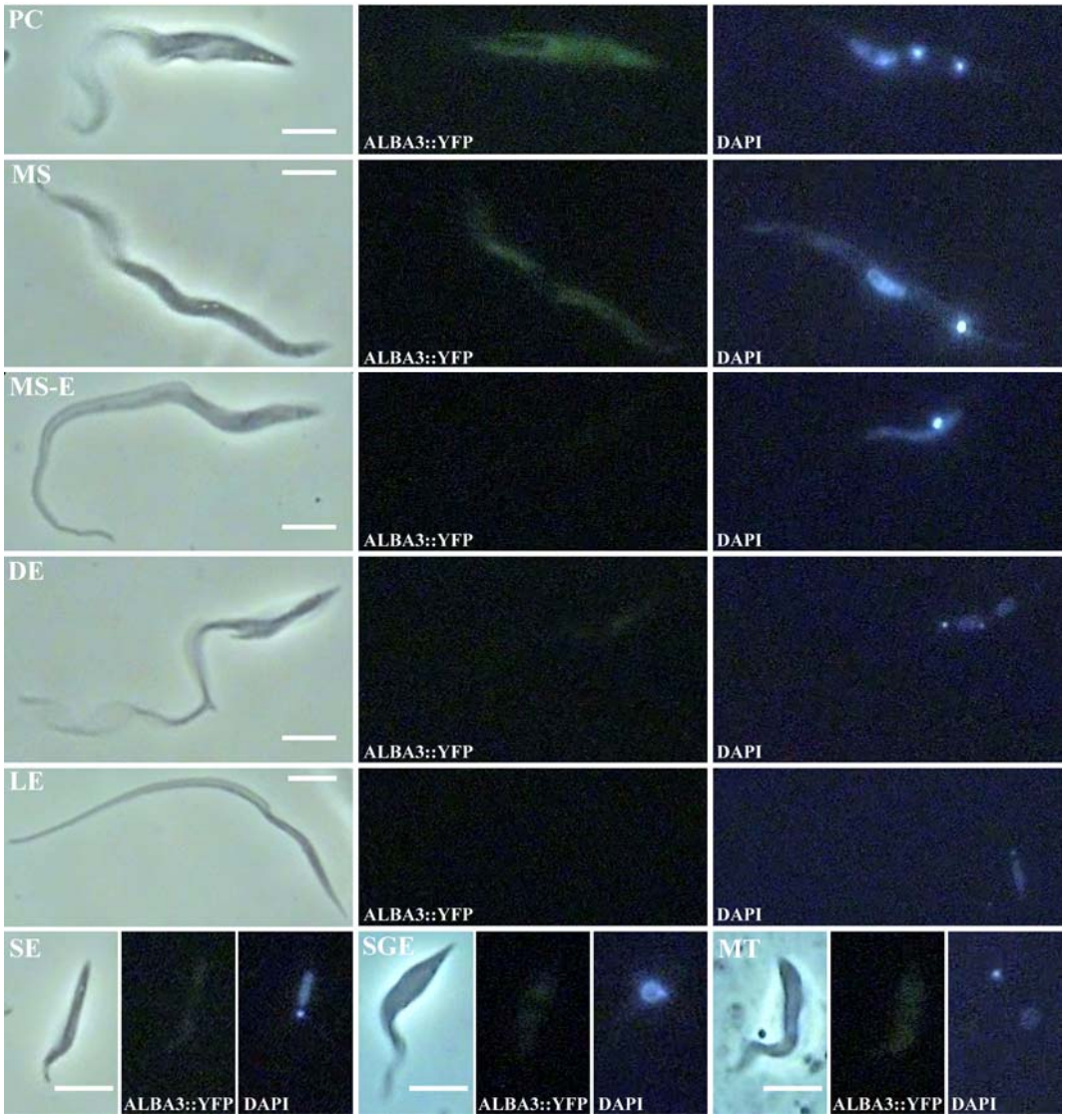

Figure 3.23: Level of ALBA3::YFP in different stages during development in the fly. Still images of movie 3 were extracted for each parasite stage in the fly. Left panel: phase contrast, middle panel: ALBA3::YFP signal and right panel: DAPI staining. Scale bars represent 5 µm.

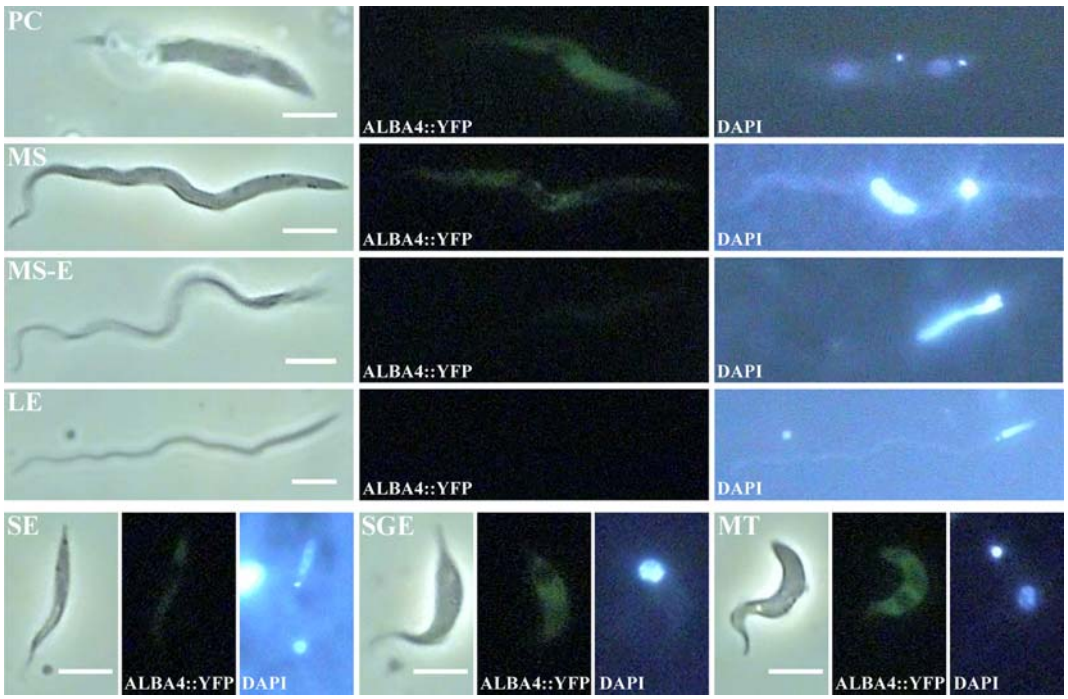

Figure 3.24: Level of ALBA4::YFP in different stages during development in the fly. Still images of movie 5 were extracted for each parasite stage in the fly. Left panel: phase contrast, middle panel: ALBA4::YFP signal and right panel: DAPI staining. Scale bars represent 5 µm.

All ALBA3::YFP cells showed a bright fluorescent signal at the procyclic stage (PC) while the parasites at the mesocyclic stage (MS) were more heterogenous (40% bright and 60% positive green cells) (Fig 3.25A). The ALBA3 fluorescence intensity dropped further during the transition of the trypo- to epimastigote form, with almost 80% of the MS-E parasites being negative. This was even more pronounced in the dividing epimastigote (DE) form (more than 90% of ALBA3::YFP negative cells) (Fig 3.25A). The ALBA signal was recovered in the short epimastigotes (SE) whereas long epimastigotes (LE) remained negative, confirming the IFA data. Finally, all trypanosome forms found in the salivary glands were positive for ALBA3 (Fig 3.25A).

The expression profile of ALBA4::YFP turned out to be very similar to that of ALBA3 (Fig 3.25B), with the exception of the DE stage with 35% of positive fluorescent cells in ALBA4 versus 10% in ALBA3. This could be explained by a re-emergence of ALBA4 protein in the future SE before cytokinesis is completed, going along with the higher percentage of SE positive cells for ALBA4 versus ALBA3 (Fig 3.25B).

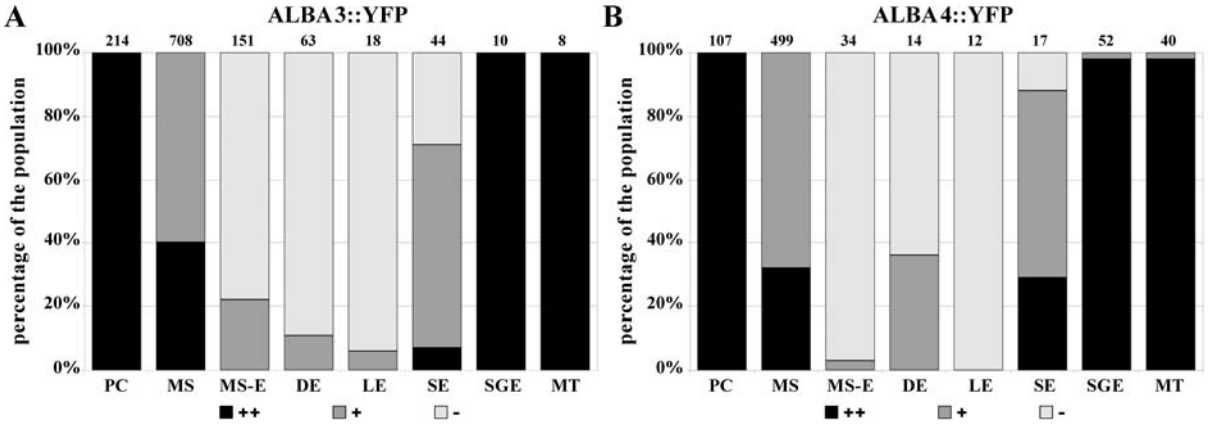

Figure 3.25: Expression profile of ALBA3::YFP and ALBA4::YFP in parasites issued from fly infection. Percentage of strong (black), positive (dark grey) and negative cells (light grey) in the different stages of the parasite cycle of AnTat1.1 parasites expressing endogenously tagged (A) ALBA3::YFP and (B) ALBA4::YFP obtained upon tsetse fly dissection. For ALBA3::YFP, data are the sum of two separate infection experiments (total of 168 flies, 68 were dissected) whereas a total of 93 flies (36 dissected) were used for ALBA4::YFP in one infection experiment. Analysis was performed on live cells and the number of counted cells is indicated on top of the bars. Cells are shown in the order of appearance during the infection cycle in the tsetse fly: procyclic (PC), mesocyclic trypomastigote (MS), parasites in transition from mesocyclic trypomastigote to epimastigote (MS-E), asymmetrically dividing epimastigote (DE) into a long (LE) and a short epimastigote (SE). In the salivary glands: salivary gland epimastigote (SGE) and metacyclic (MT).

Taken together, the combination of IFA and live video microscopy analysis showed a defined expression profile of ALBA3 and ALBA4 proteins during the trypanosome parasite cycle, marked by a significant drop when parasites change from trypo- to epimastigote conformation in the proventriculus region.

3.1.6 Consequences of ALBA3/4 over-expression on trypanosome development

3.1.6.1 Procedure for over-expression of ALBA3 or ALBA4

To understand the significance of the down-regulation of ALBA3/4 in the proventricular stages, we selected to over-express these proteins. However, regulatory elements required for specific expression at these particular stages are unknown. Hence, we selected to constitutively over-express individual ALBA3 or ALBA4 proteins using the pHD67E vector which had been reported to confer GFP reporter expression throughout the parasite cycle (Bingle et al., 2001). This construct was targeted to the *rDNA* locus and the reporter GFP protein was expressed under the control of the EP procyclin promoter. Either *ALBA3* or *ALBA4* coding region was fused upstream of the *GFP* gene into this vector. The expression as

GFP fusion was necessary to control the level of over-expression in individual cells during parasite development in the fly as western blot was not achievable at the stage-specific level. Procyclic trypanosomes of the AnTat1.1 strain were transfected with the plasmid pHD67E as control or with pHD67EALBA3 and pHD67EALBA4.

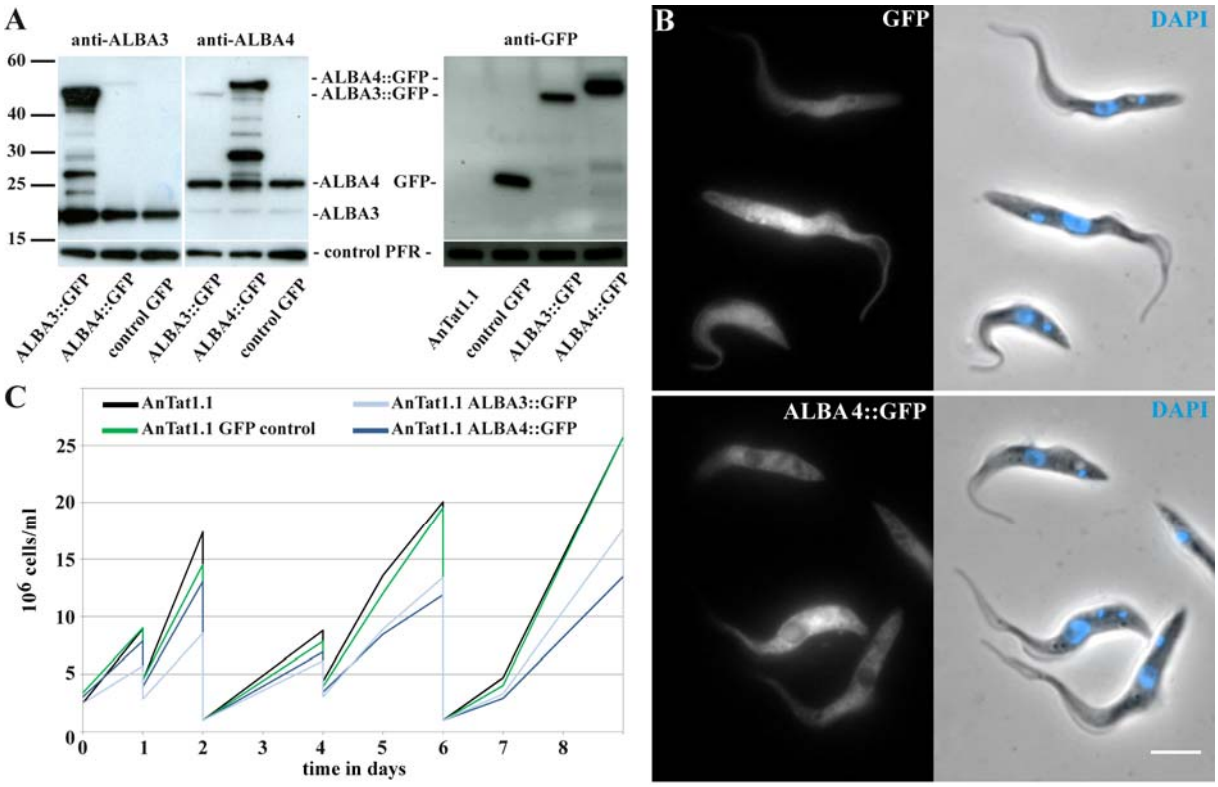

Figure 3.26: ALBA3 and ALBA4 over-expression in AnTat1.1 procyclic form in culture. (A) Western blots with 2 µg of total protein samples of WT AnTat1.1 cells, carrying a *GFP* gene (control GFP) or an extra copy of either *ALBA3::GFP* or *ALBA4::GFP*. Blots were incubated with a specific anti-ALBA3 antibody to detect the endogenous ALBA3 (expected molecular weight 21 kDa) and the ALBA3::GFP (46 kDa) protein (left), with a specific anti-ALBA4 antibody to detect the endogenous ALBA4 (25 kDa) and the ALBA4::GFP (50 kDa) protein (middle) or an anti-GFP antibody to reveal the control GFP protein (right panel) and the ALBA::GFP fusion proteins. A weak cross-reactivity of the anti-ALBA antibodies is visible. The anti-PFR antibody L13D6 was used as a loading control. (B) Procyclic cells of the strain AnTat1.1 in culture expressing either GFP or exogenous ALBA4::GFP were fixed in PFA and counterstained with DAPI (direct fluorescence on the left, phase contrast image and DNA in blue on the right, scale bar represents 5 µm). (C) Cell growth of the AnTat1.1 WT (parental strain, black curve), GFP control (green curve), *ALBA3::GFP* (light blue curve) or *ALBA4::GFP* (dark blue curve) cell lines.

Protein expression levels were first analysed by western blot in cultured procyclic cells using the specific anti-ALBA3 or anti-ALBA4 antibodies (Fig 3.26A). Fusion proteins exhibited the expected electrophoretic mobility and their abundance appeared to be equivalent to the endogenous ALBA3 or ALBA4, meaning that these cells were over-expressing at least two-

fold the amount of ALBA3 or ALBA4 compared to non-transfected cells. This exogenous expression of ALBA::GFP did not lead to a down-regulation of the endogenous ALBA protein, but additional protein bands of intermediate size were detected with both the anti-ALBA3 and anti-ALBA4 antibodies (Fig 3.26A), possibly corresponding to degradation products of the fusion protein, a feature not seen with the endogenous tagging experiments (Fig 3.2B,C). To compare the expression levels between cell lines, protein samples were probed with an anti-GFP antibody (Fig 3.26A). ALBA4::GFP was expressed to a level comparable to the control GFP whereas ALBA3::GFP turned out to be less abundant, despite the use of the same expression system (Fig 3.26A). In the GFP control cells, direct observation of fluorescence in live or fixed cells revealed that GFP was expressed and that the signal was detected in the cytoplasm as well as in the flagellum and in the nucleus (Fig 3.26B). In contrast, ALBA3::GFP and ALBA4::GFP fusion proteins were found exclusively in the cytoplasm (shown for ALBA4::GFP in Fig 3.26B). The growth in culture of the control GFP cell line was comparable to the parental AnTat1.1 cell line while the ALBA3 and ALBA4::GFP expressing cell lines showed slightly slower growth (Fig 3.26C).

3.1.6.2 ALBA3/4 over-expression during trypanosome development in the fly

Several groups of flies were infected with each of the strains and dissection was undertaken at late time points (days 25-30), when control infections should have reached maturity in the salivary glands. Infection rates were obtained by grouping data of nine independent experiments. For the GFP control strain, 52% of the flies showed midgut infections and salivary gland infections were detected in 12% of the flies, which corresponds to the levels observed in our laboratory for the AnTat1.1 wild type strain (Rotureau et al., 2011a) (Fig 3.27). One third of the established infections in the midgut led to a mature salivary gland infection. The ALBA3::GFP strain turned out to be as efficient as the control in developing midgut infections (53%) (Fig 3.27). The level of salivary gland infections was lower (6%, meaning that only 10% of the established infections in the midgut led to a mature infection in the fly saliva). Although this lower infection rate was not statistically significant, each of these flies showed an unusually high number of midgut parasites in comparison to other midgut infections observed for the same cell line (Fig 3.27). For the ALBA4::GFP strain, 50% of the flies were infected in the midgut and 17% showed parasites in the salivary glands, being very close to the control situation with one third of midgut infections leading to a mature development (Fig 3.27).

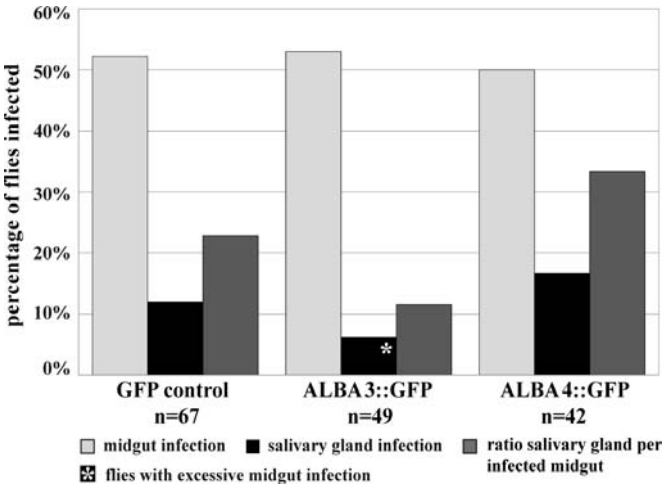

Figure 3.27: Fly infection rates of the ALBA::GFP over-expressing strains. Percentage of flies infected in the midgut (light grey bars) or the salivary glands (black bars) when challenged with AnTat1.1 cells expressing GFP control (sum of 7 infection experiments, 214 flies), ALBA3::GFP (sum of 6 infection experiments, 155 flies) or ALBA4::GFP (sum of 3 infection experiments, 143 flies)(n = number of dissected flies). Infections with the ALBA3::GFP cell line in the salivary glands were only observed in flies with a highly infected midgut (indicated by a star). The dark grey bars indicate the ratio of salivary gland infection per parasitized midgut.

Live trypanosomes from all three strains were investigated by video microscopy and scored as described for the endogenously expressing ALBA::YFP cell lines. Movie 6 shows fields of mesocyclic parasites from each strain to illustrate relative fluorescence intensities. Still images are shown in Figure 3.28.

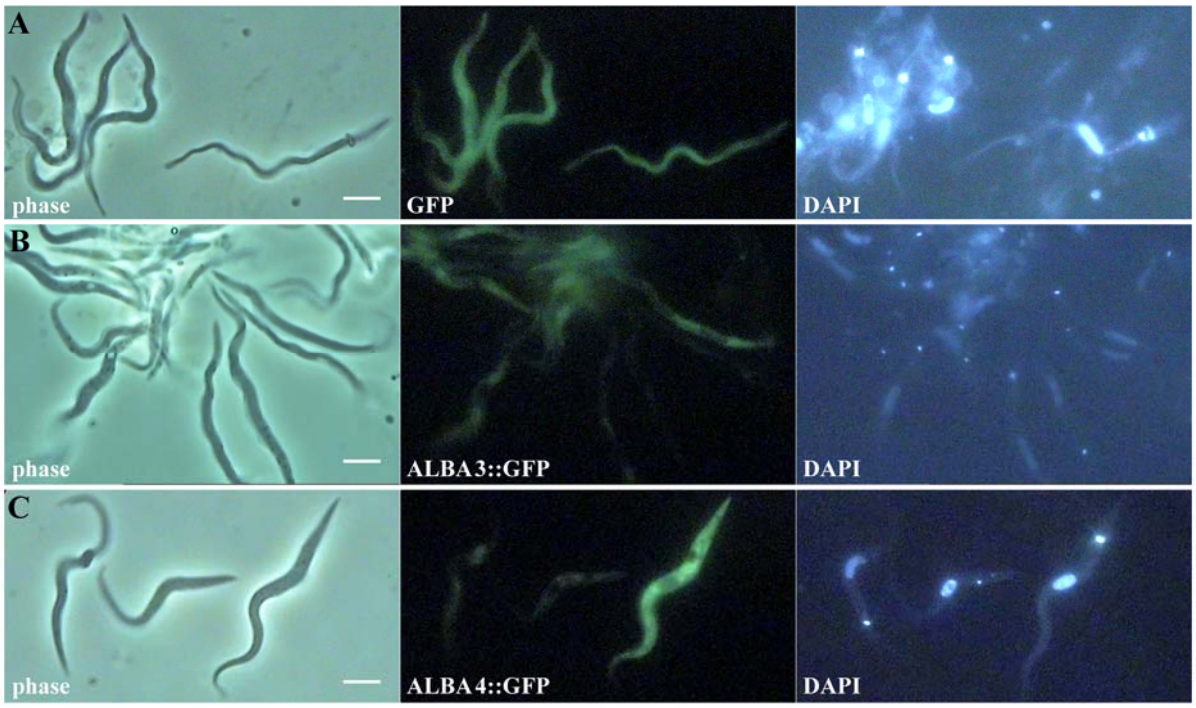

Figure 3.28: Mesocyclic parasites of GFP control and ALBA::GFP over-expressing cell lines. Representative fields of mesocyclic parasites of the (A) GFP control, (B) ALBA3::GFP and (C) ALBA4::GFP strains. Left panels: the phase contrast of each field, middle panels: the recorded green fluorescent signal and right panels: DAPI shows DNA content and localization. Scale bars represent 5 µm.

Starting with a high proportion of green fluorescent procyclic parasites (78 to 98%) in all three cases, the green signal evolved differently during progression in the parasite cycle (Fig 3.29). In the GFP control cell line, 80% of the cells were strongly positive at the midgut PC or MS stages and negative parasites were rare (Fig 3.29A). The general trend in all proventricular stages was a drop in the proportion of strongly positive parasites, but the abundance of GFP negative parasites remained constantly low around 20%. Cells in the salivary gland were positive in most cases (SGE and MT). In summary, the reporter GFP protein was present in 80 to close to 100% of the cells in all stages of the parasite cycle, although its abundance was variable (Fig 3.29A).

In contrast to the endogenous tagging experiments, different results were obtained for cells over-expressing ALBA3::GFP or ALBA4::GFP (Fig 3.29B,C). Parasites resulting from an infection with the ALBA4::GFP strain were expressing the GFP fusion protein to a high level in the majority of the cells, whereas negative parasites were a minority in all stages investigated, with the exception of long epimastigotes, a profile quite similar to the expression of the control GFP alone (Fig 3.29C). In contrast, proventricular parasites resulting from ALBA3::GFP infections showed a higher proportion of negative cells: 35% for the MS-E and up to 47% for the DE whereas the percentage of positive SE was comparable to the results obtained for ALBA4::GFP (Fig 3.29B). Only a few cells could be analysed in the salivary glands due to reduced infection levels, but all turned out to be negative or weakly positive (Fig 3.29B). These results show that over-expression of the ALBA4 protein as GFP fusion is maintained in each stage during progression of the parasite cycle without impairing the rate of fly infectivity. In contrast, although using the same expression system, the ALBA3::GFP protein appears to be down-regulated at the transition from trypo- to epimastigote stage in a pattern similar to the endogenous ALBA3 protein. Moreover, parasites expressing large amounts of ALBA3::GFP proteins were not observed in the salivary glands (Fig 3.29B), suggesting that strong over-expressers cannot complete the final part of the parasite cycle.

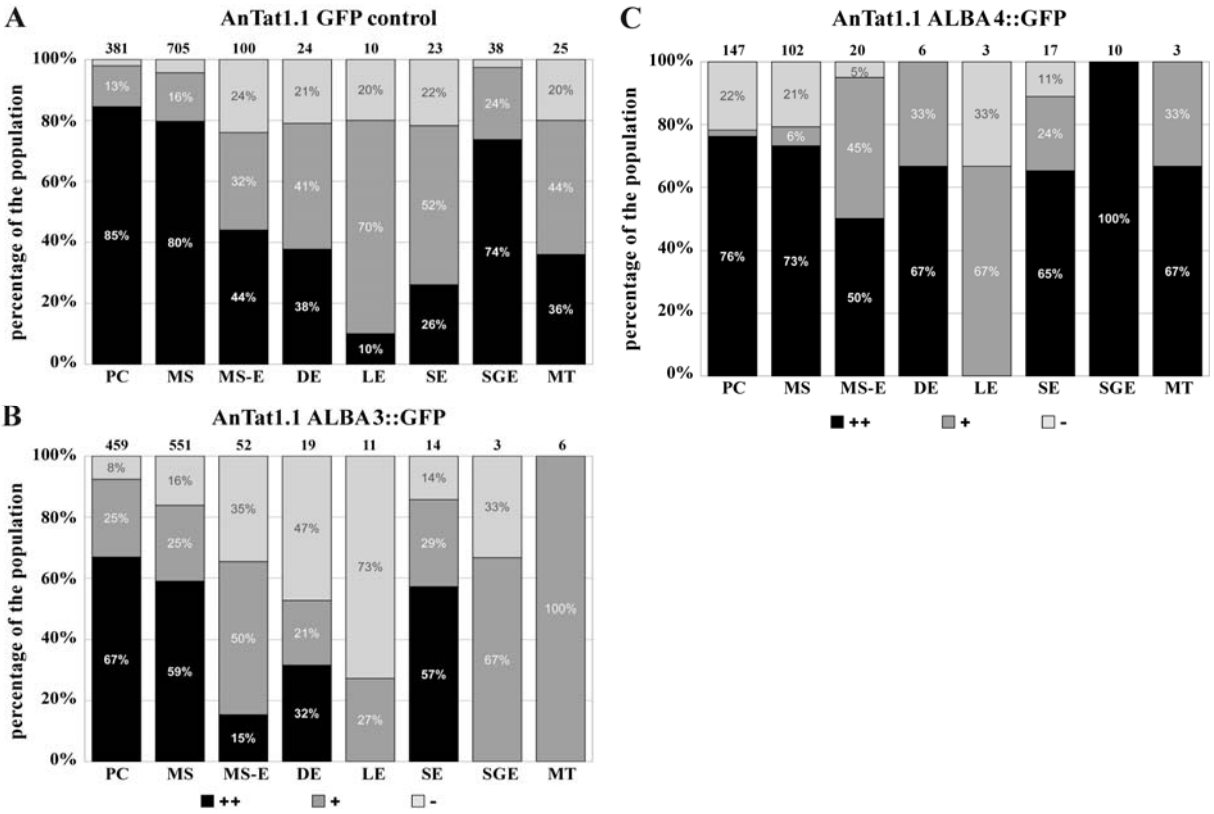

Figure 3.29: Evolution of GFP control and ALBA::GFP signal during parasite development. Percentage of bright (black), positive (dark grey) and negative cells (light grey) in the populations of each stage of AnTat1.1 parasites expressing GFP alone (A), ALBA3::GFP (B) or ALBA4::GFP (C) during the course of infection. Analysis was performed on live movies of trypanosomes filmed directly upon fly dissection and the number of counted parasites is indicated on top of the bars. Data are the sum of all independent infection experiments (GFP control: 67 flies from 7 experiments, ALBA3::GFP: 49 flies from 6 experiments and ALBA4::GFP: 42 flies from 3 experiments).

3.1.6.3 ALBA3 over-expression perturbs the progression in differentiation

During the live video analysis of the ALBA3::GFP cells (but not of the GFP control nor in the ALBA4::GFP strain) in the proventriculus, our attention was attracted by a significant proportion of parasites that showed atypical cell diameter and DNA organelle positioning (Movie 7 and Fig 3.30).

In order to characterize this atypical population, we measured several morphometric parameters: the length of the parasite (from the posterior end of the cell to the tip of the flagellum), the cell diameter, the distance between kinetoplast and nucleus centres as well as the length of the nucleus. To avoid artefacts potentially caused by fixation methods, this analysis was performed on cells from the live movies of the GFP control and the ALBA3::GFP parasites (Fig 3.30).

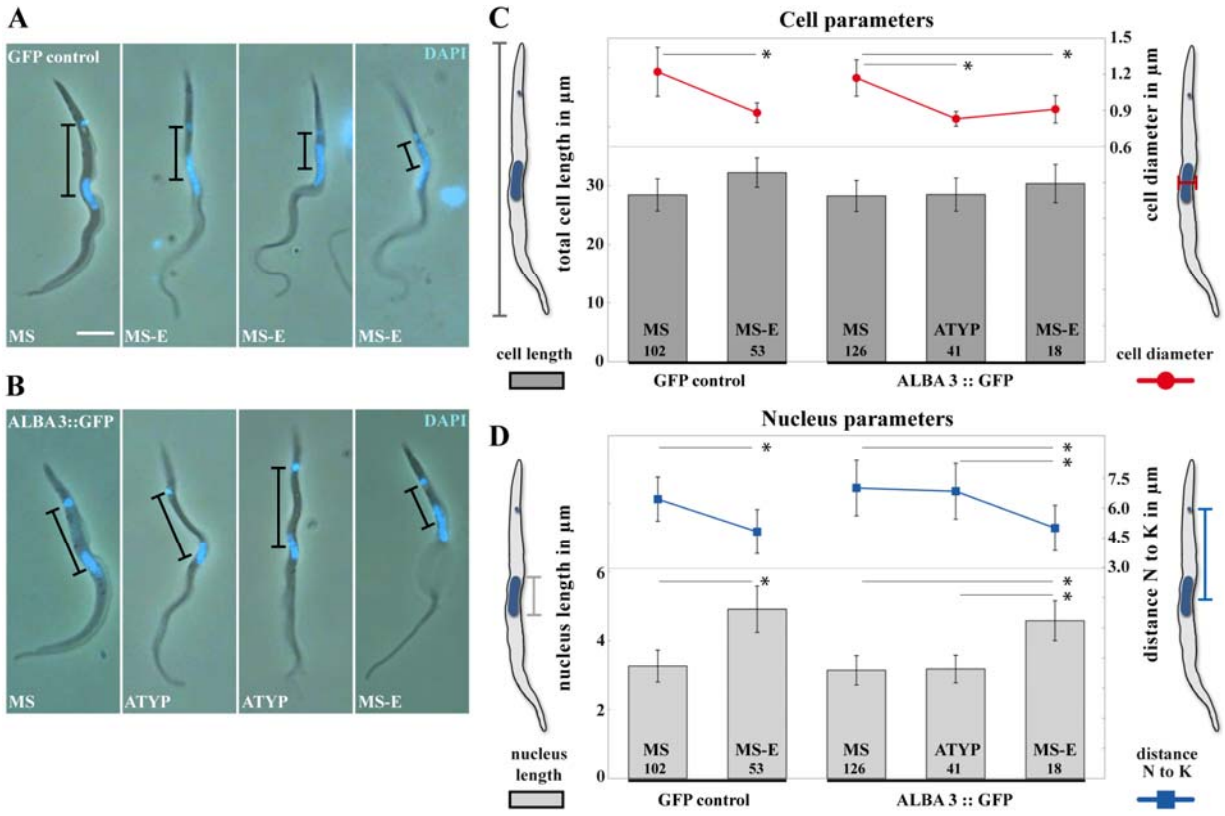

Figure 3.30: Characterization of the transition from mesocyclic to epimastigote in the GFP control and the ALBA3::GFP expressing strain. Still images extracted from movies of cells of the AnTat1.1 strains expressing (A) GFP control or (B) ALBA3::GFP after fly dissection. Phase images were superimposed with the fluorescent DAPI signal in blue. Black bars indicate the distance between the nucleus and the kinetoplast. Scale bar represents 5 µm. (C) Cellular and (D) nuclear parameters in MS, MS-E and ATYP (atypical forms found in ALBA3::GFP infected flies only). Numbers of analysed parasites are indicated in the bars. (C) On the left axis, the total cell length is plotted as dark grey bars (µm ± SD) and on the right axis the cell diameter is shown as red curve (µm ± SD). (D) On the left axis, the nucleus length is plotted as light grey bars (µm ± SD) and on the right axis the distance between the nucleus and the kinetoplast centres is shown as blue curve (µm ± SD). ANOVA tests were performed and significant comparisons by Tukey ad hoc post-tests are indicated on the histogram with * $P < 0.0001$.

Two populations were identified in the GFP control: MS cells with a fairly large diameter (1.2 µm) and with a round-shaped nucleus positioned close to the centre of the cell (102 out of 155 analysed cells) and MS-E cells with a thinner diameter (0.9 µm) and an elongated oval nucleus undergoing migration towards the posterior end of the cell (Fig 3.30A,C,D). These two phenomena were always found to occur in parallel and were never observed uncoupled. Although typical MS (126 out of 185 analysed cells) and MS-E (18 out of 185) were present, an atypical cell type (ATYP) was also observed in the ALBA3::GFP cell line (41 out of 185) (Fig 3.30B,C,D). These cells presented a pronounced thin cell diameter (0.83 ±0.06 µm)

typical for MS-E but strikingly, despite this characteristic trait, they exhibited a non-elongated nucleus (3.18 ±0.4 µm versus 4.58 ±0.58 µm in MS-E) whose position was more anterior compared to that observed in MS-E (Fig 3.30C,D). The distance to the kinetoplast was 6.84 ±1.40 µm instead of 5.0 ±1.14 µm (Fig 3.30D).

In conclusion, this atypical form encountered in the ALBA3::GFP over-expressing strain displayed the morphology of an MS-E regarding the cell diameter but the nucleus length and its distance to the kinetoplast was found to be comparable to the mesocyclic form. This suggests that the presence of the ALBA3::GFP protein delayed or inhibited migration of the nucleus towards the posterior end of the cell during the trypo- to epimastigote transition, further strengthening the hypothesis of ALBA3 implication in this differentiation process.

3.2 Novel flagellar proteins as environmental sensory candidates

Trypanosomes encounter drastic environmental changes during their journey in the tsetse fly and the perception of these modifications is likely to trigger differentiation processes. The flagellum is proposed to represent the main sensory organelle in trypanosomes. Thus, we searched for sensory protein candidates among the proteins identified by mass-spectrometry of intact flagella. Several have not been reported so far and have no attributed functions. Most of these had not been found in the flagellar skeleton and are thus good candidates to be localized in the membrane and matrix where they could act upstream of the ALBA proteins. Some of these proteins were subjected to further analyses.

Among the hypothetical proteins identified we selected ten candidates with interesting predicted domains to study their flagellar localization. Those were named by their likely localization as flagellar membrane and matrix proteins (FLAMM). We also got particularly interested in two proteins that have already been described in the literature. First, the sensory protein PAD2 (proteins associated with differentiation) (Tb927.7.5940) that re-localizes to the cell surface upon temperature drop and acts as a citrate transporter during differentiation from stumpy to procyclic forms (Dean et al., 2009). Second, the arginine kinase (AK) protein that was already described to play a role in resistance against environmental stresses in the related parasite *T. cruzi* (Miranda et al., 2006; Pereira et al., 2003).

3.2.1 FLAMM proteins as novel flagellar proteins

3.2.1.1 Selection of the FLAMM proteins

Out of 194 proteins identified in more than three mass-spectrometry experiments, and that were absent from published flagellar proteomes, we selected ten candidates for analysis. Criteria used included the presence of interesting domains and their conservation in other species. FLAMM1-10 contain interesting domains, such as the WD40 or TPR protein-protein interaction domains, known to be over-represented in flagellar proteins (Li et al., 2004), or domains with putative sensory function such as a cNMP binding or a nucleoside diphosphate kinase domain (Table 3.1).

Table 3.1: Selection of FLAMM proteins 1-10. Indicated are the gene accession numbers in TriTrypDB (www.tritrypdb.org), the predicted protein size in kDa and the predicted domains. Homology to proteins of other species was assessed by BLAST (http://blast.ncbi.nlm.nih.gov/Blast.cgi) or by following the link to the OrthoMCL database (http://orthomcl.org) directly in the description of each protein in the TriTrypDB.

	Gene	Size	Domains	Conservation
FLAMM1	Tb927.10.7230	284	6 nucleoside diphosphate kinase domains, 1 EF-hand	orthologs in flagellates
FLAMM2	Tb927.10.7290	130	nothing recognizable	kinetoplastids
FLAMM3	Tb927.8.4780	468	1 TPR like domain, 1 antimicrobial beta defensin precursor	kinetoplastids
FLAMM4	Tb927.8.7950	191	1 LRR (leucin rich repeat) in the RNI like domain	trypanosomatids
FLAMM5	Tb09.211.4280	177	1 RNI like domain, multiple WD40 repeats	kinetoplastids
FLAMM6	Tb927.3.5020	155	3 cAMP binding like domains	kinetoplastids
FLAMM7	Tb11.01.8650	228	1 TPR like, multiple IQ (calmodulin binding) and P loop domains	kinetoplastids
FLAMM8	Tb927.2.5760	330	1 virus attachment protein globular domain	kinetoplastids and green algae *Volvox*
FLAMM9	Tb927.8.940	237	2 transmembrane domains	kinetoplastids
FLAMM10	Tb927.7.5340	56.8	1 TPR like domain	trypanosomatids

3.2.1.2 Localization studies of the FLAMM proteins

The localization studies of the FLAMM were performed together with Ms Nele Reeg, a biochemistry master student at the University of Berlin (FU), who accomplished a two-months internship under my supervision. Cell lines encoding a yellow fluorescent protein (YFP) tagged version of the selected FLAMM proteins were created and first analysed by live video microscopy. In the green channel of the microscope, a clear signal was observed in the flagellum compartment for the proteins FLAMM1-8 using the parental Lister 427 WT strain as negative control. Subtle differences in localization patterns were noted and are described below. In the case of FLAMM9 and FLAMM10, no clear signal could be detected, consistent with the absence of expression. Next, in order to determine the precise localization of each FLAMM protein, cells were fixed with PFA or methanol and direct fluorescence was assessed. In PFA fixation, the fluorescence signal was weakly detectable and localization turned out to be in the flagellar compartment for FLAMM1-8. Upon methanol fixation the fluorescent signal was almost non-detectable, presumably because a lot of the proteins were lost or because the YFP molecules were denatured upon treatment.

Therefore, we used an anti-GFP antibody in order to unambiguously detect the YFP tagged FLAMM proteins in IFA. We selected methanol fixation for the analysis, as PFA fixation preserves the volume of the cells and complicates investigation of the whole length of the

flagellum that is rarely completely in focus. In parallel, FLAMM localization was assessed after membrane extraction to determine if the proteins are tightly attached to cytoskeletal structures. To analyse the relative localization of the FLAMMs to either the axoneme or the paraflagellar rod (PFR), we co-stained the cells with the monoclonal antibody mAb25, a marker of the flagellar axoneme. The axoneme structure starts immediately after the transition zone of the basal body in close proximity to the kinetoplast, while the PFR structure is build adjacent to the axoneme once the flagellum exits the flagellar pocket and runs until its distal tip. Thus, these two structures do not co-localize in IFA but appear as two parallel lines with shifted starting points. The results obtained for the localization of the FLAMM proteins are summarized in Table 3.2 and illustrated in Figure 3.31.

The proteins FLAMM1, FLAMM2 and FLAMM7 presented a linear aspect in the flagellar compartment but did not co-localize with the mAb25 axonemal staining, indicating a PFR-like localization. The FLAMM1 protein had the particularity of showing a weaker signal at the tip of the flagellum that extends the cell body.

The YFP fusion proteins of FLAMM3, FLAMM4 and FLAMM5 showed localization in the PFR structure after methanol fixation and membrane extraction of either dotty (FLAMM3/4) or discontinuous appearance (FLAMM5). FLAMM3 was found in the PFR compartment but did not extend to the flagellar tip upon methanol fixation. The staining stopped where the flagellum attachment zone (FAZ) would stop in the cell body. Interestingly, when the cellular membrane was extracted, FLAMM3::YFP was detected as two dotty lines, presumably in the FAZ of the cell body and in the flagellum on its whole length. The FLAMM4 signal was accumulated in the new flagellum of dividing cells upon methanol fixation.

FLAMM6::YFP was mostly co-localizing with the mAb25 antibody staining but showed special features, to our knowledge, never reported so far for any protein of the trypanosome flagellum. The bright staining of the FLAMM6 protein started with the axoneme at the basal body. It was observed up to the middle of the flagellum where the signal gradually disappeared and the distal half of the flagellum was negative. In dividing cells, the new flagellum stained equally for FLAMM6 in comparison to the old one, no matter its length.

FLAMM8::YFP also showed a very unusual pattern: its staining was restricted to the extreme distal tip of the flagellum. The signal was not lost upon membrane extraction and remarkably, in dividing cells, the new flagellum did not show FLAMM8 signal until it reached a certain length.

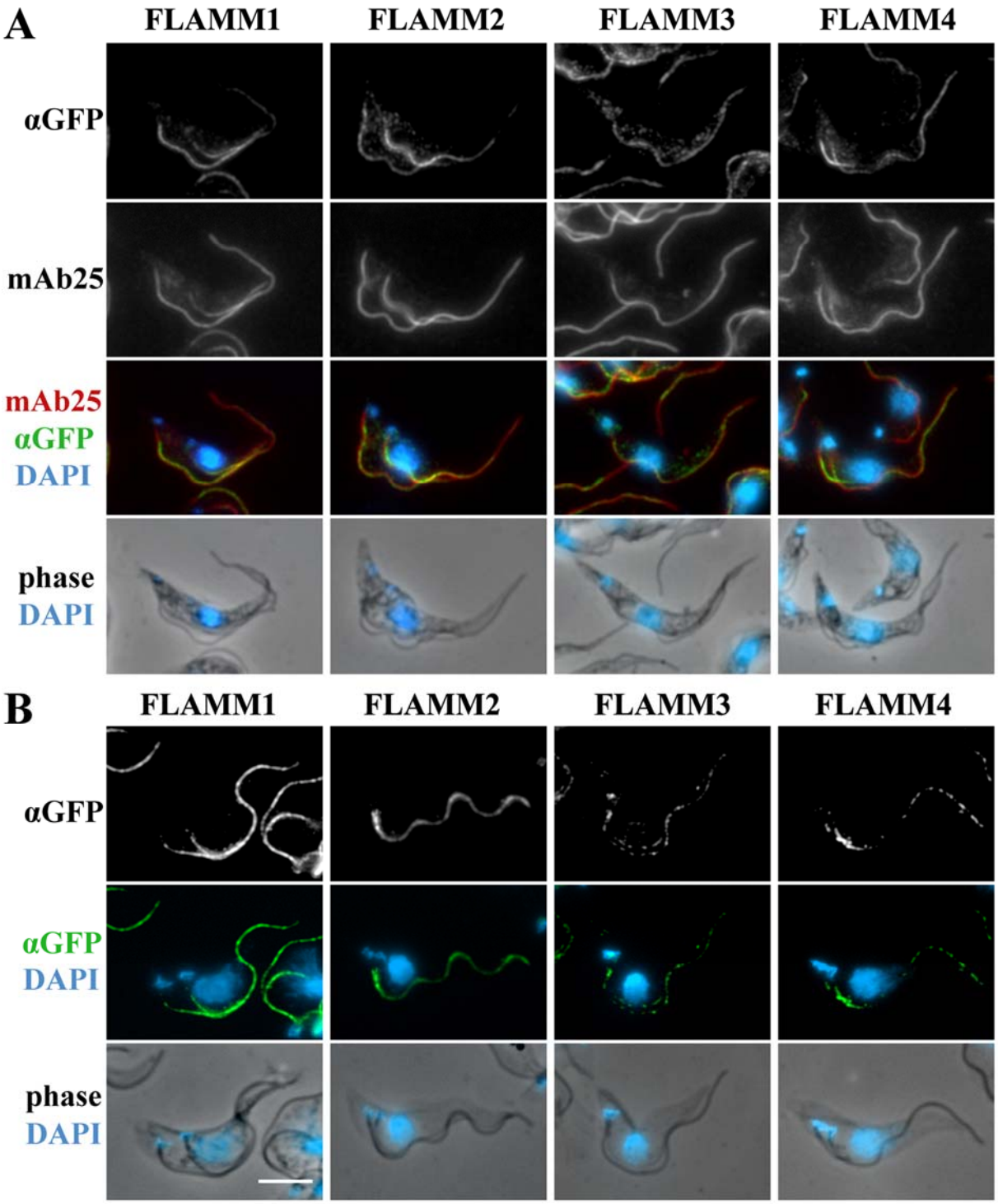

Figure 3.31: Localization of FLAMM proteins. Figure continues on page 73. Cell lines expressing FLAMM::YFP fusion proteins were analysed in IFA with an anti-GFP (in green) antibody upon (A) methanol fixation or (B) membrane extraction. To determine the localization of the FLAMM proteins in the flagellum, the cells were co-stained with the axonemal marker mAb25 (in red) and counterstained with DAPI (in cyan on the phase contrast image or the colour-merge). The scale is the same for all pictures and the scale bar represents 5 µm.

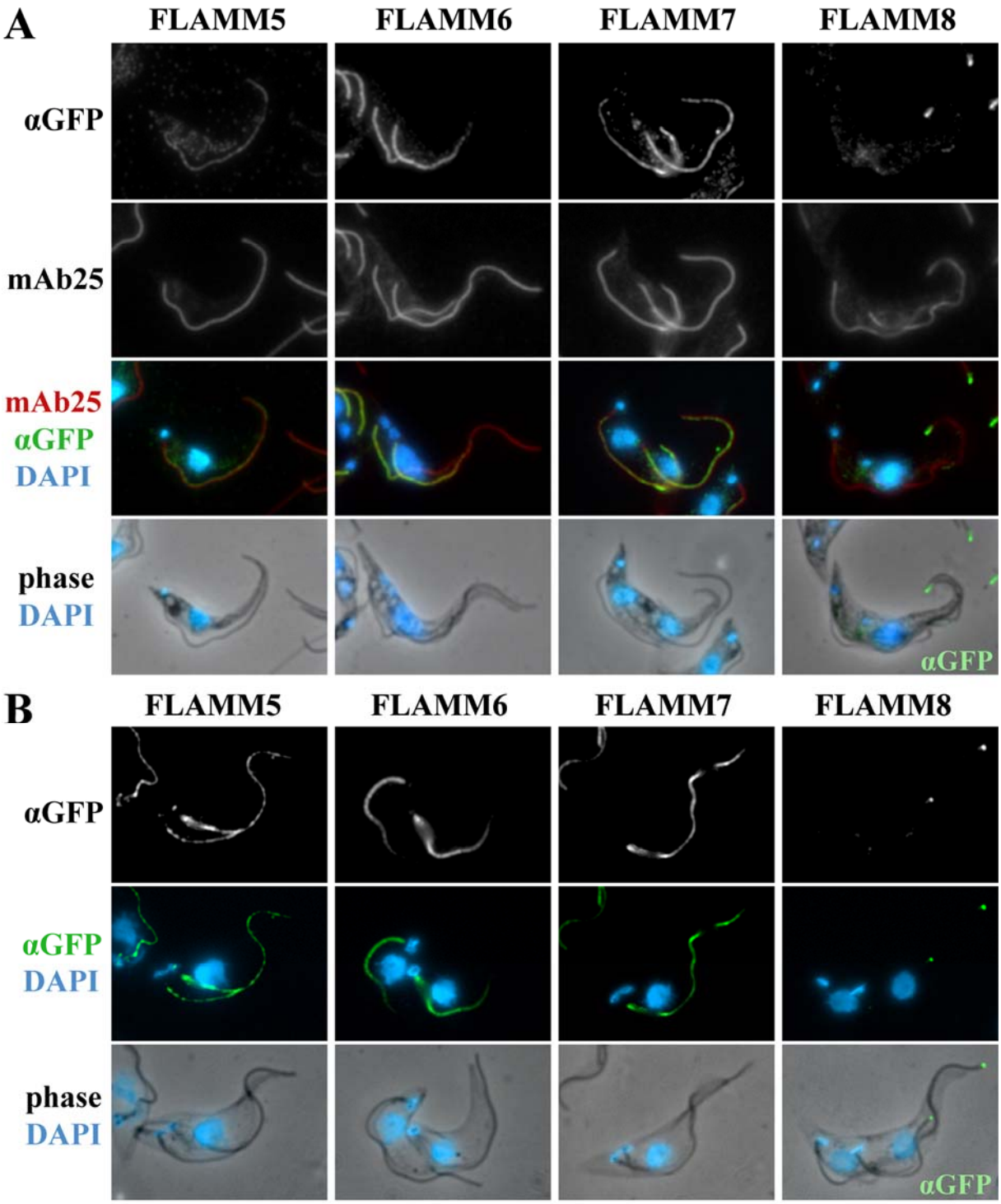

Figure 3.32: Localization of FLAMM proteins. Continuation of page 72.

Table 3.2: Localization of FLAMM proteins 1-8. Cell lines expressing FLAMM::YFP fusion proteins were analysed by IFA with an anti-GFP antibody after methanol fixation or membrane extraction. To determine the relative localization of the FLAMM proteins, the cells were co-stained with the axonemal marker mAb25. Localization was considered to be axonemal when the FLAMM signal co-localized with the staining produced by mAb25, or considered to be in the PFR when it was adjacent to it with a shifted proximal starting point.

	methanol	**membrane extraction**	**peculiarities**
FLAMM1	PFR	PFR (linear)	staining weaker at the flagellar tip
FLAMM2	PFR	PFR (linear)	
FLAMM3	PFR	PFR + FAZ (dotty)	staining does not extend to the flagellar tip in methanol, follows PFR and FAZ after membrane extraction
FLAMM4	PFR	PFR (dotty)	in methanol: some cells with brighter new flagellum
FLAMM5	PFR	PFR (discontinued line)	
FLAMM6	Axoneme	Axoneme	gradient in the flagellum, decreasing towards the tip
FLAMM7	PFR	PFR (linear)	
FLAMM8	flagellar tip	flagellar tip	signal intensity proportional to length of new flagellum

In conclusion, we showed that all these different hypothetical proteins are localized in the flagellum compartment, some of them displaying unique localization. Moreover, most of the FLAMMs being specific to the kinetoplastid order, their flagellar localization suggests a specific role of the flagellum in this lineage.

3.2.2 Investigation of PAD2 localization

The PAD2 protein was identified in the flagellar proteome of procyclic cells, so we investigated its localization in the flagellum. Published images showed stumpy parasites analysed with the anti-PAD2 antibody to visualize weak localization of the protein in the flagellum, before and after a temperature shift (Dean et al., 2009) (Fig 3.32A,B). To determine PAD2 localization in fly stages, we used parasites derived from tsetse infection with the AnTat1.1 strain and stained them with the anti-PAD2 antibody (Fig 3.32C). In procyclic and mesocyclic cells, PAD2 localization was clearly distributed all over the surface. It was difficult to see a distinct signal in the flagellum, presumably because it was masked by the intense signal of the cell body. Therefore, we examined cells with partially detached flagella from the cell body, which often occurs during the IFA procedure (Fig 3.32C, magnified images indicated by white boxes). The flagellar signal in these cells seemed very weak or absent.

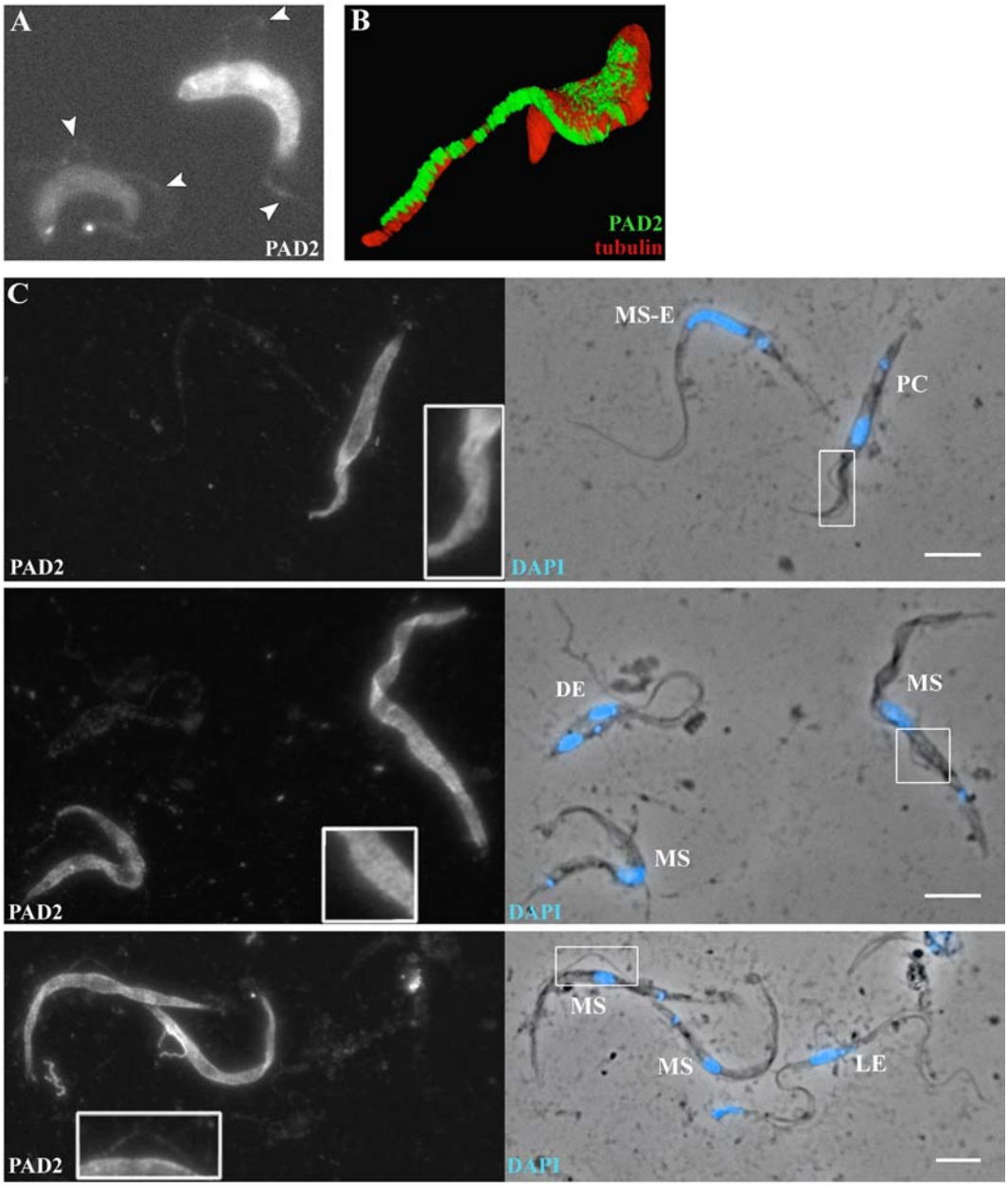

Figure 3.33: Localization of PAD2 in trypanosomes. (A,B) Adapted from Dean et al, 2009, supplementary figure 5. (A) Stumpy parasites were analysed after 1 h of cold shock (from 37° C to 20° C) with the anti-PAD2 antibody in IFA. PAD2 signal re-localizes from the flagellar pocket area (left cell) to the whole cell membrane (right cell) during cold shock. The flagellar staining is indicated by arrowheads. (B) Confocal 3D-imaging of a stumpy cell co-stained with the anti-PAD2 antibody (in green) and anti-tubulin (in red) to stain the peripheral microtubule corset. PAD2 signal is clearly visible on the flagellum. (C) AnTat1.1 cells at different developmental stages in the tsetse alimentary tract were fixed in methanol and analysed by IFA with the anti-PAD2 antibody. Cells were counterstained with DAPI (in blue on phase contrast image) and scale bars represent 5µm. Procyclics (PC), mesocyclic trypomastigotes (MS), parasites in transition from mesocyclic to epimastigote (MS-E), asymmetrically dividing epimastigotes (DE) into a long (LE) and a short epimastigotes (SE). White boxes on the phase contrast images indicate the areas of magnification shown in the images with the fluorescence signal.

Interestingly, parasites that were analysed in an advanced stage of infection, in the proventriculus of the fly, displayed a significant drop in the global PAD2 signal. In mesocylic cells in transition to the epimastigote form that undergo a nucleus migration (MS-E), the PAD2 signal was virtually absent and remained undetectable in asymmetrically dividing epimastigotes (DE) as well as in their progeny, the long (LE) and short epimastigotes (SE) (Fig 3.32C). This absence in PAD2 signal indicates that the protein is down-regulated in development. These preliminary results show that PAD2 is an interesting sensory protein that is worth being investigated in parasite stages beyond the bloodstream to procyclic differentiation.

3.2.3 Localization of arginine kinase as candidate flagellar protein

The arginine kinase (AK) was identified in *T. cruzi* (Tc00.1047053507241.30) as a cytoplasmic protein that shows differential activity according to the life cycle stage and that is implicated in resistance against nutritional, oxidative and pH stress (Miranda et al., 2006; Pereira et al., 2003; Pereira et al., 2002). In *T. brucei*, three separate genes encode proteins of slightly different sequences. They all contain the active core of AK (Miranda et al., 2009) that catalyzes the reversible translocation of a phosphate group from phosphoarginine to ADP by generating ATP (Fig 3.33). AK1 (Tb09.160.4590) is the smallest protein and contains the core only, while AK2 (Tb09.160.4570) shows a C-terminal extension with a glycosomal/peroxisomal PTS1 targeting sequence, and the larger AK3 (Tb09.160.4560) is characterized by N- and C-terminal extensions (Miranda et al., 2009) (Fig 3.33).

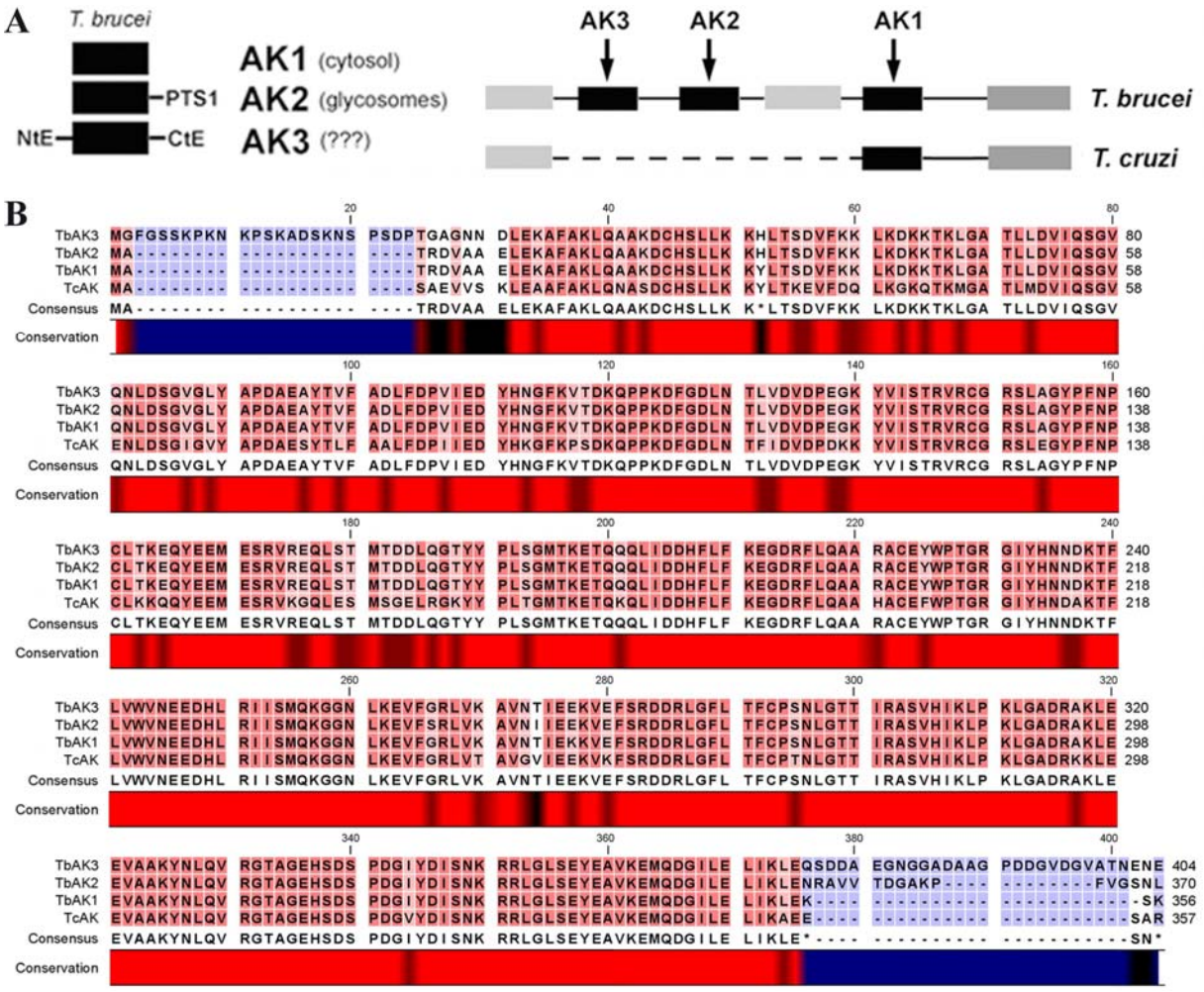

Figure 3.34: Arginine kinase proteins in *T brucei*. (A) Adapted form (Miranda et al, 2009) Left: the three isoforms of *T. brucei* AK all share the catalytic core of the enzyme (black box), AK2 has a C-terminal elongation with a predicted glycosomal (peroxisomal) targeting sequence and AK3 has N- and C-terminal extensions. Right: representation of the genetic locus of AK in *T. brucei* and *T. cruzi* as predicted by GeneDB (http://www.genedb.org/). (B) Protein sequence alignment of all *T. brucei* AK isoforms (TbAK1-3) with the *T. cruzi* AK (TcAK). High conservation is presented as dark red shading on the sequence (red on the graph conservation), conservation in more than 2 sequences in pale red (grey on the graph) and conservation in less than 2 sequences is indicated in black on the graph conservation. N- and C-terminal extensions are shown in blue for TbAK2 and TbAK3. The number of amino acids is indicated on top and right of the alignment.

To determine the localization of AK in *T. brucei* by IFA, we used the anti-arginine kinase polyclonal antibody raised in mouse against the recombinant unique AK protein of *T. cruzi* (Pereira et al., 2000) (sequence in Fig 3.33B). This antibody cross-reacted with *T. brucei* AK proteins in western blot (Canepa et al., 2011; Pereira et al., 2000).

3.2.3.1 Localization of AK in the procyclic form

IFA with the anti-AK antibody was first carried out on Lister 427 wild type procyclic cells in culture and confirmed that the antibody cross-reacted with *T. brucei* (Fig 3.34). To determine the best conditions to visualize AK proteins, we applied three different procedures: (1) fixation in PFA (optimal for soluble proteins), (2) fixation in ice-cold methanol (optimal for skeletal proteins) and (3) membrane extraction with NP40 followed by fixation in PFA to expose skeletal associated epitopes (Fig 3.34).

Using these fixation methods, three different localization patterns of AK proteins were distinguished. After PFA fixation, the antibody produced a signal in the cytoplasm of the cells and a double line delimiting the flagellum, indicating localization in the flagellar membrane (Fig 3.34A magnification box). After methanol fixation, the protein was found in the flagellum and in a lesser extent in the cytoplasm (Fig 3.34B). After detergent extraction, the signal became very weak in the flagellum and could be detected at the basal bodies (Fig 3.34C). Regardless the fixation method, the new flagellum in duplicating cells showed a staining comparable to the old flagellum, no matter its length (Fig 3.34 arrowheads).

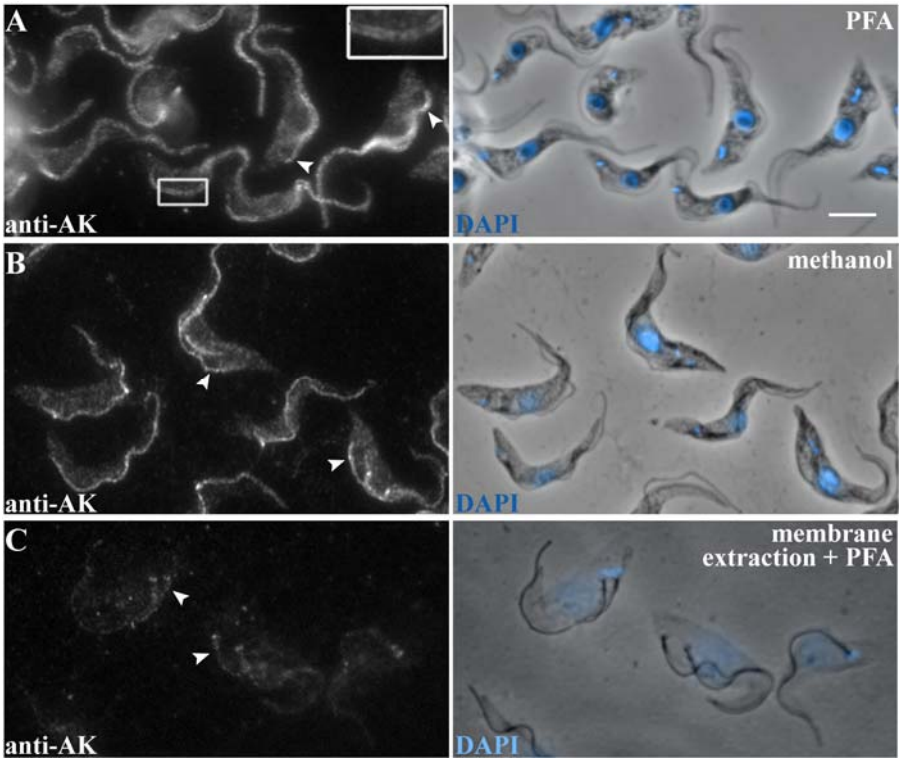

Figure 3.35: Localization of AK in different fixation conditions. PC cells (427 WT) were fixed in (A) PFA, (B) methanol or (C) fixed in PFA after membrane detergent-extraction before IFA with the anti-AK antibody. Cells were stained with DAPI (in blue on the phase contrast image). The scale bar represents 5 µm. White boxes indicate the area of magnification, arrowheads point at the new flagellum in dividing cells.

We investigated the localization of AK as a potential membrane associated flagellar protein upon PFA fixation in co-localization studies with the mAb25 antibody and L8C4 (Fig 3.35A), to mark the flagellar axoneme or the PFR respectively. The AK signal was forming a tube-

like structure that encompassed the axoneme and the PFR staining (Fig 3.35A, magnified panels on the right). The starting point of the AK signal corresponded to that of the axoneme staining and not to that of PFR that was only present after the exit of the flagellum from the flagellar pocket. In methanol fixation, we performed co-labelling with the mAb25 antibody and the anti-IFT172 (intraflagellar transport protein 172) (Fig 3.35B). In methanol fixation the AK signal draw a thick line in the flagellum suggesting that it was associated to membrane that collapsed during the dehydrating fixation procedure and co-localized with IFT172 and the axoneme (Fig 3.35B, magnified panels on the right).

These results obtained by IFA confirmed the hypothesis that at least one isoform of AK is localized in the flagellar membrane of *T. brucei*.

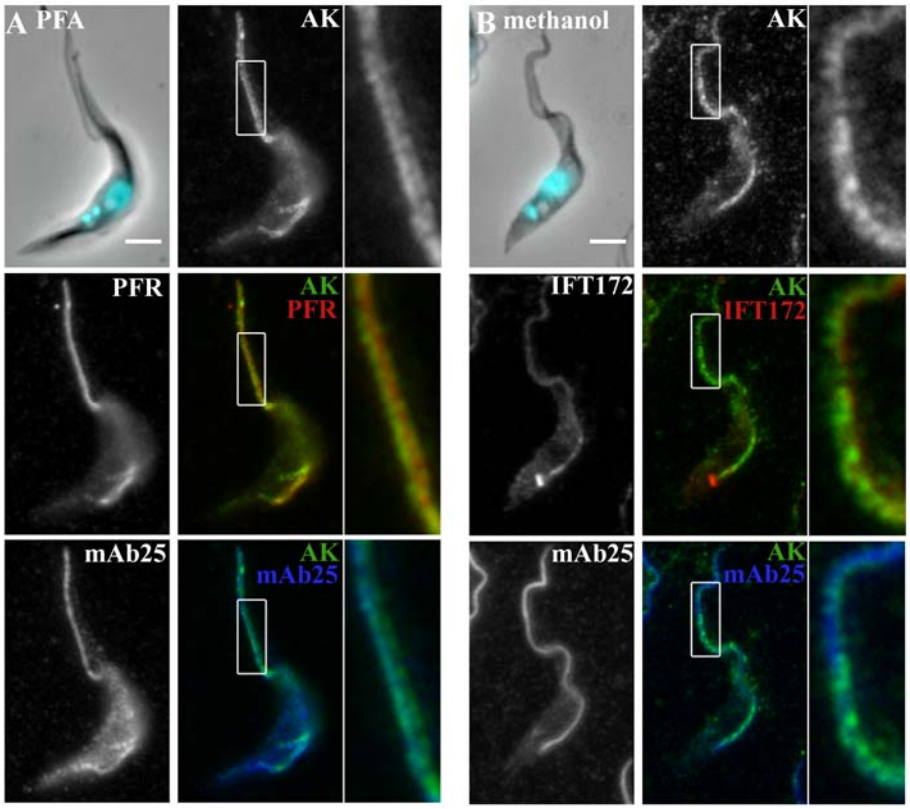

Figure 3.36: Co-localization of AK with PFR, axoneme and IFT172. PC cells were fixed in (A) PFA or (B) methanol before IFA with the anti-AK antibody, mAb25 (axoneme) and either (A) L8C4 (PFR) or (B) anti-IFT172. Cells were stained with DAPI (in cyan on the phase contrast image). Scale bars represent 3 µm. White boxes indicate the area of magnification shown on the right-hand side of each panel.

3.2.3.2 Localization of AK in parasite stages from the tsetse fly

The localization and expression level of AK in the developmental stages of trypanosomes found in the tsetse fly was assessed using the AnTat1.1 strain. In order to obtain a sufficient high number of parasites, we used methanol fixation before performing IFA with the anti-AK antibody. In all trypanosome cells issued from the alimentary tract (PC, MS, MS-E, DE, LE+SE) and the salivary gland of the tsetse fly (SGE, pre-MT and MT), the AK signal was

weakly detected in the cytoplasm but strongly present in the flagellum (Fig 3.36). In contrast to ALBA, the signal was not reduced in proventricular stages. The AK signal in flagella of short epimastigotes appeared stronger than in long epimastigotes, analysed in the same field, before and after cell division (Fig 3.36).

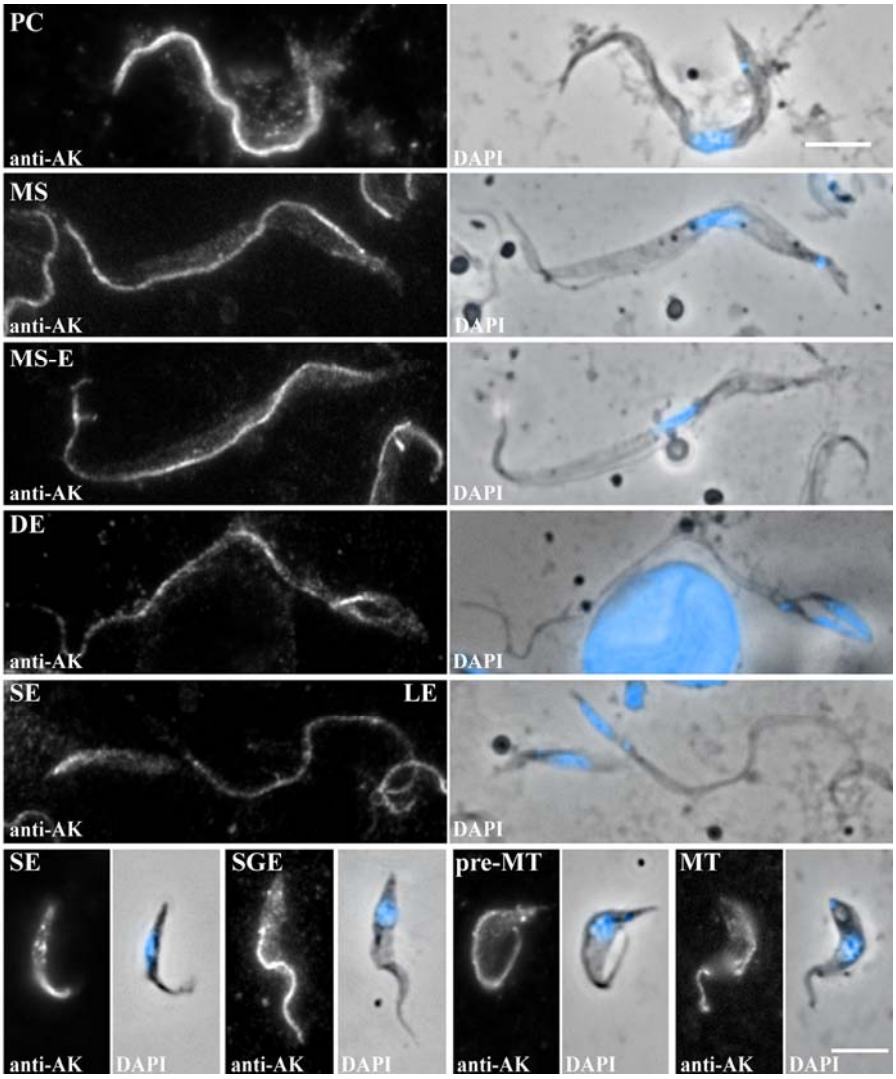

Figure 3.37: Localization of AK during parasite development in the fly. AnTat1.1 cells at different developmental stages in the tsetse alimentary tract (PC, MS, MS-E, DE, LE+SE) and salivary glands (SGE, pre-MT and MT), were fixed in methanol and analysed by IFA with the anti-AK antibody. Cells were counterstained with DAPI (in blue on phase contrast image) and scale bar represents 5µm. Cells are shown in the order of appearance during the parasite cycle: procyclic (PC), mesocyclic trypomastigote (MS), parasites in transition from mesocyclic trypomastigote to epimastigote (MS-E), asymmetrically dividing epimastigote (DE) into a long (LE) and a short epimastigote (SE). In the salivary glands: salivary gland epimastigote (SGE), pre-metacyclic (pre-MT) and mature metacyclic (MT).

3.2.3.3 Localization of AK in the mutant *Fla1*^{RNAi}

The mutant cell line *Fla1*^{RNAi} was used for the purification of intact flagella that turned out to contain a high abundance of AK. We confirmed this result by IFA with the anti-AK upon PFA fixation. Non-induced *Fla1*^{RNAi} cells showed a flagellar signal comparable to that observed in WT cells (Fig 3.37). After a two day induction period, detached flagella were visible in a high proportion of cells. These flagella displayed similar signal intensities in

comparison to flagella of non-induced cells. However, we also noticed a small proportion of detached flagella with weaker AK signal (Fig 3.37).

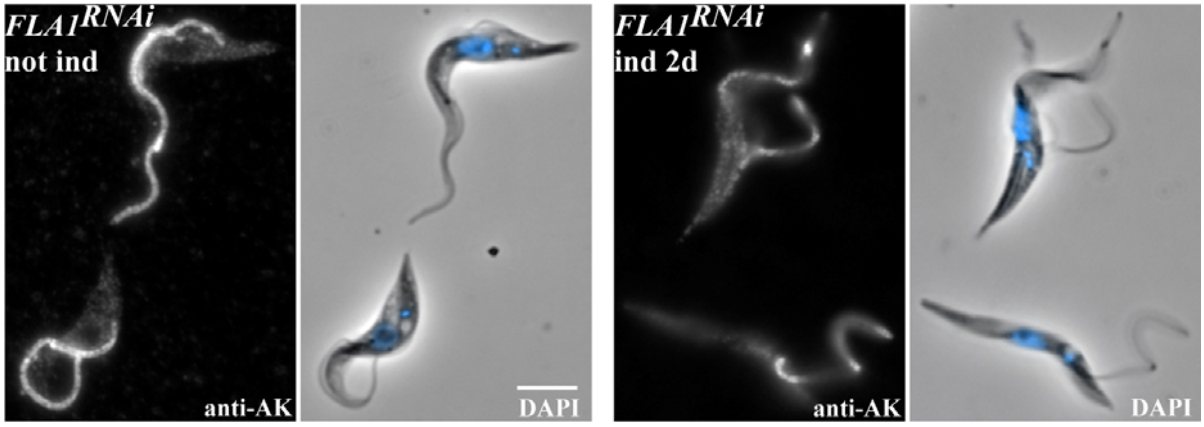

Figure 3.38: AK in flagella of the *Fla1*^{RNAi} cell line. *Fla1*^{RNAi} cells non-induced and induced for 2 d with tetracycline were fixed in PFA and treated with the anti-AK antibody in IFA. Cells were counterstained with DAPI (in blue merged with the phase contrast image), scale bar represents 5 µm.

3.2.4 Functional analysis of arginine kinase

3.2.4.1 Knockdown of AK

In order to determine the function of AK in trypanosomes two strategies were designed (Fig 3.38). First, all three mRNA were targeted by RNAi selecting a 406 bp common region for dsRNA expression (*AK1-3*^{RNAi}) (Fig 3.38A, blue box). Second, we created a cell line silencing *AK3* alone (*AK3*^{RNAi}) by targeting its unique 3'coding sequence and 3'UTR sequence (Fig 3.38A, orange box). The silencing of AK3 should allow determination of its localization, as it is the only isoform for which no prediction was made (Fig 3.33A) (Miranda et al., 2009). The investigation of this cell line is still pending.

RNAi against *AK1-3* was induced for 4 days with tetracycline and the efficiency of protein knock-down was assessed by IFA using the anti-AK antibody. In PFA fixation, the non-induced cells showed the previously described pattern: a weak signal in the cytoplasm and a strong signal in the flagellum (Fig 3.38B,C left panels). In contrast, the induced cells were completely negative in the flagellum and retained only a weak cytoplasmic signal (Fig 3.38B,C right panels). This analysis was performed for two clones of the same transfection experiment and both showed the same result (Fig 3.38B,C). We therefore concluded that RNAi silencing was efficient at least for the AK localized in the flagellar compartment and the results confirmed the specificity of the antibody at least for the flagellar

isoform. The induced cells analysed by IFA were also screened for morphological abnormalities or aberrations in their DNA content. The induced cells were indistinguishable from the non-induced ones so that no visible phenotype could be determined. However, although the growth rate after induction of RNAi appeared normal during the four days of analysis, it needs to be determined if AK knock-down impairs growth after longer periods.

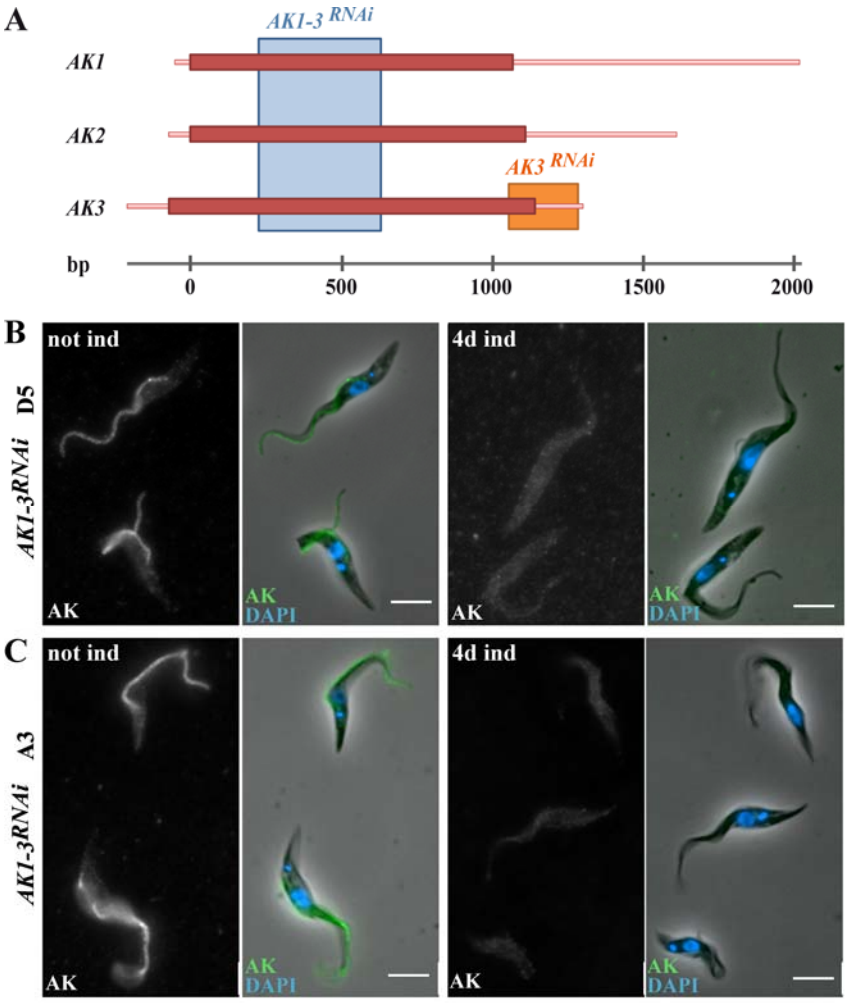

Figure 3.39 : Knockdown of AK by RNAi. (A) Schematic representation of the DNA sequences of *AK1*, *AK2* and *AK3*. Coding sequences are shown in dark red and UTRs in pale red. Boxes indicate the region used to generate dsRNA against *AK1-3* (blue box) or against *AK3* (orange box). Drawn to scale (the number of base pairs is represented below). (B,C) Analysis performed upon PFA fixation followed by IFA with the anti-AK antibody on two clones of the *AK1-3*^{RNAi} cell line: (B) D5 and (C) A3 either non-induced (left panel) or induced for 4 days (right panel). Cells were stained with DAPI (in blue), the scales represent 5 µm.

3.2.4.2 Kinetics of the knockdown of AK proteins

Very little is known about flagellar membrane proteins in general and their transport to and the turnover within the flagellum. Efficient silencing of the AK localized in the flagellum was observed upon IFA after 4 days of induction of RNAi. Thus, it was of special interest to analyse the knock-down kinetics of the flagellar AK as a membrane-associated protein. Cells of the *AK1-3*^{RNAi} cell line were processed by IFA with the anti-AK antibody upon PFA fixation and analysed at different time points of induction (8 h, 16 h and 24 h) (Fig 3.39). The amount of the proteins in both old and new flagella was highly reduced after 8 h especially in

the D5 clone (Fig 3.39A). The signal further decreased until the protein was maximally silenced in the flagellum and cytoplasm of clone D5 24 h after induction of RNAi (Fig 3.39A). The silencing kinetics was slower in clone A3 and less efficient after 24 h of RNAi. In cells with two flagella, the new flagellum stained equally in comparison with the old flagellum, meaning that the AK pool in the two flagella was equally affected (Fig 3.39, arrowheads and arrows).

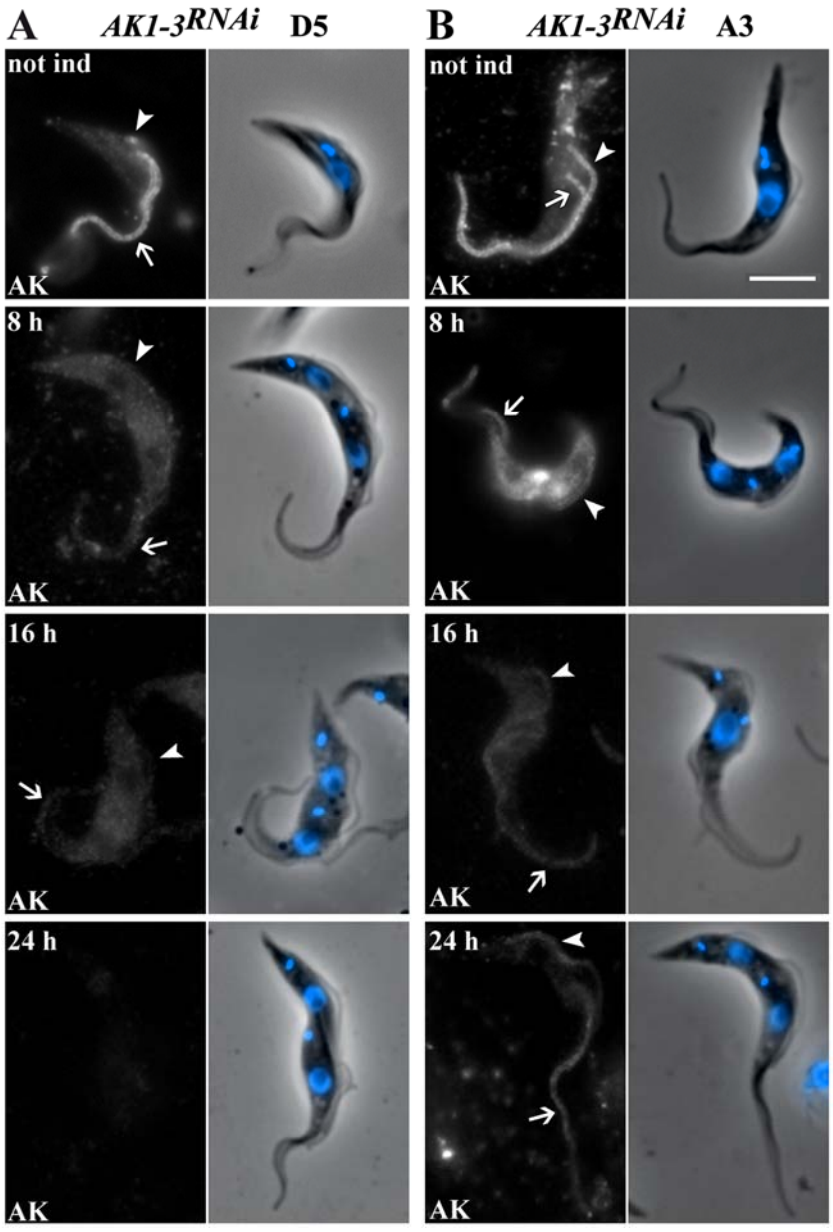

Figure 3.310: Kinetics of AK silencing by RNAi. Analysis performed upon PFA fixation followed by IFA with the anti-AK antibody in two clones of the *AK1-3*^{RNAi} cell line: (A) D5 and (B) A3 either non-induced or induced for 8 h, 16 h and 24 h as indicated. Cells were counterstained with DAPI (in blue merged on the phase contrast image). All cells have two flagella: a new elongating one, indicated by arrowheads and an old one, indicated by arrows. The scale bar represents 5 µm.

4 DISCUSSION

4.1 ALBA proteins and trypanosome development

4.1.1 ALBA proteins show a distinct expression pattern during development

We used endogenous tagging and monitoring of fluorescent fusion proteins by live microscopy to assess expression of ALBA3 and ALBA4 in all stages of the *T. brucei* parasite. This method has the advantage to enable investigation at the individual cell level. Combined with immunofluorescence detection, it revealed a drastic drop in the amount of both ALBA3/4 during trypanosome differentiation in the fly proventriculus region. In bloodstream and procyclic trypomastigotes in culture, the ALBA3/4 proteins are expressed in comparable amounts to procyclic trypanosomes in the fly midgut. However, the ALBA3/4 signal slightly diminishes during the transition to the mesocyclic stage. This reduction could be due to ~14% increase in cell volume (Rotureau et al., 2011a) and possible protein dilution. ALBA3/4 become barely detectable during trypo- to epimastigote differentiation when the nucleus is very elongated and starts to migrate to the posterior end of the cell. A dilution effect is excluded as the cell volume remains constant during this transition (Rotureau et al., 2011a). ALBA3/4 protein abundance remains low in the dividing epimastigote and in the long epimastigote. In contrast, in the short epimastigote, the abundance of ALBA3/4 proteins rises rapidly and apparently prior to completion of cytokinesis. High amounts of ALBA3/4 proteins are detected in all subsequent stages in the salivary glands.

ALBA proteins could undergo different post-translational modifications during development that could influence protein function. For example, ALBA3 is found in a phosphorylated state in the procyclic form (Nett et al., 2009). Acetylation of a distinct lysine residue has been shown to influence Alba protein activity in the archaeal counterparts (Bell et al., 2002). While this specific residue is not conserved in most eukaryotic Alba proteins (Aravind et al., 2003) including ALBA3/4, other residues could undergo acetylation. In Archaea, the acetylation state of Alba is controlled by Sir2 which is unlikely to occur in trypanosomes as the three Sir2 homologues are localized either in the nucleus or in the mitochondrion (Alsford et al., 2007; Garcia-Salcedo et al., 2003).

The drop in ALBA3/4 protein abundance during a specific time window of the parasite cycle suggests it could be a prerequisite for differentiation. This step of the life cycle is a one-way decision: mesocyclic trypomastigotes issued from fly dissection and transferred to culture medium are able to transform back to the proliferating procyclic form after 5 days, in contrast

to post-mesocyclic forms that are committed to differentiation (Van Den Abbeele et al., 1999).

This differentiation process is likely to involve changes in protein levels other than the ALBA3 and ALBA4 proteins but few studies were conducted in tsetse derived parasites. We recently reported molecular remodelling of cytoskeletal structures during the trypo- to epimastigote transition. As soon as the nucleus starts to migrate to the posterior pole of the cell, two proteins belonging to the FAZ filament: FAZ1 (recognized by the antibody L3B2) and the antigen recognized by the DOT1 antibody, were no longer detected (Rotureau et al., 2011a). This could be due to a true down-regulation or to a remodelling of the filament leading to reduced access to the two antigens. The overall FAZ structure was not taken apart, as shown by the unaltered presence of the FLA1 protein, another FAZ marker (Rotureau et al., 2011a). Another study focused on proteins involved in the endocytotis pathway during trypanosome development (Natesan et al., 2007). Here, the ER marker protein BiP was reported to be subsequently down-regulated during the transition from trypomastigote to epimastigote. The authors attributed this to a decrease in cell volume, a fact that was refuted in a more recent study showing that cell volume during this transition stays mostly constant (Rotureau et al., 2011a). However, in comparison to ALBA3/4, the BiP signal is already decreased starting from the mesocyclic stage and does not re-emerge in the short epimastigote. In contrast, the abundance of the p67 protein, a marker of the lysosome, was described to stay constant during the whole parasite cycle (Natesan et al., 2007). Although these findings of changes in protein expression during the trypo- to epimastigote differentiation are of high interest, they deal with markers associated to specific compartments of the trypanosome cell and the evolution of cytosolic proteins has yet to be described. In our study, we monitored DHH1 as cytosolic protein marker, initially to search for a negative control, and were able to show a drop in protein abundance at the transition from trypo- to epimastigote by immunolabelling, closely following the pattern of the ALBA3/4 proteins. This result confirms the hypothesis that multiple proteins show differential expression patterns during this important differentiation step in trypanosome development.

4.1.2 Reduced ALBA protein levels mimic changes observed in development

As ALBA protein abundance *in vivo* is reduced starting from the mesocyclic stage, it was obvious to question the effects of ALBA protein silencing on the cultured procyclic form.

Remarkably the resulting phenotypes mimic some signatures of the early differentiation steps towards the epimastigote stage: (1) cell cycle arrest, (2) elongation of the posterior end by *de novo* microtubule polymerisation ("nozzle" phenotype) and (3) migration of the nucleus towards the posterior end.

The slow growth phenotype in the induced *ALBA3/4*^{RNAi} cell line and the scoring of the DNA containing organelles during the induction time course suggests that absence of ALBA3/4 proteins leads to a cell cycle arrest in a large proportion of the cell population. Growth did not stop completely presumably because a small number of ALBA positive cells (detected by IFA) were still able to sustain the culture. To verify at which step of the cell cycle the induced *ALBA3/4*^{RNAi} cell population is arrested, we scored DNA containing organelles. The proportion of the different cell types initially observed in the non induced state did not change drastically over the time of RNAi induction. Cells did not become multi-nucleated. However, after 4 days of induction a high proportion of zoids (1K0N cells) was present and reached 15% of the population after 6 days. Zoids were initially defined as cells containing a kinetoplast but no nucleus (Robinson et al., 1995). As trypanosomes lack a mitosis to cytokinesis checkpoint (Hammarton et al., 2003; Li et al., 2003; Robinson et al., 1995), zoids occur as daughter cells from dividing trypanosomes that are blocked or delayed in mitosis by the drug rhizoxin (Robinson et al., 1995). In order to assess the hypothesis of a mitotic cell cycle arrest in the induced *ALBA3/4*^{RNAi} cell line, we performed DNA-FISH. The experiments showed that nuclei in several cells are very enlarged, with an aberrant number of large and minichromosomes, suggesting an arrest of these cells just before the initiation of mitosis. Some cells were undergoing mitosis but with an unusual distribution of chromosomes. We propose that defects in mitosis are responsible for the high number of zoids (1K0N) in the *ALBA3/4*^{RNAi} induced population.

Posterior elongation by active microtubule polymerisation occurs in the trypanosome development during bloodstream to procyclic differentiation (Matthews et al., 1995) and during the procyclic to epimastigote transition (Rotureau et al., 2011a; Sharma et al., 2008). Nozzle cells (procyclic cells displaying an unusual long posterior end) have been reported in mutant procyclic cells after knock-down of cyclin CYC2 that blocks progression through G1 phase (Hammarton et al., 2004) or double RNAi against cdc2 related kinases CRK1 and CRK2 (Tu and Wang, 2004; Tu and Wang, 2005a; Tu and Wang, 2005b). Ectopic over-expression of zinc finger proteins TbZFP2 and TbZFP3 in procyclics also leads to nozzle formation and G1 arrest (Hendriks et al., 2001; Paterou et al., 2006). All these results suggest that procyclic cells elongate their posterior end as a result of cell cycle arrest. A high

proportion of *ALBA3/4*^{RNAi} induced cells is actively elongating at the posterior end as shown by YL1/2 staining (anti-tyrosinated tubulin antibody) and measurements of cell parameters, leading to a high number of nozzle cells (almost 50% after 5 days of induction).

In trypanosome development, the mesocyclic trypomastigote cell is almost one third longer than the midgut procyclic form (Rotureau et al., 2011a; Sharma et al., 2008). As proposed by Vickerman et al (Vickerman, 1985) and van den Abbeele et al (Van Den Abbeele et al., 1999), mesocyclic cells arise as a non-dividing endpoint form in the midgut. They are undergoing nuclear S-phase but then get arrested in the G2 phase of the cell cycle and do not enter mitosis prior to differentiation to the epimastigote form (Sharma et al., 2008; Van Den Abbeele et al., 1999). We propose that knock-down of ALBA mimics the differentiation towards the mesocyclic cells: posterior elongation and cell-cycle arrest after nuclear S-phase.

In vivo, a mesocyclic cell transforms to an epimastigote by nucleus migration towards the posterior side of the kinetoplast. This does not involve kinetoplast movement as the distance between posterior end and kinetoplast remains constant (Sharma et al., 2008). Mitosis is only initiated when the nucleus has reached a posterior position to the kinetoplast and after duplication of the latter. The *ALBA3/4*^{RNAi} induced cell line is blocked in the cell cycle just before mitosis as shown by DNA-FISH that revealed enlarged nuclei with multiple DNA content. In addition, over 20% of the *ALBA3/4*^{RNAi} cells induced for 6 days show either a juxtaposed posterior or clear posterior positioning of the nucleus. This is unique to the ALBA3/4 protein knockdown and was, to our knowledge, never reported so far. In all other mutants, observed to be blocked in the cell cycle and displaying a nozzle phenotype, the nucleus remains in its position anterior to the kinetoplast (Hammarton et al., 2004; Hendriks et al., 2001; Tu and Wang, 2004; Tu and Wang, 2005a). We propose that ALBA3/4 knock-down does not only mimic the procyclic to mesocyclic development but also the development from mesocyclic to epimastigote marked by nucleus migration to the posterior end of the cell.

However, knock-down of ALBA3/4 does not lead to a properly differentiated epimastigote cell in terms of cellular and nuclear morphology. This is presumably because other elements are involved and are not temporally coordinated such as *in vivo*. In addition, cells are not synchronized when ALBA knock-down is initiated, a requirement important for example in bloodstream to procyclic differentiation. Other factors that could influence differentiation could be ALBA3/4 partners, for example the ALBA1 and or ALBA2 protein (Mani et al., 2011). The down-regulation of DHH1 protein at exactly the same stage suggests a possible interplay between these two proteins. Environmental factors could be involved in this differentiation processes such as changes in viscosity, osmolarity or nutriment availability

when the parasite number increases dramatically in the midgut. The passage of the parasite through the peritrophic membrane or to the proventriculus in combination with high parasite load can also influence the nutriment composition. It is conceivable that factors secreted by the parasite itself influence differentiation by a quorum sensing mechanism, as described for the stumpy inducing factor in bloodstream forms. To track down the triggers for differentiation of the parasite in the proventriculus, additional knowledge on sensing proteins expressed in these particular stages is needed. Interestingly the PAD2 protein, a citrate/cis-aconitate transporter involved in trypanosome differentiation from bloodstream to procyclic form (Dean et al., 2009), is completely down-regulated during trypomastigote to epimastigote differentiation. It remains to be determined whether this is a cause or a consequence of differentiation.

The *T. brucei* ALBA proteins were investigated in a parallel study by Mani and colleagues (Mani et al., 2011). The knock-down experiments conducted on both ALBA3 and ALBA4 proteins in the procyclic form also led to a down-regulation of proteins ALBA1 and ALBA2 but produced no striking phenotypes, although a cell growth phenotype was reported upon ALBA3 knock-down. Two major technical differences need to be highlighted. First, in contrast to our study, knock-down was not achieved by double stranded RNA generated from opposing promoters but by a hairpin dsRNA structure. In addition, Mani and colleagues performed ALBA RNAi studies in the AnTat1.1 strain 90-13 while we used the strain Lister 427 29-13. The AnTat1.1 strain is pleomorphic, whereas the Lister 427 strain is mostly used for *in vitro* experiments but cannot establish salivary gland infections in the fly (Herder et al., 2007).

4.1.3 ALBA3 over-expression impairs transition to the epimastigote stage

GFP expression under the control of the procyclin promoter and with the *actin* 3’ UTR is supposed to be constitutive over the development phases in the tsetse fly (Bingle et al., 2001). We used this construct to express ALBA::GFP fusion proteins and tsetse flies were fed with the recombinant parasites. Unexpectedly, differences in expression levels were observed between ALBA3 and ALBA4. At the PC stage in culture, ALBA4::GFP showed the strongest signal by western blot using an anti-GFP antibody, contrasting with a lower abundance of ALBA3::GFP. The endogenous protein levels of ALBA, assessed with the anti-ALBA antibodies, were unaltered. Differences in expression level of the GFP fusion proteins were also observed during the development in the tsetse fly. The ALBA4::GFP expression profile

was mostly comparable to that of the GFP control. In contrast, ALBA3::GFP was down-regulated during the trypo- to epimastigote transition and in dividing epimastigotes, a behaviour close to that of the endogenous protein suggesting a strong control of ALBA3 protein during development. While ALBA 4 over-expressing trypanosomes were normally completing the cycle, parasites of the ALBA3::GFP strain were not as efficient to invade the salivary glands even if over-expression was limited. Only 11 % of the midgut infections with the ALBA3::GFP strain led to salivary gland infection, compared to over 23% in the control and over 30% in the ALBA4::GFP. In addition, this was only observed in flies heavily infected in the midgut, meaning that the higher the parasite load the higher the chance to pass the bottleneck towards the salivary glands (Oberle et al., 2010). Moreover, parasites that reached the salivary glands displayed reduced ALBA 3::GFP amounts compared to their ALBA 4 counterpart. This is in contrast to the endogenous tagging experiment, where all parasites found in the salivary glands showed comparable strong signal for both ALBA3 and ALBA4 cell lines. This suggests that differentiation might be impaired when ALBA3 protein is too abundant. This is in agreement with the presence of numerous individuals displaying an intermediate situation between the transition of trypo- to epimastigote. In these stages, the cell diameter shrank as expected but the nucleus elongation and migration to the posterior end was either blocked or slowed down. This is exclusively observed in ALBA3::GFP expressing cells and is the converse of what was observed during RNAi: no cell shrinking but nucleus repositioning at the posterior end of the cell. These data support the view of an important role for ALBA3 and provide the first molecular and cellular data on a protein involved in the control of differentiation during this essential and limiting step of the parasite cycle.

4.2 ALBA proteins control mRNA levels during differentiation

4.2.1 ALBA are RNA-binding proteins

In eukaryotes, Alba domain containing proteins can be divided into two major groups: Pop7/Rpp20 and Rpp25/Mdp2. Most members are found in the nucleus consistent with association to the nuclear RNase P complex, but yeast RNase P was found in both the nucleus and in a defined focus in the cytoplasm (Gill et al., 2006). More recent data in parasitic protozoa reveal localization in the cytoplasm of *Plasmodium* species (Mair et al., 2010) or dual localization in the cytoplasm and the nucleus in *Toxoplasma* (Olguin-Lamas et al., 2011).

The presence of protozoan ALBA proteins in the protein complex of RNase P/RNase MRP remains elusive. In trypanosomes the nuclear RNase P has not been characterized to date but the mitochondrial counterpart has been purified as a 70 kDa protein complex from mitochondrial matrix (Salavati et al., 2001). However, the protein composition of this mtRNase P has not been further specified but we can probably exclude ALBA3/4 proteins as members because of their cytosolic localization. Moreover, the down-regulation of all ALBA members did not affect precursors of tRNA processing, excluding a direct association with RNaseP (Mani et al., 2011).

We propose that ALBA 3/4 are RNA-binding proteins that interact with mRNA during the parasite cycle. First, ALBA 3 and ALBA 4 localize exclusively to the cytoplasm. Second, ALBA proteins aggregate in cytoplasmic granules upon starvation, as reported for several trypanosome RNA binding proteins (Cassola et al., 2007; Kramer et al., 2008) where they partially co-localize with polyA$^+$ RNA. This could determine the fate of mRNA targets towards storage (Cassola et al., 2007) or degradation. In other organisms, the presence of the decapping enzyme Dcp1 defines the P-body, a microdomain where degradation of the mRNA occurs (Anderson and Kedersha, 2009). As the search of a decapping homologue in trypanosomes was unsuccessful to date, the discrimination between storage or degradation granule cannot be made at this stage (Milone et al., 2002).

The parallel study of Mani and colleagues confirmed the localization of all ALBA proteins in cytoplasmic granules upon nutritional stress, but with perfect co-localization with polyA$^+$ RNA (Mani et al., 2011). However, this analysis was restricted to an epifluorescent microscope whose capacity to discriminate close, but separate small structures, is limited. When we examined our samples with such a microscope, signals of ALBA and polyA$^+$ RNA also appeared perfectly co-localized, in contrast to confocal analysis.

In the same study, Mani and colleagues proved the RNA-binding capacity of all four trypanosome ALBA members when they were found associated with the GRE element in mobility shift assays. This is a 25 nucleotide region found in the regulatory loop II of the 3' UTR of the *GPEET* transcript (Hehl et al., 1994), encoding one of the surface proteins of procyclic parasites. Intriguingly, the down-regulation of all ALBA members did not show any regulatory effect on the *GPEET* transcript abundance (Mani et al., 2011) nor major changes on the overall levels of mRNA transcripts in procyclic cells in a system-wide analysis (Nilsson et al., 2010). Hence, if ALBA proteins regulate mRNA expression their role is more likely to be at the translational level. This coincides well with the fact that all ALBA members were co-precipitated with the ribosomal protein P0 but only the interaction with ALBA2 and

ALBA3 was resistant to RNase A treatment, suggesting a possible physical interaction with ribosomes (Mani et al., 2011). The ALBA3 protein was also shown to interact with the elongation factor eIF4E4 in an RNA-dependent manner. In addition, all ALBA proteins can form complexes with at least one other ALBA member, with ALBA3 acting as a core component (Mani et al., 2011). These data are in agreement with our results that showed a central role for ALBA3 during parasite development. We propose that ALBA proteins could interact with developmentally regulated mRNA.

4.2.2 ALBA proteins control developmentally regulated mRNA

To adapt to different environments, *T. brucei* modulates gene expression. Gene expression in trypanosomes is largely controlled at the post-transcriptional level and trans-acting RNA binding proteins such as ALBA proteins could act on multiple levels on their mRNA targets: leading to stabilization or degradation, to altered localization or accessibility for translation.

At least two views can be considered of how ALBA proteins regulate mRNA involved in development. First, ALBA proteins could act as negative regulator by inhibiting their translation through sequestering mRNA into cytoplasmic foci. Second, ALBA proteins could stabilize mRNA and promote their translation. Both hypothesis can be considered and may depend on the developmental stage and/or the interaction with ribosomes and protein partners.

Their role as negative regulator could be the suppression of the expression of certain transcripts that encode proteins involved in unique processes of a given stage or transition between stages. Therefore, ALBA proteins would need to be down-regulated exclusively during MS-E transition. This would imply interaction with specific mRNAs, as demonstrated by the IFA coupled to FISH results where ALBA3/4 localize only to certain polyA$^+$ RNA containing granules. Restricted localization of proteins to certain granules is known for mammalian cells where P-bodies remain distinct from stress granules although they exchange some of the material (Kedersha et al., 2005; Wilczynska et al., 2005). In trypanosomes, the granules formed upon starvation remain separate from those observed upon heat shock (Kramer et al., 2008). The XRN1 protein for example shows a distinct focus at the extreme posterior end of the cell upon heat shock in which no other known protein could be found (Kramer et al., 2008).

ALBA 3/4 aggregate in foci upon nutritional stress which is more likely to happen in the peritrophic space and proventriculus region of the fly. However, it needs to be stated that cytoplasmic granules were never observed in our dissection experiments, directly after release

of either stage of ALBA::YFP or ALBA::GFP expressing parasites from the fly tissues. In contrast, *T. cruzi* epimastigote parasites analysed *ex vivo* from their host intestine tract show granules in more than 70% of the cells in IFA with a recognized marker of starvation granules (Cassola et al., 2007). These parasites were likely to have undergone extreme starvation conditions as their insect host had not fed during 10 days after being infected with trypanosomes (Cassola et al., 2007). Tsetse flies used in our study normally feed twice a week which is less than in the field (Aksoy et al. 2003), suggesting possible starvation conditions. Perhaps trypanosomes are so well adapted to their host environment that living in a tsetse does not cause a stress situation that is as dramatic as the applied *in vitro* starvation conditions using PBS and granule formation might milder and more transient.

P-bodies are constantly present in trypanosome cells, at least in culture (Kramer et al., 2008) and their number increases in stress conditions, so they could play a major role in efficiently adapting gene expression in situations when trypanosomes encounter changing environments by sequestering or releasing specific mRNA. This idea together with the identified binding partners of ALBA (Mani et al., 2011) supports a more general concept towards the existence of “post-transcriptional operons”, where ribonucleoprotein complexes control the destiny of a subset of functionally related mRNA in a jointly fashion (Keene, 2007). ALBA co-localizes with the DHH1 protein in cytoplasmic granules, although direct interactions were not detected (Mani et al., 2011). DHH1 controls developmentally regulated mRNA (Kramer et al., 2010) and although the protein outnumbers the total mRNA molecules in the cell, it is still selective for many developmentally regulated transcripts. This is not exclusive as other mRNA transcripts differentially expressed in bloodstream and procyclic do not rely on DHH1 (Kramer et al., 2010). ALBA proteins could fulfil this function. The ALBA protein amount is present in large excess compared to its only identified target *GPEET* transcript (Mani et al., 2011), suggesting it could interact with several mRNA. A theory that is also consistent with the fact, that ALBA proteins are found in a large number of cytoplasmic foci. Like the ZFP3, it could play a dual role in blocking or promoting translation of different transcripts.

In a second view, ALBA could be a positive actor, stimulating the expression of multiple mRNA that participate to the control of cell proliferation, and hence would be present in most parasite stages. During the trypo- to epimastigote differentiation, ALBA degradation would be associated to destabilization of RNA transcripts important for proliferation and would lead to cell cycle arrest. As this was shown to be a prerequisite for differentiation from stumpy bloodstream to procyclic (Matthews and Gull, 1994; Shapiro et al., 1984), it would be interesting to investigate ALBA levels and function in the stumpy parasite.

Cell cycle arrest in the mesocyclic form would be associated with nucleus migration and establishment of the dividing epimastigote situation, features that are impaired upon over-expression of ALBA3. After division, ALBA *de novo* expression in the short epimastigote would allow the restoration of cell cycle elements needed in the salivary gland proliferating form. This re-emergence of ALBA is not observed in the long epimastigote that appears to be sacrificed (Sharma et al., 2008).

The “stabilizing” hypothesis effect is reinforced by the finding that ALBA proteins are bound to the *GPEET* 3’UTR in procyclic cells (Mani et al., 2011). At the early procyclic stage, ALBA proteins are highly expressed suggesting that they could have a positive effect on GPEET production. GPEET is almost completely exchanged with the EP protein when procyclics penetrate through the peritrophic membrane into the ectoperitrophic space (Acosta-Serrano et al., 2001; Sharma et al., 2008; Vickerman et al., 1988). Mesocyclic and mesocyclic to epimastigote parasites show tiny remnants of GPEET on their surface, while dividing epimastigotes and their progeny are completely negative. ALBA protein is down-regulated at these stages of the parasite cycle. It can be speculated that the absence of ALBA protein is correlated with the destabilization of the *GPEET* transcript either directly or by allowing the access of an RNA-binding complex to the *GPEET* 3’UTR involved in translational silencing. In both cases it would lead to the clearance of GPEET from the cell surface. Accordingly, in the absence of ALBA proteins, the expression of a reporter protein carrying the *GPEET* 3’UTR is down-regulated (Mani et al., 2011).

The role of ALBA proteins in protists starts to be unveiled. In the apicomplexan *Plasmodium berghei*, they were identified in oocyte P granules, whose protein content is conserved throughout the eukaryotic lineage. It ensures the storage of certain mRNAs in translationally silent mRNP granules before the fertilization of gametes (Mair et al., 2010). The crucial transformation step in sexual development completely relies on the translation of mRNA initially stored in the P granules. However, the pool of mRNA in these granules is still unknown. Three *Plasmodium* ALBA members were found in the oocyte P granule, each of which contains a single N-terminal Alba domain and one member with a C-terminal RGG extension (Alba1) (Mair et al., 2010). Phylogenetic studies place Alba1 and Alba2 in the Rpp25/MDP2 group and Alba3 into the Pop7/Rpp20 group of the superfamily branches defined by Aravind and colleagues (Aravind et al., 2003; Mair et al., 2010). More recently, in the apicomplexan *Toxoplasma gondii* two Alba proteins were identified in a screen of nuclear factors that are bound to a promoter sequence (Olguin-Lamas et al., 2011). However, these

Alba proteins showed a more prominent localization in the cytoplasm than in the nucleus. It still remains elusive which function they might play in these organisms.

In the *T. brucei* related *Leishmania infantum* species, Alba proteins were identified in a pull-down assay using a U-rich regulatory element of the 3' UTR of the amastin transcript as a bait (Dupé, A and Papadopoulou, B, personal communication). This transcript encodes a major surface protein of the intracellular amastigote form of the parasite. It further supports the idea of the role of RNA-binding ALBA proteins in the regulation of differential protein expression during development of *T. brucei*.

Alba proteins are involved in developmental processes and are participating in RNA-binding, likely controlling translational regulation. With these properties they are perfect candidates to play a role in developmental processes in protozoan parasites that rely on post-transcriptional control such as kinetoplastids. Alba proteins are found in numerous eukaryotic organisms, so these proteins could be developmental regulators in a larger view, as possibly the ciliary MDP2 during macronucleus development. In metazoan organisms, Alba-like proteins are encoded in addition to the RNase subunits Rpp20 and Rpp25 which could be important in the developmental fine tuning in certain cell types.

4.3 Investigation of the candidate flagellar sensing proteins

4.3.1 Identification of novel flagellar proteins

The proteomic analysis of intact flagella of *T. brucei* revealed a large number of proteins not previously reported to be associated to the flagellum. We selected 14 proteins for analysis, 12 in this study of which 10 turned out to be present in the flagellum compartment, therefore validating the quality of the flagella preparation.

The ten undescribed FLAMM proteins with unknown function were tagged with YFP and localization in the flagellum for eight of them was demonstrated. At this stage it is still possible that the other two proteins could be in the flagellum. Indeed, the tagged versions were not detectable and the experiment is still inconclusive. For example FLAMM9 shows two transmembrane domains and the YFP tag could perturb the correct expression or targeting of this protein to the membrane. Work on FLA1 has shown that adding a tag to flagellum-associated transmembrane proteins can be tricky (Rotureau, unpublished).

In addition to the validation of eight FLAMM proteins, we confirmed the presence of PAD2 in the flagellum. Although the staining is weak, it was clearly visible in some flagella that were detached from the cell body (as staining on the cell surface masks the flagellar signal when properly attached). This result is in agreement with the fact that this protein was not enriched in the flagellum proteome versus whole cells. Nevertheless, our analysis revealed that PAD2 is differentially expressed during development in the tsetse fly. Although comparably abundant on the surface of procyclic and mesocyclic cells, it is completely absent in stages found in the proventriculus region: in those that transform into epimastigotes as well as in short and long epimastigotes. Therefore, this recognized sensing protein could also be involved in developmental switches other than the bloodstream to procyclic differentiation, a hypothesis that remains to be investigated.

The arginine kinase (AK) was found to be amongst the most abundant proteins in the *T. brucei* flagellar proteome. In this organism, three gene copies are present and all encode proteins that contain the general core of the protein. Enzymatic activity in *T. brucei* is comparable to that of *T. cruzi* but it remains to be clarified if all protein isoforms contribute to this enzymatic activity. Two of them possess N- and/or C-terminal extensions that could target the protein to specific compartments. AK2 has a predicted small C-terminal targeting sequence to the peroxisome-related organelles called glycosomes (Miranda et al., 2009), that

are specialized in kinetoplastids as they contain the whole machinery for glycolysis. AK3 is the largest of the three proteins and shows an extension at the N- and C-terminus. Evidence suggests that AK3 is localized in the flagellar compartment. First, on western blots comparing whole cell proteins with the flagellar preparation, the anti-AK antibody produced two bands, at molecular weights of 41 and 45 kDa in whole cells, but only the 45 kDa band is present in flagella (Julkowska, unpublished data) (Fig 4.1). This band likely represents AK3, the largest isoform.

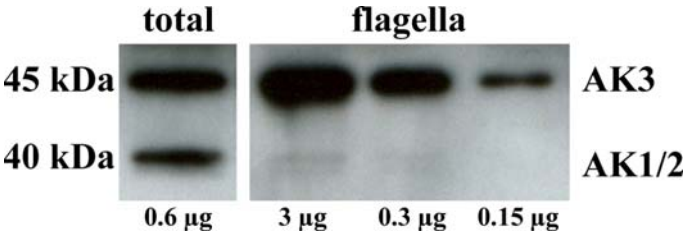

Figure 4.1: Flagellar localization of AK3. Western blot with the anti-AK antibody on the total protein fraction or proteins from purified flagella. The amount of protein in each lane is indicated at the bottom. The expected molecular weight of the AK1/2 and AK3 proteins is indicated on the left

Second, IFA indicates that AK is associated to the membrane of the flagellum. This is also the case of some calcium binding proteins, such as the three calflagins in *T. brucei* or FCaBP in *T. cruzi* (Emmer et al., 2009; Godsel and Engman, 1999). Their first residues in the N-terminus are important for their targeting to the flagellar membrane. The glycine residue (at position 2) is myristoylated and provokes association to the cellular membrane, while the palmitoylation of an adjacent cysteine residue targets the protein to the flagellar membrane (Fig 4.2). However, these acylation events are presumably not the only determinants. Several lysine residues that are conserved in the N-termini of these proteins allow the association of *T. cruzi* FCaBP to lipid rafts which are proposed to traffic membrane proteins to the flagellum (Emmer et al., 2009; Maric et al., 2011). Sequence comparison of the N-terminal extension of AK3 with that of calflagins and FCaBP show no apparent conservation apart from the second glycine residue and an SK pair (residues 6 and 7 in all proteins) with unknown function (Fig 4.2). Similarly to the calcium binding proteins, AK3 is marked by several lysine residues in its N-terminal sequence and although they do not align with those of calflagin or CaBP, their importance for lipid raft association and flagellar membrane targeting of AK3 remains to be investigated. It should be noted that N-terminal extensions also act in targeting proteins to flagellar structural compartments. This is the case for three members out of seven in the adenylate kinase (ADK) family. Only these three present long N-terminal extensions and are either targeted to the flagellar PFR (ADKA and ADKB) or to the flagellar axoneme in the case of ADKE (Ginger et al., 2005).

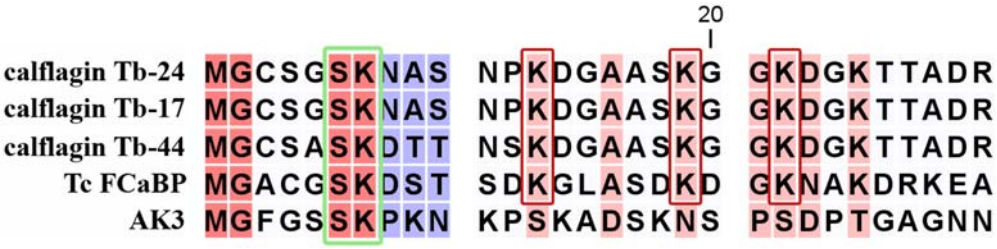

Figure 4.2: Alignment of the N-terminal domains of trypanosome flagellar membrane proteins. The AK3 N-terminal extension was aligned with the N-extensions of the three calflagins Tb-24, Tb-17 and Tb-44 and the calcium binding protein FCaBP from T. cruzi. Dark red shading indicates conservation in all, light red shading conservation in four sequences, white shading shows parts that are conserved in three sequences (mostly the calflagins), while blue regions are the most divergent. The conserved SK motif in all is marked by a green box. The conserved lysins that were shown to be important for association of Tc FCaBP with lipid rafts are indicated by red frames. Although their position is not conserved in AK3, the AK3 sequence shows several lysins in their proximity.

The localization of several other proteins identified by mass spectrometry was investigated in parallel by colleagues in the laboratory. Using IFA, Diego Huet validated the flagellar localization of a 14-3-3 like protein, involved in kinase signalling events in mammalian cells (Pozuelo Rubio et al., 2004) and necessary in *T. brucei* for cell motility, cytokinesis and correct progression in the cell cycle (Inoue et al., 2005). The flagellum proteome also revealed the presence of aquaporin3 (AQP3) that has been described as a glycerol and water channel involved in osmoregulation in *T. brucei* (Uzcategui et al., 2004). A *Leishmania* homolog, the aquaporin 1 (LmAQP1) protein, shows 81% identity with TbAQP3, and localizes to the flagellum and the flagellar pocket membrane (Figarella et al., 2007). Daria Julkowska created a *T. brucei* cell line expressing an AQP3::YFP fusion protein and found the protein enriched in the flagella pocket area.

4.3.2 Dynamics of novel flagellar proteins

The determination of the FLAMM proteins localization was assessed in cell lines expressing YFP fusion proteins form an endogenous locus, by replacing one copy of the *FLAMM* gene. Direct YFP fluorescence was visible in live cells but the signal was often very weak, possibly because the proteins are expressed in low amounts or because the YFP tagged version is in competition with the non-tagged protein when incorporated in the flagellum. In addition, the presence of the YFP tag could interfere with protein stability or efficient targeting of the protein to the flagellum compartment. This technical limitation of tools could be

circumvented in the future by knocking out the remaining wild-type allele, by replacing it with the YFP version or by producing antibodies for each FLAMM.

When the cell lines expressing a YFP fusion were fixed in either PFA or methanol, we used an anti-GFP antibody to detect the YFP tagged version and perform co-staining with the axoneme marker mAb25 antibody. This stains the axoneme from the top of the transition zone to the distal end of the flagellum (Pradel et al., 2006). Six out of eight FLAMM proteins did not completely co-localize with the mAb25 staining, especially at the proximal part of the flagellum, suggesting that they are associated to the PFR structure. This result is preliminary and needs to be confirmed by co-staining with a marker of the PFR. Why 75% of the analyzed FLAMMs are found in the PFR might have different explanations. The PFR structure is a characteristic of kinetoplastid species and most of the selected FLAMM have no homologues in other organisms, being either restricted to kinetoplastids (*Leishmania* and *trypanosomes*) or only to *Trypanosoma* species (but not *Leishmania*). The mass spectrometry analysis of intact flagella identified a higher number of proteins that are known to localize to the PFR in comparison to the investigation of the flagellar skeletal proteome (Broadhead et al., 2006). This suggests that there are several proteins in the matrix of the PFR that could be washed away when flagella are treated with detergent and high salt. However, most of the proteins are, to a certain extent, resistant to detergent, as membrane extraction using detergent still allows their detection with the anti-GFP antibody. Pullen and colleagues proposed the PFR lattice as a platform for proteins in a “solid-phase” environment where they could act in pathways involved in metabolism and signalling (Pullen et al., 2004).

The PFR structure in the flagellum is found in close proximity to the cell body and transmission electron microscopy images show that filaments appear to contact the FAZ region (Fig 2.9). FLAMM3 displays an interesting dual localization pattern: a line along the cell body presumably following the FAZ and another one in the PFR that does not reach its tip. This protein has no transmembrane domain but is large (470 kDa) and displays a high number of repetitive sequences, a feature already reported for both FAZ and PFR proteins (Imboden et al., 1995; Vaughan et al., 2008; Woodward et al., 1994). With its dual localization it could be involved in communication processes between the flagellum and the cell body.

The FLAMM8 protein is restricted to the flagellar tip. When the parasite swims, it is the first part of the cell to make contact with the environment. It could be involved in detecting signals and interact with a downstream receptor. The distal tip of the flagellum could also be a platform where sensing molecules are accumulated as observed in sensory cilia in *C. elegans*.

Recently, a calcium-dependant cysteine protease of the calpain family (TbCALP1.3) has been found in the membrane of the extreme distal tip of the flagellum (Liu et al., 2010) with a similar pattern to FLAMM8. FLAMM8 contains a predicted virus globular attachment domain (Uniprot 2011_07) that is found in virus proteins where it plays a role in the attachment to surface receptors. The protein sequence shows significant similarity with the microtubule-associated Gb4 protein identified in most kinetoplastids (Cotrim et al., 1995; Rindisbacher et al., 1993). In *T. brucei*, Gb4 is localized at the posterior end of the cell of procyclics where it is proposed to cap the plus ends of microtubules (Rindisbacher et al., 1993). In agreement with the postulated role of Gb4 on cytoplasmic microtubules, FLAMM8 is also resistant to detergent treatment and could cap the microtubule ends in the flagellum. As described in our study, FLAMM8 is only fully incorporated at the distal tip when the flagellum reached a certain length, but is absent in new and growing flagella. Therefore, its presence could define the elongation status of the flagellar axoneme microtubules. Additional functional analysis of FLAMM8 could give more insight in its role at this specific part of the flagellum, especially during the parasite cycle.

Structural flagellar elements are transported by the IFT machinery where they are incorporated at the distal tip during flagellar elongation (Bastin et al., 1999). This was also reported for tubulin and radial spoke proteins in *Chlamydomonas* (Johnson and Rosenbaum, 1992). Several of the identified new flagellar proteins might have different incorporation and turnover dynamics. Silencing of AK leads to an equal drop of AK signal in both the new and the old flagellum. This is the complete opposite of structural elements, where protein knockdown leads to a negative new flagellum whereas the old flagellum still possesses wild-type amount of material (Bastin et al., 2000). This suggests that the turnover for flagellar membrane proteins such as AK3 might be much faster. This also indicates that the flagellum membrane protein pool could be constantly exchanged even between two flagella of different age and status. In addition, the AK staining was more pronounced in the flagella of the short epimastigote assayed after fly dissection with the anti-AK antibody. While this could reflect a direct role for the AK function in the flagellum at this developmental stage, it could also be a way to pre-accumulate the protein in a flagellum that is expected to rapidly elongate and expand its membrane in the next parasite stage, the attached epimastigote. A perhaps related pattern was observed for the FLAMM4 protein that was more concentrated in the new flagellum of procyclic cells, especially when it is very short. It could be a mechanism to store the maximum protein amount needed in the whole flagellum, starting from the beginning of its assembly. During elongation, the FLAMM4 content could then spread over the whole

flagellar length. This has been shown to be the case for IFT proteins in *Chlamydomonas*. These organisms have the technical advantage to be de-flagellated by pH shock and start to subsequently regrow their flagella when put back in normal conditions (Marshall and Rosenbaum, 2001). This allows experiments with synchronous cell populations that are all constantly elongating their flagella over time. Flagella were purified at increasing time points during regrowth meaning that each individual sample contains flagella of homogenous length and that samples collected at increasing time points of the experiment each contain flagella of increasing length. These samples were analyzed by IFA and western blot, revealing that the amounts of IFT proteins are constant no matter the length of the flagella, suggesting that the total pool of IFT proteins is incorporated into the flagellum already before its elongation (Marshall et al., 2005).

FLAMM6 is co-localizing with the axonemal marker starting from the basal body area. It displayed a strong signal in the proximal part of the flagellum and its abundance decreased in a gradient in the mid-region of the flagellum and was not detected in the distal half. This could be due to competition with the non-tagged version, but we can probably exclude this option, as newly built flagella show comparable signal intensities in their proximal part to old flagella, and display the gradient as soon as the flagellum reaches half of its final length. This protein incorporation mechanism is the opposite of the established one for structural flagellar elements. Thus, we can speculate that FLAMM6 is implicated in signalling processes with its three cNMP binding domains and that its gradient distribution in the flagellum could play a role in amplifying signals towards the base of the flagellum.

After having demonstrated their flagellar localization, the next step would be to identify the roles of these new proteins and their implications in trypanosome biology, especially in sensing mechanisms. Knock-down studies were performed for a large range of trypanosome mRNA (Alsford et al., 2011) and revealed that FLAMM1, FLAMM3 and FLAMM7 would be essential for proliferation in procyclic trypanosomes, based on readouts of cell growth in multi-well plates. For these proteins, it could be of interest to investigate the phenotype upon knock-down with an inducible RNAi system. For all the other FLAMMs, as well as for the AK, knock-out procyclic cell lines could be produced and analyzed during progression in the parasite cycle. Parameters such as proliferation and infection efficiency, behavior or morphology of the parasite stages during their development could be observed in their natural environment and the implication of these candidate proteins in sensing pathways investigated.

5 MATERIALS AND METHODS

5.1 Databases and softwares

Sequences for genes and proteins were retrieved from the database Tritrypdb (tritrypdb.org/), Blast searches were performed with (http://blast.ncbi.nlm.nih.gov/Blast.cgi) and information about different proteins were consulted on (http://pfam.sanger.ac.uk/) and (http://www.uniprot.org/). For sequence alignments we used the CLC Free workbench (version 4.0.3) or performed it directly online using the ClustalW2 program (http://www.ebi.ac.uk/Tools/msa/clustalw2/).

Statistical analyses were performed with the programme Kaleidagraph (version4). For image and video analysis the software used is indicated in the respective chapters.

5.2 Trypanosome strains and culture

The *Trypanosoma brucei brucei* procyclic cell line Lister 427 strain was used in this study for *in vitro* experiments or its derivative Lister 427 29-13 was chosen for the RNAi experiments. The latter disposes of a tetracycline inducible system for dsRNA expression by T7 RNA polymerase (Wirtz et al., 1999). The equivalent bloodstream cell line Lister 427 90-13 was used to investigate levels of ALBA3/4 proteins in this parasite stage. The pleomorphic strain AnTat1.1 was used for experiments in tsetse flies (Le Ray et al., 1977).

Lister 427 procyclic parasites were cultured at 27°C in SDM79 (PAA) (Brun and Schönenberger, 1979) supplemented with 2.5 mg/ml Hemin (Sigma) and 10% heat-inactivated foetal calf serum (PAA). Bloodstream form parasites were grown at 37° C with 5% CO_2 in HMI9 medium (Hirumi and Hirumi, 1989) (IMDM basic component from Gibco, supplements from Sigma). Cell density in procyclic cultures was assessed with the Beckman coulter Z2, bloodstream form cells were counted in KOVA plastic slides with grids (HYCOR, Stratagene).

Fly infection was carried out with freshly differentiated procyclic parasites of the AnTat1.1 strain. Therefore, bloodstream forms were plated on, with agar solidified HMI9 culture medium to induce stumpy differentiation (Carruthers and Cross, 1992; Vassella et al., 1997). Stumpy parasites were then taken up in DTM medium (components from Sigma) containing 20% foetal calf serum and differentiation to the procyclic form was triggered by the addition of 6 mM *cis*-aconitate (Sigma) and temperature shift from 37° C to 27° C (Brun and Schonenberger, 1981). Early procyclic AnTat1.1 parasites were then maintained in SDM79 culture medium and 20 mM glycerol (Panreac).

Cryo-stabilates of trypanosomes were made by mixing the ice-cold cell pellet of 10 ml densely grown culture with the respective glycerol-containing medium to obtain a final concentration of 7% glycerol. Tubes were immediately transferred to -80° C and for long-term storage further transferred to liquid nitrogen after one day. For defreezing, cryostabilates were thawed in a 37° C water-bath and immediately transferred to pre-warmed medium. Cells were washed 2 times in at least 10 ml fresh medium each time.

5.3 Stress experiments

To induce nutritional stress, parasites were washed twice for 5 min in PBS at room temperature and incubated 2 h at 27°C in an appropriate volume of PBS at cell densities between 5 and 10 million cells per ml (Cassola et al., 2007). To induce heat shock, parasites in their culture medium were transferred to 41° C for 2 h (Kramer et al., 2008).
Cycloheximide and puromycin (both from Sigma) were added starting from the beginning of the nutritional stress experiment in concentrations of 100 µg/ml.

5.4 Western blot

Cells were washed in PBS and boiled in Laemmli sample buffer (2x stock: 0.5 M Tris pH=6.8, 20% Glycerol, 4% DTT, 4% SDS, Bromphenolblue) before SDS-PAGE separation, loading 2 µg (~0.2 million cells) total cell protein per lane. The Criterion system (Biorad) was used for electrophoresis: Criterion XT precast gels with XT Mops running buffer (20x stock solution) in the Criterion electrophoresis cell (at 200 V constant). Proteins were transferred to PVDF membranes (Hybond-P from Amersham) in the Criterion blotter (Biorad) for 45 min at 100 V constant in TG buffer (10x stock: 0.25 mM Tris pH 8.3, 1.92 mM glycine). The membrane was blocked overnight with 5% skimmed milk in PBS and incubated with primary antibodies diluted in 1% milk and 0.1% Tween20 in PBS for 1 h. Membrane washes were performed with 0.2% Tween20 in PBS. Species specific secondary antibodies coupled to HRP (GE Healthcare) were diluted 1/20,000 in 1% milk and 0.1% Tween20 in PBS and incubated with the membranes for 1 h. Final detection was carried out by using an ECL kit according to manufacturer's instructions (Amersham) and exposure of Hyperfim-ECL (Amersham).

5.5 Immunofluorescence analysis

For immunodetection parasites obtained from the fly were taken up in SDM79 medium without serum and spread directly on poly-L-lysine coated slides (Menzel-Gläser,

Braunschweig) before fixation. Cultured parasites were washed twice in the respective medium without serum before treatment.

Three main methods of fixation were used. For methanol fixation, parasites were settled on poly-L-lysine coated slides, air dried and fixed in methanol at – 20 °C for 5 minutes followed by a rehydration step for 10 minutes in PBS. For PFA (Sigma) fixation, parasites were incubated for 10-30 min at room temperature with a 4% PFA solution in PBS at pH 7 and left to settle on poly-L-lysine coated slides. After a permeabilization step with 0.1% Nonidet P-40 (Fluka), samples were blocked for 1 hour with 1% bovine serum albumin (BSA) in PBS. To obtain de-membranated parasites, the cells were left to settle on poly-L-lysine coated slides for 10 min, rinsed in PBS and treated for 7 sec with detergent: 1% NP40 in PEM buffer (0.1 M PIPES pH 6.9, 2 mM EGTA, 1 mM $MgSO_4$). After thorough washes, the samples were fixed in 4% PFA in PBS for 30 min and washed again.

For immunodetection, slides were incubated with the appropriate dilution of the first antibody in 0.1% BSA in PBS for 1 hour. After three 5 minute-washes, species and subclass-specific secondary antibodies (from Jackson ImmunoResearch) coupled to a fluorochrome (Alexa 488, Cy3 or Cy5) were applied for 1 hour, diluted 1/400 in 0.1% BSA in PBS. Cells were stained with a 1µg/ml solution of the DNA-dye DAPI (Roche) and mounted with the ProLong antifade reagent (Invitrogen). Slides were stored at -20° C or immediately analyzed, either with a DMR microscope (Leica) and images captured with a CoolSnap HQ camera (Roper Scientific) or with a DMI4000 microscope (Leica) and images acquired with a Retiga-SRV camera (Q-Imaging). Pictures were analyzed using the IPLab Spectrum 3.9 software (Scanalytics & BD Biosciences) and were merged and superimposed using Adobe Photoshop (CS2). Measurements of cell parameters were performed on phase contrast images with the ImageJ 1.38X software (NIH) that was also used to determine fluorescent signal intensities.

5.6 Antibodies for western blot or IFA

The ALBA antibodies for this work have been generated by Thierry Blisnick and Sandra Ngwabyt. For either ALBA3 or ALBA4 full length protein, 8 different antisera were obtained from mouse immunization experiments. In western blot they were used at dilutions 1/2000, one seemed more specific for ALBA3, named anti-ALBA3 (initially 2040/4) and one more specific for ALBA4, named anti-ALBA4 in this study (initially 2030/8). All the others were recognizing both ALBA proteins, but some antibodies showed stronger signals than others, and one of those was used in the experiments shown, named anti-ALBA3/4 (initially 2040/1).

In IFA, the anti-ALBA3 showed the strongest signal and the best signal-to noise ratio of all antibodies tested and was used for most experiments. The anti-ALBA4 was much weaker in IFA. All ALBA antibodies produced were functional in IFA at dilutions of 1/750.
The following table summarizes all other antibodies used in this work for western blot and IFA studies (Table 5.1).

Table 5.1: Antibodies used in western blot and IFA. Indicated are the name of the antibody, the antigen they recognize, the species or origin, the reference when published or the person who kindly provided them. Finally, technical details about the methods used and the dilution of the respective antibody are given.

antibody	antigen	species of origin	from /reference	technique and dilution
Aldolase	*T. brucei* aldolase	rabbit poly	Paul Michels	Western blot 1/2000
AK	*T. cruzi* arginine kinase rec.	mouse poly	Claudio Pereira (Pereira et al., 2000)	IFA (PFA, methanol 30sec) 1/100, (membrane extraction) 1/50
DHH1	*T.brucei* DHH1 rec	rabbit poly	Mark Carrington (Kramer et al., 2008)	IFA (PFA) 1/1500
GFP	GFP	rabbit poly	Invitrogen	IFA (methanol, membrane extraction) 1/500,
GFP	GFP	mouse mix of 2 monoclonal	Roche	Western blot 1/100
IFT172	*T. brucei* IFT172 rec	mouse mono	Thierry Blisnick (this laboratory)	IFA (methanol) 1/500
L13D6	PFR1/PFR2	mouse mono	(Kohl et al., 1999)	Western blot 1/50
L3B2	FAZ	mouse mono	(Kohl et al., 1999)	IFA (methanol) non diluted
L8C4	PFR2	mouse mono	(Kohl et al., 1999)	IFA (PFA, methanol) non diluted
mAb25	Axonemal Prp25	mouse mono	Derick Robinson (Pradel et al., 2006)	IFA (PFA, methanol) 1/4
PAD2	PAD2 peptide	rabbit poly	(Dean et al., 2009)	IFA (methanol 30 sec) 1/50
YL1/2	tyrosinated tubulin	rat mono	(Sherwin and Gull, 1989)	IFA (methanol) 1/2

5.7 RNA-FISH coupled to IFA

For detection of total poly (A+) RNA by FISH, parasites were harvested, washed, allowed to adhere to poly-lysine-coated microscope slides and fixed with 8% paraformaldehyde in PBS for 20 min. Slides were incubated for 10 min with a 25 mM solution of NH_4Cl (Sigma) and washed with PBS. Cells were simultaneously permeabilized and blocked for 1 h in 0.5% saponin (Sigma) and 2% BSA in PBS. Prehybridisation was performed for 2 h at room

temperature in hybridization solution: 2% BSA, 5x Denhardt (Sigma), 4x SSC buffer (20x stock, Invitrogen), 5% dextran sulphate (Sigma), 35% deionized formamide (Sigma), 0.5 mg/ml wheat germ tRNA (Sigma) and 10 U/ml RNasin (Promega). Hybridization was performed overnight in the dark at room temperature in a humid chamber in the presence of 1 ng/ml Alexa488-conjugated oligo-$(dT)_{30}$ probe (Eurogentec) in hybridization solution. Samples were protected from light sources during the rest of the procedure. Slides were washed at 5 min intervals: once in 4x SSC plus 35% deionized formamide, once in 4x SSC, once in 2x SSC and finally in PBS for 10 min. Before performing immunodetection with antibodies (as described in chapter 5.5), blocking is performed during 30 min with 10% foetal calf serum (PAA) in PBS.

Slides were analyzed in collaboration with Pascal Roux and Christophe Machu at the Imaging Platform of the Institut Pasteur (Plate-Forme Imagerie Dynamique) using a Zeiss inverted microscope (Axiovert 200) equipped with an oil immersion objective (magnification x63 with a 1.4 numerical aperture) and a spinning disk confocal head (CSU22, Yokogawa). Images were acquired using Volocity software with an EMCCD camera (C-9100, Hamamatsu). For presentation purposes only, the contrast of the images was optimized by the same settings for every panel in Adobe Photoshop after their analysis.

5.8 DNA-FISH

DNA-FISH was performed as previously reported (Ersfeld and Gull, 1997), with the only exception that labelling of the DNA-probes was achieved with dUTP coupled to either Cy3 (used for minichromosomes) or Alexa488 (in the case of large chromosomes), both from Invitrogen.

5.9 Fluorescence analysis and live video microscopy

Parasites expressing a fluorescent fusion protein were either analysed after fixation for 30 min in a 4% PFA solution in PBS or directly by live video microscopy. In both cases, DNA was stained using DAPI (1µg/ml).

Parasites found in the fly were obtained from dissection in a drop of medium without serum directly on microscope slides. 5 µl of a solution of DAPI at 1 µg/ml was added to the drop and cells were covered by a coverslip and observed with a DMI4000 microscope (Leica). Videos were acquired using the camera COHU 460LI (Pieper) coupled to a DVD recorder (Sony RDR-HX725). This is an analogical system in which neither exposure time nor other parameters can be adapted. The different fluorescence signals were acquired by changing the

filters directly on the microscope. With this system we were able to acquire a maximum number of parasites that have a limited lifespan after being removed from the tsetse tissues. Movies were processed using the software Mpeg Streamclip 1.8 (Squared 5) and ImageJ 1.38X (NIH) and were assembled with iMovie (Apple). Still images were extracted with the ImageJ 1.38X (NIH) software. Fluorescence intensity of each cell was assessed on the performed movies by eye, thereby determining three categories: strong signal, intermediate signal, no visible signal.

5.10 Tsetse fly infection, maintenance and dissection

Teneral males of *Glossina morsitans morsitans* from 8 to 96 hours post eclosion were obtained from the TRYPANOSOM - UMR 177 IRD CIRAD, Campus International de Baillarguet, Montpellier, France. Tsetse flies were infected with cultured parasites during their first meal through a silicone membrane (Rotureau et al., 2011a). Freshly differentiated cultured procyclic AnTat1.1 were used at 10 million cells per ml in SDM79 medium supplemented with 10 % FCS, 60 mM N-acetylglucosamine (Sigma) (Peacock et al., 2006) and 2.5% (w/v) bovine serum albumin (Sigma) (Kabayo et al., 1986). Tsetse flies were subsequently maintained in Roubaud cages at 27°C and 70% hygrometry and fed twice a week through a silicone membrane with fresh rabbit blood in heparin. Flies were starved for at least 48 hours before being dissected 18 to 35 days post-ingestion. As described (Rotureau et al., 2011a), salivary glands were immediately isolated upon dissection. Whole tsetse alimentary tracts, from the distal part of the foregut to the rectum, were dissected in a drop of PBS or SDM79 without serum and hemin (the latter to avoid nutritional stress), and arranged lengthways to screen for parasite presence. Foregut and proventriculus were then separated from the midgut. Parasites were released from tissues in the medium/PBS drop and were immediately processed. The AnTat1.1 ALBA3::YFP cell line was proposed to 168 flies in 2 independent experiments (68 flies could be dissected of which 54% were infected in the midgut and 10.3% in the salivary glands). The AnTat1.1 ALBA4::YFP cell line was proposed to 93 flies in 1 experiment (36 flies could be dissected of which 33% were infected in the midgut and 11% in the salivary glands). For the GFP and ALBA::GFP over-expression experiments a total of 512 flies were infected. Fly batches were usually split in two so to have half of the flies infected with the GFP control strain and half with the cell line expressing ALBA::GFP. The AnTat1.1 GFP control cell line was proposed to 214 flies in 7 independent experiments (67 flies could be dissected of which 52% were infected in the midgut and 12%

in the salivary glands). The ALBA3::GFP cell line was proposed to 155 flies in 6 independent experiments (49 flies could be dissected of which 53% were infected in the midgut and 6% in the salivary glands). The ALBA4::GFP cell line was proposed to 143 flies in 3 independent experiments (42 flies could be dissected of which 50% were infected in the midgut and 17% in the salivary glands).

5.11 Semi-quantitative RT-PCR

Total RNA was extracted from cells grown with or without tetracycline for the indicated period of time and purified using Trizol (Invitrogen) as described by the manufacturer. DNA was eliminated by DNase treatment and RNA purity was confirmed by conventional PCR. After primer calibration and determination of optimal conditions, semi-quantitative RT-PCR was performed as described (Durand-Dubief et al., 2003) using the Superscript III One-step kit (Invirtogen). It turned out, that optimal conditions for ALBA were achieved with 50 ng RNA per assay with 25 cycles of PCR. For *ALBA3* and *ALBA4* a common forward primer was used: CAAAAACGAGGGTGCTAAG, in combination with specific reverse primers: *ALBA3* CACCAATCCCTTCATACTC and *ALBA4* CCACGACTGATTTGGGAAC. As independent control, we performed RT-PCR in parallel with described primers for *TbODA7* (Tb11.01.5550) (Duquesnoy et al., 2009). Primers were ordered from Eurogentec.

5.12 Plasmids and constructs

For plasmid construction, primers were ordered from Eurogentec and fragments amplified from trypanosome Lister 427 DNA using the high-fidelity Phusion polymerase (Finnzymes) in a PCR reaction according to the manufacturers' indications. The PCR fragment was directly ligated in the pCR*2.1-TOPO* vector (Invitrogen) and transformed into electrocompetent TOP10 bacteria (Invitrogen) following the manufacturers' instructions. Bacteria colonies were tested for successful insertion of the fragment by colony-PCR. Positive clones were amplified and plasmid DNA purified using the Nucleospin plasmid MINIprep Kit (Macherey & Nagel). The fragment is then excised using the appropriate restriction enzymes (either from New England Biolabs or Fermentas), purified and ligated into the prepared, purified final vector backbone (T4 ligase Fermentas). A new round of bacteria transfection and verification of positive colonies will be followed by preparation of plasmid DNA in high

amount using the Nucleobond xtra MAXI plus kit (Macherey & Nagel) following the manufacturers' instructions and sequencing analysis (Cogenics) for final verification.

***pZJM* vectors (Wang et al., 2000) for protein knock-down by RNAi**

The insert in this vector is flanked by T7 promoters facing each other allowing tetracycline-inducible dsRNA expression in cell lines PC 29-13 or BS 90-13 that encode a T7 RNA-Polymerase and tetracycline repressor (Wirtz et al., 1999). The *pZJMALBA3/4* plasmid was already available from a previous laboratory member Mickaël Durand-Dubief. For single RNAi, the sequences for dsRNA expression were selected using the RNAit algorithm (Redmond et al., 2003), for *ALBA3* a fragment of 300 bp (the last 75 bp of the 3' of the CDS and the first 227 bp of its 3'UTR) and for *ALBA4* of 350 bp (the last 77 bp of the 3' of the CDS and the first 272 bp of its 3'UTR) (see also Fig 3.18). The *pZJMALBA3* and the *pZJMALBA4* plasmids were ordered from GeneCust Europe (Dudelange, Luxembourg), where the selected *ALBA* sequences were chemically synthesized and subcloned into the *pZJM* vector after excision of the existing stuffer sequence by XhoI and HindIII.

For RNAi against *arginine kinase* (*AK*) suitable targeting sequences were selected with RNAit and two *pZJM* constructs were cloned (see also Fig 3.38). The first was selected to target all *AK1-3* and contains an insert of 406 bp common to all *AK* (spanning bp 226 to 631, when the numbering was set to zero at the *AK1* sequence start). The fragment was amplified using the primers: forward 5' AAGCTTACTGTGTTTGCCGACCTCTT '3 (HindIII site underlined) and reverse 5' CTCGAGAGATACCACGACCAGTTGGC '3 (XhoI site underlined). The other vector is meant to target *AK3* alone, but as most of its sequence is conserved in *AK1* and *AK2*, the insert was thus selected in the extreme 3' region of the coding sequence (the last 90 nucleotides) and the first part of the 3' UTR (140 nucleotides). It was amplified using the forward primer AAGCTTCAATCCGATGATGCAGAGG (HindIII site underlined) and reverse primer CTCGAGGGAATCATCACATGCTACCCT (XhoI site underlined).

Before transfection into trypanosomes, all pZJM plasmids were linearized at the unique NotI site in the rDNA intergenic targeting region. For *pZJMAK1-3* linearization was performed with ClaI, as the fragment contains a NotI recognition sequence.

Over-expression of ALBA as GFP fusion

For exogenous over-expression of ALBA proteins as GFP tagged versions, the complete coding sequence of *ALBA3* and *ALBA4* was cloned in the plasmid pHD67E (Bingle et al.,

2001) upstream of the *GFP* sequence using the HindIII restriction site. A common forward primer was used GCACAATAAGCTTATGCCTTCATATCCG (HindIII site underlined) in combination with specific reverse primers, GCACTAAGCTTCGCTCCTCATTGCCACC (HindIII site underlined) for *ALBA3* and GCACTAAGCTTCGGTTGCCTTCACCCAA (HindIII site underlined) for *ALBA4.* Before transfection, the plasmids were linearized at the unique NotI site for targeting to the *rDNA* intergenic region.

Endogenous tagging of ALBA and FLAMM

Endogenous tagging is achieved with plasmids that contain a fragment of the target gene sequence flanked by either YFP or mCherry in 5' or 3' positions. Before transfection, the plasmid will be linearized in the target gene sequence, allowing homologous recombination with the target allele. The expression of this fluorescent fusion protein will be under the control of one of the UTRs from the gene locus and one coming from the inserted plasmid. Different vectors for endogenous tagging were used that are described in (Kelly et al., 2007) and sequences are found in (http://web.me.com/mc115/mclab/resources.html). The p3329 allows tagging with eYFP at the C-terminal end of the protein and selection by puromycin (Fig 5.1). Alternatively, the vector p2705 was chosen to tag ALBA4 at the C-terminus with mCherry bearing a neomycin resistance cassette. N-terminal tagging with eYFP was chosen for some FLAMM proteins and was achieved using the p2675 vector with puromycin resistance. All the target sequence fragments were chemically synthesized by GeneCust Europe (Dudelange, Luxembourg) and subcloned into the corresponding endogenous tagging vectors.

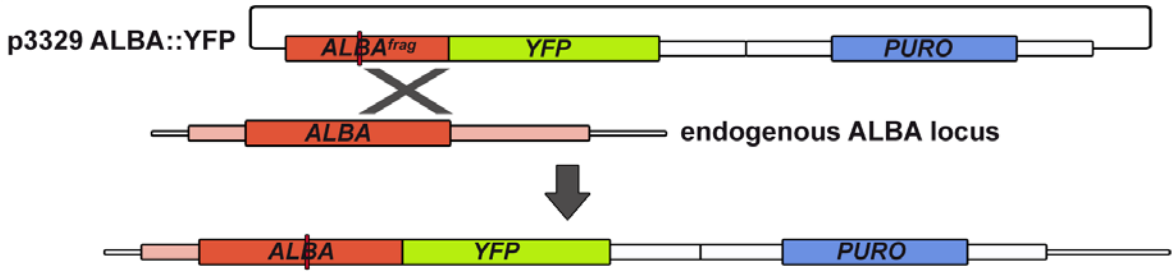

Figure 5.1: Endogenous tagging procedure. Schematic representation of the procedure used for endogenously tagging ALBA proteins with eYFP. The plasmid p3329, containing a fragment of the *ALBA* gene upstream of the *YFP* sequence and a puromycin resistance cassette, is linearized (red line) within the *ALBA* sequence before transfection. This allows homologous recombination with one of the endogenous *ALBA* copies to create YFP tagged ALBA. Its expression is under the control of the ALBA 5'UTR (light red) and of the 3'UTR from the plasmid (white).

The following table shows the different vectors used in this study (Table 5.2). The plasmid for the endogenous expression of the mCherry tagged version of DHH1 was linearized as described with NheI and transfectants selected with blasticidin (Kramer et al., 2008).

Table 5.2: Plasmids for endogenous tagging with eYFP and mCherry. Fragments of the target gene at either the 5' or the 3' end (without stop codon) were synthesized containing restriction enzyme recognition sequences. They were cloned into the respective plasmid backbone, either p3329 (allows C-terminal eYFP tagging), p2705 (allows mCherry C-terminal tagging) and p2675 (allows N-terminal tagging with eYFP). Before transfection in trypanosomes the plasmids were linearized in the target fragment with the indicated restriction enzymes and according to the plasmid, selection was applied with either puromycin (PURO) or with G418 (NEO).

target	fragment	cloned with	plasmid	linearization	selection
ALBA3	3' 520 bp	KpnI / BamHI	*p3329ALBA3*	AfeI	PURO
ALBA4	3' 393 bp	KpnI / BamHI	*p3329ALBA4*	FspAI	PURO
ALBA4	3' 393 bp	EcoRV / BamHI	*p2705ALBA4*	FspAI	NEO
FLAMM1	3' 324 bp	KpnI / BamHI	*p3329FLAMM1*	XhoI	PURO
FLAMM2	3' 231 bp	KpnI / BamHI	*p3329FLAMM2*	ApaI	PURO
FLAMM3	3' 573 bp	PaeI / BamHI	*p3329FLAMM3*	FspAI	PURO
FLAMM4	5' 419 bp	Hind III / ApaI	*p2675FLAMM4*	BbsI	PURO
FLAMM5	3' 391 bp	KpnI / BamHI	*p3329FLAMM5*	BsmI	PURO
FLAMM6	3' 460 bp	KpnI / BamHI	*p3329FLAMM6*	BbsI	PURO
FLAMM7	5' 535 bp	HindIII / ApaI	*p2675FLAMM7*	ClaI	PURO
FLAMM8	3' 500 bp	KpnI / BamHI	*p3329FLAMM8*	NruI	PURO
FLAMM9	3' 250 bp	KpnI / BamHI	*p3329FLAMM9*	SphI	PURO
FLAMM10	3' 494 bp	KpnI / BamHI	*p3329FLAMM10*	SphI	PURO

5.13 Stable transformation of trypanosomes

Trypanosomes were transfected with the linearized plasmid constructs by Nucleofector® technology (Lonza, Italy) as described (Burkard et al., 2007). Transgenic cell lines were selected in medium supplemented with the respective antibiotics (Table 5.3).

Resistance	Selection	Concentration (µg/ml)
NEO	G418	15
HYG	Hygromycin	25 - 50
BLE	Phleomycin	2.5
PUR	Puromycin	1 - 3
BSR	Blasticidin	10

Table 5.3: Antibiotics used for the selection of transgenic trypanosome procyclic cell lines. The resistance cassette is indicated as well as the antibiotics for selection used at different concentrations (all from Invivogen).

For induction of RNAi, tetracycline (Sigma) was added to the medium at each dilution step at a final concentration of 1 µg/ml.

In order to obtain clonal cell lines, the selected population was serially diluted and the dilutions spread to 96-well plates to obtain ¼ of the wells with 50 cells/well, ¼ of wells with 5 cells/well and half with in theory 0.5 cells/well. For this procedure, to facilitate growth of procyclic cells at low densities they were diluted in conditioned medium (medium that had been used to culture procyclic forms up to a density of 10^7 cells/ml, then has been centrifuged and the supernatant filtered through a filter with pores of 0.2 µm diameter from Millipore).

6 BIBLIOGRAPHY

Absalon, S., Kohl, L., Branche, C., Blisnick, T., Toutirais, G., Rusconi, F., Cosson, J., Bonhivers, M., Robinson, D. and Bastin, P. (2007). Basal body positioning is controlled by flagellum formation in *Trypanosoma brucei*. *PLoS One* 2, e437.

Acosta-Serrano, A., Vassella, E., Liniger, M., Kunz Renggli, C., Brun, R., Roditi, I. and Englund, P. T. (2001). The surface coat of procyclic *Trypanosoma brucei*: programmed expression and proteolytic cleavage of procyclin in the tsetse fly. *Proc Natl Acad Sci U S A* 98, 1513-8.

Adhiambo, C., Blisnick, T., Toutirais, G., Delannoy, E. and Bastin, P. (2009). A novel function for the atypical small G protein Rab-like 5 in the assembly of the trypanosome flagellum. *J Cell Sci* 122, 834-41.

Aksoy, S., Gibson, W. C. and Lehane, M. J. (2003). Interactions between tsetse and trypanosomes with implications for the control of trypanosomiasis. *Adv Parasitol* 53, 1-83.

Alsford, S., Kawahara, T., Isamah, C. and Horn, D. (2007). A sirtuin in the African trypanosome is involved in both DNA repair and telomeric gene silencing but is not required for antigenic variation. *Mol Microbiol* 63, 724-36.

Alsford, S., Turner, D. J., Obado, S. O., Sanchez-Flores, A., Glover, L., Berriman, M., Hertz-Fowler, C. and Horn, D. (2011). High-throughput phenotyping using parallel sequencing of RNA interference targets in the African trypanosome. *Genome Res* 21, 915-24.

Ammermann, D., Steinbruck, G., von Berger, L. and Hennig, W. (1974). The development of the macronucleus in the ciliated protozoan *Stylonychia mytilus*. *Chromosoma* 45, 401-29.

Anderson, P. and Kedersha, N. (2009). RNA granules: post-transcriptional and epigenetic modulators of gene expression. *Nat Rev Mol Cell Biol* 10, 430-6.

Aravind, L., Iyer, L. M. and Anantharaman, V. (2003). The two faces of Alba: the evolutionary connection between proteins participating in chromatin structure and RNA metabolism. *Genome Biol* 4, R64.

Archer, S., Queiroz, R., Stewart, M. and Clayton, C. (2008). Trypanosomes as a model to investigate mRNA decay pathways. *Methods Enzymol* 448, 359-77.

Archer, S. K., Luu, V. D., de Queiroz, R. A., Brems, S. and Clayton, C. (2009). *Trypanosoma brucei* PUF9 regulates mRNAs for proteins involved in replicative processes over the cell cycle. *PLoS Pathog* 5, e1000565.

Balana-Fouce, R. and Reguera, R. M. (2007). RNA interference in *Trypanosoma brucei*: a high-throughput engine for functional genomics in trypanosomatids? *Trends Parasitol* 23, 348-51.

Barrett, M. P. (2010). Potential new drugs for human African trypanosomiasis: some progress at last. *Curr Opin Infect Dis* 23, 603-8.

Bastin, P., Ellis, K., Kohl, L. and Gull, K. (2000). Flagellum ontogeny in trypanosomes studied via an inherited and regulated RNA interference system. *J Cell Sci* 113 (Pt 18), 3321-8.

Bastin, P., MacRae, T. H., Francis, S. B., Matthews, K. R. and Gull, K. (1999). Flagellar morphogenesis: protein targeting and assembly in the paraflagellar rod of trypanosomes. *Mol Cell Biol* 19, 8191-200.

Bell, S. D., Botting, C. H., Wardleworth, B. N., Jackson, S. P. and White, M. F. (2002). The interaction of Alba, a conserved archaeal chromatin protein, with Sir2 and its regulation by acetylation. *Science* 296, 148-51.

Benne, R., Van den Burg, J., Brakenhoff, J. P., Sloof, P., Van Boom, J. H. and Tromp, M. C. (1986). Major transcript of the frameshifted coxII gene from trypanosome mitochondria contains four nucleotides that are not encoded in the DNA. *Cell* 46, 819-26.

Berriman, M. Ghedin, E. Hertz-Fowler, C. Blandin, G. Renauld, H. Bartholomeu, D. C. Lennard, N. J. Caler, E. Hamlin, N. E. Haas, B. et al. (2005). The genome of the African trypanosome *Trypanosoma brucei*. *Science* 309, 416-22.

Bingle, L. E., Eastlake, J. L., Bailey, M. and Gibson, W. C. (2001). A novel GFP approach for the analysis of genetic exchange in trypanosomes allowing the in situ detection of mating events. *Microbiology* 147, 3231-40.

Biou, V., Shu, F. and Ramakrishnan, V. (1995). X-ray crystallography shows that translational initiation factor IF3 consists of two compact alpha/beta domains linked by an alpha-helix. *Embo J* 14, 4056-64.

Boekhoff, I., Tareilus, E., Strotmann, J. and Breer, H. (1990). Rapid activation of alternative second messenger pathways in olfactory cilia from rats by different odorants. *Embo J* 9, 2453-8.

Branche, C., Kohl, L., Toutirais, G., Buisson, J., Cosson, J. and Bastin, P. (2006). Conserved and specific functions of axoneme components in trypanosome motility. *J Cell Sci* 119, 3443-55.

Brems, S., Guilbride, D. L., Gundlesdodjir-Planck, D., Busold, C., Luu, V. D., Schanne, M., Hoheisel, J. and Clayton, C. (2005). The transcriptomes of *Trypanosoma brucei* Lister 427 and TREU927 bloodstream and procyclic trypomastigotes. *Mol Biochem Parasitol* 139, 163-72.

Briggs, L. J., McKean, P. G., Baines, A., Moreira-Leite, F., Davidge, J., Vaughan, S. and Gull, K. (2004). The flagella connector of *Trypanosoma brucei*: an unusual mobile transmembrane junction. *J Cell Sci* 117, 1641-51.

Broadhead, R., Dawe, H. R., Farr, H., Griffiths, S., Hart, S. R., Portman, N., Shaw, M. K., Ginger, M. L., Gaskell, S. J., McKean, P. G. et al. (2006). Flagellar motility is required for the viability of the bloodstream trypanosome. *Nature* 440, 224-7.

Bruce, D. (1895). Preliminary Report on Tsetse Fly Disease or Nagana in Zululand. *Bennet and Davis* Durban, 18 pp.

Brun, R., Blum, J., Chappuis, F. and Burri, C. (2009). Human African trypanosomiasis. *Lancet* 375, 148-59.

Brun, R. and Schönenberger. (1979). Cultivation and in vitro cloning of procyclic culture forms of *Trypanosoma brucei* in a semi-defined medium. Short communication. *Acta Trop* 36, 289-92.

Brun, R. and Schonenberger, M. (1981). Stimulating effect of citrate and cis-Aconitate on the transformation of *Trypanosoma brucei* bloodstream forms to procyclic forms in vitro. *Z Parasitenkd* 66, 17-24.

Burkard, G., Fragoso, C. M. and Roditi, I. (2007). Highly efficient stable transformation of bloodstream forms of *Trypanosoma brucei*. *Mol Biochem Parasitol* 153, 220-3.

Campbell, D. A., Thomas, S. and Sturm, N. R. (2003). Transcription in kinetoplastid protozoa: why be normal? *Microbes Infect* 5, 1231-40.

Canepa, G. E., Carrillo, C., Miranda, M. R., Saye, M. and Pereira, C. A. (2011). Arginine kinase in *Phytomonas*, a trypanosomatid parasite of plants. *Comp Biochem Physiol B Biochem Mol Biol* 160, 40-3.

Carruthers, V. B. and Cross, G. A. (1992). High-efficiency clonal growth of bloodstream- and insect-form *Trypanosoma brucei* on agarose plates. *Proc Natl Acad Sci U S A* 89, 8818-21.

Cassola, A., De Gaudenzi, J. G. and Frasch, A. C. (2007). Recruitment of mRNAs to cytoplasmic ribonucleoprotein granules in trypanosomes. *Mol Microbiol* 65, 655-70.

Chamberlain, J. R., Lee, Y., Lane, W. S. and Engelke, D. R. (1998). Purification and characterization of the nuclear RNase P holoenzyme complex reveals extensive subunit overlap with RNase MRP. *Genes Dev* 12, 1678-90.

Chang, D. D. and Clayton, D. A. (1987). A novel endoribonuclease cleaves at a priming site of mouse mitochondrial DNA replication. *Embo J* 6, 409-17.

Chappuis, F., Lima, M. A., Flevaud, L. and Ritmeijer, K. (2010). Human African trypanosomiasis in areas without surveillance. *Emerg Infect Dis* 16, 354-6.

Chen, Y., Hung, C. H., Burderer, T. and Lee, G. S. (2003). Development of RNA interference revertants in *Trypanosoma brucei* cell lines generated with a double stranded RNA expression construct driven by two opposing promoters. *Mol Biochem Parasitol* 126, 275-9.

Chou, C. C., Lin, T. W., Chen, C. Y. and Wang, A. H. (2003). Crystal structure of the hyperthermophilic archaeal DNA-binding protein Sso10b2 at a resolution of 1.85 Angstroms. *J Bacteriol* 185, 4066-73.

Clayton, C. and Shapira, M. (2007). Post-transcriptional regulation of gene expression in trypanosomes and leishmanias. *Mol Biochem Parasitol* 156, 93-101.

Cotrim, P. C., Paranhos-Baccala, G., Santos, M. R., Mortensen, C., Cano, M. I., Jolivet, M., Camargo, M. E., Mortara, R. A. and Da Silveira, J. F. (1995). Organization and expression of the gene encoding an immunodominant repetitive antigen associated to the cytoskeleton of *Trypanosoma cruzi*. *Mol Biochem Parasitol* 71, 89-98.

Cross, G. A. (1977). Antigenic variation in trypanosomes. *Am J Trop Med Hyg* 26, 240-4.

Czichos, J., Nonnengaesser, C. and Overath, P. (1986). *Trypanosoma brucei*: cis-aconitate and temperature reduction as triggers of synchronous transformation of bloodstream to procyclic trypomastigotes in vitro. *Exp Parasitol* 62, 283-91.

Daniels, J. P., Gull, K. and Wickstead, B. (2010). Cell biology of the trypanosome genome. *Microbiol Mol Biol Rev* 74, 552-69.

De Gaudenzi, J., Frasch, A. C. and Clayton, C. (2005). RNA-binding domain proteins in Kinetoplastids: a comparative analysis. *Eukaryot Cell* 4, 2106-14.

Dean, S., Marchetti, R., Kirk, K. and Matthews, K. R. (2009). A surface transporter family conveys the trypanosome differentiation signal. *Nature* 459, 213-7.

Domenicali Pfister, D., Burkard, G., Morand, S., Renggli, C. K., Roditi, I. and Vassella, E. (2006). A Mitogen-activated protein kinase controls differentiation of bloodstream forms of *Trypanosoma brucei*. *Eukaryot Cell* 5, 1126-35.

Duquesnoy, P., Escudier, E., Vincensini, L., Freshour, J., Bridoux, A. M., Coste, A., Deschildre, A., de Blic, J., Legendre, M., Montantin, G. et al. (2009). Loss-of-function mutations in the human ortholog of *Chlamydomonas reinhardtii* ODA7 disrupt dynein arm assembly and cause primary ciliary dyskinesia. *Am J Hum Genet* 85, 890-6.

Durand-Dubief, M., Kohl, L. and Bastin, P. (2003). Efficiency and specificity of RNA interference generated by intra- and intermolecular double stranded RNA in *Trypanosoma brucei*. *Mol Biochem Parasitol* 129, 11-21.

Eckert, R., Naitoh, Y. and Friedman, K. (1972). Sensory mechanisms in *Paramecium. I*. Two components of the electric response to mechanical stimulation of the anterior surface. *J Exp Biol* 56, 683-94.

Elias, R. V., Sezate, S. S., Cao, W. and McGinnis, J. F. (2004). Temporal kinetics of the light/dark translocation and compartmentation of arrestin and alpha-transducin in mouse photoreceptor cells. *Mol Vis* 10, 672-81.

Ellis, D. S. and Evans, D. A. (1977). Passage of *Trypanosoma brucei rhodesiense* through the peritrophic membrane of *Glossina morsitans morsitans*. *Nature* 267, 834-5.

Ellis, J., Sarkar, M., Hendriks, E. and Matthews, K. (2004). A novel ERK-like, CRK-like protein kinase that modulates growth in *Trypanosoma brucei* via an autoregulatory C-terminal extension. *Mol Microbiol* 53, 1487-99.

Ellis, J. C., Barnes, J. and Brown, J. W. (2007). Is Alba an RNase P subunit? *RNA Biol* 4, 169-72.

Emmer, B. T., Souther, C., Toriello, K. M., Olson, C. L., Epting, C. L. and Engman, D. M. (2009). Identification of a palmitoyl acyltransferase required for protein sorting to the flagellar membrane. *J Cell Sci* 122, 867-74.

Engstler, M. and Boshart, M. (2004). Cold shock and regulation of surface protein trafficking convey sensitization to inducers of stage differentiation in *Trypanosoma brucei*. *Genes Dev* 18, 2798-811.

Ersfeld, K. and Gull, K. (1997). Partitioning of large and minichromosomes in *Trypanosoma brucei*. *Science* 276, 611-4.

Estevez, A. M. (2008). The RNA-binding protein TbDRBD3 regulates the stability of a specific subset of mRNAs in trypanosomes. *Nucleic Acids Res* 36, 4573-86.

Evans, D. A. and Ellis, D. S. (1975). Penetration of mid-gut cells of *Glossina morsitans morsitans* by *Trypanosoma brucei rhodesiense*. *Nature* 258, 231-3.

Ferguson, M. A., Haldar, K. and Cross, G. A. (1985). *Trypanosoma brucei* variant surface glycoprotein has a sn-1,2-dimyristyl glycerol membrane anchor at its COOH terminus. *J Biol Chem* 260, 4963-8.

Ferguson, M. A., Homans, S. W., Dwek, R. A. and Rademacher, T. W. (1988). Glycosyl-phosphatidylinositol moiety that anchors *Trypanosoma brucei* variant surface glycoprotein to the membrane. *Science* 239, 753-9.

Fernandez-Moya, S. M. and Estevez, A. M. (2010). Posttranscriptional control and the role of RNA-binding proteins in gene regulation in trypanosomatid protozoan parasites. *Wiley Interdisciplinary Reviews - RNA* 1.

Fetzer, C. P., Hogan, D. J. and Lipps, H. J. (2002). A PIWI homolog is one of the proteins expressed exclusively during macronuclear development in the ciliate *Stylonychia lemnae*. *Nucleic Acids Res* 30, 4380-6.

Field, M. C. and Carrington, M. (2009). The trypanosome flagellar pocket. *Nat Rev Microbiol* 7, 775-86.

Field, M. C., Lumb, J. H., Adung'a, V. O., Jones, N. G. and Engstler, M. (2009). Macromolecular trafficking and immune evasion in african trypanosomes. *Int Rev Cell Mol Biol* 278, 1-67.

Figarella, K., Uzcategui, N. L., Zhou, Y., LeFurgey, A., Ouellette, M., Bhattacharjee, H. and Mukhopadhyay, R. (2007). Biochemical characterization of *Leishmania major* aquaglyceroporin LmAQP1: possible role in volume regulation and osmotaxis. *Mol Microbiol* 65, 1006-17.

Forterre, P., Confalonieri, F. and Knapp, S. (1999). Identification of the gene encoding archeal-specific DNA-binding proteins of the Sac10b family. *Mol Microbiol* 32, 669-70.

Fragoso, C. M., Schumann Burkard, G., Oberle, M., Renggli, C. K., Hilzinger, K. and Roditi, I. (2009). PSSA-2, a membrane-spanning phosphoprotein of *Trypanosoma brucei*, is required for efficient maturation of infection. *PLoS One* 4, e7074.

Furger, A., Schurch, N., Kurath, U. and Roditi, I. (1997). Elements in the 3' untranslated region of procyclin mRNA regulate expression in insect forms of *Trypanosoma brucei* by modulating RNA stability and translation. *Mol Cell Biol* 17, 4372-80.

Garcia-Gonzalo, F. R., Corbit, K. C., Sirerol-Piquer, M. S., Ramaswami, G., Otto, E. A., Noriega, T. R., Seol, A. D., Robinson, J. F., Bennett, C. L., Josifova, D. J. et al. (2011). A transition zone complex regulates mammalian ciliogenesis and ciliary membrane composition. *Nat Genet* 43, 776-84.

Garcia-Salcedo, J. A., Gijon, P., Nolan, D. P., Tebabi, P. and Pays, E. (2003). A chromosomal SIR2 homologue with both histone NAD-dependent ADP-ribosyltransferase and deacetylase activities is involved in DNA repair in *Trypanosoma brucei*. *Embo J* 22, 5851-62.

Garcia-Salcedo, J. A., Nolan, D. P., Gijon, P., Gomez-Rodriguez, J. and Pays, E. (2002). A protein kinase specifically associated with proliferative forms of *Trypanosoma brucei* is functionally related to a yeast kinase involved in the co-ordination of cell shape and division. *Mol Microbiol* 45, 307-19.

Gibson, W., Peacock, L., Ferris, V., Williams, K. and Bailey, M. (2008). The use of yellow fluorescent hybrids to indicate mating in *Trypanosoma brucei*. *Parasit Vectors* 1, 4.

Gill, T., Aulds, J. and Schmitt, M. E. (2006). A specialized processing body that is temporally and asymmetrically regulated during the cell cycle in *Saccharomyces cerevisiae*. *J Cell Biol* 173, 35-45.

Gill, T., Cai, T., Aulds, J., Wierzbicki, S. and Schmitt, M. E. (2004). RNase MRP cleaves the CLB2 mRNA to promote cell cycle progression: novel method of mRNA degradation. *Mol Cell Biol* 24, 945-53.

Ginger, M. L., Blundell, P. A., Lewis, A. M., Browitt, A., Gunzl, A. and Barry, J. D. (2002). Ex vivo and in vitro identification of a consensus promoter for VSG genes expressed by metacyclic-stage trypanosomes in the tsetse fly. *Eukaryot Cell* 1, 1000-9.

Ginger, M. L., Ngazoa, E. S., Pereira, C. A., Pullen, T. J., Kabiri, M., Becker, K., Gull, K. and Steverding, D. (2005). Intracellular positioning of isoforms explains an unusually large adenylate kinase gene family in the parasite *Trypanosoma brucei*. *J Biol Chem* 280, 11781-9.

Godin, K. S. and Varani, G. (2007). How arginine-rich domains coordinate mRNA maturation events. *RNA Biol* 4, 69-75.

Godsel, L. M. and Engman, D. M. (1999). Flagellar protein localization mediated by a calcium-myristoyl/palmitoyl switch mechanism. *Embo J* 18, 2057-65.

Gong, Z., Son, W., Chung, Y. D., Kim, J., Shin, D. W., McClung, C. A., Lee, Y., Lee, H. W., Chang, D. J., Kaang, B. K. et al. (2004). Two interdependent TRPV channel subunits, inactive and Nanchung, mediate hearing in *Drosophila*. *J Neurosci* 24, 9059-66.

Gopalan, V., Vioque, A. and Altman, S. (2002). RNase P: variations and uses. *J Biol Chem* 277, 6759-62.

Graham, S. V., Matthews, K. R., Shiels, P. G. and Barry, J. D. (1990). Distinct, developmental stage-specific activation mechanisms of trypanosome VSG genes. *Parasitology* 101 Pt 3, 361-7.

Graham, S. V., Terry, S. and Barry, J. D. (1999). A structural and transcription pattern for variant surface glycoprotein gene expression sites used in metacyclic stage *Trypanosoma brucei*. *Mol Biochem Parasitol* 103, 141-54.

Guerrier-Takada, C., Eder, P. S., Gopalan, V. and Altman, S. (2002). Purification and characterization of Rpp25, an RNA-binding protein subunit of human ribonuclease P. *Rna* 8, 290-5.

Guo, R., Xue, H. and Huang, L. (2003). Ssh10b, a conserved thermophilic archaeal protein, binds RNA in vivo. *Mol Microbiol* 50, 1605-15.

Hada, K., Nakashima, T., Osawa, T., Shimada, H., Kakuta, Y. and Kimura, M. (2008). Crystal structure and functional analysis of an archaeal chromatin protein Alba from the hyperthermophilic archaeon *Pyrococcus horikoshii* OT3. *Biosci Biotechnol Biochem* 72, 749-58.

Haile, S. and Papadopoulou, B. (2007). Developmental regulation of gene expression in trypanosomatid parasitic protozoa. *Curr Opin Microbiol* 10, 569-77.

Hajduk, S. L. (1984). Antigenic variation during the developmental cycle of *Trypanosoma brucei*. *J Protozool* 31, 41-7.

Hamm, B., Schindler, A., Mecke, D. and Duszenko, M. (1990). Differentiation of *Trypanosoma brucei* bloodstream trypomastigotes from long slender to short stumpy-like forms in axenic culture. *Mol Biochem Parasitol* 40, 13-22.

Hammarton, T. C. (2007). Cell cycle regulation in *Trypanosoma brucei*. *Mol Biochem Parasitol* 153, 1-8.

Hammarton, T. C., Clark, J., Douglas, F., Boshart, M. and Mottram, J. C. (2003). Stage-specific differences in cell cycle control in *Trypanosoma brucei* revealed by RNA interference of a mitotic cyclin. *J Biol Chem* 278, 22877-86.

Hammarton, T. C., Engstler, M. and Mottram, J. C. (2004). The *Trypanosoma brucei* cyclin, CYC2, is required for cell cycle progression through G1 phase and for maintenance of procyclic form cell morphology. *J Biol Chem* 279, 24757-64.

Hands-Taylor, K. L., Martino, L., Tata, R., Babon, J. J., Bui, T. T., Drake, A. F., Beavil, R. L., Pruijn, G. J., Brown, P. R. and Conte, M. R. (2010). Heterodimerization of the human RNase P/MRP subunits Rpp20 and Rpp25 is a prerequisite for interaction with the P3 arm of RNase MRP RNA. *Nucleic Acids Res* 38, 4052-66.

Hehl, A., Vassella, E., Braun, R. and Roditi, I. (1994). A conserved stem-loop structure in the 3' untranslated region of procyclin mRNAs regulates expression in *Trypanosoma brucei*. *Proc Natl Acad Sci U S A* 91, 370-4.

Hendriks, E. F. and Matthews, K. R. (2007). Post-transcriptional control of gene expression in african trypanosomes. In: Trypanosomes after the genome. Norfolk, U.K.: Horizon Bioscience.

Hendriks, E. F., Robinson, D. R., Hinkins, M. and Matthews, K. R. (2001). A novel CCCH protein which modulates differentiation of *Trypanosoma brucei* to its procyclic form. *Embo J* 20, 6700-11.

Herder, S., Votypka, J., Jirku, M., Radrova, J., Janzen, C. J. and Lukes, J. (2007). *Trypanosoma brucei* 29-13 strain is inducible in but not permissive for the tsetse fly vector. *Exp Parasitol* 117, 111-4.

Hertz-Fowler, C., Renauld, H. and Berriman, M. (2007). The genome of *Trypanosoma brucei*. In: Trypanosomes after the genome. Norfolk, U.K.: Horizon Bioscience.

Hirumi, H. and Hirumi, K. (1989). Continuous cultivation of *Trypanosoma brucei* blood stream forms in a medium containing a low concentration of serum protein without feeder cell layers. *J Parasitol* 75, 985-9.

Hotz, H. R., Hartmann, C., Huober, K., Hug, M. and Clayton, C. (1997). Mechanisms of developmental regulation in *Trypanosoma brucei*: a polypyrimidine tract in the 3'-untranslated region of a surface protein mRNA affects RNA abundance and translation. *Nucleic Acids Res* 25, 3017-26.

Hua, S. B. and Wang, C. C. (1994). Differential accumulation of a protein kinase homolog in *Trypanosoma brucei*. *J Cell Biochem* 54, 20-31.

Huang, K., Kunkel, T. and Beck, C. F. (2004). Localization of the blue-light receptor phototropin to the flagella of the green alga *Chlamydomonas reinhardtii*. *Mol Biol Cell* 15, 3605-14.

Huangfu, D., Liu, A., Rakeman, A. S., Murcia, N. S., Niswander, L. and Anderson, K. V. (2003). Hedgehog signalling in the mouse requires intraflagellar transport proteins. *Nature* 426, 83-7.

Hunt, M., Brun, R. and Kohler, P. (1994). Studies on compounds promoting the in vitro transformation of *Trypanosoma brucei* from bloodstream to procyclic forms. *Parasitol Res* 80, 600-6.

Iizuka, M. and Smith, M. M. (2003). Functional consequences of histone modifications. *Curr Opin Genet Dev* 13, 154-60.

Imboden, M., Muller, N., Hemphill, A., Mattioli, R. and Seebeck, T. (1995). Repetitive proteins from the flagellar cytoskeleton of African trypanosomes are diagnostically useful antigens. *Parasitology* 110 (Pt 3), 249-58.

Inoue, M., Nakamura, Y., Yasuda, K., Yasaka, N., Hara, T., Schnaufer, A., Stuart, K. and Fukuma, T. (2005). The 14-3-3 proteins of *Trypanosoma brucei* function in motility, cytokinesis, and cell cycle. *J Biol Chem* 280, 14085-96.

Jacobson, M. R., Cao, L. G., Wang, Y. L. and Pederson, T. (1995). Dynamic localization of RNase MRP RNA in the nucleolus observed by fluorescent RNA cytochemistry in living cells. *J Cell Biol* 131, 1649-58.

Jarrous, N. (2002). Human ribonuclease P: subunits, function, and intranuclear localization. *Rna* 8, 1-7.

Jelinska, C., Conroy, M. J., Craven, C. J., Hounslow, A. M., Bullough, P. A., Waltho, J. P., Taylor, G. L. and White, M. F. (2005). Obligate heterodimerization of the archaeal Alba2 protein with Alba1 provides a mechanism for control of DNA packaging. *Structure* 13, 963-71.

Jensen, B. C., Sivam, D., Kifer, C. T., Myler, P. J. and Parsons, M. (2009). Widespread variation in transcript abundance within and across developmental stages of *Trypanosoma brucei*. *BMC Genomics* 10, 482.

Johnson, K. A. and Rosenbaum, J. L. (1992). Polarity of flagellar assembly in *Chlamydomonas*. *J Cell Biol* 119, 1605-11.

Johnson, P. J., Kooter, J. M. and Borst, P. (1987). Inactivation of transcription by UV irradiation of *T. brucei* provides evidence for a multicistronic transcription unit including a VSG gene. *Cell* 51, 273-81.

Jonsson, F., Wen, J. P., Fetzer, C. P. and Lipps, H. J. (1999). A subtelomeric DNA sequence is required for correct processing of the macronuclear DNA sequences during macronuclear development in the hypotrichous ciliate *Stylonychia lemnae*. *Nucleic Acids Res* 27, 2832-41.

Kabani, S., Fenn, K., Ross, A., Ivens, A., Smith, T. K., Ghazal, P. and Matthews, K. (2009). Genome-wide expression profiling of in vivo-derived bloodstream parasite stages and dynamic analysis of mRNA alterations during synchronous differentiation in *Trypanosoma brucei*. *BMC Genomics* 10, 427.

Kabayo, J. P., DeLoach, J. R., Spates, G. E., Holman, G. M. and Kapatsa, G. M. (1986). Studies on the biochemical basis of the nutritional quality of tsetse fly diets. *Comp Biochem Physiol A Comp Physiol* 83, 133-9.

Kedersha, N., Stoecklin, G., Ayodele, M., Yacono, P., Lykke-Andersen, J., Fritzler, M. J., Scheuner, D., Kaufman, R. J., Golan, D. E. and Anderson, P. (2005). Stress granules and processing bodies are dynamically linked sites of mRNP remodeling. *J Cell Biol* 169, 871-84.

Keene, J. D. (2007). RNA regulons: coordination of post-transcriptional events. *Nat Rev Genet* 8, 533-43.

Kelly, S., Reed, J., Kramer, S., Ellis, L., Webb, H., Sunter, J., Salje, J., Marinsek, N., Gull, K., Wickstead, B. et al. (2007). Functional genomics in *Trypanosoma brucei*: a collection of vectors for the expression of tagged proteins from endogenous and ectopic gene loci. *Mol Biochem Parasitol* 154, 103-9.

Kilmartin, J. V., Wright, B. and Milstein, C. (1982). Rat monoclonal antitubulin antibodies derived by using a new nonsecreting rat cell line. *J Cell Biol* 93, 576-82.

Kleine, F. K. (1909). Weitere wissenschaftliche Beobachtungen über die Entwicklung von Trypanosomen in Glossinen. *Deutsche medizinische Wochenschrift* 35, 924-925.

Kohl, L., Robinson, D. and Bastin, P. (2003). Novel roles for the flagellum in cell morphogenesis and cytokinesis of trypanosomes. *Embo J* 22, 5336-46.

Kohl, L., Sherwin, T. and Gull, K. (1999). Assembly of the paraflagellar rod and the flagellum attachment zone complex during the *Trypanosoma brucei* cell cycle. *J Eukaryot Microbiol* 46, 105-9.

Konig, E., Delius, H., Carrington, M., Williams, R. O. and Roditi, I. (1989). Duplication and transcription of procyclin genes in *Trypanosoma brucei*. *Nucleic Acids Res* 17, 8727-39.

Kramer, S. and Carrington, M. (2010). Trans-acting proteins regulating mRNA maturation, stability and translation in trypanosomatids. *Trends Parasitol*.

Kramer, S., Queiroz, R., Ellis, L., Hoheisel, J. D., Clayton, C. and Carrington, M. (2010). The RNA helicase DHH1 is central to the correct expression of many developmentally regulated mRNAs in trypanosomes. *J Cell Sci* 123, 699-711.

Kramer, S., Queiroz, R., Ellis, L., Webb, H., Hoheisel, J. D., Clayton, C. and Carrington, M. (2008). Heat shock causes a decrease in polysomes and the appearance of stress granules in trypanosomes independently of eIF2(alpha) phosphorylation at Thr169. *J Cell Sci* 121, 3002-14.

LaCount, D. J., Barrett, B. and Donelson, J. E. (2002). *Trypanosoma brucei* FLA1 is required for flagellum attachment and cytokinesis. *J Biol Chem* 277, 17580-8.

Lahm, A. and Suck, D. (1991). DNase I-induced DNA conformation. 2 A structure of a DNase I-octamer complex. *J Mol Biol* 222, 645-67.

Le Ray, D., Barry, J. D., Easton, C. and Vickerman, K. (1977). First tsetse fly transmission of the "AnTat" serodeme of *Trypanosoma brucei*. *Ann Soc Belg Med Trop* 57, 369-81.

Lewis, E. A. and Langridge, W. P. (1947). Developmental forms of *Trypanosoma brucei* in the saliva of *Glossina pallidipes* and *Glossina austeni*. *Ann Trop Med Parasitol* 41, 6-13.

Li, J. B., Gerdes, J. M., Haycraft, C. J., Fan, Y., Teslovich, T. M., May-Simera, H., Li, H., Blacque, O. E., Li, L., Leitch, C. C. et al. (2004). Comparative genomics identifies a flagellar and basal body proteome that includes the BBS5 human disease gene. *Cell* 117, 541-52.

Li, Y., Li, Z. and Wang, C. C. (2003). Differentiation of *Trypanosoma brucei* may be stage non-specific and does not require progression of cell cycle. *Mol Microbiol* 49, 251-65.

Li, Z. and Wang, C. C. (2006). Changing roles of aurora-B kinase in two life cycle stages of *Trypanosoma brucei*. *Eukaryot Cell* 5, 1026-35.

Liang, X. H., Haritan, A., Uliel, S. and Michaeli, S. (2003). trans and cis splicing in trypanosomatids: mechanism, factors, and regulation. *Eukaryot Cell* 2, 830-40.

Liu, W., Apagyi, K., McLeavy, L. and Ersfeld, K. (2010). Expression and cellular localisation of calpain-like proteins in *Trypanosoma brucei*. *Mol Biochem Parasitol* 169, 20-6.

Liu, Y., Guo, L., Guo, R., Wong, R. L., Hernandez, H., Hu, J., Chu, Y., Amster, I. J., Whitman, W. B. and Huang, L. (2009). The Sac10b homolog in *Methanococcus maripaludis* binds DNA at specific sites. *J Bacteriol* 191, 2315-29.

Livingstone, D. (1857). Missionary Travels and Researches in South Africa. *John Murray* London, 548.

Lurz, R., Grote, M., Dijk, J., Reinhardt, R. and Dobrinski, B. (1986). Electron microscopic study of DNA complexes with proteins from the Archaebacterium *Sulfolobus acidocaldarius*. *Embo J* 5, 3715-21.

Lythgoe, K. A., Morrison, L. J., Read, A. F. and Barry, J. D. (2007). Parasite-intrinsic factors can explain ordered progression of trypanosome antigenic variation. *Proc Natl Acad Sci U S A* 104, 8095-100.

Mair, G. R., Lasonder, E., Garver, L. S., Franke-Fayard, B. M., Carret, C. K., Wiegant, J. C., Dirks, R. W., Dimopoulos, G., Janse, C. J. and Waters, A. P. (2010). Universal features of post-transcriptional gene regulation are critical for *Plasmodium* zygote development. *PLoS Pathog* 6, e1000767.

Mani, J., Guttinger, A., Schimanski, B., Heller, M., Acosta-Serrano, A., Pescher, P., Spath, G. and Roditi, I. (2011). Alba-Domain Proteins of *Trypanosoma brucei* Are Cytoplasmic RNA-Binding Proteins That Interact with the Translation Machinery. *PLoS One* 6, e22463.

Maric, D., McGwire, B. S., Buchanan, K. T., Olson, C. L., Emmer, B. T., Epting, C. L. and Engman, D. M. (2011). Molecular determinants of ciliary membrane localization of *Trypanosoma cruzi* flagellar calcium-binding protein. *J Biol Chem*.

Marsh, V. L., Peak-Chew, S. Y. and Bell, S. D. (2005). Sir2 and the acetyltransferase, Pat, regulate the archaeal chromatin protein, Alba. *J Biol Chem* 280, 21122-8.

Marshall, W. F., Qin, H., Rodrigo Brenni, M. and Rosenbaum, J. L. (2005). Flagellar length control system: testing a simple model based on intraflagellar transport and turnover. *Mol Biol Cell* 16, 270-8.

Marshall, W. F. and Rosenbaum, J. L. (2001). Intraflagellar transport balances continuous turnover of outer doublet microtubules: implications for flagellar length control. *J Cell Biol* 155, 405-14.

Marszalek, J. R., Liu, X., Roberts, E. A., Chui, D., Marth, J. D., Williams, D. S. and Goldstein, L. S. (2000). Genetic evidence for selective transport of opsin and arrestin by kinesin-II in mammalian photoreceptors. *Cell* 102, 175-87.

Martinez-Calvillo, S., Vizuet-de-Rueda, J. C., Florencio-Martinez, L. E., Manning-Cela, R. G. and Figueroa-Angulo, E. E. (2010). Gene expression in trypanosomatid parasites. *J Biomed Biotechnol* 2010, 525241.

Matthews, K. R. and Gull, K. (1994). Evidence for an interplay between cell cycle progression and the initiation of differentiation between life cycle forms of African trypanosomes. *J Cell Biol* 125, 1147-56.

Matthews, K. R., Sherwin, T. and Gull, K. (1995). Mitochondrial genome repositioning during the differentiation of the African trypanosome between life cycle forms is microtubule mediated. *J Cell Sci* 108 (Pt 6), 2231-9.

Maudlin, I. and Welburn, S. C. (1989). A single trypanosome is sufficient to infect a tsetse fly. *Ann Trop Med Parasitol* 83, 431-3.

Meyer, E. and Garnier, O. (2002). Non-Mendelian inheritance and homology-dependent effects in ciliates. *Adv Genet* 46, 305-37.

Milone, J., Wilusz, J. and Bellofatto, V. (2002). Identification of mRNA decapping activities and an ARE-regulated 3' to 5' exonuclease activity in trypanosome extracts. *Nucleic Acids Res* 30, 4040-50.

Miranda, M. R., Bouvier, L. A., Canepa, G. E. and Pereira, C. A. (2009). Subcellular localization of *Trypanosoma cruzi* arginine kinase. *Parasitology* 136, 1201-7.

Miranda, M. R., Canepa, G. E., Bouvier, L. A. and Pereira, C. A. (2006). *Trypanosoma cruzi*: Oxidative stress induces arginine kinase expression. *Exp Parasitol* 114, 341-4.

Moreira-Leite, F. F., Sherwin, T., Kohl, L. and Gull, K. (2001). A trypanosome structure involved in transmitting cytoplasmic information during cell division. *Science* 294, 610-2.

Mottram, J. C., Murphy, W. J. and Agabian, N. (1989). A transcriptional analysis of the *Trypanosoma brucei* hsp83 gene cluster. *Mol Biochem Parasitol* 37, 115-27.

Muller, I. B., Domenicali-Pfister, D., Roditi, I. and Vassella, E. (2002). Stage-specific requirement of a mitogen-activated protein kinase by *Trypanosoma brucei*. *Mol Biol Cell* 13, 3787-99.

Murray, H. W., Berman, J. D., Davies, C. R. and Saravia, N. G. (2005). Advances in leishmaniasis. *Lancet* 366, 1561-77.

Natesan, S. K., Peacock, L., Matthews, K., Gibson, W. and Field, M. C. (2007). Activation of endocytosis as an adaptation to the mammalian host by trypanosomes. *Eukaryot Cell* 6, 2029-37.

Nett, I. R., Martin, D. M., Miranda-Saavedra, D., Lamont, D., Barber, J. D., Mehlert, A. and Ferguson, M. A. (2009). The phosphoproteome of bloodstream form *Trypanosoma brucei*, causative agent of African sleeping sickness. *Mol Cell Proteomics* 8, 1527-38.

Nilsson, D., Gunasekera, K., Mani, J., Osteras, M., Farinelli, L., Baerlocher, L., Roditi, I. and Ochsenreiter, T. (2010). Spliced leader trapping reveals widespread alternative splicing patterns in the highly dynamic transcriptome of *Trypanosoma brucei*. *PLoS Pathog* 6.

Oberholzer, M., Langousis, G., Nguyen, H. T., Saada, E. A., Shimogawa, M. M., Jonsson, Z. O., Nguyen, S. M., Wohlschlelgel, J. A. and Hill, K. L. (2011). Independent analysis of the flagellum surface and matrix proteomes provides insight into flagellum signaling in mammalian-infectious *Trypanosoma brucei*. *Mol Cell Proteomics*.

Oberle, M., Balmer, O., Brun, R. and Roditi, I. (2010). Bottlenecks and the maintenance of minor genotypes during the life cycle of *Trypanosoma brucei*. *PLoS Pathog* 6, e1001023.

Olguin-Lamas, A., Madec, E., Hovasse, A., Werkmeister, E., Callebaut, I., Slomianny, C., Delhaye, S., Mouveaux, T., Schaeffer-Reiss, C., Van Dorsselaer, A. et al. (2011). A novel *Toxoplasma gondii* nuclear factor TgNF3 is a dynamic chromatin-associated component, modulator of nucleolar architecture and parasite virulence. *PLoS Pathog* 7, e1001328.

Ostheimer, G. J., Barkan, A. and Matthews, B. W. (2002). Crystal structure of *E. coli* YhbY: a representative of a novel class of RNA binding proteins. *Structure* 10, 1593-601.

Overath, P., Czichos, J. and Haas, C. (1986). The effect of citrate/cis-aconitate on oxidative metabolism during transformation of *Trypanosoma brucei*. *Eur J Biochem* 160, 175-82.

Overath, P., Czichos, J., Stock, U. and Nonnengaesser, C. (1983). Repression of glycoprotein synthesis and release of surface coat during transformation of *Trypanosoma brucei*. *Embo J* 2, 1721-8.

Overath, P. and Engstler, M. (2004). Endocytosis, membrane recycling and sorting of GPI-anchored proteins: *Trypanosoma brucei* as a model system. *Mol Microbiol* 53, 735-44.

Paindavoine, P., Rolin, S., Van Assel, S., Geuskens, M., Jauniaux, J. C., Dinsart, C., Huet, G. and Pays, E. (1992). A gene from the variant surface glycoprotein expression site encodes one of several transmembrane adenylate cyclases located on the flagellum of *Trypanosoma brucei*. *Mol Cell Biol* 12, 1218-25.

Pan, J. and Snell, W. J. (2003). Kinesin II and regulated intraflagellar transport of *Chlamydomonas* aurora protein kinase. *J Cell Sci* 116, 2179-86.

Parsons, M. and Ruben, L. (2000). Pathways involved in environmental sensing in trypanosomatids. *Parasitol Today* 16, 56-62.

Paterou, A., Walrad, P., Craddy, P., Fenn, K. and Matthews, K. (2006). Identification and stage-specific association with the translational apparatus of TbZFP3, a CCCH protein that promotes trypanosome life-cycle development. *J Biol Chem* 281, 39002-13.

Pays, E., Hanocq-Quertier, J., Hanocq, F., Van Assel, S., Nolan, D. and Rolin, S. (1993). Abrupt RNA changes precede the first cell division during the differentiation of *Trypanosoma brucei* bloodstream forms into procyclic forms in vitro. *Mol Biochem Parasitol* 61, 107-14.

Pays, E., Vanhollebeke, B., Vanhamme, L., Paturiaux-Hanocq, F., Nolan, D. P. and Perez-Morga, D. (2006). The trypanolytic factor of human serum. *Nat Rev Microbiol* 4, 477-86.

Peacock, L., Ferris, V., Bailey, M. and Gibson, W. (2006). Multiple effects of the lectin-inhibitory sugars D-glucosamine and N-acetyl-glucosamine on tsetse-trypanosome interactions. *Parasitology* 132, 651-8.

Peacock, L., Ferris, V., Sharma, R., Sunter, J., Bailey, M., Carrington, M. and Gibson, W. (2011). Identification of the meiotic life cycle stage of *Trypanosoma brucei* in the tsetse fly. *Proc Natl Acad Sci U S A* 108, 3671-6.

Penketh, P. G., Divo, A. A., Shyam, K., Patton, C. L. and Sartorelli, A. C. (1991). The effects of the methylating agent 1,2-bis(methylsulfonyl)-1-methylhydrazine on morphology, DNA content and mitochondrial function of *Trypanosoma brucei* subspecies. *J Protozool* 38, 172-7.

Pereira, C. A., Alonso, G. D., Ivaldi, S., Silber, A. M., Alves, M. J., Torres, H. N. and Flawia, M. M. (2003). Arginine kinase overexpression improves *Trypanosoma cruzi* survival capability. *FEBS Lett* 554, 201-5.

Pereira, C. A., Alonso, G. D., Paveto, M. C., Iribarren, A., Cabanas, M. L., Torres, H. N. and Flawia, M. M. (2000). *Trypanosoma cruzi* arginine kinase characterization and cloning. A novel energetic pathway in protozoan parasites. *J Biol Chem* 275, 1495-501.

Pereira, C. A., Alonso, G. D., Torres, H. N. and Flawia, M. M. (2002). Arginine kinase: a common feature for management of energy reserves in African and American flagellated trypanosomatids. *J Eukaryot Microbiol* 49, 82-5.

Plimmer, H. G. and Bradford, J. R. (1899). A preliminary note on the morphology and distribution of the organism found in the tsetse fly disease. *Proc R Soc B* 65, 274-281.

Ploubidou, A., Robinson, D. R., Docherty, R. C., Ogbadoyi, E. O. and Gull, K. (1999). Evidence for novel cell cycle checkpoints in trypanosomes: kinetoplast segregation and cytokinesis in the absence of mitosis. *J Cell Sci* 112 (Pt 24), 4641-50.

Pluk, H., van Eenennaam, H., Rutjes, S. A., Pruijn, G. J. and van Venrooij, W. J. (1999). RNA-protein interactions in the human RNase MRP ribonucleoprotein complex. *Rna* 5, 512-24.

Portman, N., Lacomble, S., Thomas, B., McKean, P. G. and Gull, K. (2009). Combining RNA interference mutants and comparative proteomics to identify protein components and dependences in a eukaryotic flagellum. *J Biol Chem* 284, 5610-9.

Pozuelo Rubio, M., Geraghty, K. M., Wong, B. H., Wood, N. T., Campbell, D. G., Morrice, N. and Mackintosh, C. (2004). 14-3-3-affinity purification of over 200 human phosphoproteins reveals new links to regulation of cellular metabolism, proliferation and trafficking. *Biochem J* 379, 395-408.

Pradel, L. C., Bonhivers, M., Landrein, N. and Robinson, D. R. (2006). NIMA-related kinase TbNRKC is involved in basal body separation in *Trypanosoma brucei*. *J Cell Sci* 119, 1852-63.

Prescott, D. M. (1994). The DNA of ciliated protozoa. *Microbiol Rev* 58, 233-67.

Priest, J. W. and Hajduk, S. L. (1994). Developmental regulation of *Trypanosoma brucei* cytochrome c reductase during bloodstream to procyclic differentiation. *Mol Biochem Parasitol* 65, 291-304.

Pullen, T. J., Ginger, M. L., Gaskell, S. J. and Gull, K. (2004). Protein targeting of an unusual, evolutionarily conserved adenylate kinase to a eukaryotic flagellum. *Mol Biol Cell* 15, 3257-65.

Queiroz, R., Benz, C., Fellenberg, K., Hoheisel, J. D. and Clayton, C. (2009). Transcriptome analysis of differentiating trypanosomes reveals the existence of multiple post-transcriptional regulons. *BMC Genomics* 10, 495.

Quijada, L., Guerra-Giraldez, C., Drozdz, M., Hartmann, C., Irmer, H., Ben-Dov, C., Cristodero, M., Ding, M. and Clayton, C. (2002). Expression of the human RNA-binding protein HuR in *Trypanosoma brucei* increases the abundance of mRNAs containing AU-rich regulatory elements. *Nucleic Acids Res* 30, 4414-24.

Ralston, K. S., Lerner, A. G., Diener, D. R. and Hill, K. L. (2006). Flagellar motility contributes to cytokinesis in *Trypanosoma brucei* and is modulated by an evolutionarily conserved dynein regulatory system. *Eukaryot Cell* 5, 696-711.

Rassi, A., Jr., Rassi, A. and Marin-Neto, J. A. (2010). Chagas disease. *Lancet* 375, 1388-402.

Redmond, S., Vadivelu, J. and Field, M. C. (2003). RNAit: an automated web-based tool for the selection of RNAi targets in *Trypanosoma brucei*. *Mol Biochem Parasitol* 128, 115-8.

Reuner, B., Vassella, E., Yutzy, B. and Boshart, M. (1997). Cell density triggers slender to stumpy differentiation of *Trypanosoma brucei* bloodstream forms in culture. *Mol Biochem Parasitol* 90, 269-80.

Ridgley, E., Webster, P., Patton, C. and Ruben, L. (2000). Calmodulin-binding properties of the paraflagellar rod complex from *Trypanosoma brucei*. *Mol Biochem Parasitol* 109, 195-201.

Rindisbacher, L., Hemphill, A. and Seebeck, T. (1993). A repetitive protein from *Trypanosoma brucei* which caps the microtubules at the posterior end of the cytoskeleton. *Mol Biochem Parasitol* 58, 83-96.

Robertson, M. (1912). Notes on the polymorphism of *Trypanosoma gambiense* in the blood and its relation to the exogenous cycle in *Glossina palpalis*. *Proc. R. Soc. B.* 85, 527-539.

Robertson, M. (1913). Notes on the life history of *Trypanosoma gambiense*, with a brief reference to the cycles of *Trypanosoma nanum* and *Trypanosoma percorum* in *Glossina palpalis*. *Phil. Trans. R. Soc. Lond. (Biol.)* 203, 161-184.

Robinson, D. R. and Gull, K. (1991). Basal body movements as a mechanism for mitochondrial genome segregation in the trypanosome cell cycle. *Nature* 352, 731-3.

Robinson, D. R., Sherwin, T., Ploubidou, A., Byard, E. H. and Gull, K. (1995). Microtubule polarity and dynamics in the control of organelle positioning, segregation, and cytokinesis in the trypanosome cell cycle. *J Cell Biol* 128, 1163-72.

Roditi, I. and Clayton, C. (1999). An unambiguous nomenclature for the major surface glycoproteins of the procyclic form of *Trypanosoma brucei*. *Mol Biochem Parasitol* 103, 99-100.

Roditi, I., Furger, A., Ruepp, S., Schurch, N. and Butikofer, P. (1998). Unravelling the procyclin coat of *Trypanosoma brucei*. *Mol Biochem Parasitol* 91, 117-30.

Roditi, I. and Lehane, M. J. (2008). Interactions between trypanosomes and tsetse flies. *Curr Opin Microbiol* 11, 345-51.

Roditi, I., Schwarz, H., Pearson, T. W., Beecroft, R. P., Liu, M. K., Richardson, J. P., Buhring, H. J., Pleiss, J., Bulow, R., Williams, R. O. et al. (1989). Procyclin gene expression and loss of the variant surface glycoprotein during differentiation of *Trypanosoma brucei*. *J Cell Biol* 108, 737-46.

Rotureau, B., Morales, M. A., Bastin, P. and Spath, G. F. (2009). The flagellum-MAP kinase connection in Trypanosomatids: a key sensory role in parasite signaling and development? *Cell Microbiol*.

Rotureau, B., Subota, I. and Bastin, P. (2011a). Molecular bases of cytoskeleton plasticity during the *Trypanosoma brucei* parasite cycle. *Cell Microbiol* 13, 705-16.

Rotureau, B., Subota, I., Buisson, J. and Bastin, P. (2011b). A new asymmetric division explains the continuous production of infective trypanosomes in the tsetse fly. *Development* In review.

Rudenko, G., Chung, H. M., Pham, V. P. and Van der Ploeg, L. H. (1991). RNA polymerase I can mediate expression of CAT and neo protein-coding genes in *Trypanosoma brucei*. *Embo J* 10, 3387-97.

Salavati, R., Panigrahi, A. K. and Stuart, K. D. (2001). Mitochondrial ribonuclease P activity of *Trypanosoma brucei*. *Mol Biochem Parasitol* 115, 109-17.

Sandman, K. and Reeve, J. N. (2000). Structure and functional relationships of archaeal and eukaryal histones and nucleosomes. *Arch Microbiol* 173, 165-9.

Schlitzer, M. (2009). [Agents for the treatment of African sleeping sickness. Those developed in the last century]. *Pharm Unserer Zeit* 38, 552-8.

Schmitt, M. E. and Clayton, D. A. (1993). Nuclear RNase MRP is required for correct processing of pre-5.8S rRNA in *Saccharomyces cerevisiae*. *Mol Cell Biol* 13, 7935-41.

Scory, S., Stierhof, Y. D., Caffrey, C. R. and Steverding, D. (2007). The cysteine proteinase inhibitor Z-Phe-Ala-CHN2 alters cell morphology and cell division activity of *Trypanosoma brucei* bloodstream forms in vivo. *Kinetoplastid Biol Dis* 6, 2.

Shah, A. S., Ben-Shahar, Y., Moninger, T. O., Kline, J. N. and Welsh, M. J. (2009). Motile cilia of human airway epithelia are chemosensory. *Science* 325, 1131-4.

Shapiro, S. Z., Naessens, J., Liesegang, B., Moloo, S. K. and Magondu, J. (1984). Analysis by flow cytometry of DNA synthesis during the life cycle of African trypanosomes. *Acta Trop* 41, 313-23.

Sharma, R., Gluenz, E., Peacock, L., Gibson, W., Gull, K. and Carrington, M. (2009). The heart of darkness: growth and form of *Trypanosoma brucei* in the tsetse fly. *Trends Parasitol* 25, 517-24.

Sharma, R., Peacock, L., Gluenz, E., Gull, K., Gibson, W. and Carrington, M. (2008). Asymmetric cell division as a route to reduction in cell length and change in cell morphology in trypanosomes. *Protist* 159, 137-51.

Sherwin, T. and Gull, K. (1989a). The cell division cycle of *Trypanosoma brucei brucei*: timing of event markers and cytoskeletal modulations. *Philos Trans R Soc Lond B Biol Sci* 323, 573-88.

Sherwin, T. and Gull, K. (1989b). Visualization of detyrosination along single microtubules reveals novel mechanisms of assembly during cytoskeletal duplication in trypanosomes. *Cell* 57, 211-21.

Siegel, T. N., Hekstra, D. R., Kemp, L. E., Figueiredo, L. M., Lowell, J. E., Fenyo, D., Wang, X., Dewell, S. and Cross, G. A. (2009). Four histone variants mark the boundaries of polycistronic transcription units in *Trypanosoma brucei*. *Genes Dev* 23, 1063-76.

Siegel, T. N., Hekstra, D. R., Wang, X., Dewell, S. and Cross, G. A. (2010). Genome-wide analysis of mRNA abundance in two life-cycle stages of *Trypanosoma brucei* and identification of splicing and polyadenylation sites. *Nucleic Acids Res* 38, 4946-57.

Singla, V. and Reiter, J. F. (2006). The primary cilium as the cell's antenna: signaling at a sensory organelle. *Science* 313, 629-33.

Stern, M. Z., Gupta, S. K., Salmon-Divon, M., Haham, T., Barda, O., Levi, S., Wachtel, C., Nilsen, T. W. and Michaeli, S. (2009). Multiple roles for polypyrimidine tract binding (PTB) proteins in trypanosome RNA metabolism. *Rna* 15, 648-65.

Stolc, V., Katz, A. and Altman, S. (1998). Rpp2, an essential protein subunit of nuclear RNase P, is required for processing of precursor tRNAs and 35S precursor rRNA in *Saccharomyces cerevisiae*. *Proc Natl Acad Sci U S A* 95, 6716-21.

Strahl, B. D. and Allis, C. D. (2000). The language of covalent histone modifications. *Nature* 403, 41-5.

Strissel, K. J., Lishko, P. V., Trieu, L. H., Kennedy, M. J., Hurley, J. B. and Arshavsky, V. Y. (2005). Recoverin undergoes light-dependent intracellular translocation in rod photoreceptors. *J Biol Chem* 280, 29250-5.

Szoor, B., Ruberto, I., Burchmore, R. and Matthews, K. R. (2010). A novel phosphatase cascade regulates differentiation in *Trypanosoma brucei* via a glycosomal signaling pathway. *Genes Dev* 24, 1306-16.

Szoor, B., Wilson, J., McElhinney, H., Tabernero, L. and Matthews, K. R. (2006). Protein tyrosine phosphatase TbPTP1: A molecular switch controlling life cycle differentiation in trypanosomes. *J Cell Biol* 175, 293-303.

Talbert, P. B. and Henikoff, S. (2009). Chromatin-based transcriptional punctuation. *Genes Dev* 23, 1037-41.

Tetley, L. and Vickerman, K. (1985). Differentiation in *Trypanosoma brucei*: host-parasite cell junctions and their persistence during acquisition of the variable antigen coat. *J Cell Sci* 74, 1-19.

Thomson, R., Samanovic, M. and Raper, J. (2009). Activity of trypanosome lytic factor: a novel component of innate immunity. *Future Microbiol* 4, 789-96.

Tobin, D., Madsen, D., Kahn-Kirby, A., Peckol, E., Moulder, G., Barstead, R., Maricq, A. and Bargmann, C. (2002). Combinatorial expression of TRPV channel proteins defines their sensory functions and subcellular localization in *C. elegans* neurons. *Neuron* 35, 307-18.

Tu, X. and Wang, C. C. (2004). The involvement of two cdc2-related kinases (CRKs) in *Trypanosoma brucei* cell cycle regulation and the distinctive stage-specific phenotypes caused by CRK3 depletion. *J Biol Chem* 279, 20519-28.

Tu, X. and Wang, C. C. (2005a). Coupling of posterior cytoskeletal morphogenesis to the G1/S transition in the *Trypanosoma brucei* cell cycle. *Mol Biol Cell* 16, 97-105.

Tu, X. and Wang, C. C. (2005b). Pairwise knockdowns of cdc2-related kinases (CRKs) in *Trypanosoma brucei* identified the CRKs for G1/S and G2/M transitions and demonstrated distinctive cytokinetic regulations between two developmental stages of the organism. *Eukaryot Cell* 4, 755-64.

Tyler, K. M., Fridberg, A., Toriello, K. M., Olson, C. L., Cieslak, J. A., Hazlett, T. L. and Engman, D. M. (2009). Flagellar membrane localization via association with lipid rafts. *J Cell Sci* 122, 859-66.

Tyler, K. M., Matthews, K. R. and Gull, K. (2001). Anisomorphic cell division by African trypanosomes. *Protist* 152, 367-78.

Urwyler, S., Studer, E., Renggli, C. K. and Roditi, I. (2007). A family of stage-specific alanine-rich proteins on the surface of epimastigote forms of *Trypanosoma brucei*. *Mol Microbiol* 63, 218-28.

Uzcategui, N. L., Szallies, A., Pavlovic-Djuranovic, S., Palmada, M., Figarella, K., Boehmer, C., Lang, F., Beitz, E. and Duszenko, M. (2004). Cloning, heterologous expression, and characterization of three aquaglyceroporins from *Trypanosoma brucei*. *J Biol Chem* 279, 42669-76.

Van Den Abbeele, J., Claes, Y., van Bockstaele, D., Le Ray, D. and Coosemans, M. (1999). *Trypanosoma brucei spp.* development in the tsetse fly: characterization of the post-mesocyclic stages in the foregut and proboscis. *Parasitology* 118 (Pt 5), 469-78.

Vassella, E., Den Abbeele, J. V., Butikofer, P., Renggli, C. K., Furger, A., Brun, R. and Roditi, I. (2000). A major surface glycoprotein of *Trypanosoma brucei* is expressed transiently during development and can be regulated post-transcriptionally by glycerol or hypoxia. *Genes Dev* 14, 615-26.

Vassella, E., Kramer, R., Turner, C. M., Wankell, M., Modes, C., van den Bogaard, M. and Boshart, M. (2001). Deletion of a novel protein kinase with PX and FYVE-related domains increases the rate of differentiation of *Trypanosoma brucei*. *Mol Microbiol* 41, 33-46.

Vassella, E., Oberle, M., Urwyler, S., Renggli, C. K., Studer, E., Hemphill, A., Fragoso, C., Butikofer, P., Brun, R. and Roditi, I. (2009). Major surface glycoproteins of insect forms of *Trypanosoma brucei* are not essential for cyclical transmission by tsetse. *PLoS One* 4, e4493.

Vassella, E., Probst, M., Schneider, A., Studer, E., Renggli, C. K. and Roditi, I. (2004). Expression of a major surface protein of *Trypanosoma brucei* insect forms is controlled by the activity of mitochondrial enzymes. *Mol Biol Cell* 15, 3986-93.

Vassella, E., Reuner, B., Yutzy, B. and Boshart, M. (1997). Differentiation of African trypanosomes is controlled by a density sensing mechanism which signals cell cycle arrest via the cAMP pathway. *J Cell Sci* 110 (Pt 21), 2661-71.

Vaughan, S., Kohl, L., Ngai, I., Wheeler, R. J. and Gull, K. (2008). A repetitive protein essential for the flagellum attachment zone filament structure and function in *Trypanosoma brucei*. *Protist* 159, 127-36.

Vickerman, K. (1985). Developmental cycles and biology of pathogenic trypanosomes. *Br Med Bull* 41, 105-14.

Vickerman, K., Tetley, L., Hendry, K. A. and Turner, C. M. (1988). Biology of African trypanosomes in the tsetse fly. *Biol Cell* 64, 109-19.

Vincensini, L., Blisnick, T. and Bastin, P. (2011). 1001 model organisms to study cilia and flagella. *Biol Cell* 103, 109-30.

Walker, S. C. and Engelke, D. R. (2006). Ribonuclease P: the evolution of an ancient RNA enzyme. *Crit Rev Biochem Mol Biol* 41, 77-102.

Walrad, P., Paterou, A., Acosta-Serrano, A. and Matthews, K. R. (2009). Differential trypanosome surface coat regulation by a CCCH protein that co-associates with procyclin mRNA cis-elements. *PLoS Pathog* 5, e1000317.

Wang, G., Guo, R., Bartlam, M., Yang, H., Xue, H., Liu, Y., Huang, L. and Rao, Z. (2003). Crystal structure of a DNA binding protein from the hyperthermophilic euryarchaeon *Methanococcus jannaschii*. *Protein Sci* 12, 2815-22.

Wang, Q., Pan, J. and Snell, W. J. (2006). Intraflagellar transport particles participate directly in cilium-generated signaling in *Chlamydomonas*. *Cell* 125, 549-62.

Wang, Z., Morris, J. C., Drew, M. E. and Englund, P. T. (2000). Inhibition of *Trypanosoma brucei* gene expression by RNA interference using an integratable vector with opposing T7 promoters. *J Biol Chem* 275, 40174-9.

Wardleworth, B. N., Russell, R. J., Bell, S. D., Taylor, G. L. and White, M. F. (2002). Structure of Alba: an archaeal chromatin protein modulated by acetylation. *Embo J* 21, 4654-62.

Welburn, S. C. and Maudlin, I. (1999). Tsetse-trypanosome interactions: rites of passage. *Parasitol Today* 15, 399-403.

Welting, T. J., Peters, F. M., Hensen, S. M., van Doorn, N. L., Kikkert, B. J., Raats, J. M., van Venrooij, W. J. and Pruijn, G. J. (2007). Heterodimerization regulates RNase MRP/RNase P association, localization, and expression of Rpp20 and Rpp25. *Rna* 13, 65-75.

Welting, T. J., van Venrooij, W. J. and Pruijn, G. J. (2004). Mutual interactions between subunits of the human RNase MRP ribonucleoprotein complex. *Nucleic Acids Res* 32, 2138-46.

WHO. (2010). Human African trypanosomiasis: number of new cases drops to historically low level in 50 years. In *http://www.who.int/neglected_diseases/integrated_media/integrated_media_hat_june_2010/en/index.html*, (ed. 2011).

Wilczynska, A., Aigueperse, C., Kress, M., Dautry, F. and Weil, D. (2005). The translational regulator CPEB1 provides a link between dcp1 bodies and stress granules. *J Cell Sci* 118, 981-92.

Wirtz, E., Leal, S., Ochatt, C. and Cross, G. A. (1999). A tightly regulated inducible expression system for conditional gene knock-outs and dominant-negative genetics in *Trypanosoma brucei*. *Mol Biochem Parasitol* 99, 89-101.

Woodward, R., Carden, M. J. and Gull, K. (1994). Molecular characterisation of a novel, repetitive protein of the paraflagellar rod in *Trypanosoma brucei*. *Mol Biochem Parasitol* 67, 31-9.

Woodward, R. and Gull, K. (1990). Timing of nuclear and kinetoplast DNA replication and early morphological events in the cell cycle of *Trypanosoma brucei*. *J Cell Sci* 95 (Pt 1), 49-57.

Wright, J. R., Siegel, T. N. and Cross, G. A. (2010). Histone H3 trimethylated at lysine 4 is enriched at probable transcription start sites in *Trypanosoma brucei*. *Mol Biochem Parasitol* 172, 141-4.

Wu, J. and Grunstein, M. (2000). 25 years after the nucleosome model: chromatin modifications. *Trends Biochem Sci* 25, 619-23.

Xue, H., Guo, R., Wen, Y., Liu, D. and Huang, L. (2000). An abundant DNA binding protein from the hyperthermophilic archaeon *Sulfolobus shibatae* affects DNA supercoiling in a temperature-dependent fashion. *J Bacteriol* 182, 3929-33.

Yuan, Y., Tan, E. and Reddy, R. (1991). The 40-kilodalton to autoantigen associates with nucleotides 21 to 64 of human mitochondrial RNA processing/7-2 RNA in vitro. *Mol Cell Biol* 11, 5266-74.

Zhao, K., Chai, X. and Marmorstein, R. (2003). Structure of a Sir2 substrate, Alba, reveals a mechanism for deacetylation-induced enhancement of DNA binding. *J Biol Chem* 278, 26071-7.

Zhu, Y., Stribinskis, V., Ramos, K. S. and Li, Y. (2006). Sequence analysis of RNase MRP RNA reveals its origination from eukaryotic RNase P RNA. *Rna* 12, 699-706.

Zomerdijk, J. C., Kieft, R. and Borst, P. (1991). Efficient production of functional mRNA mediated by RNA polymerase I in *Trypanosoma brucei*. *Nature* 353, 772-5.

7 ANNEXE

7.1 Movie legends

Enclosed to this thesis is a CD containing seven movies that illustrate trypanosome division processes explained in the introduction (movie 1,2) and show representative films of cells in different developmental stages obtained from tsetse fly infection with ALBA::YFP and ALBA::GFP (movie 3-7).

Movie 1 Cell division in procyclic parasites *ex vivo* from the posterior midgut

The content of the posterior midgut of a tsetse fly infected with the trypanosome strain AnTat1.1 was analyzed by live video microscopy. Procyclic cells in subsequent phases of cell division are represented in this movie. In the sequences marked as early division the two cells are clearly distinguishable but cytokinesis was not yet initiated. In the middle stage of division, cytokinesis is well advanced, but the cells are still attached via their flagella. In late division, the two cells are clearly separated and only held together via a thin remnant of membrane. The final separation is achieved by the beating forces of the flagella that drag the cells in opposite directions.

Movie 2 Asymmetric cell division in proventricular dividing epimastigotes *ex vivo*

A proventriculus of a tsetse fly infected with the trypanosome strain AnTat1.1 was analyzed by live video microscopy and the asymmetric division process of epimastigote forms investigated. First the early division is represented: epimastigote forms with a head-like structure (containing two kinetoplasts and one nucleus) and a long flagellated tail. In the middle stage, the cell had gone through mitosis (2 kinetoplasts and 2 nuclei) and proceeded to cytokinesis, while the short daughter cell is attached along most of its posterior length to the long daughter its flagellar tip is free. Dividing epimastigotes are very fast and persistent swimmers and attach rarely to the microscope slide but in these cases mostly the short daughter attaches and one can observe the late division process. This results in two daughter cells, one short and one long epimastigote.

Movie 3 ALBA3::YFP signal monitored in trypanosomes during the parasite development in the fly

Each representative form of the parasite cycle found in the digestive tract (sequences 1-6) and salivary glands (sequences 7 and 8) of the fly infected with AnTat1.1 ALBA3::YFP

trypanosomes are shown as consecutive live movies. First, each form is shown by phase contrast and its name indicated, second its ALBA3::YFP fluorescent signal is visualized by adding a green filter and third, DAPI is visualized by adding a blue filter to show DNA content and localization. The stages are shown in the order of their appearance during fly infection: (1) procyclic form; (2) a mixed field containing the proventricular parasites: mesocyclic (MS), mesocyclic to epimastigote (MS-E) and dividing epimastigote (DE); (3) a form in mesocyclic to epimastigote transition; (4) dividing epimastigote; (5) long epimastigote, (6) short epimastigote; (7) salivary gland epimastigote and (8) metacyclic.

Movie 4 ALBA3::YFP signal monitored in fields with mixed trypanosome forms

Different fields of mixed trypanosome forms, found in the proventriculus of the fly infected with AnTat1.1 ALBA3::YFP trypanosomes, are shown as consecutive live movies. First, each form is shown by phase contrast and its name indicated, second its ALBA3::YFP fluorescent signal is visualized and third, DAPI is visualized to show DNA content and localization. Mixed fields contain the following proventricular forms: (1) mesocyclic (MS), mesocyclic to epimastigote (MS-E) and dividing epimastigote (DE); (2) mesocyclic (MS) and mesocyclic to epimastigote (MS-E); (3) a field containing different parasites in mesocyclic to epimastigote transition (MS-E); (4) mesocyclic to epimastigote (MS-E) and dividing epimastigote (DE); (5) mesocyclic (MS), dividing epimastigote (DE) and short epimastigote (SE); (6) mesocyclic (MS) and long epimastigote (LE); (7) mesocyclic (MS) and dividing epimastigote (DE).

Movie 5 ALBA4::YFP signal monitored in trypanosomes along the parasite development in the fly

Each representative form of the parasite cycle found in the digestive tract (sequence 1-6) and salivary glands (sequences 7 and 8) of the fly infected with AnTat1.1 ALBA4::YFP trypanosomes are shown as consecutive live movies. First, each form is shown by phase contrast and its name indicated, second its ALBA3::YFP fluorescent signal is visualized and third, DAPI is visualized to monitor DNA content and localization. The stages are shown in the order of appearance during fly infection: (1) procyclic form; (2) mesocyclic form; (3) a mixed field containing the proventricular parasites: mesocyclic (MS) and mesocyclic to epimastigote (MS-E); (4) a mesocyclic to epimastigote transition; (5) long epimastigote; (6) short epimastigote; (7) salivary gland epimastigote and (8) metacyclic.

Movie 6 AnTat1.1 GFP control and ALBA::GFP over-expression

Fields of mesocyclic parasites, as representative form, of the strains AnTat1.1 GFP control, ALBA3::GFP and ALBA4::GFP are shown as consecutive live movies. First, the phase contrast of each field is shown, second the green fluorescent signal is visualized and third, DAPI is visualized by adding a blue filter to show DNA content and localization.

Movie 7 Mesocyclic to epimastigote transition during ALBA3::GFP over-expression

Parasites of the AnTat1.1 strain over-expressing ALBA3::GFP found in the proventriculus of the fly are shown. First, the phase contrast of each field indicating the name of the forms, second, green fluorescent signal of ALBA3::GFP is visualized and third, DAPI is visualized to monitor DNA content and localization. Following forms are represented: (1) a field of mesocyclic; (2) mesocyclic (MS) and mesocyclic to epimastigote (MS-E); (3) mesocyclic to epimastigote; (4-7) four different atypical cells displaying thin cell diameter (typical for MS-E) and a nucleus in a very anterior position (typical for MS).

7.2 Publication list

1. The study about ALBA proteins in trypanosome development is submitted to the journal " Molecular Biology Of The Cell " where a revised version of the manuscript is currently in revision. Manuscript number E11-06-0511R.

Authors: Subota Ines, Rotureau Brice, Blisnick Thierry, Ngwabyt Sandra, Durand-Dubief Mickaël, Engstler Markus and Bastin Philippe

Title: ALBA Proteins are Stage-Regulated during Trypanosome Development in the Tsetse Fly and Participate in Differentiation

Abstract: The protozoan parasite *Trypanosoma brucei* is responsible for sleeping sickness and alternates between mammal and tsetse fly hosts, where it has to adapt to different environments. In this report, we investigated the role of two members of the ALBA family that encodes hypothetical RNA-binding proteins conserved in most eukaryotes. We show that ALBA3/4 proteins colocalize with the DHH1 RNA-binding protein and with a subset of polyA+ RNA in stress granules upon starvation. Depletion of ALBA3/4 proteins by RNA interference in the cultured procyclic stage produces cell modifications mimicking several morphogenetic aspects of trypanosome differentiation that usually take place in the fly midgut. A combination of immunofluorescence data and video-microscopy analysis of live trypanosomes expressing endogenously ALBA fused with fluorescent proteins revealed that ALBA3/4 are present throughout the development of the parasite in the tsetse fly, with the striking exception of the transition stages found in the proventriculus region. This involves migration of the nucleus towards the posterior end of the cell, a phenomenon that is perturbed upon forced expression of ALBA3 during the differentiation process, showing for the first time the involvement of an RNA-binding protein in trypanosome development in vivo.

2. The second part of the thesis about the identification of novel flagellar proteins and their initiated functional analysis will be part of a manuscript currently in preparation.

Authors: Julkowska Daria, **Subota Ines**, Reeg Nele, Blisnick Thierry, Buisson Johanna, Duchateau Magalie, Huet Diego, Vincensini Laetitia, Namane Abdelkader and Bastin Philippe

Title: Identification of novel membrane and matrix protein reveals differential protein dynamics in the trypanosome flagellum.

3. The extensive analysis of trypanosome developmental forms in the organs of the tsetse fly by live video-microscopy allowed the validation of the presence of living asymmetrically dividing epimastigote forms in the salivary glands, initially identified by Brice Rotureau in fixed cells. In addition, I contributed to this work by analyzing the occurrence of the BARP surface protein in the different trypanosome developmental forms in the proventriculus and the salivary glands of the tsetse fly.
This manuscript is submitted to the journal " Development " and is currently in review. Manuscript identification number: DEVELOP/2011/072611.

Authors: Rotureau Brice, **Subota Ines**, Buisson Johanna and Bastin Philippe

Title: A new asymmetric division explains the continuous production of infective trypanosomes in the tsetse fly

Abstract: African trypanosomes are flagellated protozoan parasites causing sleeping sickness and are transmitted by the bite of the tsetse fly. To complete their life cycle in the insect, trypanosomes reach the salivary glands and transform into the infective form. The latter are expelled with the saliva at each blood meal during the whole life of the insect. Here, we reveal the means by which the continuous production of infective parasites is ensured. Dividing trypanosomes present in the salivary glands of infected tsetse flies were monitored by live video-microscopy and by quantitative immunofluorescence analysis using specific molecular markers for the cytoskeleton and for surface antigens. This revealed the existence of two distinct modes of

trypanosome proliferation occurring simultaneously in the salivary glands. The first cycle produces two equivalent cells that are not competent for infection and attached to the epithelium. It is predominant at the early steps of infection, ensuring a rapid colonization of the glands. The second mode is more frequent at later stages of infection and involves an asymmetric division. It produces a daughter cell that matures into the infective form released in the saliva, as demonstrated by the expression of specific molecular markers, the calflagins. The amount of these calciumbinding proteins increases exclusively in the new flagellum during the asymmetric division, showing the commitment of the future daughter cell to differentiation. The coordination of these two alternative cell cycles explains the continuous production of infective parasites, turning the tsetse fly into an efficient and long-lasting vector for African trypanosomes.

4. The following study about cytoskeletal dynamics and the molecular components during the trypanosome parasite cycle is published in " Cellular Microbiology ", Volume 13, Issue 5, pages 705–716, in May 2011. I contributed to this work with fly infections and discussions. The article as it was published is found on the next pages 138-149.

Authors: Rotureau Brice, **Subota Ines** and Bastin Philippe

Title: Molecular bases of cytoskeleton plasticity during the *Trypanosoma brucei* parasite cycle

Cellular Microbiology (2011) **13**(5), 705–716
doi:10.1111/j.1462-5822.2010.01566.x
First published online 18 January 2011

Molecular bases of cytoskeleton plasticity during the *Trypanosoma brucei* parasite cycle

Brice Rotureau,* Ines Subota and Philippe Bastin
Institut Pasteur, Trypanosome Cell Biology Unit, Paris, France.

Summary

African trypanosomes are flagellated protozoan parasites responsible for sleeping sickness and transmitted by tsetse flies. The accomplishment of their parasite cycle requires adaptation to highly diverse environments. These transitions take place in a strictly defined order and are accompanied by spectacular morphological modifications in cell size, shape and positioning of organelles. To understand the molecular bases of these processes, parasites isolated from different tissues of the tsetse fly were analysed by immunofluorescence with markers for specific cytoskeleton components and by a new immunofluorescence-based assay for evaluation of the cell volume. The data revealed striking differences between proliferative stages found in the midgut or in the salivary glands and the differentiating stage occurring in the proventriculus. Cell proliferation was characterized by a significant increase in cell volume, by a pronounced cell elongation marked by microtubule extension at the posterior end, and by the production of a new flagellum similar to the existing one. In contrast, the differentiating stage found in the proventriculus does not display any increase in cell volume neither in cell length, but is marked by a profound remodelling of the posterior part of the cytoskeleton and by changes in molecular composition and/or organization of the flagellum attachment zone.

Introduction

African trypanosomes are protozoan parasites responsible for human African trypanosomiasis or sleeping sickness, a fatal tropical disease in the absence of treatment. They also infect cattle with major socio-economic consequences, mainly in east Africa (Simarro *et al.*, 2008). *Trypanosoma brucei* parasites are exclusively transmitted by the bite of the tsetse fly. In the mammalian host, trypanosomes develop in the bloodstream as extracellular parasites, and at later stages of infection, they can cross the blood–brain barrier and provoke severe neurological symptoms ultimately leading to death (Brun *et al.*, 2009). There is currently no vaccine available whereas drug treatments are difficult to apply in the field and have severe side-effects (Brun *et al.*, 2009).

A tsetse fly gets infected when it picks up trypanosomes during a blood meal on an infected mammal. To be infective for humans, parasites need to reach the tsetse saliva and to transform into the so-called metacyclic stage. This is not direct and requires several intermediate stages taking place in a strictly defined chronological order at different locations in the midgut, proventriculus and foregut, and finally in the salivary glands of the tsetse fly (Vickerman *et al.*, 1988; Roditi and Lehane, 2008) (Fig. 1). This requires specific adaptation to the varying environment, involving metabolism, cell surface proteins or striking morphological modifications (Vickerman *et al.*, 1988; Fenn and Matthews, 2007).

Trypanosomes possess a nucleus (N) and a single mitochondrion whose genetic material is condensed in a structure named kinetoplast (K) that is linked to the basal body apparatus of the flagellum (Robinson and Gull, 1991). The flagellum is attached to the cell body and tracts the trypanosome forward, hence defining the anteroposterior axis of the cell. Two main characteristic morphotypes have been defined according to the relative position of the kinetoplast to the nucleus (Hoare and Wallace, 1966). In trypomastigotes, the kinetoplast localizes between the nucleus and the posterior end of the cell. The two bloodstream forms found in mammals are the dividing slender trypomastigote and the non-dividing tsetse-infective stumpy trypomastigote that is observed at peaks of parasitaemia. After ingestion, stumpy parasites rapidly differentiate into procyclic trypomastigotes in the posterior midgut of the fly where they multiply (Fig. 1). Then, some of these procyclic parasites elongate and migrate to the anterior part of the midgut as non-proliferative mesocyclic trypomastigotes (Fig. 1). Once in the proventriculus, mesocyclic cells become thinner and adopt an epimastigote configuration, defined by the localization of the kinetoplast between the nucleus and the anterior end of the

Received 19 October, 2010; revised 25 November, 2010; accepted 7 December, 2010. *For correspondence. E-mail rotureau@pasteur.fr; Tel. (+33) 1 40 61 38 33; Fax (+33) 1 40 61 38 25.

A

Morphotype	Stage	Parasite cycle → Mammalian host: Blood	Tsetse fly vector: Midgut	Tsetse fly vector: Proventriculus and foregut	Tsetse fly vector: Salivary glands
Trypomastigote	Slender *	SL			
	Stumpy	ST	ST		
	Procyclic *		PC		
	Mesocyclic		MS	MS	
Epimastigote	Dividing *			DE	
	Long			LE	
	Short			SE	SE
	Attached *				AE
Trypomastigote	Metacyclic				MT

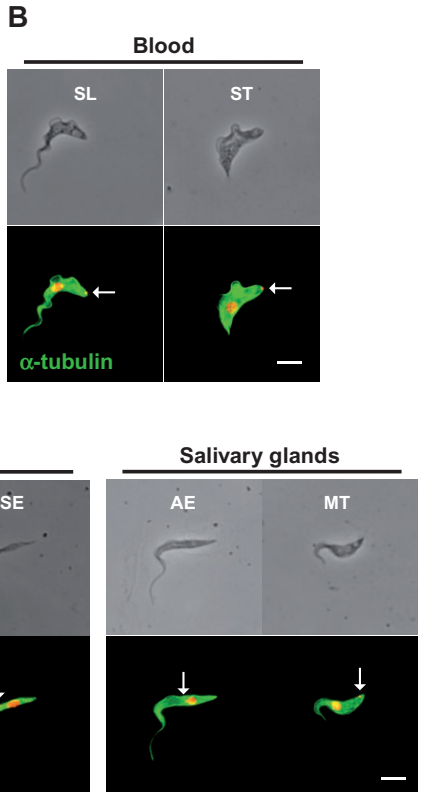

Fig. 1. Morphological changes in trypanosomes during the parasite cycle.
A. Simplified table showing the localization of each stage during the parasite cycle. Proliferative stages are indicated with *. ST, MS and SE in white boxes are only found transiently in the specified organs.
B–C. The 10 main morphological stages of the *T. brucei* parasite cycle, found in the mammalian bloodstream (B) and in the tsetse fly vector (C), were fixed in methanol and stained with DAPI (red) and the TAT1 antibody (green) recognizing α-tubulin. The α-tubulin is homogeneously distributed at the cell periphery in all stages. The scale bar represents 5 μm and the old (arrow) and new (arrowhead) basal body positions are indicated.
All stages are presented in a chronological order and the following name code has been used throughout the legends. SL: slender trypomastigote; ST: stumpy trypomastigote; PC: procyclic trypomastigote; MS: mesocyclic trypomastigote; E: proventricular epimastigote; DE: asymmetrically dividing epimastigote; LE: long epimastigote; SE: short epimastigote; AE: attached epimastigote; MT: metacyclic trypomastigote.

cell. This is due to the posterior migration of the nucleus to the other side of the kinetoplast (Sharma *et al.*, 2008). These long spermatozoa-like epimastigotes divide asymmetrically in the proventriculus and foregut to produce a long and a short epimastigote (Van Den Abbeele *et al.*, 1999) (Fig. 1). It has been proposed that, once in the salivary glands, the latter parasites attach to the epithelium via their flagellum and elongate (Sharma *et al.*, 2009) (Fig. 1). Finally, parasites adopt again the trypomastigote configuration when they transform into the metacyclic form and become competent for infecting mammalian hosts upon release in the saliva.

Parasite proliferation is encountered in three different situations: in the bloodstream (slender stage), in the midgut (procyclic stage) and in the salivary glands (attached epimastigotes). The progression of trypanosomes in the cell cycle can be monitored by a simple DNA staining as cells with one kinetoplast and one nucleus (1K1N) are in the G1/S phase, those with two kinetoplasts and one nucleus (2K1N) are in G2/M, and individuals with two kinetoplasts and two nuclei (2K2N) are about to undergo cytokinesis (Sherwin and Gull, 1989a; Woodward and Gull, 1990). Cellular and molecular information about cytoskeleton organization, composition and evolution during the cell cycle have been obtained from studies mostly carried out on the cultured procyclic form of the parasite (Gull, 1999; Ralston *et al.*, 2009). In trypanosomes, the shape of the cell is defined by a peripheral corset of microtubules that are cross-linked to each other and to the plasma membrane (Sherwin and Gull, 1989a). All these microtubules have the same polarity with their positive end at the posterior part of the cell (Robinson *et al.*, 1995). The flagellum is attached along most of the length of the cell body where a complex structure called the flagellum attachment zone (FAZ) is present. The FAZ has been defined as comprising the FAZ filament present in a gap between two microtubules of the corset, and the specialized microtubule quartet, associated to the smooth

endoplasmic reticulum (Robinson *et al*., 1995). Its elongation is co-ordinated with that of the flagellum (Kohl *et al*., 1999). From observation of procyclic parasites in culture, the FAZ has been proposed to control cell division by defining the cleavage furrow for cytokinesis (Robinson *et al*., 1995). The positioning of the new flagellum is defined by the flagella connector, a short pyramidal structural that connects the tip of the new flagellum to the side of the old flagellum (Moreira-Leite *et al*., 2001). Restricting the elongation of only the new flagellum by inactivation of intraflagellar transport is accompanied by the construction of a shorter FAZ filament, whose length is correlated with that of the new flagellum (Kohl *et al*., 2003). When such cells divide, the progeny inheriting the new flagellum is shorter, with a direct correlation between cell size and flagellum and FAZ length (Kohl *et al*., 2003). This is accompanied by a failure in basal body migration (Davidge *et al*., 2006; Absalon *et al*., 2007).

To understand the molecular bases of the numerous morphological changes occurring during the parasite cycle (Van Den Abbeele *et al*., 1999; Sharma *et al*., 2008; 2009), we have investigated the evolution of key cytoskeleton components *in vivo* using a panel of specific molecular markers for the sub-pellicular microtubules, the flagellum and the FAZ. A new immunofluorescence-based assay for evaluation of the cell volume with 3D reconstruction was developed. We reveal that whereas the three proliferative stages exhibit common points in terms of cytoskeletal rearrangements during their cell cycle, the transition from the procyclic trypomastigote to the short epimastigote form in the proventriculus and foregut happens very differently. The FAZ filament is partially remodelled, concomitantly with the migration of the nucleus towards the posterior end. Strikingly, the entire sub-pellicular microtubule cytoskeleton of the future short epimastigote daughter cell appears to be remodelled before the asymmetric division, a phenomenon that takes place without visible modification of the cell volume.

Results

To investigate cytoskeleton dynamics during trypanosome development in the tsetse fly, a total of 3992 *Glossina morsitans morsitans* tsetse flies were infected with cultured *Trypanosoma brucei brucei* strain AnTat1.1 parasites in 49 separate experiments. Out of the 761 flies dissected $\geq$ 14 days post-ingestion, 36.5% were carrying trypanosomes in the midgut and 13.5% presented infection of the salivary glands. These results indicate that the infection reached maturity in 37.1% of the infected flies. Phase-contrast microscopy coupled to 4,6-diamidino-2-phenylindole (DAPI) staining of nuclear and mitochondrial DNA confirmed the validity of the experimental set-up as all the reported parasite stages were detected upon fly dissection (Fig. 1).

Dynamics of the cytoskeleton during the parasite cycle

Overall, the total length of the parasite measured from the tip of the flagellum to the posterior end of the cell ranged from 11.5 $\pm$ 2.0 μm in short epimastigotes up to 35.3 $\pm$ 4.9 μm in epimastigotes found in the proventriculus (mean $\pm$ SD, Table S1). To understand the molecular mechanisms underlying these extensive variations of the cytoskeleton, we first monitored the distribution of sub-pellicular microtubules upon staining with the monoclonal antibody TAT1 that recognizes α-tubulin (Woods *et al*., 1989). The antibody produced a bright signal underlying the plasma membrane in all stages (Fig. 1). This was exploited to estimate the cell volume by *in silico* 3D reconstruction of confocal z-stack pictures of α-tubulin-labelled parasites (Fig. 2). In parallel, microtubule dynamics was investigated using the monoclonal antibody YL1/2 (Kilmartin *et al*., 1982) that stains tyrosinated α-tubulin and is a recognized marker of new tubulin assembly (Sherwin *et al*., 1987; Sherwin and Gull, 1989b) (Figs 3A–D and S1).

The cell volume of 1K1N parasites varied from 20 $\pm$ 3 μm^3 in short epimastigotes up to 65 $\pm$ 8 μm^3 in mesocyclic trypomastigotes (mean $\pm$ SD, Fig. 2A). Variations in cell volume between two consecutive stages were somehow correlated with those in cell length but far from direct (Fig. 2B). During the transition from the slender to the stumpy bloodstream form, the decrease in cell length (–16%) was accompanied by an increase in cell volume (+18%), with limited insertion of new tubulin at the posterior end, suggesting a rearrangement of the existing microtubules (Figs 2B and S1). In the posterior midgut of the vector, the differentiation from the stumpy to the procyclic form (Figs 2B and S1) was marked by an important elongation of the posterior end (+42%) but only a discrete increase in cell volume (+7%). Then, during the transition to the mesocyclic stage, an intense microtubule polymerization activity was detected at the tip of the flagellum and at the posterior end of cells (Fig. S1). This was accompanied by an increase in cell volume (+8 μm^3/+14%) and a lengthening of the cell (+8.9 μm/+30%), suggesting that mesocyclic parasites become thinner (Fig. 2B).

The next step of the parasite cycle is the trypomastigote to epimastigote differentiation occurring in the anterior midgut and during which both the cell length and volume remained relatively constant (Fig. 2B). After migration of the long thin nucleus towards the posterior side of the kinetoplast, the cell became very narrow while the duplicated kinetoplasts began to divide, as shown by the presence of two basal bodies labelled by

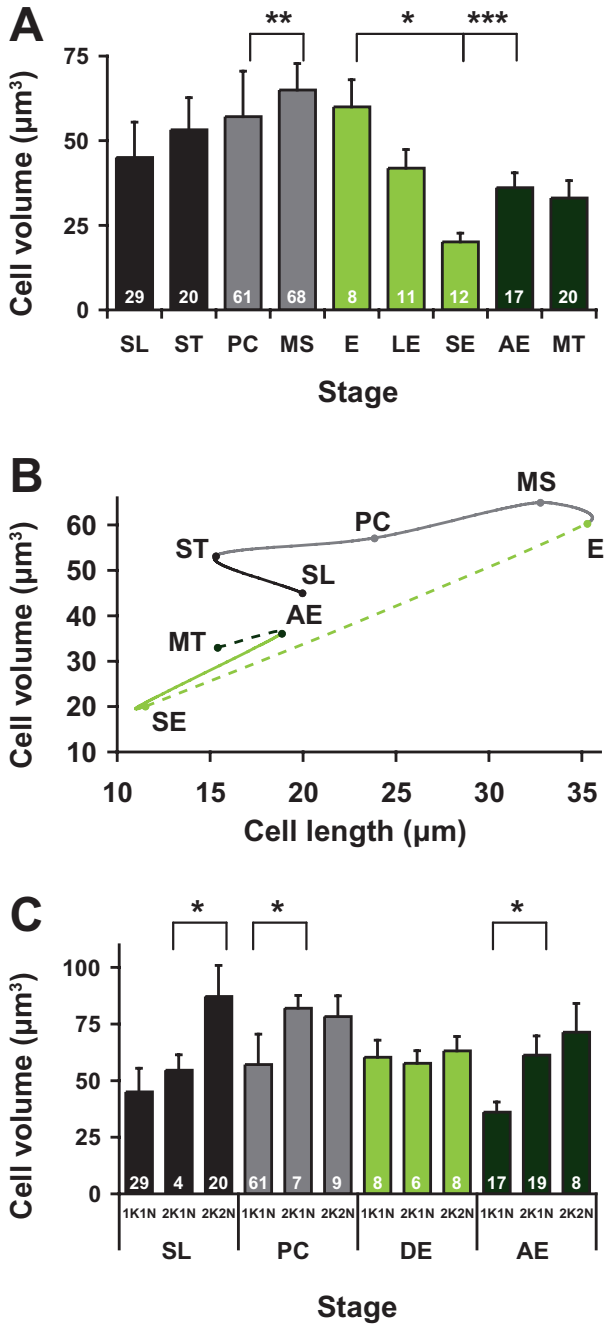

Fig. 2. Cell volume variation during the parasite cycle. The 10 main morphological stages of the *T. brucei* parasite cycle (A) and the four dividing forms (C) were fixed in PFA and stained with DAPI and the TAT1 antibody recognizing α-tubulin. The cell volume was calculated after 3D reconstruction of 200 nm confocal z-stack pictures. The number of cells studied is shown inside each column. An ANOVA test was performed and significant comparisons between two consecutive stages by Tukey *ad hoc* post-tests were indicated on the histogram with $*P < 0.0001$, $**P < 0.001$ or $***P < 0.01$.

A. Mean cell volumes ± SD (µm³) of 1K1N cells at each stage of the parasite cycle.

B. Variations of the mean cell volume ± SD (µm³) ($n = 246$) as a function of the mean total cell length ± SD (µm) of each stage ($n = 1273$). Full lines stand for differentiations and dotted lines for asymmetric divisions.

C. Mean cell volumes ± SD (µm³) of 1K1N, 2K1N and 2K2N cells in each of the four dividing stages of the parasite cycle. Stages are presented in a chronological order and the name code is given in Fig. 1.

the YL1/2 antibody (Figs 3A–D and S2). Surprisingly, binucleated epimastigotes displayed a unique YL1/2 staining pattern as the signal completely encompassed the two nuclei, corresponding to the dilated posterior part of the cell (Fig. 3B). This was further confirmed by detailed confocal observations of dividing epimastigotes using 200 nm optical sections that revealed a bright fluorescent signal drawing the entire posterior part of the cell (Figs 3E and S2). After asymmetric cell division, the staining was restricted to the tip of the flagellum, the basal body and the far posterior end of both long (Fig. 3C) and short (Fig. 3D) epimastigote cells. In contrast to the YL1/2 staining, the pattern of acetylated tubulin (Schneider *et al.*, 1987) followed faithfully the global shape of the cell, including the anterior part, as in all the other stages of the parasite cycle (Fig. S2). These results indicate an active remodelling of the posterior part of the microtubule corset concomitant to nuclear mitosis in dividing epimastigotes.

To correlate these modifications of the peripheral microtubule corset with morphological changes, the evolution of the cell volume during the cell cycle was first monitored in all three proliferating stages of the parasite cycle (bloodstream long slender, midgut procyclic and attached epimastigote in the salivary glands), and then compared with the proventricular dividing epimastigote form. A significant increase in cell volume was observed in all three proliferative stages in correlation with cell elongation (Fig. 2C). In sharp contrast, the cell volume of the epimastigotes found in the proventriculus and foregut remained constant at every step of their existence at 60 ± 8 µm³, no matter the stage of the cell cycle (from 1K1N to 2K2N, Fig. 2C). The asymmetric division resulted in the net production of a long epimastigote (42 ± 6 µm³) and a short epimastigote cell (20 ± 3 µm³).

The probable transition from this short epimastigote to the parasite attached to the salivary gland was then accompanied by a significant increase in cell volume, close to a doubling (+16 µm³/+80%), and by an important elongation of the posterior end (+7.3 µm/+48%) (Fig. 2B). Finally, trypomastigote metacyclic cells were found to be slightly smaller than their epimastigote precursors (Fig. 2B). These data reveal striking differences in the mechanisms involved in morphological modifications between proliferative stages and the differentiating stage in the proventriculus.

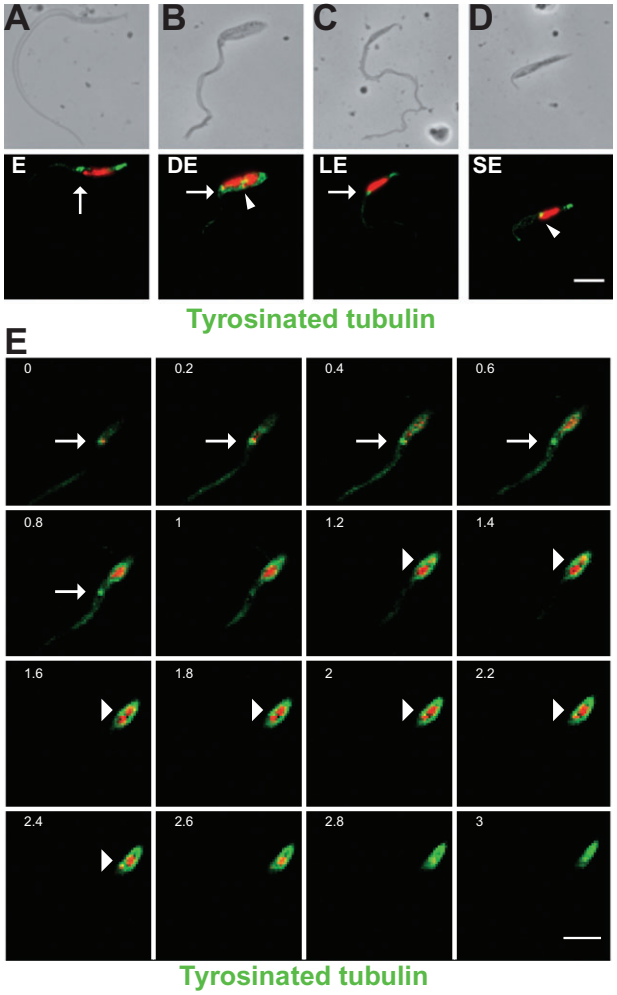

Fig. 3. Cytoskeleton remodelling during the asymmetric division in the proventriculus. Proventricular cells were fixed in methanol (A–D) or in PFA (E) and stained with DAPI (red) and the YL1/2 antibody (green) recognizing tyrosinated tubulin.
A–D. Whereas tyrosinated tubulin is found at the posterior end and the basal body of epimastigotes (A), long epimastigotes (C) and short epimastigotes (D), an intense signal was present in a larger posterior region engulfing the two nuclei in dividing epimastigotes (B). Stages are presented in a chronological order and the name code is given in Fig. 1.
E. A z-stack confocal observation of a 2K2N dividing epimastigote labelled with YL1/2 was represented from the bottom (anterior end) to the top (posterior end). A bright fluorescent signal is found around the entire peripheral microtubule corset of the future short epimastigote. The scale bars represent 5 μm and the old (arrow) and new (arrowhead) basal body positions are indicated.

Flagellum/FAZ evolution during the trypanosome parasite cycle

Because the flagellum has been shown to participate to cell morphogenesis (Robinson *et al*., 1995; Kohl *et al*., 2003; Vaughan, 2010), we monitored the evolution of typical molecular markers using the monoclonal antibodies MAb25 (Pradel *et al*., 2006) (data not shown) and L8C4 (Kohl *et al*., 1999) (Fig. S3), respectively, labelling the axoneme and the paraflagellar rod, an extra-axonemal structure that runs alongside the axoneme [review in (Portman and Gull, 2009)]. Immunofluorescence produced a clear signal throughout the length of the flagellum in all stages analysed. The length of the flagellum was measured either from the phase contrast picture or from immunofluorescence images obtained upon MAb25 or L8C4 staining (Fig. S3 and Table S1). The three sets of data correlated well, with slightly shorter values for PFR2 as expected from the position of the PFR that is only present when the flagellum exits from the flagellar pocket (Fig. S3). Flagellum length ranged from only 2.9 ± 0.6 μm in the short epimastigote up to 29.0 ± 3.8 μm in epimastigote cells found in the proventriculus (mean ± SD, with MAb25, Fig. S3 and Table S1). Although flagellum length variations followed the same trends as cell length, the amplitude was at least three times more pronounced, reaching a 1 to 10 ratio.

The presence and localization of four distinct components of the FAZ was examined by immunofluorescence. The FAZ-associated microtubule quartet was probed with the monoclonal antibody 1B41 that recognizes a particular isoform of β-tubulin (Gallo *et al*., 1988) (Fig. 4A). By immunofluorescence analysis, this antibody exclusively stains the quartet and does not produce a signal on any other microtubules (axonemal, sub-pellicular or mitotic microtubules). Antibodies recognizing three distinct components of the FAZ filament were used: L3B2 for the FAZ1 protein (Kohl *et al*., 1999) (Fig. S4), DOT1 for a distinct, yet unknown, protein (Woods *et al*., 1989; Kohl and Gull, 1998) (Fig. S5), and an antiserum against the FLA1 protein (Nozaki *et al*., 1996), recently shown to belong to the FAZ filament (B. Rotureau *et al*., unpubl. data). FAZ1 is a large repetitive protein only present in the FAZ that plays important roles in trypanosome cell division, but is not essential for assembly of the filament (Vaughan *et al*., 2008). FLA1 is a transmembrane protein whose extracellular domain is heavily glycosylated; its absence results in flagellum detachment in *T. brucei* (LaCount *et al*., 2002) and in the related parasite *Trypanosoma cruzi* (Cooper *et al*., 1993). All three proteins are tightly associated to the FAZ filament as they remain present after detergent extraction of the cytoskeleton. The anti-FLA1 and the anti-microtubule-quartet antibodies produced a positive signal in all stages (Fig. 4A). Measurements of the length of the FAZ filament based on these immunofluorescence images revealed an evolution correlated with the length of the flagellum (Fig. 4B and Table S1). The length of the FAZ ranged from 4.9 ± 2.4 μm in the short epimastigotes up to 22.9 ± 3.4 μm in mesocyclic cells (mean ± SD, $n = 289$ with the anti-FLA1 antibody) (Fig. 4B and Table S1). A close correlation was observed between the length of the FAZ filament and that of the quartet of microtubules (data not

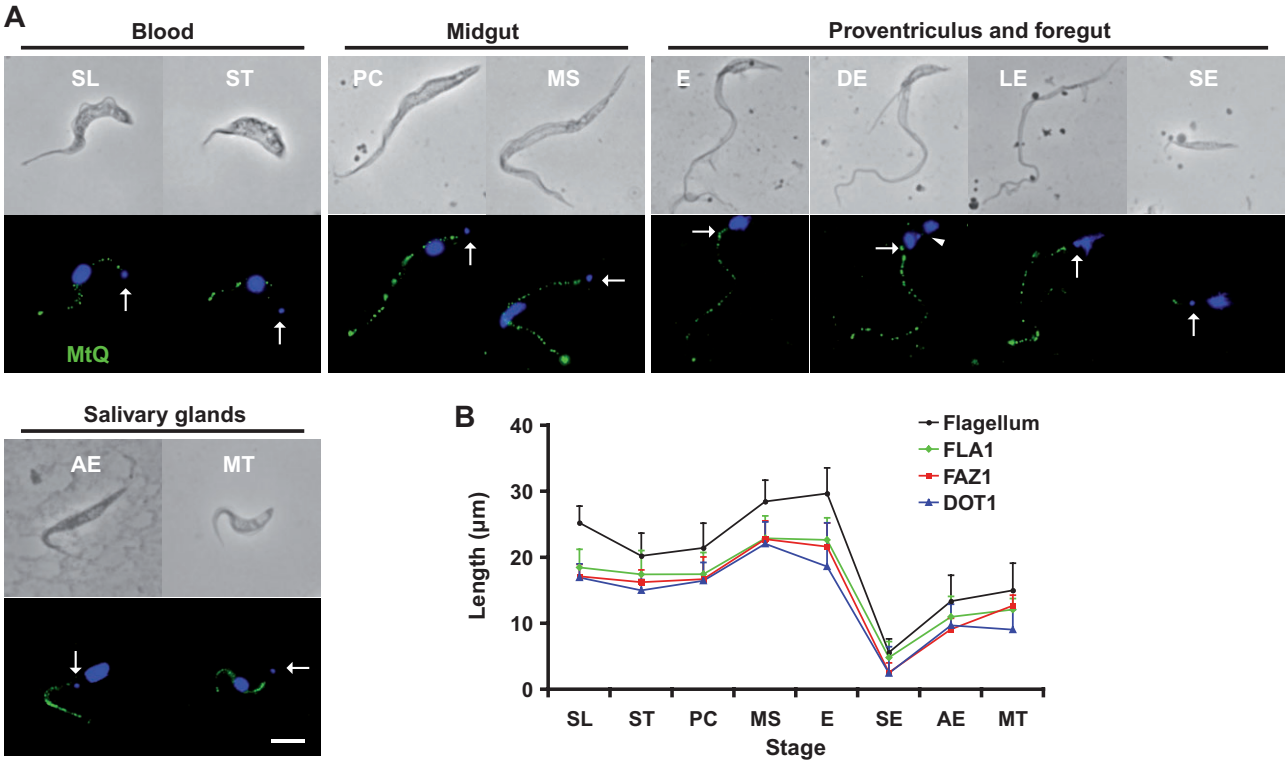

Fig. 4. The FAZ is present in all stages and its length follows that of the flagellum. Cells were fixed in methanol and stained with DAPI (blue in A) and the following antibodies.
A. Staining with the 1B41 antibody recognizing the microtubule quartet associated to the FAZ (MtQ in green). The scale bar represents 5 µm and the old (arrow) and new (arrowhead) basal body positions are indicated. Stages are presented in a chronological order and the name code is given in Fig. 1.
B. Staining with the MAb25 antibody targeting the axoneme, the antibody recognizing the transmembrane protein FLA1, or one of the two distinct markers of the FAZ filament L3B2 and DOT1. Length of the fluorescent signals was measured (Table S1) and presented as means ± SD (in µm) for each stage. Flagellar axoneme ($n = 307$), FLA1 ($n = 289$), FAZ1 ($n = 365$) and DOT1 ($n = 239$).

shown). However, from the beginning of nucleus migration towards the posterior end of the cell in the late mesocyclic stage, to the asymmetrically dividing epimastigote parasites, a dramatic reduction in the intensity of the fluorescent signal was observed for both the L3B2 and DOT1 probes. Comparison of parasites from the proventriculus in the same microscope field showed a dramatic drop in signal intensity for both L3B2 (80%, $n = 65$) and DOT1 (82%, $n = 28$) in long epimastigotes and dividing epimastigotes compared with mesocyclic trypomastigotes, which exhibited a signal intensity similar to that of procyclic trypomastigotes (Fig. 5C–F). The signal became detectable again associated to the FAZ in close vicinity of the flagellum in short epimastigote cells and in all subsequent stages (Figs S4 and S5). In contrast, single or simultaneous immuno-labelling of FLA1 or the four FAZ-associated microtubules remained unchanged in all proventricular stages (Fig. 5A, B and F). These data reveal important remodelling of the FAZ filament during the transition from the trypomastigote to the epimastigote configuration.

Discussion

In this study, we investigated the evolution of the cytoskeleton and of the flagellar apparatus during trypanosome differentiation in the tsetse fly. First, we confirmed that all previously characterized parasite stages could be identified in our hands, although the chronology of events was shifted by about 1 week compared with published reports (Van Den Abbeele *et al.*, 1999; Peacock *et al.*, 2007; Sharma *et al.*, 2008; Oberle *et al.*, 2010). Nevertheless, measurement of parasite length at various stages of infection was in good agreement with data from the literature (Van Den Abbeele *et al.*, 1999; Sharma *et al.*, 2008).

Cytoskeleton dynamics and cell volume evolution

As in many protists, the trypanosome cytoskeleton is not depolymerized during mitosis. Instead, a complete microtubule corset is inherited by each daughter cell in a semi-conservative manner, as shown in cultured procyclic cells (Sherwin and Gull, 1989b). Tubulin and acetylated

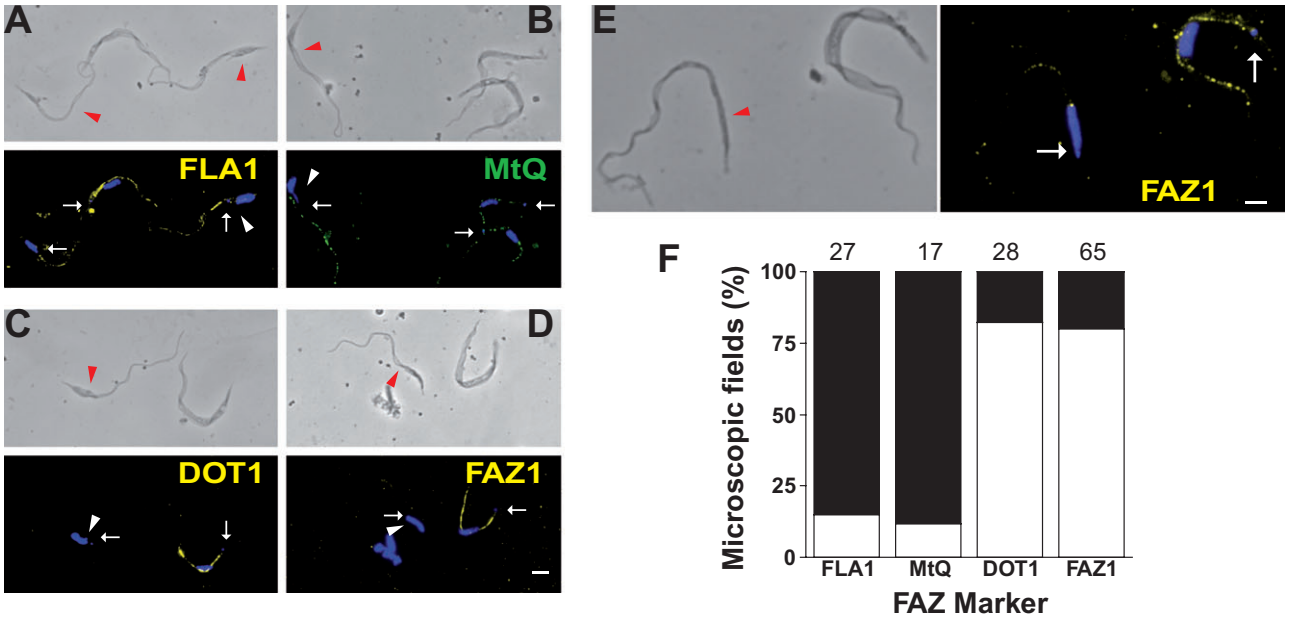

Fig. 5. Remodelling of the FAZ filament during differentiation in the proventriculus. Cells were fixed in methanol and stained with DAPI (blue in A–E), the antibody recognizing the transmembrane protein FLA1 (A, yellow), the 1B41 antibody targeting the MtQ (B, green), and two distinct markers of the FAZ filament DOT1 (C, yellow) and L3B2 (D and E, yellow). A–E. The scale bars represent 5 μm and the old (white arrow) and new (white arrowhead) basal body positions are indicated. Epimastigote cells are shown with red arrowheads.
F. The intensity of the signals obtained for the anti-FLA1, 1B41, L3B2 and DOT1 were compared between proventricular forms of the parasites in the same microscope fields. The occurrence of an equal or lower (black bars) or higher (white bars) fluorescent signal in mesocyclic cells compared with epimastigotes/dividing epimastigotes were counted and plotted as percentage of the total number of fields observed (*n* at the top of the bars).

α-tubulin staining confirmed the existence of the corset at all investigated stages. We have exploited this feature to set up a novel method to estimate cell volume. To our knowledge, estimations of the *T. brucei* cell volume have only been reported for bloodstream stages, in culture (Grunfelder *et al*., 2002) or isolated from infected rats (Opperdoes *et al*., 1984; Reuner *et al*., 1997). Our cell volume calculations (45 and 53 μm^3 for slender and stumpy cells, respectively) are close to the previously published estimations: 36 μm^3 obtained by electronic pulse area analysis (Reuner *et al*., 1997), 52 μm^3 calculated by stereological analysis of electron microscopic images (Grunfelder *et al*., 2002), 58 μm^3 estimated by the inulin exclusion method (Opperdoes *et al*., 1984) and 59 μm^3 evaluated in 3D microscopic images of fluorescent living cells (Grunfelder *et al*., 2002), validating our approach.

Tyrosinated α-tubulin is a recognized marker of recently assembled tubulin and was used in cultured procyclic trypanosomes to monitor microtubule dynamics during the cell cycle, revealing elongation of microtubules at the posterior end and intercalation of new microtubules within the existing network (Sherwin *et al*., 1987; Sherwin and Gull, 1989b). We confirmed these data on procyclic parasites obtained from the midgut and showed that all three proliferative stages (bloodstream form, procyclic stage and attached epimastigote) exhibit microtubule elongation at the posterior end, a process coupled to a significant increase in total cell volume.

Cytoskeleton elongation at the posterior end is also a feature of two differentiating stages: stumpy to procyclic (Matthews *et al*., 1995) and procyclic to mesocyclic (Hammarton *et al*., 2004). These two steps involve increase in cell length but modest increase in cell volume. In sharp contrast, no apparent increase in tubulin polymerization was observed during the thinning of the cell body and the nucleus migration occurring from the pre-epimastigote to the epimastigote stage in the proventriculus. Cell volume did not increase either before cytokinesis in asymmetrically dividing epimastigotes. Once anaphase is clearly initiated, the posterior end appears more dilated and becomes brightly positive for tyrosinated tubulin, a staining that encompasses the two nuclei. These changes indicate the dynamic formation of new microtubules and/or the remodelling of existing ones. This is the first observation of tubulin tyrosination without posterior elongation in trypanosomes. This could imply a depolymerization of some sub-pellicular microtubules before assembly in a new configuration, a phenomenon compatible with the observed stability of the cell volume. This could be related to the formation of a much smaller daughter cell (the short epimastigote) at the asymmetric division and to the assembly of a very short flagellum.

Roles of the FAZ in trypanosome development in the tsetse fly

The morphometric measurements produced here demonstrate that the evolution of cell length is more closely related to variations in flagellum length than in cell volume. In cultured procyclic trypanosomes, morphogenesis has been shown to be associated to flagellum length (Kohl *et al*., 2003). The FAZ has been proposed to define the position and the direction of the cleavage furrow, hence defining morphogenesis (Robinson *et al*., 1995). Intraflagellar transport RNAi mutants undergo an asymmetric division with the formation of a cell of normal length inheriting the normal old flagellum/FAZ and a short cell inheriting the short new flagellum/FAZ, with a direct correlation with flagellum length (Kohl *et al*., 2003). As it has previously been hypothesized (Sharma *et al*., 2008), such a mechanism could explain the asymmetric division observed in epimastigotes of the proventriculus. A second postulated function of the FAZ is the control of basal body and flagellar pocket positioning (Absalon *et al*., 2007; Bonhivers *et al*., 2008a). Tomography studies showed that the microtubule quartet wraps around the flagellar pocket and that the FAZ filament is in close contact with the collar of the flagellar pocket (Lacomble *et al*., 2009). An involvement of the FAZ in basal body positioning is further supported by the location of the basal body at the extreme posterior end of the cell in the *BILBO1*^{RNAi} mutant that lacks the flagellar pocket collar and fails to assemble a new FAZ (Bonhivers *et al*., 2008b).

In cultured procyclic cells, the FAZ elongates at the same rate as the flagellum (Kohl *et al*., 1999). Our data show that the molecular composition of the FAZ, with a typical dotty pattern along the adhesion region, is conserved over the parasite development in the tsetse fly, despite the exhaustive modifications of flagellum length. One striking exception to this rule is the differentiation from the mesocyclic trypomastigote to the epimastigote form. This transition results from a thinning of the cell body and a relative movement of the nucleus towards the posterior end of the cell, and occurs at the same time as the initiation of mitosis (Sharma *et al*., 2008). We revealed that a remodelling of the FAZ filament initiates as soon as the elongated nucleus starts its migration towards the posterior end. The protein FAZ1 and the distinct antigen recognized by the monoclonal antibody DOT1 (Kohl and Gull, 1998) fell below detection level whereas neighbouring mesocyclic parasites were still positive. This could be due to either absence of these two proteins, or to reduced accessibility to the epitopes that could result from post-translational modifications or changes in molecular configuration, but in any case, it reveals a modification in FAZ filament organization. It should be reminded here that FAZ1 is not required for the construction of the FAZ filament *per se* (Vaughan *et al*., 2008). As working model, we propose that this re-organization is related to the movement of the nucleus in a more posterior position. Indeed, treatment of extracted trypanosome cytoskeletons with calcium depolymerizes the sub-pellicular microtubules, leaving behind only the flagellum, the FAZ filament and the nucleus that appears to be associated with the filament (Absalon *et al*., 2007). Thus, we suggest that the observed changes in molecular disposition of the FAZ filament could somehow liberate and/or guide the nucleus for posterior migration, for example by the action of motors that remain to be identified. These could be associated to the microtubule quartet of the FAZ that remains present in these cells.

In contrast to the differentiation between bloodstream stumpy and midgut procyclic stages, which occurs during a G1 arrest (Matthews and Gull, 1994), the differentiation of mesocyclic trypomastigotes to epimastigotes occurs at the beginning of the asymmetric cell division cycle (Van Den Abbeele *et al*., 1999; Sharma *et al*., 2008). We observed that both L3B2 and DOT1 markers were recovered after the asymmetric division in the short epimastigote daughter cells but not in the long siblings. This observation is in accordance with the fact that the long epimastigote daughter cell does not enter S-phase, as judged by the lack of expression of the cohesin component SCC1, and is likely to degenerate as many are observed with diffuse or dispersed nuclear staining (Sharma *et al*., 2008). Further understanding of the role of the FAZ in these important morphogenetic processes awaits the identification of novel molecular components for functional investigation. It should be stressed that all FAZ components identified so far are specific to trypanosomatid parasites and could represent promising drug target in the future given the essential role of this sub-cellular structure.

Our results bring molecular evidence for cytoskeleton shaping that takes place during trypanosome differentiation. Several functions could be proposed to link the specific morphological and molecular modifications with trypanosome behaviour, alongside previously published observations (Vickerman *et al*., 1988; Van Den Abbeele *et al*., 1999; Peacock *et al*., 2007; Sharma *et al*., 2008; Oberle *et al*., 2010). First, the high motility of procyclic trypomastigotes found in the posterior midgut could be involved in crossing of the peritrophic membrane that separates the blood meal from the midgut epithelium, hence escaping the more aggressive environment of the gut lumen. Their proliferative status is linked to the early settlement and amplification of the parasite population, and subsequently, with the maintenance of the midgut infection during the whole life of the vector. In contrast, cells at the mesocyclic stage do not show signs of proliferation but are longer and thinner. These elongated

parasites swim together sometimes at high density (B. Rotureau *et al*., unpubl. data) all along the midgut, from its posterior part to the proventriculus. Such a characteristic shape could remarkably fit their migratory function. Then, the relatively long journey of epimastigote parasites to the salivary gland implies passage via the foregut and the hypopharynx, and finally through the narrow salivary gland duct. The few but long, thin and highly motile dividing epimastigote parasites found in these regions could be well-adapted to deliver free short epimastigote cells, whose motility properties appear more limited, directly in the salivary glands. In these conditions, the elongated shape might offer less friction and facilitate migration. Anterior positioning of the flagellum in short epimastigotes could be explained by the necessity for adhesion to the salivary gland epithelium, as these parasites are not yet infective: they do not possess the VSG coat but display a specific cell surface protein called BARP (Urwyler *et al*., 2007). Proliferation of attached epimastigotes is likely required to ensure colonization of the epithelium and sustained production of infective parasites in the saliva. After their attachment to the epithelium, epimastigotes elongate their posterior end, adopting characteristic protrusions. As the flagellum is attached, these protusions oscillating in the lumen offer a significant surface that could be involved in sensing and/or molecular exchanges with the environment. Upon release in the saliva, free infective metacyclic trypomastigotes are shaped like bloodstream forms and possess a VSG coat but are small enough to travel through the narrow ducts of the tsetse mouthparts. The trypomastigote morphotype could ensure more efficient swimming in a crowded environment such as encountered in the blood with millions of erythrocytes (Engstler *et al*., 2007). In all cases, the flagellum tracts the cell forward, with its tip always extending beyond the cell body. Such a configuration would ensure that the tip of this organelle is the first one to be in contact with new environments, making it a strong sensing candidate (Rotureau *et al*., 2009). These are only conjectures but it emphasizes the link between the multiple cytoskeletal modifications, including those of the flagellum, and the adequate functions of each trypanosome stage in its specific environment in the insect.

Experimental procedures

Trypanosome strain and cultures

The pleomorphic strain *Trypanosoma brucei brucei* AnTat1.1 (Le Ray *et al*., 1977) was used throughout this study. Slender bloodstream parasites were cultured in HMI9 medium supplemented with 10% foetal bovine serum (Hirumi and Hirumi, 1989). Alternatively, they were plated on solid HMI9 medium supplemented with 10% fetal bovine serum to induce their differentiation into the stumpy form (Carruthers and Cross, 1992; Vassella *et al*., 1997). Stumpy parasites were then triggered to differentiate into the procyclic culture form in DTM medium containing 20% fetal bovine serum by the addition of 6 mM *cis*-aconitate and a temperature shift from 37°C to 27°C (Brun and Schonenberger, 1981). Procyclic trypanosomes were maintained in SDM79 medium (Brun and Schonenberger, 1979) supplemented with 10% fetal bovine serum and 20 mM glycerol.

Tsetse fly infection, maintenance and dissection

Teneral males of *Glossina morsitans morsitans* from 8 to 96 h post-eclosion were obtained from the 'TRYPANOSOM' UMR177 IRD-CIRAD, Campus International de Baillarguet, Montpellier, France. Tsetse flies were allowed to ingest parasites in culture medium during their first meal through a silicone membrane. We used either (i) stumpy cells at 10^6 cells per millilitre in HMI9 medium supplemented with 10% foetal bovine serum, 60 mM N-acetylglucosamine (Peacock *et al*., 2006) and 2.5% (w/v) bovine serum albumin (Kabayo *et al*., 1986), or (ii) procyclic cultured trypanosomes at 5.10^6 cells per millilitre in SDM79 medium supplemented with 10% foetal bovine serum, 60 mM N-acetylglucosamine (Peacock *et al*., 2006) and 2.5% (w/v) bovine serum albumin (Kabayo *et al*., 1986). Tsetse flies were subsequently maintained in Roubaud cages at 27°C and 70% hygrometry and fed twice a week through a silicone membrane with fresh rabbit blood in heparin.

Flies were starved for at least 48 h before being dissected at different time points from 14 to 55 days after ingestion of the infected meal. Salivary glands were first dissected into a drop of PBS or SDM79 medium. Whole tsetse alimentary tracts, from the distal part of the foregut to the rectum, were then dissected and arranged lengthways for assessment of parasite presence. Foregut and proventriculus were physically separated from the midgut in distinct PBS/SDM79 drops. Tissues were dilacerated and recovered parasites were treated for further experiments no more than 15 min after dissection.

Immunofluorescence

For immunofluorescence, cells were washed in PBS or SDM79 medium, settled on poly-L-lysine coated or uncoated slides and fixed in 4% para-formaldehyde (PFA) for 10 min. Fixed cells were permeabilized with 0.5% Nonidet P-40 in PBS for 10 min and samples were rinsed to remove the excess of detergent. Blocking was performed by an incubation of 45 min in PBS containing 1% bovine serum albumin. Alternatively, cells were fixed in methanol at –20°C for at least 5 min and re-hydrated in PBS for 10 min. In all cases, slides were incubated with primary antibodies for 60 min at room temperature. They were washed and incubated with the appropriate secondary antibodies coupled to Alexa 488 (Invitrogen) or Cy3 (Jackson). Slides were stained with DAPI for visualization of kinetoplast and nuclear DNA content, and mounted under cover slips with ProLong antifade reagent (Invitrogen).

The TAT1 (IgG2b) (Woods *et al*., 1989) antibody recognizes α-tubulin. MAb25 (IgG2a) labels a protein found all along the axoneme (Pradel *et al*., 2006), while the monoclonal antibody L8C4 (IgG1) specifically recognizes PFR2, localized throughout the PFR (Kohl *et al*., 1999). The YL1/2 antibody (IgG) (Kilmartin *et al*., 1982) labels tyrosinated α-tubulin while the C3B9 antibody

(IgG2b) detects acetylated α-tubulin (Woods *et al*., 1989). Concerning the FAZ components, a polyclonal antibody was used to stain the transmembrane protein FLA1 (Nozaki *et al*., 1996), the 1B41 antibody recognizes the microtubule quartet associated to the FAZ filament (Gallo *et al*., 1988), and the two markers of the FAZ filament L3B2 (Kohl *et al*., 1999) and DOT1 (Woods *et al*., 1989), respectively, target FAZ1 and a distinct yet unknown protein (Kohl and Gull, 1998). For each antibody, IFA experiments were repeated on trypanosomes issued from 3 to 13 different flies and from at least 3 distinct experimental infections.

Measurements and analyses

Samples were observed either with (i) a DMR microscope (Leica) and images were captured with a CoolSnap HQ camera (Roper Scientific) (ii) with a DMI4000 microscope (Leica) and images were acquired with a Retiga-SRV camera (Q39 Imaging) or (iii) with a digital D-Eclipse EZ-C1si confocal system (Nikon) installed on an Eclipse TE2000-E inverted microscope (Nikon). Pictures were analysed and cell parameters were measured using the IPLab Spectrum 3.9 software (Scanalytics & BD Biosciences), the ImageJ 1.38X software (NIH) or the NIS-elements software (Nikon). For clarity purposes, brightness and contrast of several pictures presented in figures were adjusted after their analysis in accordance with editorial policies. The scale bars represent 5 μm in all figures. The cell volumes were calculated from *in silico* 3D reconstructions of 200 nm confocal z-stack pictures of PFA-fixed cells stained with TAT1. Calculations were done in the ImageJ-derived Fiji package after an 'intermodes' auto-threshold normalization of the fluorescence. Statistical analyses and plots were performed in Excel or with the KaleidaGraph V.4.0 software (Synergy Software). Lengths (μm) and volumes (μm^3) were plotted as means ± SD. One-way ANOVA tests were performed with intergroup comparisons between two consecutive stages by Tukey *ad hoc* post-tests with $a = 0.05$ and significant results were indicated with $^{*}P < 0.0001$, $^{**}P < 0.001$ and $^{***}P < 0.01$ (Fig. 2).

Acknowledgements

We thank B. Tchicaya and J. Janelle from the UMR177 IRD-CIRAD team headed by G. Cuny (Montpellier, France) for generously providing tsetse flies. We are grateful to J. Van Den Abbeele for providing the trypanosome AnTat 1.1 cell line. We acknowledge L. Kohl, D. Robinson and K. Gull for providing various antibodies. We thank P. Reiter and A. Scherf for providing access to the insectarium and to the confocal microscope respectively. We thank G. Milon, D. Julkowska, G. Spaeth, F. Bringaud and D. Robinson for critical reading of the manuscript. This work was funded by the CNRS, the Institut Pasteur and by a MIE grant from the ANR. BR is funded by a Roux post-doctoral fellowship from the Institut Pasteur and IS by a FNR fellowship. The authors declare no competing financial interests.

References

Absalon, S., Kohl, L., Branche, C., Blisnick, T., Toutirais, G., Rusconi, F., *et al*. (2007) Basal body positioning is controlled by flagellum formation in *Trypanosoma brucei*. *PLoS ONE* **2:** e437.

Bonhivers, M., Landrein, N., Decossas, M., and Robinson, D.R. (2008a) A monoclonal antibody marker for the exclusion-zone filaments of *Trypanosoma brucei*. *Parasit Vectors* **1:** 21.

Bonhivers, M., Nowacki, S., Landrein, N., and Robinson, D.R. (2008b) Biogenesis of the trypanosome endo-exocytotic organelle is cytoskeleton mediated. *PLoS Biol* **6:** e105.

Brun, R., and Schonenberger, M. (1979) Cultivation and in vitro cloning or procyclic culture forms of *Trypanosoma brucei* in a semi-defined medium. Short communication. *Acta Trop* **36:** 289–292.

Brun, R., and Schonenberger, M. (1981) Stimulating effect of citrate and cis-Aconitate on the transformation of *Trypanosoma brucei* bloodstream forms to procyclic forms in vitro. *Z Parasitenkd* **66:** 17–24.

Brun, R., Blum, J., Chappuis, F., and Burri, C. (2009) Human African trypanosomiasis. *Lancet* **375:** 148–159.

Carruthers, V.B., and Cross, G.A. (1992) High-efficiency clonal growth of bloodstream- and insect-form *Trypanosoma brucei* on agarose plates. *Proc Natl Acad Sci USA* **89:** 8818–8821.

Cooper, R., de Jesus, A.R., and Cross, G.A. (1993) Deletion of an immunodominant *Trypanosoma cruzi* surface glycoprotein disrupts flagellum-cell adhesion. *J Cell Biol* **122:** 149–156.

Davidge, J.A., Chambers, E., Dickinson, H.A., Towers, K., Ginger, M.L., McKean, P.G., and Gull, K. (2006) Trypanosome IFT mutants provide insight into the motor location for mobility of the flagella connector and flagellar membrane formation. *J Cell Sci* **119:** 3935–3943.

Engstler, M., Pfohl, T., Herminghaus, S., Boshart, M., Wiegertjes, G., Heddergott, N., and Overath, P. (2007) Hydrodynamic flow-mediated protein sorting on the cell surface of trypanosomes. *Cell* **131:** 505–515.

Fenn, K., and Matthews, K.R. (2007) The cell biology of *Trypanosoma brucei* differentiation. *Curr Opin Microbiol* **10:** 539–546.

Gallo, J.M., Precigout, E., and Schrevel, J. (1988) Subcellular sequestration of an antigenically unique beta-tubulin. *Cell Motil Cytoskeleton* **9:** 175–183.

Grunfelder, C.G., Engstler, M., Weise, F., Schwarz, H., Stierhof, Y.D., Boshart, M., and Overath, P. (2002) Accumulation of a GPI-anchored protein at the cell surface requires sorting at multiple intracellular levels. *Traffic* **3:** 547–559.

Gull, K. (1999) The cytoskeleton of trypanosomatid parasites. *Annu Rev Microbiol* **53:** 629–655.

Hammarton, T.C., Engstler, M., and Mottram, J.C. (2004) The *Trypanosoma brucei* cyclin, CYC2, is required for cell cycle progression through G1 phase and for maintenance of procyclic form cell morphology. *J Biol Chem* **279:** 24757–24764.

Hirumi, H., and Hirumi, K. (1989) Continuous cultivation of *Trypanosoma brucei* blood stream forms in a medium containing a low concentration of serum protein without feeder cell layers. *J Parasitol* **75:** 985–989.

Hoare, C.A., and Wallace, F.G. (1966) Developmental Stages of Trypanosomatid Flagellates: a New Terminology. *Nature* **212:** 1385–1386.

Kabayo, J.P., DeLoach, J.R., Spates, G.E., Holman, G.M., and Kapatsa, G.M. (1986) Studies on the biochemical

basis of the nutritional quality of tsetse fly diets. *Comp Biochem Physiol A Comp Physiol* **83:** 133–139.
Kilmartin, J.V., Wright, B., and Milstein, C. (1982) Rat monoclonal antitubulin antibodies derived by using a new nonsecreting rat cell line. *J Cell Biol* **93:** 576–582.
Kohl, L., and Gull, K. (1998) Molecular architecture of the trypanosome cytoskeleton. *Mol Biochem Parasitol* **93:** 1–9.
Kohl, L., Sherwin, T., and Gull, K. (1999) Assembly of the paraflagellar rod and the flagellum attachment zone complex during the *Trypanosoma brucei* cell cycle. *J Eukaryot Microbiol* **46:** 105–109.
Kohl, L., Robinson, D., and Bastin, P. (2003) Novel roles for the flagellum in cell morphogenesis and cytokinesis of trypanosomes. *EMBO J* **22:** 5336–5346.
Lacomble, S., Vaughan, S., Gadelha, C., Morphew, M.K., Shaw, M.K., McIntosh, J.R., and Gull, K. (2009) Three-dimensional cellular architecture of the flagellar pocket and associated cytoskeleton in trypanosomes revealed by electron microscope tomography. *J Cell Sci* **122:** 1081–1090.
LaCount, D.J., Barrett, B., and Donelson, J.E. (2002) *Trypanosoma brucei* FLA1 is required for flagellum attachment and cytokinesis. *J Biol Chem* **277:** 17580–17588.
Le Ray, D., Barry, J.D., Easton, C., and Vickerman, K. (1977) First tsetse fly transmission of the 'AnTat' serodeme of *Trypanosoma brucei*. *Ann Soc Belg Med Trop* **57:** 369–381.
Matthews, K.R., and Gull, K. (1994) Evidence for an interplay between cell cycle progression and the initiation of differentiation between life cycle forms of African trypanosomes. *J Cell Biol* **125:** 1147–1156.
Matthews, K.R., Sherwin, T., and Gull, K. (1995) Mitochondrial genome repositioning during the differentiation of the African trypanosome between life cycle forms is microtubule mediated. *J Cell Sci* **108** (Part 6)**:** 2231–2239.
Moreira-Leite, F.F., Sherwin, T., Kohl, L., and Gull, K. (2001) A trypanosome structure involved in transmitting cytoplasmic information during cell division. *Science* **294:** 610–612.
Nozaki, T., Haynes, P.A., and Cross, G.A. (1996) Characterization of the *Trypanosoma brucei* homologue of a *Trypanosoma cruzi* flagellum-adhesion glycoprotein. *Mol Biochem Parasitol* **82:** 245–255.
Oberle, M., Balmer, O., Brun, R., and Roditi, I. (2010) Bottlenecks and the maintenance of minor genotypes during the life cycle of *Trypanosoma brucei*. *PLoS Pathog* **6:** e1001023.
Opperdoes, F.R., Baudhuin, P., Coppens, I., De Roe, C., Edwards, S.W., Weijers, P.J., and Misset, O. (1984) Purification, morphometric analysis, and characterization of the glycosomes (microbodies) of the protozoan hemoflagellate *Trypanosoma brucei*. *J Cell Biol* **98:** 1178–1184.
Peacock, L., Ferris, V., Bailey, M., and Gibson, W. (2006) Multiple effects of the lectin-inhibitory sugars d-glucosamine and N-acetyl-glucosamine on tsetse-trypanosome interactions. *Parasitology* **132:** 651–658.
Peacock, L., Ferris, V., Bailey, M., and Gibson, W. (2007) Dynamics of infection and competition between two strains of *Trypanosoma brucei* brucei in the tsetse fly observed using fluorescent markers. *Kinetoplastid Biol Dis* **6:** 4.
Portman, N., and Gull, K. (2009) The paraflagellar rod of kinetoplastid parasites: from structure to components and function. *Int J Parasitol* **40:** 135–148.
Pradel, L.C., Bonhivers, M., Landrein, N., and Robinson, D.R. (2006) NIMA-related kinase TbNRKC is involved in basal body separation in *Trypanosoma brucei*. *J Cell Sci* **119:** 1852–1863.
Ralston, K.S., Kabututu, Z.P., Melehani, J.H., Oberholzer, M., and Hill, K.L. (2009) The *Trypanosoma brucei* flagellum: moving parasites in new directions. *Annu Rev Microbiol* **63:** 335–362.
Reuner, B., Vassella, E., Yutzy, B., and Boshart, M. (1997) Cell density triggers slender to stumpy differentiation of *Trypanosoma brucei* bloodstream forms in culture. *Mol Biochem Parasitol* **90:** 269–280.
Robinson, D.R., and Gull, K. (1991) Basal body movements as a mechanism for mitochondrial genome segregation in the trypanosome cell cycle. *Nature* **352:** 731–733.
Robinson, D.R., Sherwin, T., Ploubidou, A., Byard, E.H., and Gull, K. (1995) Microtubule polarity and dynamics in the control of organelle positioning, segregation, and cytokinesis in the trypanosome cell cycle. *J Cell Biol* **128:** 1163–1172.
Roditi, I., and Lehane, M.J. (2008) Interactions between trypanosomes and tsetse flies. *Curr Opin Microbiol* **11:** 345–351.
Rotureau, B., Morales, M.A., Bastin, P., and Spath, G.F. (2009) The flagellum-MAP kinase connection in Trypanosomatids: a key sensory role in parasite signaling and development? *Cell Microbiol* **11:** 710–718.
Schneider, A., Sherwin, T., Sasse, R., Russell, D.G., Gull, K., and Seebeck, T. (1987) Subpellicular and flagellar microtubules of *Trypanosoma brucei* brucei contain the same alpha-tubulin isoforms. *J Cell Biol* **104:** 431–438.
Sharma, R., Peacock, L., Gluenz, E., Gull, K., Gibson, W., and Carrington, M. (2008) Asymmetric cell division as a route to reduction in cell length and change in cell morphology in trypanosomes. *Protist* **159:** 137–151.
Sharma, R., Gluenz, E., Peacock, L., Gibson, W., Gull, K., and Carrington, M. (2009) The heart of darkness: growth and form of *Trypanosoma brucei* in the tsetse fly. *Trends Parasitol* **25:** 517–524.
Sherwin, T., and Gull, K. (1989a) The cell division cycle of *Trypanosoma brucei* brucei: timing of event markers and cytoskeletal modulations. *Philos Trans R Soc Lond B Biol Sci* **323:** 573–588.
Sherwin, T., and Gull, K. (1989b) Visualization of detyrosination along single microtubules reveals novel mechanisms of assembly during cytoskeletal duplication in trypanosomes. *Cell* **57:** 211–221.
Sherwin, T., Schneider, A., Sasse, R., Seebeck, T., and Gull, K. (1987) Distinct localization and cell cycle dependence of COOH terminally tyrosinolated alpha-tubulin in the microtubules of *Trypanosoma brucei* brucei. *J Cell Biol* **104:** 439–446.
Simarro, P.P., Jannin, J., and Cattand, P. (2008) Eliminating human African trypanosomiasis: where do we stand and what comes next? *PLoS Med* **5:** e55.
Urwyler, S., Studer, E., Renggli, C.K., and Roditi, I. (2007) A family of stage-specific alanine-rich proteins on the surface of epimastigote forms of *Trypanosoma brucei*. *Mol Microbiol* **63:** 218–228.
Van Den Abbeele, J., Claes, Y., van Bockstaele, D., Le Ray, D., and Coosemans, M. (1999) *Trypanosoma brucei* spp.

development in the tsetse fly: characterization of the post-mesocyclic stages in the foregut and proboscis. *Parasitology* **118** (Part 5)**:** 469–478.
Vassella, E., Reuner, B., Yutzy, B., and Boshart, M. (1997) Differentiation of African trypanosomes is controlled by a density sensing mechanism which signals cell cycle arrest via the cAMP pathway. *J Cell Sci* **110** (Part 21)**:** 2661–2671.
Vaughan, S. (2010) Assembly of the flagellum and its role in cell morphogenesis in *Trypanosoma brucei*. *Curr Opin Microbiol* **13:** 453–458.
Vaughan, S., Kohl, L., Ngai, I., Wheeler, R.J., and Gull, K. (2008) A Repetitive Protein Essential for the Flagellum Attachment Zone Filament Structure and Function in *Trypanosoma brucei*. *Protist* **159:** 127–136.
Vickerman, K., Tetley, L., Hendry, K.A., and Turner, C.M. (1988) Biology of African trypanosomes in the tsetse fly. *Biol Cell* **64:** 109–119.
Woods, A., Sherwin, T., Sasse, R., MacRae, T.H., Baines, A.J., and Gull, K. (1989) Definition of individual components within the cytoskeleton of *Trypanosoma brucei* by a library of monoclonal antibodies. *J Cell Sci* **93** (Part 3)**:** 491–500.
Woodward, R., and Gull, K. (1990) Timing of nuclear and kinetoplast DNA replication and early morphological events in the cell cycle of *Trypanosoma brucei*. *J Cell Sci* **95** (Part 1)**:** 49–57.

Supporting information

Additional Supporting Information may be found in the online version of this article:

Fig. S1. Distribution of tyrosinated α-tubulin in parasite stages found in mammalian bloodstream and tsetse midgut. Cells were fixed in methanol and stained with DAPI (blue) and the YL1/2 antibody (green) recognizing α-tyrosinated tubulin. The scale bar represents 5 μm and the basal body position is indicated with an arrow. Stages are presented in a chronological order and the name code is given in Fig. 1.
Fig. S2. Distribution of acetylated and tyrosinated α-tubulin during asymmetric division in 2K2N dividing epimastigotes observed by epifluorescence and confocal microscopy. Proventricular cells were fixed in methanol (epifluorescence) or in PFA (confocal) and stained with DAPI (red) and the YL1/2 antibody (green) recognizing tyrosinated tubulin or the C3B9 antibody (green) labelling acetylated tubulin. The scale bar represents 5 μm and the old (arrow) and new (arrowhead) basal body positions are indicated.
Fig. S3. Flagellar axoneme and PFR2 localization and length variations during trypanosome development. The 10 main morphological stages of the *T. brucei* parasite cycle were fixed in methanol and stained with DAPI (blue in A), the L8C4 antibody recognizing the PFR2 protein (green in A) or the mAb25 antibody labelling the axoneme (not shown). The scale bar represents 5 μm and the old (arrow) and new (arrowhead) basal body positions are indicated. Stages are presented in a chronological order and the name code is given in Fig. 1.
B. Variations (mean ± SD in μm) of flagellum length measured on phase contrast pictures ('Flagellum', $n = 1221$), or upon L8C4 ('PFR', $n = 218$) or MAb25 staining ('axoneme', $n = 307$), compared with the evolution of total trypanosome length from the tip of the flagellum to the posterior end of cell (Total, $n = 1273$).
Fig. S4. FAZ1 localization during trypanosome development. The 10 main morphological stages of the *T. brucei* parasite cycle were fixed in methanol and stained with DAPI (blue) and the L3B2 antibody (green) labelling FAZ1. Note that the FAZ1 labelling is present in all stages, except in epimastigotes and dividing epimastigotes in the proventriculus. In these stages, the fluorescent signal is absent, or is restricted to a few areas of reduced intensity. The scale bar represents 5 μm and the old (arrow) and new (arrowhead) basal body positions are indicated. Stages are presented in a chronological order and the name code is given in Fig. 1.
Fig. S5. Localization of the antigen recognized by the DOT1 marker during trypanosome development. The 10 main morphological stages of the *T. brucei* parasite cycle were fixed in methanol and stained with DAPI (blue) and the DOT1 antibody (green). Note that the DOT1 labelling is present in all stages, except in epimastigotes and dividing epimastigotes in the proventriculus. As for L3B2, the fluorescent signal is absent, or is restricted to a few areas of reduced intensity. The scale bar represents 5 μm and the old (arrow) and new (arrowhead) basal body positions are indicated. Stages are presented in a chronological order and the name code is given in Fig. 1.
Table S1. Morphometric measurements in trypanosome stages. The main morphological stages of the *T. brucei* parasite cycle were fixed in methanol and stained with DAPI and various antibodies (cf. section *Experimental procedures*). This table summarizes all the morphometric measurements performed in the present study in 1K1N parasites. The mean lengths ± SD, ranges and numbers of cells studied are given in μm for nine parameters: the total length of the cell from the tip of the flagellum to the posterior end of the cell (Total), the length of the flagellum in phase contrast pictures (Flagellum), the distance between the centre of the nucleus and the kinetoplast (N–K), the distance between the centre of the nucleus and the posterior end of cell (N-Post), the lengths of the fluorescent signals observed after staining of FLA1, FAZ1 (even in E when it was possible), DOT1 (even in E and DE when it was possible), PFR2 and the axoneme. A total of 1276 parasites was analysed. Stages are presented in a chronological order and the name code is given in Fig. 1.

7.3 List of figures and tables

Figures

Tables

7.4 List of abbreviations

ADK	adenylate kinase
AK	arginine kinase
Alba	acetylation lowers binding affinity (domain and protein)
ALBA	acetylation lowers binding affinity protein (nomenclature in *T. brucei*)
AQP	aquaporin
ATYP	atypical forms found with ALBA3::GFP
BARP	brucei alanine rich protein
BS	bloodstream form
DAPI	4',6-diamidino-2-phenylindole
DE	dividing epimastigote
ER	endoplasmic reticulum
FAZ	flagellum attachment zone
FISH	fluorescence *in situ* hybridization
FLA1	flagellum adhesion glycoprotein 1
FLAMM	flagellar membrane and matrix proteins
GFP	green fluorescent protein
GPI	glycosylphosphatidylinositol
HAT	Human African Trypanosomiasis
IF3	translation initiation factor 3
IFA	immunofluorescence analysis
IFT	intraflagellar transport machinery
K	kinetoplast
LE	long epimastigote
MAPK	mitogen activated protein kinase
MDP	macronuclear development protein
MG	midgut
MS	mesocyclic trypomastigote
MS-E	mesocyclic trypomastigote to epimastigote
MT	metacyclic trypomastigote
N	nucleus
PAD	proteins associated with differentiation
P-bodies	processing bodies
PBS	phosphate buffered saline
PC	procyclic trypomastigote
PFA	paraformaldehyde
PFR	paraflagellar rod
Pol	RNA polymerase
PTP	protein tyrosine phosphatase
RABL5	Rab-like 5 protein
RBP	RNA-binding proteins
RNAi	RNA interference
Rnase MRP	ribonuclease mitochondrial RNA processing
Rnase P	ribonuclease P

Rpp20	ribonuclease P protein subunit p20
Rpp25	ribonuclease P protein subunit p25
RT-PCR	reverse transcription - polymerase chain reaction
SD	standard deviation
SE	short epimastigote
SG	salivary gland
SGE	salivary gland epimastigote
Sir	silent information regulator
siRNA	small interfering RNA
SL	splice leader
SSR	strand switch region
UTR	untranslated region
VSG	variant surface glycoprotein
WT	wild type
YFP	yellow fluorescent protein
ZFK	zinc finger kinase
ZFP	zinc finger protein

7.5 Acknowledgements

I thank Dr. Philippe Bastin, thank you so much to have welcomed me to the TRYPA lab, your scientific enthusiasm is inspiring! Thanks for guiding me through these four years, helping me discover so many facets of trypanosome biology and offering me all the possibilities to improve scientifically. The friendly atmosphere in the lab and the parties you encourage made these years a very enjoyable time.

Ich danke Prof. Markus Engstler, du hast mich jederzeit unterstützt und maßgeblich dazu beigetragen, dass ich meinen Weg in der Wissenschaft gehen kann. Dein jederzeit offenes Ohr und deine Hilfe sind unbezahlbar.

Herrn Prof. Thomas Rudel möchte ich herzlich für die Übernahme des Gutachtens dieser Arbeit danken.

Un énorme merci à toute l'équipe TRYPA, ce fut un plaisir de partager ces années avec vous. Tant de temps pour en profiter et d'apprendre d'être plus « française ». Merci à Sabrina Absalon pour ta grande aide au début, à Daria Julkowska pour le temps passé entre filles « étrangères », à Johanna Buisson de partager l'aventure pas toujours facile de faire une thèse, à Thierry Blisnick j'ai énormément apprécié nos discussions autour de plein de choses différentes, à Laetitia Vincensini pour ton esprit toujours positif et posé et à Diego Huet pour tes desserts mexicains (j'adore les ronds de cacahuètes). Un grand merci à Brice Rotureau, sans toi une grande partie de cette thèse n'existerai pas et merci pour ton aide généreuse autour des corrections du papier et de ce manuscrit. Merci à Anne Cozanet, tu m'as tellement aidée pour l'administratif mais aussi pour les « petites » choses de la vie quotidienne. Nele, dir vielen Dank für deine Hilfe, du warst wirklich eine Musterpraktikantin.

Thanks to all the members of BIHP, your day-to-day company in the P2 is really a pleasure. Surtout merci à Emeric Roux pour nos longues discussions. Merci à Arnaud Chène pour les échanges sur les ALBA et ton aide pour la correction d'une partie de la thèse.

I am very grateful to Dr. Mark Carrington and Dr. Susanne Kramer from the University of Cambridge for having provided several plasmids and giving me the opportunity to come and study my cells in an experienced laboratory. Thanks to all those who provided the antibodies and the cell lines for this work. J'aimerai aussi remercier B. Tchicaya, J. Janelle et G. Cuny de l'équipe UMR177 IRDCIRAD à Montpellier d'avoir fourni les mouches tsé-tsé pour les expériences de cette thèse.

Thanks to Dr. Carla Saleh, for taking the time tutoring me and for your experienced advice. Vielen Dank an Dr. Gerald Späth, für dein Interesse an meinem Projekt und das Korrekturlesen des ALBA Papers. Merci au Dr. Geneviève Milon, vos attentions et votre sourire sont d'une bonté rare.

I would like to thank the Fonds National de la Recherche Luxembourg for having given me the opportunity to benefit from the fellowships BFR/AFR during the 4 years of my thesis. Thanks to Prof. Artur Scherf and the CNRS who agreed to finance the last months of my thesis.

Ich danke meinen Freunden herzlichst für ihre stete Unterstützung und positive Energie trotz dieser örtlichen Distanz während der letzten Jahre!
Im Besonderen danke ich Ben, dafür dass du an mich glaubst, mich unentwegt bestärkst wenn ich zweifle und sogar versuchst zu verstehen was ich erforsche. Deine Liebe war mir eine unbeschreibliche Hilfe während der Doktorarbeit.
Außerordentlich dankbar bin ich meinen Eltern und Großeltern, ihr unterstützt mich mit all eurer Kraft und Liebe. Ihr gebt mir stetige Sicherheit und den Rückhalt meinen Weg zu gehen.

7.6 Erklärungen gem. §4 (3) der Promotionsordnung

Hiermit erkläre ich ehrenwörtlich, die vorliegende Dissertation in allen Teilen selbständig angefertigt und keine anderen als die angegebenen Quellen und Hilfsmittel benutzt zu haben.

Diese Dissertation wurde betreut durch Dr. Philippe Bastin (Institut Pasteur, Paris, Frankreich) zusammen mit Prof. Dr. Markus Engstler (Universität Würzburg) und hat weder in gleicher noch in ähnlicher Form in einem anderen Prüfungsverfahren bereits vorgelegen.

Ein Verzeichnis der bisher eingereichten und veröffentlichten wissenschaftlichen Arbeiten ist im Abschnitt 7.2 zu finden.

Des Weiteren erkläre ich, dass ich früher außer dem Studienabschluss der Diplom Biologin an der Ludwig-Maximilians-Universität München keine weiteren akademischen Grade erworben habe, oder zu erwerben versucht habe.

Ines Subota